Investigating the function of novel players of iron homeostasis, heme metabolism and steroid hormone biosynthesis in *Drosophila melanogaster*

by

Sattar Soltani

A thesis submitted in partial fulfillment of the requirements for the degree of

Doctor of Philosophy

in

Molecular Biology and Genetics

Department of Biological Sciences

University of Alberta

Abstract

Iron is a transition metal that is known to be essential for all organisms in trace amounts. It participates in biological reactions in the form of different enzymatic cofactors such as a single atom to an iron-sulfur cluster and heme. Therefore, iron functions in numerous biological and cellular processes such as oxygen transport, electron transfer, steroid hormone biosynthesis and DNA synthesis. Unbalanced cellular iron levels result in divergent disorders, including iron deficiency anemia, iron overload hemochromatosis, porphyrias and neurodegenerative disorders. While extensive efforts have focused on general aspects of systemic and cellular iron regulation, little is known about iron homeostasis in tissues with dynamic iron demands. The *Drosophila* prothoracic gland (PG) is an excellent model for investigating dynamic iron regulation and characterizing novel functions of genes or genes with hitherto unknown links to iron. The PG is a part of the endocrine gland known as the ring gland (RG) and is the primary tissue responsible for the biosynthesis of the steroid hormone ecdysone in insects. The PG has been demonstrated to require substantial amounts of iron. Indeed, the PG releases pulses of ecdysone throughout the *Drosophila* life cycle to govern developmental transitions such as the molts and puparium formation. Multiple cytochrome P450 enzymes (P450s) with dynamic and remarkably high expression in the PG cells produce ecdysone. These P450 enzymes require iron in the form of heme cofactors. Therefore, the PG has to import a high amount of iron or release stored iron to keep up with the ecdysone biosynthesis.

My thesis focuses on three distinct projects aiming at understanding the regulatory mechanisms of heme synthesis, iron homeostasis and ecdysone biosynthesis. First, I investigated the roles of a gene referred to as Ecotropic viral integration site 5 (*Evi5)* in the PG cells' iron trafficking and heme production. Evi5 is a GTPase-activating protein (GAP) that regulates the small GTPase Rab11. Depletion of *Evi5* function in the PG cells causes larval developmental retardation, pupal lethality and cellular accumulation of heme precursors (known as the porphyria-like phenotype). These phenotypes are due to impaired vesicular trafficking and reduced cellular iron level that can be rescued with dietary heme administration. Further investigation suggested a hitherto unknown role for Evi5 in iron homeostasis and trafficking. I found that Evi5 interacts with the iron storage protein ferritin and autophagy components such as dynamin, Clathrin and Hsc70-4. These results led to the hypothesis that Evi5 regulates iron release from ferritin via autophagy-lysosomal degradation.

The second project was to evaluate the transcriptional responses to dietary iron manipulation. I carried out an RNA sequencing (hereafter RNA-Seq) analysis using the larval brain ring gland complex (BRGC), larval gut, and whole larval body (WB) to identify differentially expressed genes (DEGs). This study aimed at identifying novel iron homeostasis genes. My approach determined that in PG cells, the heat shock proteins encoded by *Hsp22* and *Hsp70* are iron-responsive genes. Both proteins appear to participate in cellular iron homeostasis by binding to NFS1, a component of iron-sulfur (Fe-S) cluster assembly machinery, Fe-S cluster recipient proteins, and ferritin. Further analysis of all significant DEGs indicated decreased food iron levels boost the immune responses and chitin metabolism. Given these findings, I propose that chitin acts as a novel iron deficiency immune responsive molecule that creates a physical barrier against pathogens. Furthermore, this work demonstrated that Dietary and metabolic glutamate transporter (dmGlut) and modifier of mdg4 (mod(mdg4)) have significant homology to unidentified ferroportin (FPN1) and ATF2 transcription factor in *Drosophila*, respectively. These findings added more knowledge to the current information about iron biology.

I also studied novel functions of the Spen protein in ecdysone biosynthesis. Spen is a corepressor transcription factor that governs gene expression by binding to regulatory sequences in the nucleus or to mRNA in the cytosol. PG-specific loss of *Spen* function altered the RG morphology of the larvae and reduced the numbers of PG cells. This results in a larval developmental arrest due to ecdysone deficiency that can be rescued with ecdysone or precursors of the ecdysone pathway. I further found evidence that Spen is a regulatory protein downstream of the MAPK/ERK signaling pathway that controls ecdysone biosynthesis. The exact regulatory mechanism of Spen is currently unknown, but expressing a constitutively active form of Ras in the PG cells also rescues the arrested animals and improves the RG morphology. These preliminary data suggest a novel role for Spen in ecdysone biosynthesis.

This thesis is dedicated to the doctors, nurses and medical staff who lost their valuable lives during the Covid-19 pandemic.

Acknowledgments

I would like to express my deepest appreciation to my supervisor Dr. Kirst King-Jones for giving me the opportunity to join his lab. I am very grateful to him for being a patient, supportive and encouraging supervisor during my program. I would like to further thank him for his constant encouragement and critical feedback on my projects, presentations, and writings that helped me to develop my career and perform better as a researcher. My deepest gratitude also goes to my committee members Dr. Martin Srayko and Dr. Andrew Waskiewicz for providing useful feedback and suggestions on my projects.

I am very thankful for the help and support of all the past and current members of the King-Jones lab, especially Dr. Qiuxiang Ou. I would also like to specifically thank Pendleton Cox, Dr. Jie Zeng, and Dr. Brian Phelps for all their comments on my project during the coffee breaks that we had.

Lastly, I would like to say thanks to my family and friends. I am very grateful to my parents for their love and support that enabled me to cope with the stresses that I had and always encouraged me to continue my work. I am also extending my thanks to my friends who made me feel happy and provided me a time to escape from my work and supported me during the hard days that I had.

Finally, my thanks go to all the people at the University of Alberta who have helped me to do my research directly or indirectly.

Table of Contents

List of Figures

Chapter 1

Chapter 3

Chapter 4

Chapter 5

Appendix

List of Tables

Chapter 1

Chapter 2

Chapter 3

Chapter 4

Abbreviations

20E	20-hydroxyecdysone
5βk	5β-ketodiol
7DC	7-dehydrocholesterol
Ag5r	Antigen 5-related
ALAD	Aminolaevulinic acid dehydratase
ALAS	5-Aminolevulinate synthase
Atg	Autophagy-related protein
BPS	Bathophenanthrolinedisulfonic acid disodium salt hydrate
BPS-up	BPS upregulated genes
BRGC	Brain Ring gland complex
CA	Corpus Allatum
Cas9	CRISPR-associated nuclease
CC	Corpus Cardiaca
CC	Coiled-coil domain
cDNA	Complementary DNA
Chc	Clathrin heavy chain
CNS	Central nervous system
coIP	Coimmunoprecipitation
CPOX	Coproporphyrinogen III oxidase
CRISPR	Clustered Regularly Interspaced Short Palindromic Repeats
CT	Threshold Cycle
CyP450	Cytochromes P450
Dap 160	Dynamin associated protein 160
DEG	Differentially expressed gene
Desi	Desiccate
DGRC	*Drosophila* Genome Resource Center
DHR3	*Drosophila* Hormone receptor 3

DHR4	*Drosophila* Hormone receptor 4
Dib	Disembodied
Dl	Delta, Notch signaling ligand
DMT1	Divalent metal transporter 1
DNA	Deoxyribonucleic acid
DRSC	*Drosophila* RNAi Screening Center
DsRed	Discosoma red fluorescent protein
Dup99B	Ductus ejaculatorius peptide 99B
E75	Ecdysone-induced protein 75
EcR	Ecdysone Receptor
EE	Early endosome
EEA1	Early Endosomal Autoantigen 1
eGFP	enhanced Green Fluorescent Protein
EGFR	Epidermal growth factor receptor signaling
Eps-15	Epidermal growth factor receptor pathway substrate clone 15
ER	Endoplasmic reticulum
ERK	Extracellular signal-regulated kinase
Evi5	Ecotropic viral integration site 5
FAC	Ferric Ammonium iron(III) citrate
FAC-up	FAC upregulated genes
FECH	Ferrochelatase
FLP	Flippase
FPN1	Ferroportin
FRT	Flippase Recombination Target
FTH1	Ferritin heavy chain 1
FTL1	Ferritin light chain 1
G1-G5	Generation one to generation five
GAP	GTPase-activating proteins

GCS2β	Glucosidase 2 β subunit
GDP	Guanosine diphosphate
GEF	Guanine nucleotide exchange factor
gRNA	guide RNA
Gst	Glutathione S transferase
GTP	Guanosine triphosphate
H	Ferritin Heavy chains
HDAC	Histone deacetylase
HO	Oxygenase enzyme
Hp	Hephaestin
Hsc70-4	Heat shock protein cognate-4
Hsp	Heat shock protein
IF	Immunofluorescence
ILP	Insulin-like peptide
IM4	Immune induced molecule 4
InR	Insulin-like receptor
IP	Immunoprecipitation
IP-MS	Immunoprecipitation followed by Mass-spectrometry
IRE	Iron Responsive Element
IRP	Iron Regulatory Protein
L	Ferritin Light chains
L1	First instar
L2	Second instar
L3	Third instar
LK	Leucokinin
Lsp	Larval serum protein
mAcon1	Mitochondrial aconitase 1
MAPK	Mitogen-activated protein kinase

MCF-7	Human adenocarcinoma cells
Mco4	Multicopper oxidase 4
ml	Millilitres
MS	Multiple sclerosis
MtF	Mitochondrial ferritin
Mvl	Malvolio
MZF-1	Myeloid zinc-finger 1
NCOA-4	Nuclear receptor coactivator–4
Ng3	New glue 3
Nvd	Neverland
PBGD	Porphobilinogen deaminase
PBS	Phosphate buffered Saline
PCA	Principal component analysis
PG	Prothoracic gland
Phm	Phantom
PPIX	Protoporphyrin IX
PPOX	Protoporphyrinogen IX oxidase
PTTH	Prothoracicotropic hormone
qPCR	Quantitative Real-time PCR
Ras85D	Ras oncogene at 85D
RBM15	RNA-binding motif protein 15
RFeSP	Rieske iron-sulfur protein
RG	Ring gland
RNA	Ribonucleic acid
RNA-seq	RNA-sequencing
RNAi	RNA interference
ROS	Reactive oxygen species
RPKM	Reads per Kilobase of transcript per Million mapped reads

RRM	RNA Recognition Motif
S2	Schneider S2 cells
Sad	Shadow
SdhB	Succinate dehydrogenase subunit B
Ser	Serrate, Notch signaling ligand
Shd	Shade
SNP	Single nucleotide polymorphism
Sod3	Superoxide dismutase
SP	Signal peptide
SPOC	Spen Paralog and Ortholog C-terminal domain
Spok	Spookier
SRA	Steroid Receptor RNA Activator
Sroß	Shroud
StAR	Steroidogenic acute regulatory protein
Su(H)	Suppressor of Hairless
TBC	Tre-2, Bub2, and Cdc16 domain
TEM	Transmission Electron microscopy
TfR	Transferring receptor
TRIP	Transgenic RNAi Resource Project
Tsf	Transferrin
UAS	Upstream activation sequence
Ugt	UDP-glycosyltransferase
UPS	Ultraspiracle
UROD	Uroporphyrinogen decarboxylase
UROS	Uroporphyrinogen III synthase
UV	Ultraviolet
VDRC	Vienna *Drosophila* Resource Center
W1118	White mutant *Drosophila* flies, Control flies

WB	Whole larval body
Wg	Wingless
ZnPP	Zinc-protoporphyrin IX
αE	α-ecdysone
βFtz-F1	β-fushi tarazu transcription factor 1
µM	Micrometer

Chapter 1 Introduction

My research focused on iron homeostasis in the context of steroid hormone production in the *Drosophila melanogaster* model organism. Here, I will describe the general aspects of iron biology, and then I will elaborate on the link between iron hemostasis and steroid hormone production in *Drosophila*.

1.1 General concepts of iron biology

1.1.1 Iron is an obligate element in cellular biology

Iron cycles between a ferrous (Fe^{2+}) and a ferric form (Fe^{3+}) to act as a cofactor in a variety of electron transfer reactions. This coordination chemistry of iron in cycling between two relatively stable and different oxidative forms makes it a fundamental element in biological processes [1,2]. It has an obligatory role in a broad range of proteins, from oxygen transport/storage by hemoglobin and myoglobin to energy production by mitochondrial cytochrome electron transports and in diverse enzymatic pathways such as DNA synthesis and lipid metabolism [3–8].

Despite being an essential micronutrient, iron imposes several problems on living organisms. In fact, the redox activity/ability of iron can lead to free radical production via the Fenton reaction [9]. Excess of free ferrous iron can form oxygen superoxide (O_2^-), which in turn is converted to highly toxic hydroxyl free radicals (^0OH) [9]. These radicals can readily damage proteins, nucleic acids, carbohydrates and further initiate lipid peroxidation [9]. For this reason, evolution has not limited iron to be freely accessible, and instead has generated diverse iron-binding proteins first to sequester free iron and second to transport it to the sites where iron is highly needed [10].

The iron-binding proteins' misregulation can progress into a series of health problems associated with iron deficiency and iron overload (Table 1.1). For example, iron deficiency anemia, a worldwide health problem, is characterized by abnormal microcytic hypochromic red blood cells. Furthermore, any condition in which iron levels do not meet demands will cause iron-deficient erythropoiesis that adversely affects children's growth and development [11]. On the other hand, when the iron content exceeds cellular capacity (iron overload), it results in other disorders. The hereditary hemochromatosis syndromes are the most and the best-understood iron overload diseases [12]. At the early stages, hemochromatosis causes abnormal skin pigmentation, depression, and infertility [13], but as the disease progresses, patients indicate hepatic inflammation and fibrosis

[12]. Secondary hemochromatosis (non-hereditary hemochromatosis) arises from intense cellular iron usage that results in lethality due to severe liver and heart failure [14].

Finally, iron is a potential risk factor for different cancers such as breast, lung, gastric and esophageal cancers [15]. It has been demonstrated that iron promotes malignant tumor formation by impairing immunity and inducing cell proliferation [16,17]. Therefore, the regulation of iron homeostasis is one of the central cellular functions in nearly all living organisms.

1.1.2 Mammalian systemic iron homeostasis

The body iron content of adult humans is approximately 3-5 g. A large proportion of this iron pool is present in the hemoglobin of erythrocytes (65-70%), but the remaining iron is either stored (20%) or utilized as a cofactor in different proteins (10-15%) [18]. These cellular iron paths are highly dynamic and are tightly regulated by a constant iron flux between tissues. Nearly 4 mg of iron in the form of protein-bound is circulating in the bloodstream, but a substantial amount of iron is taken up from the plasma every day (serum iron) [19]. This iron supply is predominantly used for hemoglobin synthesis during erythropoiesis in the bone marrow (30 mg per day). However, serum iron is further delivered to other sites of iron utilization, such as the liver (5 mg) and muscle cells (300 mg) [20].

To maintain the daily balance of serum iron, the same amount of iron should be restored and released into the blood. White blood cell phagocytes (macrophages) play a central role in this process. These cells recognize, engulf and digest old or damaged erythrocytes to recycle iron into the bloodstream [21]. The autophagic process (lysosomal degradation) of cellular iron-containing components such as mitochondria and storage proteins also release and restore iron. Furthermore, intestinal cells absorb 1-2 mg of iron from the diet every day to replace the unavoidable loss of iron from the skin and the urinary system [18]. Therefore, this dynamic flux of iron among different tissues suggests that organisms need the precise transportation, storage and secretion systems for iron. This maintains the iron in an oxidatively inactive but easily accessible form that can be utilized at a time when needed.

1.1.3 Mammalian cellular iron uptake

Before gaining access to the plasma circulatory proteins, iron must be absorbed by duodenal enterocytes. Dietary iron is found in two forms: a heme iron (organic) and a non-heme

iron (inorganic). Heme is discussed later in this chapter (Section 1.2.2). Therefore, in this section, I will mainly focus on the non-heme dietary iron (Figure 1.1).

The Fe^{3+} (aka ferric) iron, which accounts for a large extent of the non-heme dietary iron (~90%), is incapable of passing the enterocytes' membrane. Thus, in the acidic gastric environment, the ferrireductase enzyme (Dcytb) first converts the Fe^{3+} iron to Fe^{2+} iron [22]. Next, ferrous iron is imported into the enterocytes by the divalent metal transporter 1 (DMT1) at the apical surface of cells [19,23]. The DMT1 is a glycoprotein endomembrane transporter of the Zip protein family that transports a broad range of divalent metals such as Fe^{2+}, Zn^{2+}, Mn^{2+}, Co^{2+}, Cd^{2+}, Cu^{2+}, Ni^{2+} and Pb^{2+} [24,25]. In enterocytes, iron is stored in the cytoplasm if it is not required immediately. But if needed, iron is transported across the basolateral membrane of the cells by the iron transporter ferroportin (FPN1) [19,23]. It is worth mentioning that heme is also imported into enterocytes, and its iron is released by the heme oxygenase enzyme. Once all iron of enterocytes is exported into the plasma, it is oxidized into ferric iron before being trafficked to target tissues by the transferrin (Tsf) proteins. The oxidation step is facilitated with the multicopper ferroxidase Hephaestin (Hp) in a copper-dependent oxidation manner [26–28].

Mammalian cells encode several transferrin proteins, including serum transferrin, lactoferrin, ovotransferrin and Melanotransferrin [29]. Transferrins are secreted glycoproteins with two iron-binding lobes (N–terminal and C-terminal halves). Each lobe binds to a Fe^{3+} by forming a hydrophobic cleft that harbors iron-binding residuals [30]. It is proposed that the two iron-binding lobes arose from a gene duplication and fusion event due to the high sequence similarity [31]. The serum Tsf is one of the most abundant plasma proteins (~2-4 mg/ml) that, under normal conditions, bind to all of the circulatory iron (Figure 1.1). It is found in a diferric transferrin (holo-form), mono-ferric transferrin and iron-free apo-transferrin [18]. Furthermore, serum transferrin is proposed to be an immune response protein that sequesters iron when there is an infection, or if there is a sudden increase in the iron level [10,32]. In target tissues, such as bone marrow or hepatocytes, holo-Tsf binds to its receptor, the transferrin receptor (TfR) (Figure 1.1). There are two TfR proteins (TfR1 and TfR2), but holo-Tsf binds to TfR1 with significantly higher affinity than TfR2 [33]. TfR1 is expressed in almost all cells, but it is has elevated levels in cells with an higher iron demand (such as developing erythrocytes) [34]. *TfR2* expression, on the other hand, is restricted to hepatocytes and only expressed under iron overload conditions [35]. Upon binding at the cell surface,

the TfR1-holo-Tsf complex enters into cells via Clathrin-mediated endocytosis. The iron-containing complex in early endosomes is then sorted to late or recycling endosomes [36]. The acidic lumen of the endosomal structures facilitates the release of iron from the TfR1-holo-Tsf complex. Ferric iron is then converted to ferrous iron and is exported into the cytosol by the DMT1 protein. In the recycling endosomes, the TfR1-apoTsf complex is returned to the plasma membrane. The higher pH of the extracellular space induces the release of the apo-Tsf from TfR1. This results in free Tsf and TfR1 that can repeat the iron uptake cycle again.

In addition to transferrin-mediated iron uptake, cells may use other proteins to import iron in different ways. For example, neurons and retina cells express two members of the Zip protein family, DMT1 and Zip8, to import iron directly from the plasma (Figure 1.1) [37,38]. Furthermore, it is thought that the iron storage protein ferritin further functions in the intracellular iron trafficking pathway via possibly the ligand-receptor mediated endocytosis (similar to transferrin) [39–41].

1.1.4 Mammalian cellular iron usage, storage and release

Not all of the imported iron is utilized for iron-dependent biological processes in the cell. Up to ~4500 iron atoms can be stored in the ferritin nano-cage (Figure 1.1). Cytosolic ferritin is a spherical structure that acts as a nano-cage for iron, and is composed of 24 subunits of two different proteins (12 subunits per each). It has a heavy chain subunit (H) with a ferroxidase activity to facilitate iron oxidation and storage into the cage and a light chain subunit (L) that promotes iron composition with phosphate and oxygen in cooperation with the H subunit [39,42,43]. The genes encoding the ferritin subunits, *FTH1* and *FTL1* (encode H and L chains, respectively), are expressed in various cells from duodenal to skin, muscles and brain cells [39,43]. Furthermore, in vertebrate and insects ferritin has been identified within different cellular components, such as cytosol, mitochondria, nucleus, and vesicular compartments, but the cytosolic protein is the primary iron storage ferritin.

Mitochondrial ferritin (FTMT) is encoded by a single gene (*FTMT)*. It is similar to cytosolic ferritin, it has 24-subunits (homopolymers) with ferroxidase activity. FTMT has been demonstrated to protect mitochondria from the oxidative damage caused by iron misregulation [42,44]. In vertebrates, ferritin also has been identified in the nucleus, mainly in the H-form. It is proposed that nuclear ferritin protects DNA from iron-induced oxidative damage and involved in gene regulation [45,46]. Moreover, ferritin has been identified in autophagosomes and lysosomes

when cells suffer from iron deficiency (Figure 1.1) [47]. This process is termed ferritinophagy and is initiated in vertebrates by holoferritin interacting with nuclear receptor coactivator–4 (NCOA-4) [48]. The ferritinophagy targets ferritin to the lysosomes and results in iron release upon lysosomal protein degradation [47–50]. This restores a large amount of iron that can be exported into the cytosol to be utilized under iron starvation (Figure 1.1).

Finally, ferritin is secreted into the extracellular space analogous to the transferrins. The exact function of serum ferritin has not been characterized yet. However, it is proposed to sequester serum iron during iron overload or in response to the infection with iron-using pathogens [40]. Besides, many studies suggest that serum ferritin is involved in systemic iron trafficking (Figure 1.1). Little is known about this aspect of ferritin function, but it is thought that it imports iron into the cells by a receptor-mediated endocytosis/exocytosis process. If such a cell surface receptor for ferritin exists is still unclear.

1.1.5 Mammalian cellular iron homeostasis

Cells have adapted several regulatory procedures to adjust protein functions in response to iron status. One of the key intracellular iron homeostasis mechanisms is the translational control of iron-related mRNAs by the iron-regulatory proteins (IRP1 and IRP2) [51]. The IRPs govern the expression of iron genes by binding to iron-regulator elements (IREs) in the untranslated region (UTRs) of their respective mRNAs [51]. The binding of IRP to IREs within the 3'UTR stabilizes mRNAs and increases protein synthesis. On the other hand, the interaction of IRPs with 5'UTR IREs represses the translation process [52].

IRP1 plays a critical role in post-transcriptional regulation during iron stress. IRP1 cycles between two distinct forms depending on the iron level. When cells have normal iron levels, IRP1 functions as an aconitase enzyme because it is bound to an 4Fe-4S iron-sulfur cluster [53]. But when the iron is deficient, the 4Fe-4S cluster is disassociated from the protein, and IRP1 becomes an mRNA binding protein. The IRP1/IRE regulation system is restricted to few iron-related genes. The TfR1 and DMT1 mRNAs harbor each 3'UTR IREs while the *FTH1*, *FTL1*, *FPN1* and *AlAS2* (5-aminolevulinic acid synthase 2 in the heme pathway) genes encode mRNAs with 5'UTR IREs [52,54,55]. IRP2 acts in a different manner to regulate iron-related genes post-transcriptionally. Cells

promote the expression of IRP2 under the low iron conditions, but the IRP2 is degraded when the iron level is normal [56].

The hepatic peptide hormone hepcidin further regulates the iron homeostasis of mammalian cells [57]. The hepcidin hormone promotes the lysosomal degradation of FPN1 and DMT1 upon binding to them at the cell surface [57,58]. The hepatic synthesis and secretion of hepcidin are controlled transcriptionally. Elevated hepatic iron content activates the expression of hepcidin to reduce the plasma iron levels [20]. Furthermore, anemia, hypoxia and iron deficiency downregulate hepcidin expression, suggesting that the iron status creates a feedback loop to regulate the hepcidin levels [59]. TfR2 is also expressed in hepatocytes and functions as an iron sensor to regulate hepcidin levels [60]. This suggests that hepcidin coordinates systemic iron uptake and trafficking in response to different stimuli.

1.1.6 Insect iron biology

The integrated and conserved biological responses to iron on the one hand, and the functional and structural specificities of iron proteins, on the other hand, make insects an interesting model to study iron biology. Some of the iron pathways are not present in insects, or they have modified distinctly. Differences in responses would indicate how iron homeostasis has been differentiated and evolved across the species. However, similar to mammals, insect cells must create a balance between iron toxicity and iron utilization. Most of our knowledge about the iron biology in insects has been derived from studies in *Drosophila melanogaster* [61]. Therefore, I will consider here the similarities and differences of iron regulation between *Drosophila* and mammals.

In *Drosophila*, dietary iron uptake occurs in the apical surface of the midgut epithelial cells. It then passes the basal membrane surface and is released into the hemolymph, which is the circulating fluid or blood in insects. Hemolymph iron is then taken up by individual tissues and is utilized or stored in the cells. Despite the resemblance to mammals, only a few players of these events have been identified in *Drosophila* (Table1.1). At the site of absorption, only the DMT1 homolog called Malvolio (Mvl) has been characterized in *Drosophila*, and the functional orthologs of the ferrireductase enzyme (Dcytb), ferroportin (FPN1) and ferroxidase Hephaestin (Hp) iron exporter have not been identified yet (Table1.1).

At the systemic iron trafficking level, *Drosophila* has three Tsf homologs (Tsf1-3). Tsf1 is the ortholog of serum Tsf and is found in the hemolymph abundantly [62,63]. However, Tsf1 lacks the C-terminal iron-binding lobe and is considered a mono-ferric iron transporter [64]. Tsf2 is the homolog of mammalian melanotransferrin that has two iron binding halves and a GPI anchor moiety [65]. Tsf3 is the least studied member of the *Drosophila* transferrins with no knowledge about its role. Surprisingly, despite the presence of three transferrin genes in the fly genome, *Drosophila* and other insects lack an ortholog for the vertebrate (*TfR1* and *TfR2*) transferrin receptor. Therefore, it remains unclear how the holo-Tsf proteins are endocytosed or exocytosed into/out of insect cells.

Drosophila ferritin is similar to its mammalian homolog and is composed of the H-chain and L-chain subunits with homologous roles [64]. The *Fer1HCH* and *Fer2LCH* genes encode the two subunits and are orthologs of FTH1 and FTL1, respectively [64]. Unlike the mammalian homologs, however, the Fer1HCH and Fer2LCH protein subunits carry a canonical secretion signal that predominantly targets ferritin into the hemolymph by the ER-Golgi secretion machinery [66,67]. The hemolymph ferritin level is induced in response to iron and pathogens, suggesting that it may transfer iron between the cells. *Drosophila* also expresses the mitochondrial ferritin (Fer3HCH) that has a critical role in mitochondrial iron regulation during spermatogenesis [68,69].

There are two orthologs for vertebrate IRP1 in *Drosophila* named IRP1A and IRP1B [70,209]. It has been indicated that IRP1A and IRP1B have the cytosolic aconitase activity [70,209]. However, the IRP1A is considered to be the primary (functional) homolog for the IRP1 in cellular iron homeostasis [209]. It cycles between the holo (4Fe-4S bound) and apo (aconitase form) conformations, and the fly IRP1A/IRE system regulates the translation of Fer1HCH and SdhB (succinate dehydrogenase subunit B) mRNAs [209]. Remarkably, holo-IRP1A displays nuclear localization in some *Drosophila* tissues, where it is believed to regulate iron homeostasis via the regulation of specific target genes [70]. This nuclear function has not been reported for the mammalian IRP1 yet. *Drosophila* IRP1B, however, appears to be restricted to act as an aconitase, but it is found in nuclei also.

To conclude, *Drosophila* shares many of the key players in mammals' iron metabolism, but it has evolved different mechanisms with novel players corresponding to its unique physiology.

Finally, it is worth mentioning that in this section, I only mention the functionally characterized orthologs and not the uncharacterized candidate genes (Table 1.1).

1.2 Steroid hormone and iron homeostasis

1.2.1 Iron is an obligatory component of the *Drosophila* steroid hormone ecdysone

The *Drosophila* life cycle consists of several distinct developmental stages, including one embryonic, three larval (L1, L2, L3), one pupal and one adult stages (Figure 1.2) [71]. Extensive studies over the past decades indicated that the *Drosophila* developmental transitions are operated by pulses of the steroid hormone ecdysone [72]. Steroids or external signals regulate multiple biological processes upon binding to a nuclear receptor in the target tissues. This triggers transcriptional responses that eventually regulate glucose metabolism, immune responses, cellular osmotic balance, and sexual and developmental puberty [73–76].

All larval stages of *Drosophila* are considered growth stages where animals continue feeding until metamorphosis. Pulses of ecdysone govern developmental transitions of all three larval stages and raise the question of how ecdysone production is balanced with dietary nutrients. After all, a lack of essential nutrients will stall or slow down development if an organism has not sufficient stores of the nutrient in question (assuming it cannot be synthesized) (Figure 1.2). Thus, nutrient availability is critical for the ecdysone pulse, as a pulse of ecdysone regulates the duration of each developmental stage precisely. Iron is an essential nutritional element for ecdysone biosynthesis. In fact, steroid hormone production in mammals and insects is heavily dependent on iron, since the corresponding enzymes require cofactors in the form of heme and Fe-S clusters [77,78].

Ecdysone is synthesized in the larval prothoracic gland (PG) from dietary sterols such as cholesterol (C). The PG, which is the major part of a tripartite endocrine gland named the ring gland (RG), utilizes a series of enzymes called Halloween enzymes to synthesize ecdysone (Figure 1.3) [79,80]. The pathway initiates with Neverland (Nvd), which converts cholesterol to 7-dehydrocholesterol (7DC). 7DC is then hydrolyzed to 5β-ketodiol (5βk) by several unknown steps. This part of the pathway is referred to as the "black box" because the intermediates and participating enzymes are poorly understood. However, Shroud (Sro), Spookier (Spok) and Cyp6t3 Halloween enzymes have been demonstrated to function in the black box (the order remains unclear). Next, the enzymatic reactions of Phantom (Phm), Disembodied (Dib) and Shadow (Sad)

form the prohormone α-ecdysone (αE) from the 5βk. α-ecdysone is an inactive hormone that is released into the hemolymph. It is converted to the active hormone 20-hydroxyecdysone (20E) in the target tissues by the last enzyme in the pathway, Shade (Shd). Except for Shroud, all other Halloween enzymes require iron in different forms as a cofactor. The Neverland is a Rieske electron oxygenase that harbors an Fe-S cluster, whereas the rest are cytochrome P450 monooxygenase enzymes that contain heme as a cofactor [81,82].

The PG-specific depletion of Halloween gene function or regulatory proteins of the ecdysone pathway causes various ecdysone deficiency phenotypes. Consequently, animals fail to complete their development, and they exhibit embryonic lethality, larval lethality (arrested L1, L2 and L3 animals), larval developmental delay, or pupal lethality.

Dr. Kirst King-Jones' lab is mainly studying the regulatory factors involved in the formation of the ecdysone peak at the end of the L3 larval stage that is needed for the onset of metamorphosis. The transcriptional analysis of the PG cells indicated that Halloween gene expression is dramatically upregulated prior to an ecdysone peak [83,84]. This dynamic expression pattern suggests that substantial amounts of iron in PG cells have to be bioavailable prior to the ecdysone pulse to be used for heme and Fe-S cluster synthesis (Figure 1.4B).

1.2.2 Heme biosynthesis and cellular iron balance

Heme is a cofactor for a divergent group of proteins (Hemoproteins) involved in critical cellular processes such as oxygen transport, steroid hormones production, oxidative phosphorylation, gas sensing, circadian rhythm, glucose metabolism and microRNA processing [85–88]. Eight enzymes synthesize the heme in the cytosol and mitochondria (Figure 1.4A). The heme biosynthetic enzymes are structurally and functionally conserved between mammals and *Drosophila*. The first step is conducted by the 5-Aminolevulinate synthase (ALAS) enzyme that forms 5-aminolevulinic acid (ALA) from succinyl-CoA and glycine inside the mitochondrial matrix. The ALAS is the rate-limiting enzyme in mammals and most likely in the *Drosophila* heme pathway as well, and its function is governed by heme levels via a negative feedback loop [89]. The high levels of heme are sensed by the nuclear repressor proteins that down-regulate ALAS expression [89]. On the contrary, when heme levels have dropped, ALAS expression is induced to maintain the intracellular heme levels. Furthermore, unlike the single *ALAS* gene in *Drosophila*, mammals have two ALAS genes (*ALAS1* and *ALAS2*). ALAS1 is constitutively expressed in the

majority of cells and is under control of heme levels. However, ALAS2 expression is restricted to erythrocytes and is governed by the IRP/IRE system [52].

The subsequent four steps of the pathway are carried out by the aminolevulinic acid dehydratase (ALAD), porphobilinogen deaminase (PBGD), uroporphyrinogen III synthase (UROS), and uroporphyrinogen decarboxylase (UROD) enzymes in the cytosol. These enzymes convert the linear ALA intermediate to a cyclic tetrapyrrole structure referred to as a porphyrin ring. The porphyrin rings have unique photochemistry that autofluoresce red when exposed to UV light and to air [90–92]. This photochemistry is the hallmark of a group of heme biosynthetic disorders (see 1.2.3 section). The porphyrin ring undergoes further structural changes in the mitochondria by coproporphyrinogen III oxidase (CPOX) and protoporphyrinogen IX oxidase (PPOX) enzymes to become the protoporphyrin IX (PPIX) [93]. Finally, ferrochelatase (FECH), the last enzyme in the pathway, inserts a ferrous iron (Fe^{2+}) into protoporphyrin IX to form the final heme molecule [93]. Furthermore, FECH has an affinity to other metals, such as zinc and cobalt, and is able to insert them into the PPIX [94]. Moreover, these metalloporphyrins are found in animals' diets, but they cannot function as the cofactor in the hemoproteins such as P450s [95]. Thus, the FECH enzyme further exchanges these metals in the PPIX with Fe^{2+} to produce functional heme [94].

Similar to iron, free heme is a potent cytotoxic and hydrophobic component that cannot be stored per se in cells, and it is thus thought that all cellular heme is bound to target proteins that require heme as a cofactor. Free heme promotes protein degradation and lipid peroxidation and induces free radical formation and oxidative damage [96]. Cells can further detoxify excess heme or dietary heme by heme oxygenase enzyme (HO). HO breaks down heme into Fe^{2+}, biliverdin and carbon monoxide [97]. The released iron can be further utilized immediately, or it can be stored in ferritin nano-cages. Thus, tissues with high heme demands during development (like the PG in *Drosophila*) must either import heme or synthesize heme when demand increases. Besides, iron import/mobilization has to be balanced with heme biosynthesis in this tissue to address the cellular heme requirements at the time of demand.

1.2.3 Heme defects reduce ecdysone levels and induce porphyria phenotypes

Interfering with the function of heme biosynthetic genes reduces cellular heme levels and compromises the formation of ecdysone pulses. This results in a lowered ecdysone level that

causes developmental defects. For example, animals with depleted ALAS and PPOX expression fail to complete the L3 to prepupal transition [70]. PG-specific loss of *PPOX* causes dramatic ALAS upregulation in this tissue. The induction of ALAS causes the accumulation of porphyrins and results in red autofluorescing PG cells [70]. This phenotype resembles the symptoms of porphyria patients, which are characterized by mutations in heme biosynthetic genes.

The porphyrias are a group of metabolic disorders that are specified by various symptoms based on the defects in the heme enzymes (Table 1.2). They are categorized into two groups: acute and cutaneous porphyrias [98,99]. The acute forms of porphyria are usually induced by external and internal stimuli, such as drugs and steroid hormones, that elevate ALAS1 expression. Acute porphyria patients are distinguished by abdominal pain, vomiting and neuropathy symptoms. Reducing the product of the ALAS1 enzyme (ALA) is one of the main treatments for this type of porphyria [98]. The cutaneous porphyrias, on the other hand, are distinguished by severe skin lesions because of increased heme precursors in the liver, skin and circulatory fluids [100]. Moreover, the hepatic expression of ALAS2 is remarkably induced in these types of disease [101]. Similar to PG loss of *PPOX*, the photosensitivity (redness and red autofluorescence) is the principal manifestation of the cutaneous porphyrias that appears immediately after exposure to light [100]. The patients' blood, teeth, and urine under UV light exhibit the porphyria red autofluorescence phenotype [100].

1.3 Thesis outline

My thesis focuses on three distinct projects. The first two projects are aimed at studying heme metabolism and iron homeostasis. In the first project, I have characterized the roles of Evi5 in iron trafficking with regard to ecdysone production of PG cells. The second part was to examine the transcriptional responses to dietary iron manipulation using RNA-Seq in whole body and tissue-specific samples. The objective of the third project, however, was to study the regulatory functions of Spen, a transcriptional corepressor, upstream of the ecdysone pathway.

1.3.1 Understanding the roles of Evi5 in heme and iron metabolism during ecdysone production

Ecotropic viral integration site 5 (Evi5) is a GTPase-activating protein that interacts with the small GTPase Rab11. I started to investigate the function of Evi5 in the context of ecdysone

production. PG-specific loss of Evi5 function caused an ecdysone deficiency phenotype and resulted in the accumulation of heme precursors, evidenced by the presence of red autofluorescence. The porphyria-like phenotype and developmental defects could be rescued with hemin (protoporphyrin IX-Fe^{3+}) supplementation, an analogous compound to heme. Subsequent experiments indicated that depletion of Evi5 impairs vesicle trafficking for iron delivery, and I could demonstrate that it blocks the trafficking and secretion of transferrin proteins. Furthermore, I identified a candidate protein for transferrin receptors in my project, which is absent in *Drosophila*. I established that the transferrin proteins interact with Eps-15, which is a principal component of endocytosis.

I also report here that mutant Evi5 PG cells engulf an extended number of vesicles and electron-dense lysosomes. By conducting further in vivo and ex vivo tests, I was able to show that Evi5 interacts with ferritin heavy chain (Fer1HCH) and with components of endosomal trafficking and autophagy, such as dynamin, Clathrin and Hsc70-4. These findings suggest a novel role for Evi5 in the ferritin autophagy process coupled with iron metabolism during ecdysone synthesis. These findings indicate a novel function for Evi5 in iron homeostasis and heme metabolism that are not reported prior to my study.

1.3.2 Evaluating differential genomic responses to iron deficiency and iron overload.

The principal objective of this project was to perform a high throughput genome-wide study using RNA-Seq and to identify genes that respond to dietary iron. I designed a unique experimental approach and collected brain-ring gland complex (BRGC), gut and whole larval body (WB) samples to elucidate the maximal genomic responses to iron level. By conducting a series of downstream analyses, I identified subsets of unique novel genes and further genes with an already known iron biology function. I could indicate that the Hsp22 and Hsp70 are iron-responsive proteins in the ring gland (RG) that interact with ferritin and Fe-S cluster biogenesis and recipient proteins. Moreover, I identified that chitin biosynthesis is promoted under iron starvation to probably create a physical barrier against pathogens during iron deficiency. Finally, I found candidates for previously unidentified orthologs for ferroportin (FPN1) and ATF2 iron-responsive transcription activator protein via data mining analyses. These findings added new dimensions to our knowledge about the cellular responses to the medium iron manipulations.

1.3.3 Understanding the mechanisms by which Spen regulates ecdysone production

The goal of the last project was to determine the undiscovered functions of the Spen protein. Spen is a member of the Spen protein family that has a dual function in regulating gene expression. It binds to repressor transcription factors and also binds to mRNAs to govern gene expression in the nucleus or post-transcriptionally in the cytosol. Knocking down of Spen in PG cells perturbes the RG morphology, which I refer to here as "malformed" RGs, and reduces the PG cell numbers. The PG-specific loss of *Spen* function further results in larval arrest at the L3 stage. I found that feeding arrested animals with 20E and specific precursors of the ecdysone pathway could rescue the malformed RG phenotype and led to normal adult formation. Additionally, I found evidence that Spen is a regulatory protein downstream of the MAPK/ERK signaling pathway that controls ecdysone biosynthesis, probably at the mRNA level. Expressing a constitutively active form of Ras in the PG cells of arrested animals can improve larval RG morphology and rescue the developmental defects.

1.4 Figures

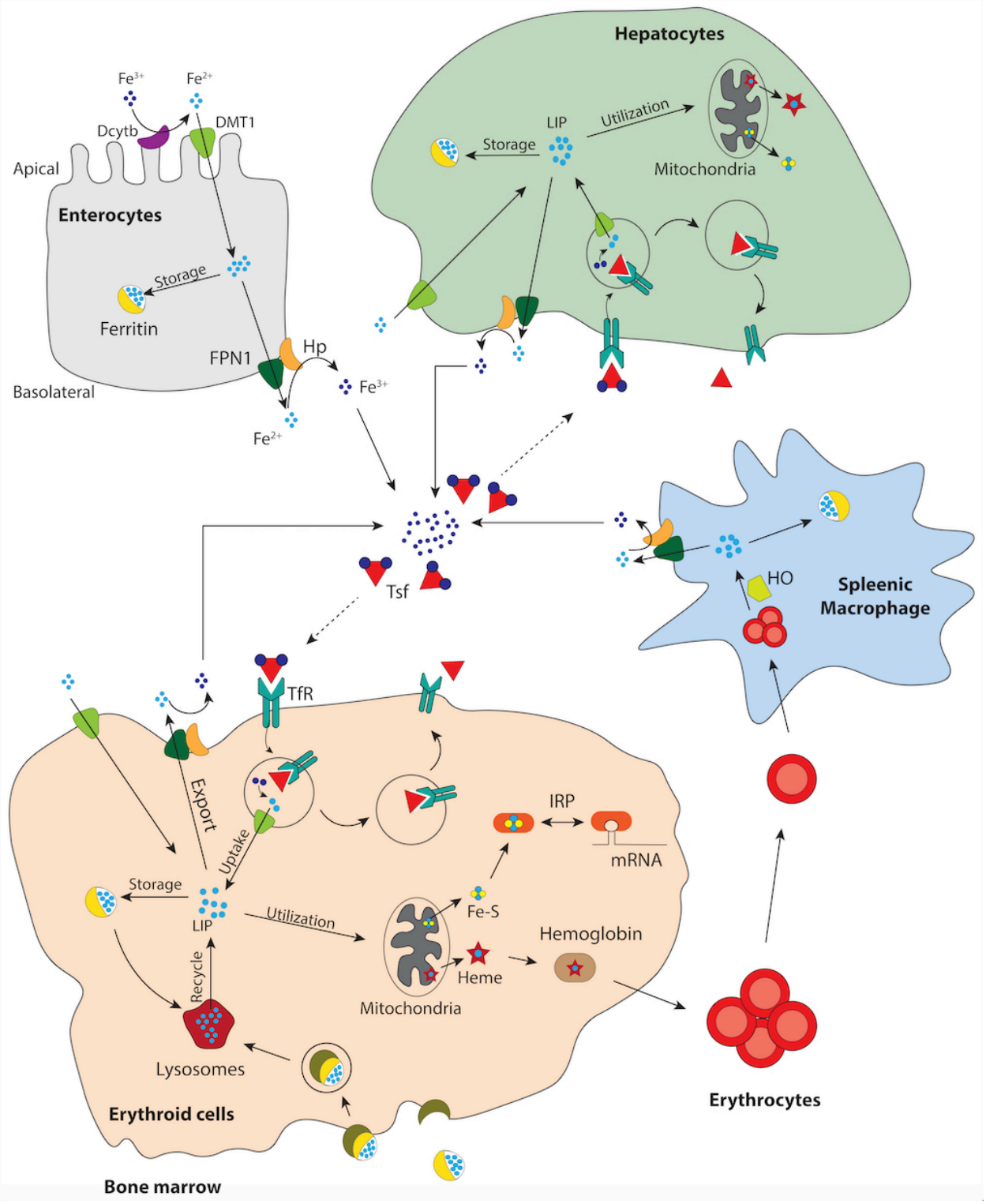
Hepatocytes
Fe3+
Fe2+
Dcytb
DMT1
Apical
Enterocytes
Storage
Ferritin
FPN1
Hp
Basolateral
Fe3+
Fe2+
LIP
Utilization
Storage
Mitochondria
Tsf
HO
Spleenic Macrophage
TfR
Export
Uptake
IRP
mRNA
Storage
LIP
Utilization
Fe-S
Hemoglobin
Heme
Recycle
Mitochondria
Lysosomes
Erythroid cells
Erythrocytes
Bone marrow

Figure 1. 1 Iron trafficking and homeostasis in mammals

In the intestinal lumen's apical site, Fe^{3+} is reduced to Fe^{2+} by duodenal cytochrome b (DCytb) and then is taken up by divalent metal transporter 1 (DMT1) into the enterocytes. Fe^{2+} is either stored in ferritin or exported to the serum by Ferroportin (FPN1). The Hephaestin (Hp) oxidizes the Fe^{2+} into Fe^{3+} at the enterocytes' basolateral site. This is critical for the iron loading of serum transferrin (Tsf). The holoTsf proteins deliver iron to target tissues via the bloodstream upon binding to the transferrin receptor (TfR).

High amounts of iron are used for erythrocyte production in the bone marrow. The labile iron pool (LIP) of the erythroid cells is created via the iron uptake by holoTsf-TfR complex-mediated endocytosis and exocytosis and direct import of iron by iron-importers (DMT1). Serum ferritin is further imported into cells with high demand for iron. Ferritin lysosomal degradation can further add iron to the LIP. Iron is then imported into the mitochondria for heme and Fe-S cluster biosynthesis. The heme and Fe-S clusters are then exported into the cytosol. The Fe-S is used as the cofactor in different proteins such as iron regulatory protein (IRP), but heme is utilized for hemoglobin and erythrocytes synthesis.

Most of the utilized iron is recycled in specialized macrophages in different tissues such as the spleen by heme oxygenase. The recycled iron can be exported into the bloodstream or stored in the ferritin.

Hepatocytes further acquire dietary iron by different proteins such as Tsf and DMT1. Iron is then stored in ferritin or utilized for cellular requirements such as heme and Fe-S cluster biosynthesis.

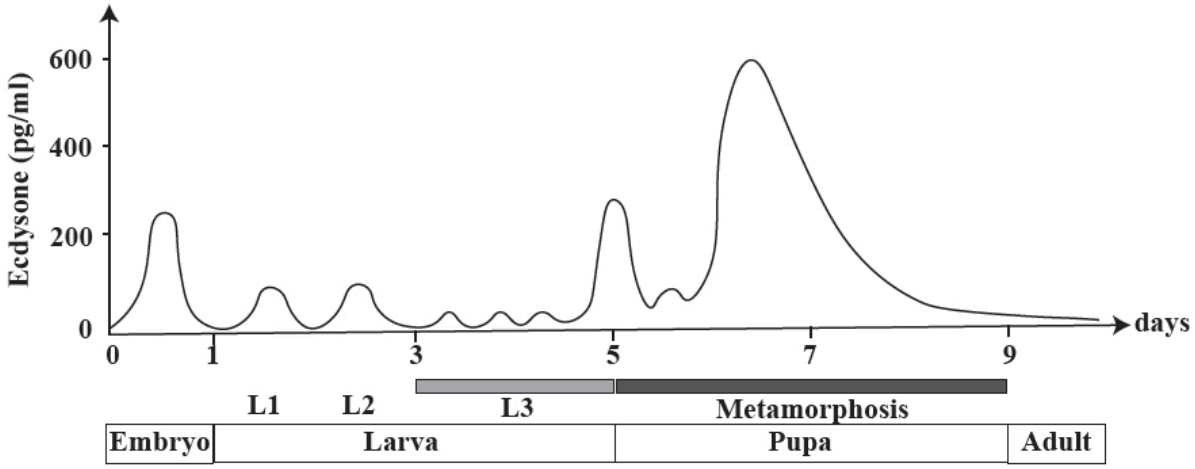

Figure 1. 2 Ecdysone regulates *Drosophila* developmental transition

The *Drosophila* life cycle consists of four distinct stages, including embryonic, larval, pupal and adult stages. The ecdysone (ecdysteroids) have been measured throughout the *Drosophila* life cycle. A pulse of ecdysone governs the duration and onset of the next developmental stage.

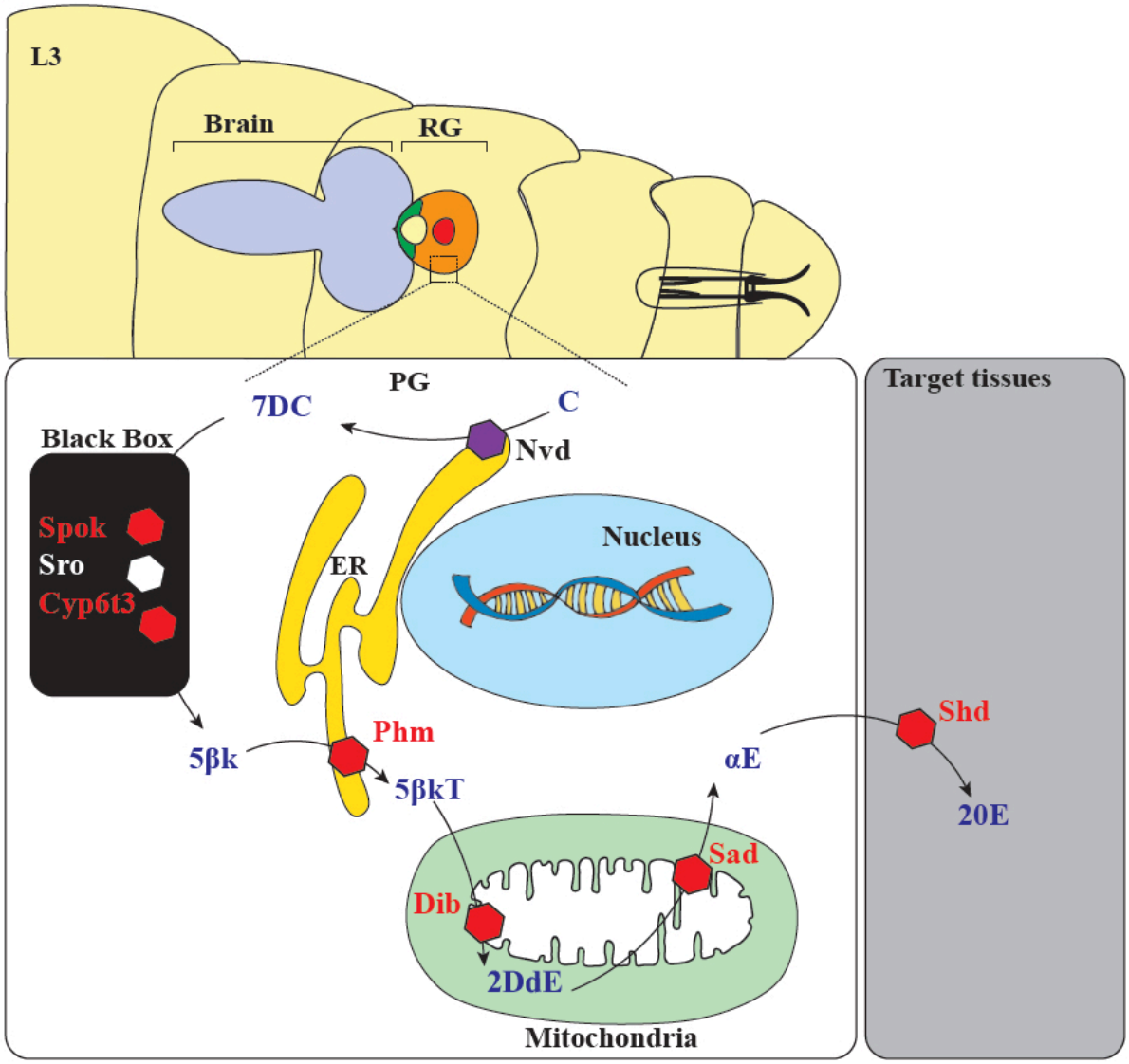

Figure 1. 3 Ecdysone biosynthesis in *Drosophila* Larval stage

At the larval stage (L1, L2, and L3 stages), ecdysone is synthesized in the prothoracic gland (PG) by the Halloween enzymes. The PG is the major part of a tripartite endocrine gland that along with the corpus allatum (CA) and corpus cardiaca (CC) forms the ring gland (RG). In PG cells, the Neverland enzyme (Nvd), which is localized in the ER, converts cholesterol (C) to 7-dehydrocholesterol (7DC). Next, the 5β-ketodiol (5βk) is produced through several unknown steps in the "black box". The black box intermediates and enzymes are not fully characterized yet, but

Spookier (Spok) Shroud (Sro) and Cyp6t3 enzymes are believed to function in the black box. 5βk is converted to 5β-ketotriol (5βkT) in the ER by Phantom (Phm). The 5βkT is then transported into the mitochondria and converted to 2-dexoyecdysone (2DdE) and α-ecdysone (αE) by Disembodied (Dib) and Shadow (Sad). αE is released into the hemolymph and taken up by target tissues. In the target tissues, Shade (Shd) oxidizes αE to produce the active hormone 20-hydroxyecdysone (20E), which regulates numerous biological processes. The Nvd enzyme harbors an Fe-S cluster as the cofactor, and enzymes that are shown in red are cytochrome P450 that contain a prosthetic heme group.

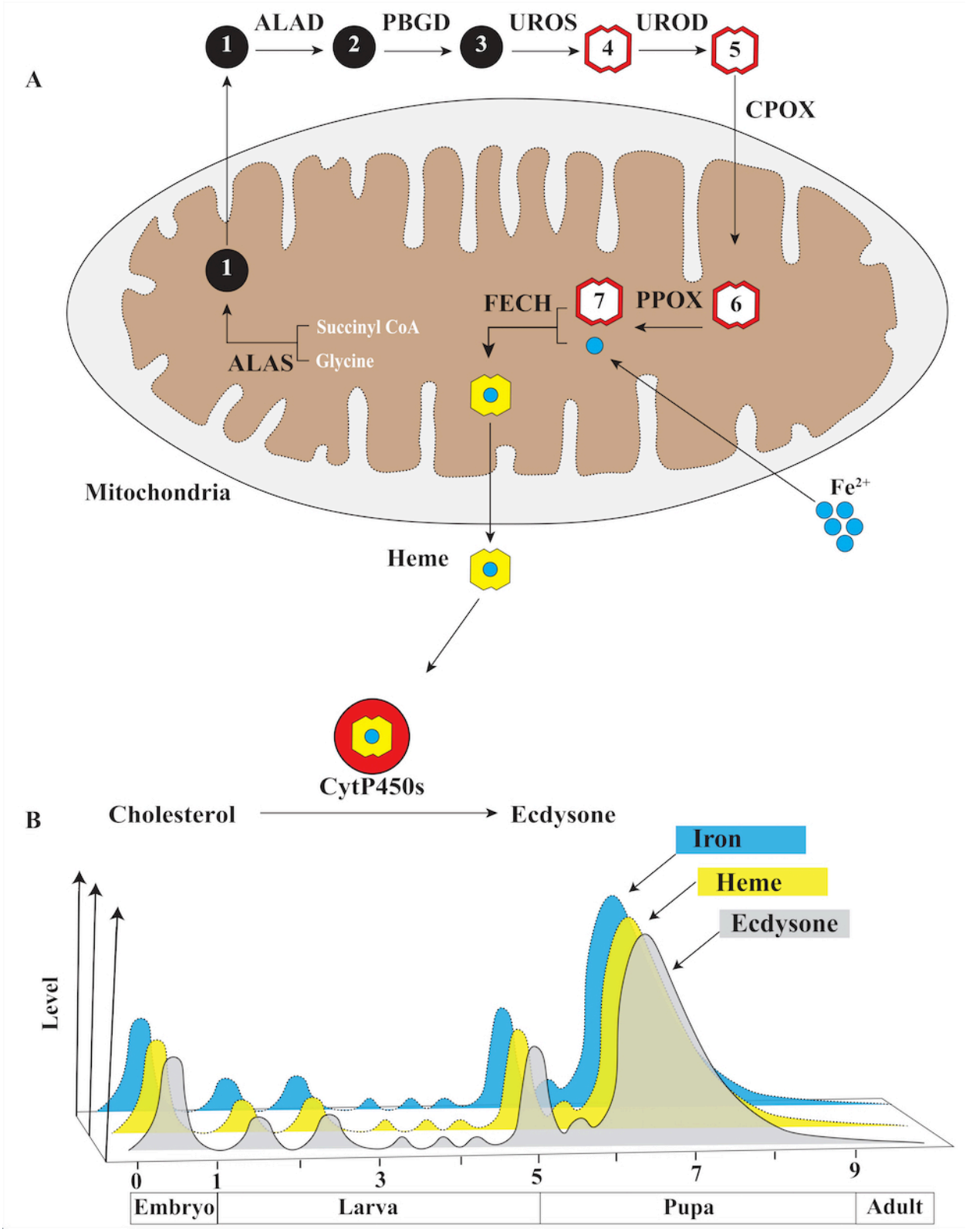
A
1
ALAD
2
PBGD
3
UROS
4
UROD
5
CPOX
1
FECH
7
PPOX
6
Succinyl CoA
ALAS
Glycine
Mitochondria
Fe2+
Heme
CytP450s
B
Cholesterol
Ecdysone
Iron
Heme
Ecdysone
Level
0
1
3
5
7
9
Embryo
Larva
Pupa
Adult

Figure 1. 4 Relationship between Heme biosynthesis, iron mobilization and ecdysone biosynthesis

A) An overview of the conserved heme biosynthesis pathway in mitochondria and the cytoplasm. Aminolevulinate synthase (ALAS) initiates by the formation of the first precursor (ALA) from succinyl CoA and glycine in the mitochondria. The next four steps are carried out in the cytosol to convert precursor one to the tetracyclic porphyrin rings (the red precursors of steps 4 to 7). These ring precursors are shown in red as they are able to autofluoresce red when exposed to UV light or air. Ferrochelatase (FECH) in the last step incorporates a ferrous iron (blue circle) into the last precursor to form heme. Heme is then exported into the cytoplasm and utilized for hemoprotein synthesis, such as P450 enzymes in the PG cells. Other heme enzymes are aminolevulinic acid dehydratase (ALAD), porphobilinogen deaminase (PBGD), uroporphyrinogen III synthase (UROS), uroporphyrinogen decarboxylase (UROD), coproporphyrinogen III oxidase (CPOX) and protoporphyrinogen IX oxidase (PPOX). **B)** Heme and iron are in highly demand in PG cells, since the ecdysone biosynthetic enzymes are present at very high levels. Since excess free iron and heme promote the formation of free radicals that damage the cells, I propose that cellular iron availability (green) and heme production (yellow) are synchronized with ecdysone synthesis (black) throughout the *Drosophila* life cycle.

1.5 Tables

Table 1. 1 Comparison of Iron genes between humans and *Drosophila*.

Human genes	**Function**	**Human disease database[A]**	***Drosophila* Genes**
Duodenal cytochrome b (*DCytb*)	Ferric reductase	Hemochromatosis, Type 1, Siderosis	*CG1275*
Divalent metal transporter 1 (*DMT1*)	Ferrous iron importer	Frontotemporal Dementia, Hemosiderosis	Malvolio (mvl)
Ferroportin (*FPN1*)	Ferrous iron exporter	Ulcerative Colitis, Neuroblastoma	*UN[B]*
Hephaestin (*Hp*)	Ferroxidase	Hemosiderosis, Rare Hereditary Hemochromatosis,	*MCO1, MCO3*
Ferritin heavy chain (*FTH1*)	Ferritin subunit, Iron storage	Hemochromatosis, Type 5, Retinitis Pigmentosa	*Fer1HCH*
Ferritin light chain (*FTL1*)	Ferritin subunit, Iron storage	Huntington Disease	*Fer2LCH*
Mitochondrial ferritin (*FTMT*)	Mitochondrial iron storage and metabolism	Myelodysplastic Syndrome, Friedreich Ataxia	*Fer3HCH*
Serum Transferrin (*Tf*)	Ferric iron transporter	Atransferrinemia, Iron Deficiency Anemia	*Tsf1*
Melanotransferrin (*MELTF*)	Ferric iron transporter	Melanoma, Alzheimer Disease	*Tsf2*

Transferrin receptor 1 (*TfR1*)	Transferrin receptor binding, iron uptake	Hemosiderosis, Rare Hereditary Hemochromatosis	*UN*
Transferrin receptor 2 (*TfR2*)	Transferrin receptor binding, iron sensor	Hemochromatosis, Type 3 Hemochromatosis, Type 1	*UN*
Iron regulatory protein 1 (*IRP1*)	Aconitase enzyme, iron homeostasis	Polycythemia Huntington Disease	*IRP1A*
Iron regulatory protein 2 (*IRP2*)	Iron homeostasis	Lung Cancer Hemosiderosis	*IRP1B*

[A] The top two disorders in the Malacards human disease database [150].

[B] UN: Unidentified

Table 1. 2 Porphyria types and comparison of heme biosynthetic genes between humans and *Drosophila*.

Human genes	**Enzyme product**	**Porphyria type**	**Prevalence[A]**	***Drosophila* genes**
ALAS1 *ALAS2*	Aminolevulinic acid (ALA)	X-linked protoporphyria	Unknown	*ALAS*
ALAD	Porphobilinogen (PBG)	ALA dehydratase deficiency	7.2	*Pbgs*
HMBS	Hydroxymethylbilane	acute intermittent porphyria	0.33	*l(3)02640*
UROS	Uroporphyrinogen III (UROIII)	congenital erythropoietic porphyria	40	*Uros1* *Uros2*
UROD	Coproporphyrinogen III	Porphyria cutanea tarda	1	*Urod (updo)*
CPOX	Protoporphyrinogen IX	Hereditary coproporphyria	3.2	*Coprox*
PPOX	Protoporphyrin IX	Variegate porphyria	9.2	*Ppox*
FECH	Heme	Erythropoietic protoporphyria	Unknown	*FeCH*

[A] Prevalence of symptomatic porphyria per million [99]

Chapter 2 Materials and methods

This Chapter includes the experimental and computational approaches that have been used in my study.

2.1 *Drosophila* Flies maintenance and husbandry

A list of fly strains that have been used in my study is provided in Table 2.1. All fly stocks were reared on a standard corn-based media for general maintenance. Two backup vials were kept at 18°C, and they were transferred into new food every four weeks. The active stocks were maintained at 25°C and 70% humidity in a walk-in incubation chamber. For expanding the population, flies were transferred into bottles.

For conducting all experiments, "Nutri-Fly" media (Genesee Scientific, Cat. # 66113) was used and prepared based on a standard recommended recipe from the Bloomington *Drosophila* Stock Center (https://bdsc.indiana.edu/information/recipes/bloomfood.html). Overall, for one liter of food, 186 grams of food powder was added to 1 liter of autoclaved milli-Q water and boiled on a heater for 5 minutes. When the mixture is cooled down (approximately 50°C, 4.5 ml of propionic acid (Sigma, Cat. # P1368) was added. The required compounds for experimental foods were added to the mixture at this step with the desired concentrations (see next section). Then, approximately 5 ml of prepared food was poured off into the vials or 50 ml was added into bottles. For crossing and maintaining the flies, 8-10 flies in each vial and 80-100 flies in each bottle, with a 1:1 ratio for male and female flies, were kept.

For experiments where fly eggs/embryos were required, grape-juice agar plates were prepared according to the Cold Spring Harbor Protocols and stored at 4°C (http://cshprotocols.cshlp.org/content/2007/9/pdb.rec11113.full). In brief, to prepare 1 liter of solution, 30 grams agar, 300 ml grape juice concentrate, 10 ml ethanol, and 0.5 g methylparaben was added to 700 ml autoclaved milli-Q water. The mixture was autoclaved and added to 35mm x 10mm sterile plastic Petri dishes to be solidified. To collect eggs, first, flies were allowed to lay eggs on agar plates three times with a 1-hour interval and plates discarded to remove old embryos and non-fertilized eggs. For each vial, 50 embryos were collected and rinsed thoroughly with 1X PBS and then transferred gently to fly media/vials.

The prepared media were kept in plastic bags at room temperature (RT, 22°C) for a short time of storage (1 week). However, a 4°C fridge was used to store foods for extended periods (6 weeks). Three biological repeats were used for the entire experiment.

2.2 *Drosophila* food analysis for developmental and survival studies

The desired compounds with proper concentrations (listed in Table 2.2) were added to the standard Nutri-Fly food to conduct media analysis. In addition, the supplements of each compound (ethanol and NaOH) were added to the media to create control foods.

For developmental analysis, control and experimental were first set. Then, 50 embryos of control and experimental crosses were transferred to a freshly made food to analyze flies' developmental progression. Vials were checked carefully from the beginning of metamorphosis (three days after egg collection) to the eclosion time in an 8-hours interval. The number of pupae in each vial were then counted. Finally, each genotype was compared with the control flies by graphing the observed data (amount of time) in Microsoft Excel (Version 16.44).

Similarly, the survival experiments were done by transferring 50 embryos to each vial and counting the number of 3rd instar larvae, pupae and adult flies. A black filter paper (AHLSTROM, Cat. # 8613-0900) was placed in a 15 mm petri dish. Then, 1 ml of 1X PBS was added to wet the filter paper. Next, media with crawling L3 larvae were transferred on the filter paper. Animals were counted while they were transferred into new food gently.

All scores were curved in Microsoft Excel. Furthermore, all experiments were conducted with three biological replicates. All vials and cages were kept in 25°C.

2.3 Schneider 2 (S2) cells culturing and Transfecting

S2 cells were grown in the 25 ml flask with Schneider's *Drosophila* medium (Sigma, Cat. # S0146-6X500ML) containing 10% heat-inactivated FBS (Thermo Scientific, Cat. # A4766801) and 1 % Penicillin-Streptomycin (Sigma, Cat. # P4333-100ML). Flasks were maintained in a 28°C incubator. When cell cultures had a final density of 2 to 4 x 10^6 cells/ml were transferred into a complete fresh medium (with a ratio of 1:4). Cells were then stained with Trypan blue dye (Abcam, Cat.# ab233465) to measure the cell density [102]. Cells were mixed with Trypan blue stain with a 1:1 ratio and 10 ul of mixture added to a hemocytometer. The total number of stained (viable) and unstained (non-viable) cells were counted and normalized to 1 ml cells (calculated number multiply to 2 and 100). The density of the cells was calculated by measuring the percentage of viable cells. Staining was repeated 10 times, and the average number of cells was used for the final calculation.

Cells transfection was carried out with the calcium phosphate transfection method from the Invitrogen Life Technologies company (Cat. # R690-07). In brief, 3 x 10^6 cells were seeded in the 6-well plates and incubated at 28°C overnight. To transfect each well to a microcentrifuge tube: 36 µl 2 M CaCl2, 15 µg desired plasmid (See Table 2.3 for the plasmid list) and cell culture sterile water to a final volume of 300 µl. Next, 300 µl of 2X HEPES-Buffered Saline (Sigma Cat. # 51558-50ML, 50 mM HEPES, 1.5 mM Na2HPO4, 280 mM NaCl, pH 7.1) were added to the microcentrifuge tube and incubated for 30 min at RT. The transfecting solution was then added to the plate wells dropwise and plates incubated at 28°C for 24 hours. Cells were collected, centrifuged (4000 rpm, 4°C, 5 min) and washed 2X with the complete fresh medium to remove the calcium phosphate solution. Transfected cells were then incubated in the 28°C incubator for 48 hours for Western blot, Mass spectrometry and co-immunoprecipitation assay.

For cell immunostaining, a clean heat-sterilized coverslip was placed into each well of the plate when the old medium was removed. Transfected cells on coverslip then were incubated in the 28°C incubator for 48 hours.

2.4 S2 cells constructs for transfection

To generate plasmid construct for S2 cell transfection, pAc5-STABLE2-neo (Addgene, Catalog # 32426), pAFW-3XFLAG (Addgene) and pAMW-5XMyc were used (Addgene). The full-length cDNAs of all interested genes (Table 2.4) were ordered from DGRC (*Drosophila* Genomics Resource Center, https://dgrc.bio.indiana.edu/Home). All cDNA fragments were first amplified and cloned into a small plasmid backbone with an Ori and AmpR gene. All clones were sequenced prior to use for any experiments. These clones were further used for other purposes such as site-directed mutagenesis, adding C-terminus 3X FLAG, 5X MYC, eGFP or mCherry and removing signal peptides.

For single transfection, cDNAs were amplified and cloned into pAFW-3XFLAG and pAMW-5XMyc via the Gibson assembly master mix (New England Biolabs Inc. Cat. # E2611) according to the manufacturer's instruction. The backbone of pAFW-3XFLAG plasmid without FLAG tags was further amplified and used for creating constructs with cDNA-eGFP and cDNA-mCherry.

For co-transfection constructs, two strategies were used. First, a mix of two constructs of cDNAs with different epitope tags was made based on transfection protocol DNA requirement (See S2

cells culturing and transfecting section). Second, in a small plasmid backbone, two cDNAs with different C-terminus tags were cloned, then a sequence of the T2A viral peptide [103] was added to the middle of two genes in frame. Finally, the whole fragments that include two tagged cDNAs and T2A were amplified and cloned into the digested pAc5-STABLE2-neo plasmid with KpnI (Thermo Scientific™, Cat. # FERFD0524) and BamHI (Thermo Scientific™, Cat. # FD0054) restriction enzymes.

All plasmid and primes are listed in Table 2.3 and table 2.10, respectively. The Q5 High-Fidelity DNA Polymerase (New England Biolabs Inc. Catalog No. M0491S) was used for all PCR amplification.

2.5 S2 cell immunostaining and imaging

As described in the S2 cell culture and transfection section, cells were allowed to adhere to a coverslip for 48 hours. Coverslips were then placed into a clean transfection plate, and cells were fixed with the fixative buffer for 20 minutes. The fixation buffer was replaced with PBST by gentle pipetting. This step was repeated three times. Cells then were incubated with blocking solution (1X PBST with 5% goat serum) for 30 min and washed with PBST (1X PBS with 0.1% Triton, Sigma Cat. # T9284) five times with gentle pipetting. Next, the primary antibody solution (antibody in 1X PBST with 1% BSA) was added to the samples for 4 hours at 4°C. The primary antibody was washed away with PBST for 5X. Then, cells were incubated with a secondary antibody solution for 1 hour at RT. Samples were then washed with PBST three times and mounted in VECTASHIELD mounting medium (DAPI containing mounting medium, Cell signaling Cat. # 4083). Finally, all images were taken with Nikon C2si Confocal Microscope. All antibodies are listed in Table 2.6.

2.6 Tissue immunostaining

The control and experimental flies were raised at 25°C in the proper media to collect tissues for immunostaining. Next, larvae were carefully staged until they molted from 2nd to 3rd instar larvae (L2 to L3 molt). Then the newly molted L3 larvae were collected and transferred to new vials of corresponding media. At 40 to 44 hours after L2/L3 molt, the Brain-Ring Gland Complexes (BRGC) and Whole Gut (WG) larval tissues were dissected in 1X ice-cold PBS buffer. Samples were then fixed in the fixative buffer (1X PBS with 4% formaldehyde) for 30 minutes and followed by washing in PBST (1X PBS with 0.1% Triton, Sigma Cat. # T9284) for 3X 15

minute on a rocking shaker at RT. Samples were then blocked for 1 hour in blocking solution (1X PBST with 5% goat serum) and washed 3X in PBST for 15 min each at RT. Samples were next incubated with the primary antibody solution (the manufacturer recommended concentration of antibody in 1X PBST with 1% BSA) overnight at 4°C on a rocking shaker. The following day, samples were washed 3X in BPST and incubated with the secondary antibody for 1 hour at RT. Samples were then washed three more times in PBST and mounted in VECTASHIELD mounting medium (DAPI counting mounting medium, Cell signaling #4083).

A Nikon C2si Confocal Microscope was used to view the samples and take confocal and brightfield images. For the list of antibodies and concentrations that are used, please see Table 2.6.

2.7 Red autofluorescence imaging

The Brain-Ring gland complexes (BRGC) of 40 to 44 hours L3 larvae from control and experimental animals were dissected in 1X ice-cold PBS buffer. Samples were mounted in the mounting medium (VECTASHIELD) immediately. Slides were viewed with UV light (Lumen Dynamics, X-Cite SERIES 120Q) or red laser channel in the Nikon C2si Confocal Microscope.

2.8 Prussian blue iron staining

For Ferric iron staining, the whole gut samples from carefully staged 3rd instar larvae (40 to 44 hours after L2 to L3 molt) were dissected in 1X PBS and then fixed in the fixative buffer (1X PBS with 4% formaldehyde) for 30 min on a rocking shaker at RT. Following three times washes with PBS for 15 min each time, the gut samples were then incubated in 1X PBST for 20 min. Next, samples were treated with Prussian blue stain solution that contains 2% $K4Fe(CN)_6$ (Sigma Cat. # P9387-100G) and 2% HCl for 45 min in the dark at RT. Samples were then washed three times with PBST and mounted in the mounting medium (50% glycerol in 1X PBS, no DAPI dye) on glass slides. A LEICA DFC500 camera and a regular dissecting microscope were used to take images. All pictures were saved in Tagged Image Format (Tiff), and final figures were made in Adobe Photoshop and Adobe Illustrator.

2.9 Transmission Electron Microscopy

The Brain-Ring gland complexes (BRGC) of 40 to 44 hours L3 larvae from control and experimental animals were dissected in 1X ice-cold PBS buffer. The dissected BRGCs were fixed overnight in the TEM fixative buffer (2.5% glutaraldehyde, 2% paraformaldehyde and 1X PBS).

The samples were then washed three times with TEM wash buffer (0.1 M PBS) for 15 min each time. Next, they were incubated in a Post-Fixative buffer (1 % osmium tetroxide in 0.1 M PBS) for one hour, followed by three times wash with 0.1M PBS. Samples were then dehydrated through a graded ethanol series as follows: 50% ethanol, 70% ethanol, 90% ethanol, 100% ethanol, 100% ethanol, 100% ethanol, for 15 to 25 min in each solution. After dehydration, samples were infiltrated in 50% super resin for 3 hours. The 50% super resin was replaced with a fresh solution every one hour. Next, samples were incubated in pure super Resin (100% super resin) overnight. The next day, the pure super resin was washed twice (~every 5 hours) with a fresh solution. The BRGC samples were embedded in flat molds with fresh super resin the following day. Samples were then aligned and placed at the desired angle for cross-sectioning in the molds using an injecting needle. The molds were placed in an oven at 70 °C for an overnight. The solidified molds were then submitted to the microscopy facility at the University of Alberta (Microscopy Unit; Room CW225; Biological Sciences Bldg.).

In brief, the solidified molds were subjected to sectioning via Reichert-Jung Ultracut_E Ultramicrotome. Sections with 70 to 90 nm thickness were prepared and collected into the TEM grids. The grids were stained with Uranyl Acetate and then Lead Citrate stain by placing them on a dye drop. Lastly, the grids were washed with distilled water and used for imaging with a Transmission Electron Microscope at 80 kV accelerating voltage (Philips FEI, Model = Morgagni 268).

2.10 High-voltage Transmission Electron Microscopy

The uranyl acetate-stained girds were prepared for the TEM microscopy by coating the girds with a carbon layer. The carbon coating was performed by the Leica ACE 600 coater. Both sides of the girds were coated with 5 nm carbon. The thickness of coating is monitored by quartz microbalance. The High-voltage TEM images were taken with a JEOL JEM-ARM200CF S/TEM electron microscope at an accelerating voltage of 200 kV. All images were taken at the microscopy facility at the University of Alberta (Microscopy Unit; Room W1-060 ECERF; nanoFAB Bldg.).

2.9 Genomic DNA and plasmid extraction

DNAzol reagent from ThermoFisher scientific company (Cat # 10503027) was used to isolate genomic DNA. The manufacturer's instruction was conducted without any manipulation and change. To start, 50 young (1-2 days after eclosion) adult flies (approximately 150-200 mg

sample) were used as the input sample. Flies were first anesthetized with CO2 gas and brushed into a 1.5 ml tube. Then tubes were placed into the liquid nitrogen, and a cold pestle (VWR™ pellet electronic mixer) was used to grind and powder the samples. This step was repeated three times, and homogenized powder samples were used as the input for genomic DNA purification by DNAzol reagent. In the last step, 8 mM NaOH was used to dissolve the DNA pellet. Samples were snap-frozen with liquid nitrogen and stored at a -20°C freezer.

Next, two different kits were used to isolate plasmid from bacteria following the manufacturer's instruction. GeneJET Plasmid Miniprep Kit (ThermoFisher Scientific, Cat. # K0503) was used to extract plasmid for regular cloning. All steps were done according to the protocol recommended by the manufacturer. However, to purify plasmids with a larger quantity and a higher quality, the QIAGEN Plasmid Midiprep kit (QIAGEN, Cat. # 10043) was used following as recommended by the QIAGEN company. A starter culture was first created by inoculating a single colony of transformed DH5α *E. coli* bacteria into 5 ml LB medium with the proper antibiotic depending on the desired plasmid (75-100 mg Ampicillin or 100 mg Chloramphenicol). The culture was incubated for 8 hours in 37°C, and then 200 µl of starter culture was added to 100 ml of fresh LB medium. Approximately 5-10 µg DNA was extracted from each reaction. The Midiprep extracted DNAs were used for S2 cell transfection and embryo injection.

A Nanodrop Spectrophotometer was used to evaluate the quality and quantity of all DNA samples. The genomic DNA samples were further checked by agarose gel electrophoresis (1% gel, 45 min, 100 V).

2.10 Transgenic *Evi5* and *transferrin* lines

Plasmids containing full-length cDNAs (Gold cDNAs collection) of Evi5 (MIP13464), Tsf1 (LP08340), Tsf2 (LD22449) and Tsf3 (FI03676) were ordered from the DGRC Center (https://dgrc.bio.indiana.edu/Home). All cDNAs were amplified and cloned into a small plasmid backbone with Ori and AmpR gene. All clones were then submitted for Sanger-sequencing by designing a set of sequencing-primers. The sequences were then compared and aligned against cDNA sequences of interesting genes in the Flybase database (http://flybase.org). After confirming all sequences, site-directed mutagenesis was used to add mVenus (Evi5-mVenus) and 3X FLAG (Tsf1-3XFLAG, Tsf2-3XFLAG and Tsf3-3XFLAG) tag to the C-terminus. The Sanger-

sequencing was carried out to ensure that all tags were in frame. Next, all tagged cDNAs were cloned into the pBID-UASC-FG (Addgene, Cat. # 35201) plasmid.

The pBID-UASC-FG is designed for the gateway cloning system and carries attR1 and attR2 sequences [104]. It also has the mini-white gene for selecting transgenic flies after embryo injection. Furthermore, the pBID-UASC-FG plasmid harbors the synthetic DSCP promoter, which consists of 10 UAS binding sites for targeted expression of desired genes by the UAS/GAL4 system [104]. The plasmid also has a gypsy insulator sequence conjunction with a phiC31 integrase compatible *attB* sequence used for site-directed insertion of transgene onto the flies' chromosomes by the phiC31 system [104].

Two pairs of primers were designed to amplify two fragments (approximately 5 kb and 2.5 kb), which include all parts of the plasmid except the attR1 and attR2 and region between them (the Gateway cloning cassette). Tagged cDNAs were then fused to these two fragments with the Gibson assembly system (New England Biolabs Inc. Catalog No. E2611). In Gibson reactions, a 1:1:3 ratio was used for Backbone Fragment1 to Backbone Fragment1 to tag cDNAs. All reactions were 15 µl and performed in a regular thermocycler at 50°C overnight. 5 µl of each reaction was used to transform competent DH5α *E. coli* bacteria according to the Gold Spring Harbor protocol (http://cshprotocols.cshlp.org/content/2006/1/pdb.prot3932.full). In brief, 10 pg-10 ng plasmid was added to 50 ml cells and incubated on ice for 30min. Cells were heat-shocked in 42°C water bath for 45 sec and placed on ice for 2-3 min. Next, one ml pre-warmed LB added to cells and incubated on a shaker incubator at 37°C, 200 rpm for one hour. Approximately, 50-75 µl of transformed cells were then plated on proper screening plates with a desired antibiotic,. Final plasmids were sequenced and used for embryo injection (See embryo injection section). The list of flies and primers used for injection is presented in Table 2.1 and Table 2.9, respectively.

2.11 Generating conditional mutant $Evi5^{FRT}$ line via CRISPR/Cas9

The main objective of this experiment was to apply HDR-CRISPR to knock-in a C-terminal FLAG-tag and flank the endogenous Evi5 locus with FRT sequences. pHD-DsRed-attP plasmid (Addgene, Cat # 51019) was used. The final plasmid was created in three steps. First, the *evi5* locus was cloned upstream of the DsRed gene into the pHD-DsRed-attP plasmid. Next, two DNA fragments with an approximate size of 1 kb were selected as homology arms as a template for the homology-directed repair process. The homology arm fragments were amplified from the outside

of the *evi5* locus (downstream of left gRNA and upstream of right gRNA) and cloned into the plasmid with the same order as genomic loci. Finally, two FRT sequences were added between homology arms and *evi5* locus and then a sequence encoding a 3X FLAG tag was added to the corresponding C-terminus site of *evi5*. The site-directed mutagenesis strategy was used to add FRT and FLAG sequences. The list of designed primers is shown in Table 2.8.

All cloned DNA fragments were amplified using the genomic DNA of fly lines that were used for injection (vasa-Cas9 strain, #51323, Table 2.1). The Gibson assembly master mix (New England Biolabs Inc. Catalog No. E2611) was used for fusing DNA fragments into the final construct. In the Gibson reactions, a 1:3 ratio was used for DNA to Backbone ratio, and all reactions were performed in a regular thermocycler for 4 hours at 50°C. The total volume of each Gibson reaction was 15 µl, and 5 µl was used for bacterial transformation. All plasmids were transformed and propagated in competent DH5α *E. coli* bacteria strain following the Gold Spring Harbor protocols (see transformation protocol in section 2.10, http://cshprotocols.cshlp.org/content/2006/1/pdb.prot3932.full). Sanger-sequencing and restriction enzyme digestion were performed to confirm the generated plasmids. Genomic DNA and plasmids were extracted as described in the genomic DNA and plasmid extraction section.

2.12 gRNA design and cloning for Evi5^{FRT} line

To design gRNAs for the Evi5^{FRT} line, first, target regions were obtained from the Flybase database and submitted to an online gRNA finder called CRISPR Optimal Target finder [105] (http://targetfinder.flycrispr.neuro.brown.edu). All program parameters were unchanged, and "*Drosophila Melanogaster* (Reference genome r_6)" was selected as the desired genome. All selected gRNAs were then confirmed by sequencing the genomic loci of fly lines that were used for injecting the final constructs.

To create gRNA constructs, first, a pair of primers (Table 2.8) that contains both forward and reverse gRNAs were designed and used to amplify the gRNA scaffold of pCFD5 plasmid (Addgene, Cat # 73914). Amplified fragments were then purified and fused to digested pCFD5 plasmid with BbsI restriction enzyme (Thermo Scientific™, Cat. # FD1014). Final constructs were sequence-verified before being used for embryo injection. All PCR reactions were performed with Q5 High-Fidelity DNA Polymerase (New England Biolabs Inc. Cat. # M0491S), and the Gibson

assembly master mix (New England Biolabs Inc. Catalog No. E2611) was used to fuse DNA fragments.

2.13 RNA extraction

RNA samples were collected from carefully staged L3 larvae at the desired time points, mainly at 4, 8, 12, 16 and 44 hours after the L2/L3 molt. RNA samples were extracted from ring glands, BRGC samples, L3 larval guts and whole L3 larval bodies. All samples were collected in triplicate. Ice-cold 1X PBS was used to dissect larvae and samples were collected, and transferred into 250 µl TRIzol (Invitrogen) on ice. Once all samples were collected, they were either flash-frozen and stored in a -80 °C freezer, or they were used to extract RNA immediately.

For small tissues such as RG and BRGC, the RNeasy Mini kit (Qiagen, Ref. #74104) was used according to the manufacturer's instructions. However, at the last step, 20-30 µl RNAse-free water (Ambion DEPC-Treated Water, Cat. #AM9906) was used to elute RNA. On the other hand, the RNA of whole larval body and gut samples was extracted with a TRIzol-based RNA extraction method. First, 150 mg (approximately five L3 larvae and 15 L3 gut samples) samples were transferred in a 1.5 ml microcentrifuge tube with 200 µl TRIzol. Samples were homogenized with pestles presoaked in 1% SDS for 15 sec. TRIzol volume was scaled up to 1 ml, and samples were vortexed and incubated on ice for 5 min. Next, 200 µl chloroform was added, and samples were shaken vigorously for 15 sec and incubated at RT for 3 min. Tubes were centrifuged for 15 min at 4°C with 12,000 rpm, and then the upper colorless aqueous phase was transferred into a new tube carefully. To each tube, 500 µl isopropanol was added, and then they were inverted five times and centrifuged for 15 min at 4°C at 12,000 rpm. The supernatant was removed and pellets were washed with 1 ml of 70% ethanol. Next, pellets were air-dried for 5 min and dissolved in 120 µl RNAse free water (Ambion, Cat. #AM9906). 200 µl chloroform was added to samples, and they were vortexed for 15 sec and were incubated at RT for 3 min. Tubes then were centrifuged for15 min at 4˚C with 12,000 rpm, and the upper aqueous phase was transferred into a new tube carefully. In the next step, 10 µl 8 M LiCl was added to tubes, and then 300 µl 100% ethanol was added, and tubes were placed on ice for 15 minutes. Finally, tubes were centrifuged (25 min, 0°C, 15000 rpm), and RNA pellets were washed, air-dried and were dissolved in 30-50 µl RNAse free water.

All samples were collected in triplicate, and they were flash-frozen in liquid nitrogen and stored at -80 °C freezer or used for generating cDNA. The quantity of all RNA samples was

measured using Qubit 2.0 Fluorometer (Invitrogen) and its Qubit RNA HS Assay Kit (Invitrogen, Cat. #Q32852). RNA integrity and quality were analyzed with Agilent 2100 Bioanalyzer on an Agilent RNA 6000 Nanochip (RNA 6000 Nano Kit).

2.14 cDNA synthesis for qPCR and RNA-sequencing

To synthesize cDNAs, the ABI High-Capacity cDNA Synthesis Kit was used (Applied Biosystems, Cat. #4368813) according to the manufacturer's protocol. 1 µg of RNA samples was used for each reaction (total RNA volume 10 µl). Based on the number of samples, a master mix (9 µl per each reaction) from 10X reverse transcriptase buffer (2 µl), 100 µM 25X dNTP mix (0.8 µl), 10x random primers (2 µl), and PCR-grade water (4.2 µl) was made and scaled up. Then, 9 µl of the master mix was added to a 0.2 ml PCR tube that contains RNA samples (RNA plus water amounted to 10 µl). Finally, the reverse transcriptase enzyme was added to each reaction tube and placed in a thermal cycler. The thermal cycler was set for 25°C for 10 min, 37°C for 120 min, 85°C for 5 sec, and hold at 4°C. cDNA samples were then diluted with a 1:20 ratio and either used for qPCR or stored at -20°C. Each biological sample was collected three times, and cDNA samples were created in triplicate.

2.15 Quantitative real-time PCR (qPCR) analysis

A list of used primers is presented in Table 2.7. Primers were first designed by an online tool from the Roche Life Science (Universal Probelibrary Assay Center, https://qpcr.probefinder.com/roche3.html). Primers were specific to *Drosophila* genes, and all transcript variants of desired genes were selected for the final design of primers. The primers' lengths were between 18-22 bp, and amplicon sizes were from 75 bp to 150 bp. Designed primers were then ordered from Integrated DNA Technologies (IDT), validated and compared to an endogenous housekeeping gene (rp49).

qPCR reactions were conducted via the SYBR Green qPCR Master Mix (Kapa Biosystems, KK4601) to validate the designed primers. The cDNA from control flies was diluted five times with a 1:4 ratio, and 2.5 µl of each dilution was added to a 0.2 ml PCR tube. Then 5 µl master mix and 2.5 µl primer mix (of 3.2 µM) was added to each tube, and QuantStudio 6 Flex Real-time PCR system from Applied Biosystems was used to run the reaction. Amplicon plot, melting curve and a relative standard curve of all primers were evaluated relative to rp49 primer.

A similar reaction to the primer validation was set to analyze a genes' relative expression (2.5 µl cDNA, 5 µl master mix and 2.5 µl primer mix). However, the cDNA samples were diluted 1:20 (see the cDNA synthesis section), and a comparative Ct (ΔΔCt) quantification program was used to run and analyze the samples. All gene expressions were normalized to the rp49 expression, and the ΔΔCt method with a confidence interval (alpha = 0.05) was used to plot expression fold changes. Each sample was evaluated with three biological samples, each in tested in triplicate. All fold change analyses were done in Microsoft Excel 365 (Version 16.44). A two-tailed unpaired Student *t*-test (P-value less than 0.05) was performed to determine statistically significant differences between data.

2.16 Iron RNA-sequencing (RNA-seq)

Samples of RNA-seq were collected by rearing the control animals (w^{1118}) on BPS supplemented medium for five generations (see "food analysis for developmental and survival studies" section). The 6th generation was carefully staged on BPS-supplemented food until the larvae reached the L2/L3 molt stage. Next, larvae were placed onto BPS-supplemented food and FAC-supplemented food (iron-supplemented). At 4, 8, 12 and 16 hours after L2/L3 molt, BRGC, whole gut and whole larval body samples were collected in duplicate (in total, 48 samples were collected). For BRGC and whole gut samples, animals were first dissected in ice-cold 1X PBS and then collected in a centrifuge 1.5 ml tube. RNA samples were isolated, evaluated and converted to cDNA as described in the RNA extraction and cDNA synthesis sections. 100 ng of RNA (total concentration) of each sample was used for generating sequencing libraries.

The Ovation *Drosophila* RNA-seq system 1-16 kit (Nugen, Cat. # 0350-32) was used to generate strand-specific RNA libraries for sequencing via the Illumina sequencing platform (ILLUMINA NOVASEQ 6000). All steps were performed as described in the kit manual. All PCR reactions were carried out in a regular thermal cycler (Eppendorf EP 384 thermal cycler). cDNA samples were fragmented with sonication and a Covaris S-Series System sonicator (Duty cycle 10%, intensity 5, cycles 200, time 180 sec, temperature, 6°C and sample volume 120 µl). Once the library construction was finished, an Agilent High Sensitivity DNA 1000 Kit (Agilent, Cat.# 5067-4626) was used to evaluate the libraries' quality on Bioanalyzer. 100 ng of high-quality libraries were prepared in 25 µl nuclease-free water and submitted to Delta Genomics company (http://www.deltagenomics.com/). Samples were then sent to the Genome Quebec Innovation

Center (https://www.mcgillgenomecentre.ca) to sequence on an Illumina Hi-Seq 2500 Sequencing System. Sequencing data was downloaded and analyzed as described in the next section (Project URL: https://genomequebec.mcgill.ca/nanuqMPS/project/ProjectPage/projectId/15439, Technology: HiSeq, Run: 4487, Libraries Order#:CCI013340, SCI020928).

2.17 Computational analysis of RNA-seq data.

The raw sequencing data were first obtained from the Genome Quebec Innovation Center website (http://www.genomequebec.com/en/innovation-center/) in a plaintext format FastQ format. The FastQ files were next tested with an online quality-controller software called FastQC (version: v0.11.8, http://www.bioinformatics.babraham.ac.uk/projects/fastqc/). None of the FastQ reads had low quality. In the next step, the HISAT2 alignment program (Version HISAT2 2.2.1) was used to map the reads to the *Drosophila* reference genome (BDGP6, https://genome-idx.s3.amazonaws.com/hisat/bdgp6.tar.gz) [106]. Next, SAMtools [107] was used to sort the sequence alignments of each gene and HTSeq was performed to assemble and calculate the reads of a gene [108]. Next, the raw reads were exported in text tab-delimited files and used for statistical analysis to identify differentially expressed genes (DEGs). Two independent parametric R packages were used to compare the output DEGs. Deseq2 and edgeR programs [247–249] were run by an adjusted p-value < 0.05 to select DEGs . Furthermore, a Principal Component Analysis (PCA) was performed to identify the experiment's most variable time points using the calibrate library function in R [109–111].

The HISAT2, SAMtool and HTSeq programs were performed in Python software (Version 3.9.1). The R (3.4.4 version) and Rstudio software (Version 1.1.414 – © 2009-2018 RStudio, Inc.) were used to run the Deseq2, edgeR and PCA analyses. The codes are presented in Appendix A.2 section.

2.18 Protein extraction and western blot

Two different lysis buffers were used for protein extraction depending on the purpose of the experiments. For western blot and SDS-page Coomassie blue staining RIPA buffer (Sigma, Cat. # R0278-50ML) was used but for protein-protein interactions (PP-interaction) and Mass-spectrometry experiments NP-40 lysis buffer (50 mM Tris pH 7.4, 250 mM NaCl, 5 mM EDTA, 50 mM NaF, 1 mM Na3VO4, 1% Nonidet P40 (NP40), 0.02% NaN_3) was used. Buffers were

aliquoted in small volume and store in a -20 freezer. Prior to use, the cOmplete™ Protease inhibitor cocktail (Roche, Cat. # 11873580001) and PMSF protease inhibitor (Thermo Scientific™, Cat.# 36978) were added to the buffer.

Next, flies were crossed with a ubiquitous Tub-GAL-4 driver and progenies were staged carefully on desired media. Samples were collected at 40 hours after L2/L3 molt. Approximately 10-15 or 100-150 L3 larvae were collected for Western blotting or mass-spectrometry, respectively. S2 cell samples were collected 48 hours after transfection (see S2 cell culturing and transfecting section). 3-5 ml transfected S2 cells were used for PP-interaction and western blot, but 10-15 ml cells were collected for mass-spectrometry experiments. Cells were centrifuged (5 min, 4°C, and 2500 rpm) and transferred into a microcentrifuge 1.5 ml tube. All samples were washed three times with cold 1X PBS for 5 min each time before being used for extraction.

Next, 300 µl of RIPA buffer was added to sample tubes, and ice-cold pestles (soaked in cold RIPA buffer) were used to homogenize samples (30 sec). For L3 larvae, this step was done five times, and for the S2 cells, only three times were performed. Tubes were incubated on ice for 5 min and centrifuged at 12000 rpm for 5 min at 4°C between each homogenizing step. Next, samples were vortexed 30 sec vigorously and centrifuged for 30 min at 4°C and 12500 rpm. Sample lysates were transferred into new microcentrifuge 1.5 ml tubes.

The same procedure was performed to isolate proteins with the NP-40 lysis buffer. However, 300 µl of buffer was used for S2 cell samples and 400 µl for L3 larvae samples. The lysis buffer was added to samples after each homogenizing-centrifuging step gradually (75-100 µl). An ice-cold Dounce homogenizer was rinsed with a cold lysis buffer and used to homogenize larval protein samples for mass- spectrometry.

A 15 µl of samples were used to measure protein concentrations with the Qubit 2.0 using a Protein Assay Kit (Invitrogen, Cat. # Q33211). Samples were stored in a -20 freezer.

2.19 Larval hemolymph collection

The hemolymph collection protocol was published by Janmejaya Bag and Monalisa Mishra [112]. The same procedure was used to collect hemolymph samples from transgenic Tsf1, Tsf2 and Tsf3 flies. Lids of 0.5 ml microcentrifuge tubes were removed, and then a small cut was created at the bottom of the tubes with a Razor blade (3-4 mm cut at the bottom center of tubes from the

back). The tubes were then put into a 1.5 ml centrifuge tube and placed on ice. Samples were then collected from carefully staged larvae at 44 hr after L2/L3 molt. Animals were washed three times in 1X PBS at RT for 10 min each time to remove all remaining foods. Next, they were transferred to a Kimwipe tissue to remove the PBS buffer. Number five forceps were used to transfer and pierce dried larvae into the prepared 0.5 ml tube. Baches of 15-20 L3 larvae were pierced by a gentle force near the larval mouth hook. Dripped hemolymph samples were collected through centrifugation for 5-10 sec at 4°C. Approximately 10-15 µl hemolymph was collected in each 1.5 ml tube, and the 0.5 ml tubes that contained larval carcass were discarded. Tubes were snap-frozen by liquid Nitrogen immediately to avoid melanization of the hemolymph and then stored in a -80 freezer.

Lastly, 10 µl 5X Laemmli protein loading buffer was added to 40 µl hemolymph. Samples were boiled at 95°C for 5 min and run on an SDS-PAGE gel to carry out western blot (see western blot and Coomassie blue staining section).

2.20 Western blot and Coomassie blue staining

Once the sample lysates were prepared, an appropriate volume of 5X Laemmli loading buffer (10% SDS, 0.25 % Bromophenol blue, 50% Glycerol, 0.25 M Tris-HCL pH 6.8) were mixed with 10 % 2-mercaptoethanol and added to protein samples (with a 1:4 ratio of loading buffer to proteins). Samples were then boiled at 95°C for 5 min, and 45 µl was loaded on the SDS-PAGE gel. Samples were run on a 6% stacking gel and 10-12% separating gel at 85V for 15 min, then at 125V for 90 min. Next, proteins on SDS-PAGE gel were transferred to a Polyvinylidene difluoride (PVDF) membrane in wet 1X transfer buffer (25 mM Tris, 190 nM Glycine, 20% Methanol) at 100V for 1 hr at 4°C. Blots were blocked in blocking solution (1X TBST with 5% non-fat skim milk) for 1 hr at RT and incubated with a proper primary antibody (Blocking solution with antibody) for an overnight at 4°C. Membranes were then washed three times with PBST for 10 min for each wash. The membranes were next incubated with the HRP secondary antibody (Blocking solution with antibody) for 1 hr at RT, followed by three washes with PBST. Protein bands were detected with ECL Prime Western Blotting Detection reagent (Sigma, Cat. # GERPN2232). A 1:1 ratio working solution was prepared based on kit protocol and added to the membrane (approximately 100 µl of working solution per 1 cm^2 of the membrane). Membranes were incubated in the dark for 5 min, and protein bands were scanned and detected with the Bio-

Rad ChemidocTM MP imaging system. All antibodies used for the western blot and their concentrations were presented in Table 2.6.

The Coomassie blue staining method was used to stain SDS-PAGE gels. First, the gels were treated in a fixative buffer (50% methanol and 10% glacial acetic acid in milli-Q water) for 1 hr at RT. Once the gel was fixed, a staining solution (0.1% Coomassie Brilliant Blue R-250, 50% methanol and 10% glacial acetic acid in milli-Q water) was added to the gel and incubated for 30 min at RT. Next, the gels were washed and treated with a destaining solution (40% methanol and 10% glacial acetic acid in milli-Q water). The solution was replenished several times (every hour) until the gel's blue background was removed. The gel was stored in a storage solution (5% glacial acetic acid in milli-Q water). Stained proteins were either submitted to the Mass-Spec facility or used to take pictures with the Bio-Rad ChemidocTM MP imaging system.

A pre-stained Protein Ladder (5 µl, Thermo Scientific™, Cat. # 26617) was used for size standards (10 to 180 kDa) on all gels.

2.21 In vivo and in vitro immunoprecipitation assay (IP and co-IP)

All protein samples (S2 cells and L3 larvae) were extracted with NP-40 lysis buffer (described in the protein extraction section). The anti-tag M2 affinity gel/beads were used to identify interacting protein complexes and evaluate protein-protein interactions. The anti-FLAG M2 affinity gel (Sigma, Cat. # A2220) was used to precipitate proteins tagged with FLAG (Evi5, Tsf1, Tsf2, Tsf3, Hsp22 and Hsp70). 40 µl of the affinity gel was added to a spin column (ChromoTek, Cat. # sct-50). The affinity gel was then equilibrated by six times washing with NP-40 lysis buffer. Next, 250-300 µl of sample lysate was added to columns and incubated on a rotating shaker at 4°C for 4 hr. Supernatants were collected into a new 1.5 ml microcentrifuge tube and stored in the -20 °C freezer for further experiments. Gel-protein complexes were then washed with buffer #1 (25 mM Na-HEPES, 75 mM NaCl, 0.5 mM EDTA, 10% glycerol, 0.1% Triton X-100, 5 mM DTT and 10 mM PMSF) and buffer 2 (25 mM Na-HEPES, 75 mM NaCl, 0.5 mM EDTA, 10% Glycerol, 10 mM PMSF). 40 µl of 5X Laemmli loading buffer was added to each column and boiled at 95°C for 5 min. Samples were then collected into a new 1.5 ml microcentrifuge tube and stored in a -20°C freezer.

IP-samples were used for either protein-protein interaction analysis with Western blot (see the Western blot section) or used for mass-spectrometry analysis. Samples were run on 10-12 %

SDS-PAGE gel at 80 V for 15 min and 120 V for 30 min. Extra parts of the gel were cut off and then stained with Coomassie Blue (see the Coomassie Blue staining section). The stained gel was then used for MALDI-TOF Mass spectrometry analysis and protein sequencing.

2.22 MALDI-TOF mass spectrometry (MS)

Coomassie blue-stained gels were submitted to the Proteomics and Mass spectrometry facility at the University of Alberta (http://apm.biochem.ualberta.ca/MassSpec.html). In brief, protein samples were digested with trypsin and extracted from the SDS-PAGE gel. Fractionated peptides were then ionized and then added to an LTQ XL-Orbitrap hybrid mass spectrometer. MS spectra of all peptides were recorded, and proteins were identified with the Proteome Discoverer software (version 1.4). The program compares the raw mass-spec data to the proteins in a (selectable) reference database. The *Drosophila* proteome database (Uniport database, Proteome ID: UP000000803, https://www.uniprot.org/proteomes/UP000000803) was used as the reference proteome in the Proteome Discoverer software. All analyses were conducted with the Proteomics and mass spectrometry facility, and final results were received in a Microsoft Excel file.

2.23 Embryo microinjection

Before starting injection first, pHD-DsRed-evi5^{FRT} (donor plasmid) and pCFD5-evi5-gRNA plasmids were propagated in *E. coli* (DH5α) and purified with the QIAGEN Midiprep kit (QIAGEN, Cat. # 10043). Plasmids were dissolved in nuclease-free water and stored at -20°C until required. In total, 1 µg DNA was used for injection, and a 1:1 ratio was used to make donor and gRNA plasmid mix. Further, *vasa-Cas9* flies (Table 2.1) were expanded into ten fly cages. Next, flies were reared on grape juice agar plates with yeast (see section 2.1) to collect embryos. Finally, a flaming/brown micropipette puller was used to prepare needles for injection (Sutter Instrument Company, model P-87) using the following parameters: heat -590, pull -250, vel -250, time 170. The needles were then opened by a gentle-touching of a sharp coverslip edge. Approximately 5 µl of the plasmid mix was added to the needle with pipette tips. 10 needles were loaded with plasmid mix and submersed in halocarbon oil (Sigma, Cat. # H8773-100ML) and stored in 4^0C until needed.

For injection, embryos were collected in a small sieve and rinsed with distilled water. Embryos were then dechorionated by immersing the sieve in a 50% bleach solution for 20-30 sec followed by rinsing thoroughly with distilled water. Next, 40-50 embryos were lined up (from

posterior to anterior site) on a small piece of grape-juice agar food and transferred on a microscope slide with glue. The glue was extracted from a double-stick tape. Approximately, 10 cm of the double-stick tape was placed into a glass bottle and 500 µl heptane (Sigma Cat. # 650536-1L) was added to the bottle. The glass bottle was placed on a rocking shaker at RT, overnight.

Then embryos were desiccated by placing slides in a desiccation chamber for 2-5 min. Time of the desiccation process varied according to the air humidity. Embryos were then covered with halocarbon oil. A loaded needle was placed on the needle holder of an inverted injection microscope with a proper bevel angle to inject embryos. Next, injected embryos were placed in a 18°C incubator for 16 hours and hatched L1 larva were transferred on a vial food. G0 flies were then crossed to w^{1118} flies, and progenies were screened for DsRed signal under UV light. Positive flies were then crossed to an X-chromosome balancer fly (*FM7a*, BDSC # 785) to create homozygous $Evi5^{FRT\text{-}DsRed}$ flies. The DsRed was excised by crossing the $Evi5^{FRT\text{-}DsRed}$ flies to piggyBac transposase expressing flies (*Cyo,Tub-PBac/Sp*, BDSC # 8283). Finally, $Evi5^{FRT}$ flies were sequenced to confirm the edited locus.

Additionally, to create transgenic lines, first pBID-UAS-cDNA-3XFLAG for Tsf1, Tsf2, and Tsf3 plasmids were transformed into DH5α *E. coli* and isolated with the QIAGEN Midiprep kit. Approximately, 20-25 µg DNA was transferred to a 1.5 ml microcentrifuge tube and submitted to GenetiVision company (https://www.genetivision.com). The G0 flies were received and crossed with W^{1118} flies. F1 generations were then screened for red eyes (mini-white transgene used as a selectable marker) and crossed with a balancer line to create homozygous flies. The transgenic lines were further confirmed with Sanger sequencing of chromosomal insertion loci. The list of injected plasmids was presented in table 2.3.

2.24 Tables

Table 2. 1 list of fly stocks that were used in my study.

Stock ID	Stock Center[A]	Name	Line	Chapter[B]
38350	BDSC	Evi5-TRIP	RNAi	Chapter 3
105146	VDRC	Evi5-VDRC	RNAi	
106479	VDRC	Tsf1	RNAi	
55936	BDSC	Tsf1	RNAi	
5236	VDRC	Tsf2	RNAi	
108470	VDRC	Tsf3	RNAi	
27299	BDSC	Rab1	RNAi	
9757	BDSC	UAS- Rab1	Overexpression	
34922	BDSC	Rab2	RNAi	
9760	BDSC	UAS- Rab2	Overexpression	
31691	BDSC	Rab3	RNAi	
9764	BDSC	UAS-Rab3	Overexpression	
33757	BDSC	Rab4	RNAi	
9768	BDSC	UAS-Rab4	Overexpression	
51847	BDSC	Rab5	RNAi	
9771	BDSC	UAS- Rab5	Overexpression	
103945	VDRC	Rab5	RNAi	
35744	BDSC	Rab6	RNAi	
9796	BDSC	UAS-Rab6	Overexpression	
27051	BDSC	Rab7	RNAi	
9778	BDSC	UAS-Rab7	Overexpression	
34373	BDSC	Rab8	RNAi	
9780	BDSC	UAS-Rab8	Overexpression	
42942	BDSC	Rab9	RNAi	
9784	BDSC	UAS-Rab9	Overexpression	
109376	VDRC	Rab9D	RNAi	
38269	BDSC	Rab9Db	RNAi	

9835	BDSC	UAS-Rab9Db	Overexpression	
109230	VDRC	Rab9Fa	RNAi	
34374	BDSC	Rab9Fb	RNAi	
9844	BDSC	UAS-Rab9Fb	Overexpression	
26289	BDSC	Rab10	RNAi	
9786	BDSC	UAS-Rab10	Overexpression	
27730	BDSC	Rab11	RNAi	
9791	BDSC	UAS-Rab11	Overexpression	
108382	VDRC	Rab11	RNAi	
28708	BDSC	Rab14	RNAi	
9795	BDSC	UAS-Rab14	Overexpression	
27665	BDSC	Rab18	RNAi	
9796	BDSC	UAS-Rab18	Overexpression	
34607	BDSC	Rab19	RNAi	
9800	BDSC	UAS-Rab19	Overexpression	
29403	BDSC	Rab21	RNAi	
9801	BDSC	UAS-Rab21	Overexpression	
28025	BDSC	Rab23	RNAi	
9802	BDSC	UAS-Rab23	Overexpression	
31177	BDSC	Rab26	RNAi	
9807	BDSC	UAS-Rab26	Overexpression	
50537	BDSC	Rab27	RNAi	
9810	BDSC	UAS-Rab27	Overexpression	
31120	BDSC	Rab30	RNAi	
9814	BDSC	UAS-Rab30	Overexpression	
28002	BDSC	Rab32	RNAi	
9815	BDSC	UAS-Rab32	Overexpression	
28342	BDSC	Rab35	RNAi	
9818	BDSC	UAS-Rab35	Overexpression	
53995	BDSC	Rab39	RNAi	

9822	BDSC	UAS-Rab39	Overexpression	
29579	BDSC	Rab40	RNAi	
9827	BDSC	UAS-Rab40	Overexpression	
28033	BDSC	RabX1	RNAi	
9837	BDSC	UAS-RabX1	Overexpression	
32360	BDSC	RabX2	RNAi	
9841	BDSC	UAS-RabX2	Overexpression	
28704	BDSC	RabX4	RNAi	
9848	BDSC	UAS-RabX4	Overexpression	
28045	BDSC	RabX5	RNAi	
9852	BDSC	UAS-RabX5	Overexpression	
50573	BDSC	RabeX-5	RNAi	
26281	BDSC	RabX6	RNAi	
9855	BDSC	UAS-RabX6	Overexpression	
63531	BDSC	Bulli	RNAi	
103378	VDRC	Mon1	RNAi	
80367	BDSC	Sprint	RNAi	
62889	BDSC	CCZ1	RNAi	
53261	BDSC	Crag	RNAi	
61915	BDSC	ParCas	RNAi	
57301	BDSC	Sbf	RNAi	
62898	BDSC	CG1695	RNAi	
57223	BDSC	CG4041	RNAi	
110700	VDRC	CG4552	RNAi	
32333	BDSC	CG5337	RNAi	
77447	BDSC	Wkd	RNAi	
32394	BDSC	CG5745	RNAi	
110561	VDRC	CG5916	RNAi	
110396	VDRC	GAPsec	RNAi	
77400	BDSC	CG6182	RNAi	

55328	BDSC	Rab3-GAP	RNAi	
34976	BDSC	CG7112	RNAi	
32929	BDSC	CG7324	RNAi	
100125	VDRC	CG7742	RNAi	
28670	BDSC	RN-tre	RNAi	
108444	VDRC	CG8155	RNAi	
24101	VDRC	CG8449	RNAi	
108736	VDRC	Sky	RNAi	
34859	BDSC	CG11490	RNAi	
33729	BDSC	CG12241	RNAi	
107134	VDRC	CG16896	RNAi	
28776	BDSC	Tbc	RNAi	
53011	BDSC	Muc14A	RNAi	
66313	BDSC	Plx	RNAi	
62385	BDSC	CG42795	RNAi	
32848	BDSC	Msp-300	RNAi	
Tsf1-3XFLAG	KKJ-Lab	UAS-Tsf1	Overexpression	
	Sattar Soltani			
Tsf2-3XFLAG	KKJ-Lab	UAS-Tsf2	Overexpression	
	Sattar Soltani			
Tsf3-3XFLAG	KKJ-Lab	UAS-Tsf3	Overexpression	
	Sattar Soltani			
$Evi5^{FRT}$	KKJ-Lab	Evi5	Conditional mutant	
	Sattar Soltani			
43632	VDRC	Hsp22	RNAi	Chapter 4
50637	BDSC	Hsp68	RNAi	
35671	BDSC	Hsp70Aa	RNAi	
35663	BDSC	Hsp70Ab	RNAi	
35672	BDSC	Hsp70Ba	RNAi	
35697	BDSC	Hsp70Bc	RNAi	

33916	VDRC	Hsp70Bbb	RNAi	
101878	VDRC	CG5157	RNAi	
105878	VDRC	CG7763	RNAi	
100234	VDRC	CG13078	RNAi	
101976	VDRC	CG33061	RNAi	
109109	BDSC	CG33270	RNAi	
51451	BDSC	CG18179	RNAi	
57710	VDRC	Ctr1B	RNAi	
106911	VDRC	Drip	RNAi	
102406	VDRC	Fer1HCH	RNAi	
106960	VDRC	Fer2LCH	RNAi	
105959	VDRC	galla-1	RNAi	
105011	VDRC	MtnA	RNAi	
106118	BDSC	MtnB	RNAi	
34095	BDSC	Ugt302E1	RNAi	
50635	VDRC	Zip99C	RNAi	
105608	VDRC	ABCA	RNAi	
102723	VDRC	CG13454	RNAi	
102275	VDRC	CG14626	RNAi	
102875	VDRC	CG33474	RNAi	
105692	BDSC	Desi	RNAi	
57147	VDRC	RpS5b	RNAi	
109040	BDSC	yellow-k	RNAi	
32954	BDSC	Zip89B	RNAi	
8283	BDSC	piggyBac transposase	Removing DsRed marker in Evi5FRT	
110620	BDSC	Fer1HCH G188	GFP reporter for ferritin	
108828	VDRC	SpenVDRC1	RNAi	Chapter 5
48846	VDRC	SpenVDRC2	RNAi	
49543	VDRC	SpenVDRC3	RNAi	

33398	BDSC	SpenTRIP1	RNAi	
41619	BDSC	SpenTRIP2	RNAi	
29319	BDSC	Ras85D	RNAi	
31038	BDSC	Raf	RNAi	
31387	BDSC	ERK	RNAi	
31502	BDSC	Notch	RNAi	
28032	BDSC	Delta	RNAi	
27174	VDRC	Serrate	RNAi	
4847	BDSC	UAS-Ras^{V12}	Overexpression	
3605	BDSC	W1118	Control flies	Chapter 3,4,5
8751	Kyoto	Insc-GAL4	GAL4 driver	
113094	BDSC	NP3084-GAL4	GAL4 driver	
-	O'Connor's lab	phm-GAL4	GAL4 driver	
-	O'Connor's lab	phmN1-GAL4	GAL4 driver	
51323	BDSC	vasa-Cas9	Injection	
784	BDSC	FM6	X chromosome balancer	
785	BDSC	FM7a	X chromosome balancer	
5570	BDSC	CyO, sp*	2nd chromosome balancer	
64205	BDSC	CyO, P{3xP3-eGFP}2	2nd chromosome balancer	
3607	BDSC	CxD	3rd chromosome balancer	
6309	BDSC	CxD	3rd chromosome balancer	
3717	BDSC	FM7a; TM2	X and 3rd chromosome balancer	
36283	BDSC	FM7a; TM3, Sb	X and 3rd chromosome balancer	
59967	BDSC	CyO; TM3, Sb	2nd and 3rd chromosome balancer	
7198	BDSC	CyO; TM3, Ser	2nd and 3rd chromosome balancer	

[A] BDSC: Bloomington *Drosophila* Stock Center, DGRC: *Drosophila* Genomics Resource Center , Kyoto: Kyoto Stock Center, VDRC: Vienna *Drosophila* Resource Center.

[B] Flies are categorized based on chapters

Table 2. 2 List media and supplements that were used in this study.

Supplement	Solvent	Concentration	Stock	Experiment	Chapter
Bathophenanthroline Sulfate (BPS)	H2O	120 μM	0.2 M	Survival analysis, Iron RNA-seq, S2 cell	3,4
Ferric Ammonium citrate (FAC)	H2O	1 mM	1 M	Survival analysis, Iron RNA-seq, S2 cell	3,4
Cholesterol	Ethanol	75 μg/ml	100 mg/ml	Survival analysis	5
7-dehydrocholesterol	Ethanol	100 μg/ml	100 mg/ml	Survival analysis	5
20-hydroxyecdysone	Ethanol	100 μg/ml	100 mg/ml	Survival analysis	3,5
Hemin	NaOH	100 μM	100 mM	Survival analysis	3
zinc protoporphyrin	DMSO	1 mM	1 M	Survival analysis	3

Table 2. 3 Plasmids that were generated in this study.

Chapter	Plasmid	Experiment
3	pHD-DsRed-evi5^{FRT}	Embryo injection, Conditional mutant line
	pCFD5-evi5-gRNA	Embryo injection, Conditional mutant line
	pBID-UAS-Tsf1-3XFLAG	Embryo injection, transgenic line
	pBID-UAS-Tsf2-3XFLAG	Embryo injection, transgenic line
	pBID-UAS-Tsf3-3XFLAG	Embryo injection, transgenic line
	pBID-UAS-Tsf1*-3XFLAG	Embryo injection, transgenic line
	pBID-UAS-Tsf2*-3XFLAG	Embryo injection, transgenic line
	pBID-UAS-Tsf3*-3XFLAG	Embryo injection, transgenic line
	pAFW-Evi5-3XFLAG	S2 cells transfection, Mass-spec analysis
	pAFW-Tsf1-3XFLAG	S2 cells transfection, Mass-spec analysis
	pAFW-Tsf2-3XFLAG	S2 cells transfection, Mass-spec analysis
	pAFW-Tsf3-3XFLAG	S2 cells transfection, Mass-spec analysis
	pAFW-Evi5-mCherry	S2 cells transfection, colocalization analysis
	pAFW-Tsf1-eGFP	S2 cells transfection, colocalization analysis
	pAFW-Tsf2- eGFP	S2 cells transfection, colocalization analysis
	pAFW-Tsf3- eGFP	S2 cells transfection, colocalization analysis
4	pAFW-Hsp22-3XFLAG	S2 cells transfection, Mass-spec analysis

	pAFW-Hsp70-3XFLAG	S2 cells transfection, Mass-spec analysis
	pAc5-STABLE2- Hsp22-3XFLAG-Fer1HCH-5XMyc	CO-IP assay, S2 cells, Protein-protein interaction
	pAc5-STABLE2- Hsp22-3XFLAG-mAcon1-5XMyc	CO-IP assay, S2 cells, Protein-protein interaction
	pAc5-STABLE2- Hsp22-3XFLAG-RFeSP-5XMyc	CO-IP assay, S2 cells, Protein-protein interaction

Table 2. 4 List of ordered plasmids.

Name	Company	Catalogue No.	Chapter
pHD-DsRed-attP	Addgene	51019	3
pCFD5	Addgene	73914	3
pBID-UASC-FG	Addgene	35201	3
pBID-UASC-MRG	Addgene	35205	3
pAc5-STABLE2-neo	Addgene	32426	3,4
pAFW-3XFLAG	Addgene	Not-available	3,4
pAMW-5XMyc	Addgene	Not-available	3,4

Table 2. 5 List of cDNAs that were used in this study.

Gene	Source	Collection	Clone No.	Flybase Id	Chapter
Evi5	DGRC	Full Length (Gold)	GH14362	FBcl0117515	3
Tsf1	DGRC	Full Length (Gold)	LP08340	FBcl0180926	3
Tsf2	DGRC	Full Length (Gold)	LD22449	FBcl0178834	3
Tsf3	DGRC	Full Length (Gold)	FI03676	FBcl0718373	3
Hsp22	DGRC	Full Length (Gold)	LD36162	FBcl0173891	4
Hsp70	DGRC	Full Length (Gold)	AT07372	FBcl0018649	4
mAcon1	DGRC	Full Length (Gold)	LD24561	FBcl0167946	4
RFeSP	DGRC	Full Length (Gold)	SD14047	FBcl0275555	4
Fer1HCH	Dr. Fanis Missirlis	Fer1HCH-RG	-	-	4

Table 2. 6 List of antibodies that were used in this study.

Antibody	Source	Dilution	Application	Company	Catalogue No.
anti-FLAG	Mouse	1-800	Immunofluorescence	Cell signaling	8146S
		1-1000	Western blot		
anti-FLAG	Rabbit	1-800	Immunofluorescence	Cell signaling	14793S
		1-1000	Western blot		
anti-Myc	Mouse	1-1000	Immunofluorescence	Cell signaling	2276S
		1-1000	Western blot		
anti-Myc	Rabbit	1-1000	Immunofluorescence	Cell signaling	2278S
		1-1000	Western blot		
anti-GFP	Mouse	1-1000	Immunofluorescence	Invitrogen	MA5-15256
		1-1000	Western blot		
anti-GFP	Rabbit	1-1000	Immunofluorescence	Invitrogen	G10362
		1-1000	Western blot		
Anti-Hrs	Mouse	1-100	Immunofluorescence	DSHB	Hrs27-4
Alexa Fluor 488	Goat anti-mouse	1-2000	Immunofluorescence	Abcam	150113
Alexa Fluor 488	Goat anti-rabbit	1-2000	Immunofluorescence	Abcam	150077
Alexa Fluor 555	Goat anti-mouse	1-2000	Immunofluorescence	Abcam	150114
Alexa Fluor 555	Goat anti-rabbit	1-2000	Immunofluorescence	Abcam	150078
IgG H&L HRP	Goat anti-mouse	1-15000	Western blot	Abcam	97023
IgG H&L HRP	Goat anti-rabbit	1-15000	Western Blot	Abcam	97051

Table 2. 7 qPCR primers list.

Primer[A]	Sequence (5'-3')	Chapter
RP49-Fwd	CGGATCGATATGCTAAGCTGT	3,4,5
RP49-Rev	GCGCTTGTTCGATCCGTA	
ALAS-Fwd	ACCAACGGAACGTCTCCTAC	3
ALAS-Rev	CTTCGACGGGGAAACCTT	
Neverland-Fwd	CCCTCACCTAGGAGCCAACT	3,4
Neverland-Rev	GGCATATAACACAGTCGTCAGC	
Shroud_Fwd	CGAATCGCTGCACATGAC	3,4
Shroud-Rev	TAGGCCCTGCAGCAGTTTAG	
Spookier-Fwd	GCGGTGATCGAAACAACTC	3,4
Spookier-Rev	CGAGCTAAATTTCTCCGCTTT	
Cyp6t3-Fwd	GGTGTGTTTGGAGGCACTG	3,4
Cyp6t3-Rev	GGTGCACTCTCTGTTGACGA	
Phantom-Fwd	GGCATCATGGGTGGATTT	3,4
Phantom-Rev	CAAGGCCTTTAGCCAATCG	
Disembodied-Fwd	GTGACCAAGGAGTTCATTAGATTTC	3,4
Disembodied-Rev	CCAAAGGTAAGCAAACAGGTTAAT	
Shadow-Fwd	CAAGCGGATATTTGTAGACTTGG	3,4
Shadow-Rev	AAGCCCACTGACTGCTGAAT	
Shade-Fwd	CCGCATTCAGCAGTCAGTGG	3,4
Shade-Rev	ACCTGCCGTGTACAAGGAGAG	
Rab5-Fwd	TTGTGAAGATTTGAAAACGACT	3
Rab5-Rev	TGCTGAGTAAGTCTTTCTGCTAAGA	
Rab11-Fwd	ACGCGCAGCATAGAGGTC	3
Rab11-Rev	CGGTAGTAGGCAGAGGTGATG	
Evi5-Fwd	ACAGCAGCAGCGCACTAAC	3
Evi5-Rev	CACATGGTGCTCCTAGTTTCG	
Tsf1-Fwd	CGCATAAGACCCACACCTG	4
Tsf1-Rev	GGCACACACAGGCGATAA	
IRP1A-Fwd	TCCATCGACAGCAAATATGAGT	4
IRP1A-Rev	CCAGCACATGAAAGTTGTCAC	
Hsp22-Fwd	GAGAGTGCCGGTATTTTCTAGATT	4
Hsp22-Rev	TTGTTAGCAGTTGGTTTGGTTTT	
Hsp68-Fwd	AACTTTGCGGTGACCTCTTC	4
Hsp68-Rev	TAGCGTCCTTGAGTGCCTTC	

Hsp70Ab-Fwd	ATCGCCAGCGAATAACCTC	4
Hsp70Ab-Rev	CCTGCTTCACATTGAAGACGTA	
Hsp70Bc-Fwd	CCAGCAACCAAGTAAATCAACTG	4
Hsp70Bc-Rev	TGAAAGTATTCAGAGTTCTCTTCTGG	
Hsp70Bbb-Fwd	GAATGTGCTCCGCATCATC	4
Hsp70Bbb-Rev	ATTGCGCTCATCCTTGAGAT	
Fer1HCH-Fwd	TGCTAGCCTGCTCCTGTTG	4
Fer1HCH-Rev	GTCCACCCAGTCCTTGGTAA	
Fer2LCH-Fwd	CGCTCTCCAAAACCACACA	4
Fer2LCH-Rev	GTGAAACTCTGAAAATCAACTGCT	
galla-1-Fwd	AGCAGCGCCAGTATCAGC	4
galla-1-Rev	CGACATCTGGCTCGTTTTG	
Mvl-Fwd	GTGGGTGCAGCGTTTTGT	4
Mvl-Rev	CGAACTCGTGGCAATCCT	
CG5157-Fwd	AGAAACCCACTCAATGACAACTC	4
CG5157-Rev	GGCAGTGACCAATCTCCTTT	
Torso-Fwd	TCCAACTCTACCCACAACATCAC	5
Torso-Rev	CAGATTCACCGCTCCCATTT	
Notch-Fwd	CCG TTC GCG GAA CTG ATA	5
Notch-Rev	CAT TCT GGC AAC CGA CAC T	
Ras-Fwd	GTC ATT GGT GGC AAT GTG G	5
Ras-Rev	TGG GTG ATG CAG ATG GAA C	
Spen-Fwd	CCTTTTGACGCCAGTCTGA	5
Spen-Rev	GTCATCGTAGTCGCCACCTC	

[A] primers are listed as the Forward (Fwd) and Reverse (Rev) pairs.

Table 2. 8 List of primers designed for Evi5FRT allele.

Primer[A]	**Sequence (5'-3')[B]**
gRNA 1 for FRT allele-Fwd	ATCCGGGTGAACTTCGTTGAAATATCTATCACATGTGTTTTAGAGCTAGAAATAGCAA G
gRNA 1 for FRT allele-Rev	TTTCTAGCTCTAAAACCAACCATAAGAAATCAAATACGACGTTAAATTGAAAATAGGT C
gRNA 2 for FRT allele-Fwd	ATCCGGGTGAACTTCGTACAAAACCCGTGCTTATAAGTTTTAGAGCTAGAAATAGCAA G
gRNA 2 for FRT allele-Rev	TTTCTAGCTCTAAAACACCATCCCATCCTCCATAGTCGACGTTAAATTGAAAATAGGTC
Evi5-genomic locus1 (left arm) for FRT allele-Fwd	gaagcaggtggaattcCCGCCTAGGCAATCAACAG
Evi5-genomic locus1 (left arm) for FRT allele-Rev	cgataagcttggatccTTTCTAGAGAATAGGAACTTCACATG
Evi5-genomic locus2 (middle) for FRT allele-Fwd	gttcctattctctagaaaGGTGACTAGCTGACAAGC
Evi5-genomic locus2 (middle) for FRT allele-Rev	cgataagcttggatccAAATGACCGAGACATGGG
Evi5-genomic locus3 (right arm) for FRT allele-Fwd	tggacgagctgtacaagtaaATTCTCTAGAAAGTATAGGAACTTC
Evi5-genomic locus3 (right arm) for FRT allele-Rev	atctagagtcgcggcccctaCTCCTTGAGCTTCTTGTG
Add FRT site to upstream-Fwd	gcgatcgcGAAGTTCCTATTCTCTAGAAAgtataggaacttcAGAAAGGTACCGGTTCCG
Add FRT site to upstream-Rev	agaataggaacttcgtcgaCTCCGGAttaattaaACATGATTAACCCTCACTAAAGG
Add FRT site to downstream-Fwd	tcgacGAAGTTCCTATTCTCTAGAAAgtataggaacttcCCCTTTAGTGAGGGTTAATTC
Add FRT site to downstream-Rev	aataggaacttcgcgatcgcAGAAGACcatatgGTATCCGCTCATGAGATTATC
Backbone 1 (left arm) for FRT allele-Fwd	TTACTTGTACAGCTCGTCCATG

Backbone 1 (left arm) for FRT allele-Rev	TAGGGGCCGCGACTCTAG
Backbone 2 (middle) for FRT allele-Fwd	TTTCTAGAGAATAGGAACTTCAC
Backbone 2 (middle) for FRT allele-Rev	GGATCCAAGCTTATCGATTTC
Backbone 3 (right arm) for FRT allele-Fwd	GAATTCCACCTGCTTCAG
Backbone 3 (right arm) for FRT allele-Rev	GGATCCAAGCTTATCGATTTC
Evi5-genomic locus1 (left arm) sequencing-Fwd	GCGACACGGAAATGTTGAATAC
Evi5-genomic locus1 (left arm) sequencing-Fwd	AAACCCGCCTAAGAATGTG
Evi5-genomic locus1 (left arm) sequencing-Fwd	CGTGGTAAAGTTGAACATACC
Evi5-genomic locus3 (right arm) sequencing-Fwd	TGGAATACGTTCTAGTTCCGATC
Evi5-genomic locus3 (right arm) sequencing-Fwd	GCCTTGTAATCGTATTTTACACG
Evi5-genomic locus2 (middle) sequencing-Fwd	GCGACACGGAAATGTTGAATAC
Evi5-genomic locus2 (middle) sequencing-Fwd	TAAGCTCATCGAGAGCGATG
Evi5-genomic locus2 (middle) sequencing-Fwd	AGTATGCGGAGTACATCAAG
Evi5-genomic locus2 (middle) sequencing-Fwd	AAGGAGTACCAGGACCTC
Evi5-genomic locus2 (middle) sequencing-Fwd	CCCAGCGAGTATTCAATAAC
Evi5-genomic locus2 (middle) sequencing-Fwd	TTACCGAGCTCAAGGAGC

Evi5-genomic locus2 (middle) sequencing-Rev	TTTGCTATGCTCACATTGC
Evi5-genomic locus2 (middle) sequencing-Fwd	CAAATGTCAAGCAGCAGG

[A] primers are listed as the Forward (Fwd) and Reverse (Rev) pairs.

[B] lowercase sequence in primers indicates overlap sequences of the Gibson assembly reaction.

Table 2. 9 List of primers designed for Transgenic lines.

Primer[A]	**Sequence (5'-3')[B]**
Backbone 1 for UAS constructs pBID-UASC-FG-Fwd	CTGCGTCCGCTATCTCTTTC
Backbone 1 for UAS construct pBID-UASC-FG-Rev	gctttttgtacaaacttgtATACCGGTGCTTGTCATCG
Backbone 2 for UAS construct pBID-UASC-FG-Fwd	ctttcttgtacaaagtgggGACGTAAGCTAGAGGATCTTTG
Backbone 2 for UAS construct pBID-UASC-FG-Rev	GAAAGAGATAGCGGACGC
Tsf1-UAS-construct-pBID-UASC-FG-Fwd	tttgtacaaaaaagcaggcttcATGATGTCGCCGCATAAG
Tsf1-UAS-construct-pBID-UASC-FG-Rev	tttgtacaagaaagctgggtCACTGCTTGGCAATCTTG
Tsf2-UAS-construct-pBID-UASC-FG-Fwd	tttgtacaaaaaagcaggcttcATGGCTAGCAGCCTCGT
Tsf2-UAS-construct-pBID-UASC-FG-Rev	tttgtacaagaaagctgggtaGAGCATTGCAACCAGCGAAC
Tsf3-UAS-construct-pBID-UASC-FG-Fwd	tttgtacaaaaaagcaggcttcATGCAGTGGCTTACACTTATTT
Tsf3-UAS-construct-pBID-UASC-FG-Rev	tttgtacaagaaagctgggtCTAGCCAAACGGCTGAC
Backbone 1 for UAS constructs pBID-UASC-GV-Fwd	CTGCGTCCGCTATCTCTTTC
Backbone 1 for UAS construct pBID-UASC-GV-Rev	gtcttaattaaGGAGCTCCGAATTCACTGC

Backbone 2 for UAS construct pBID-UASC-GV-Fwd	ttaattaaGACGTAAGCTAGAGGATCTTTG
Backbone 2 for UAS construct pBID-UASC-GV-Rev	GAAAGAGATAGCGGACGC
Evi5-UAS-construct-pBID-UASC-GV-Fwd	ggtatacacctaggcggtacGCCACCATGGCCATGACCCTGACCACAACGAC
Evi5-UAS-construct-pBID-UASC-GV-Rev	atcctctagcttacgtcttaTTACTTGTACAGCTCGTCCATGC
pBID-UASC-FG/GV sequencing 1-Fwd	ATTTAGCCGATCAATTGTGC
pBID-UASC-FG/GV sequencing 2-Fwd	GATATATCCCAATGGCATCG
pBID-UASC-FG/GV sequencing 3-Fwd	AGGTATGCTATGAAGCAGC
pBID-UASC-FG/GV sequencing 4-Fwd	CTTTGTGAAGGAACCTTACTTC
Tsf1-sequencing 1-Fwd	ATCACCAAGCTGAAGAACAC
Tsf1-sequencing 2-Fwd	TTCAGTCCACCGATTGTG
Tsf1-sequencing 3-Fwd	AACGACAAAGCCGTTCAG
Tsf2-sequencing 1-Fwd	CTTTCCGACAAACACAATCC
Tsf2-sequencing 2-Fwd	AGATGATCAGTCATTTACCAAG
Tsf2-sequencing 3-Fwd	TTCATGAAGCACACCACG
Tsf3-sequencing 1-Fwd	TTGGTCCCAGTTGCAAGG
Tsf3-sequencing 2-Fwd	TGGTGTTGGTGGATCAGG
Tsf3-sequencing 3-Fwd	TTGTTCCGTGACGACACC
Evi5-sequencing 1-Fwd	GATTCATTGTGGGCCTG
Evi5-sequencing 2-Fwd	CCGATCATACTTGGAGGTC
Evi5-sequencing 3-Fwd	GACATGTCCAACAAGGC

[A] primers are listed as the Forward (Fwd) and Reverse (Rev) pairs.

[B] lowercase sequence in primers indicates overlap sequences of the Gibson assembly reaction.

Table 2. 10 List of primers designed for S2 cells transfection.

Primer[A]	Sequence (5'-3')[B]	Chapter
General-Backbone for C 3XFlag tag-Fwd	GGCGACTACAAAGACCATGAC	3,4
General-Backbone for C 3XFlag tag-Rev	CCGCTCATGAGACAATAACCC	3,4
General-Backbone for C 5XMyc tag-Fwd	ggttattgtctcatgagcggtGATATCAGAAGCTCCGCCACCATG	3,4
General-Backbone for C 5XMyc tag-Rev	ctgtgttgtaaaacgacggcCATGGTGAGGTCGCCCAAG	3,4
General-Backbone for C 3XFlag tag-Fwd	GGCGACTACAAAGACCATGAC	3,4
General-Backbone for C 3XFlag tag-Rev	CCGCTCATGAGACAATAACCC	3,4
Ac5-STABLE1-neo Backbone1 Fwd	GGGATCCAGACATGATAAGATAC	3,4
Ac5-STABLE1-neo Backbone1 Rev	TCAGAGTTGATGCCATTCATG	3,4
Ac5-STABLE1-neo Backbone2 Fwd	CATGAATGGCATCAACTCTGA	3,4
Ac5-STABLE1-neo Backbone2 Rev	GAATTCCACCACACTGGAC	3,4
Add mCherry to pAFW backbone-Fwd	agtccagtgtggtggaattcttaattaaTTGGTACCGGAgatatcATGGCCATCATCAAGGAGTTC	3,4
Add mCherry to pAFW backbone-Rev	gggttagggataggcttaccTTTATACAGCTCGTCCATGCC	3,4
Add eGFP to pAFW backbone-Fwd	agtccagtgtggtggaattcttaattaaTTGGTACCGGAgatatcATGGTGAGCAAGGGCGAG	3,4
Add eGFP to pAFW backbone-Rev	gggttagggataggcttaccCTTGTACAGCTCGTCCATGCC	3,4

Tsf1 cDNA- for pAFW backbone with C eGFP-Fwd	agtgtggtggaattcttaatGCCACCATGGACTACAAAGAC	3
Tsf1 cDNA-for pAFW backbone with C eGFP-Rev	tcgcccttgctcaccatgatCTGCTTGGCAATCTTGTTAGCA	3
Tsf1 cDNA-no signal-P for pAFW backbone with N 3XFlag and C eGFP-Fwd	ggttattgtctcatgagcggGCCACCATGGACTACAAAG	3
Tsf1 cDNA-no signal-P for pAFW backbone with N 3XFlag and C eGFP-Rev	cgataaatgggttccatcatGAAGCCTGCTTTTTTGTACAAAC	3
Tsf2 cDNA- for pAFW backbone with C eGFP-Fwd	agtgtggtggaattcttaatATGGCTAGCAGCCTCGT	3
Tsf2 cDNA-for pAFW backbone with C eGFP-Rev	tcgcccttgctcaccatgatctaCTTGTCATCGTCATCCTTGTAATCG	3
Tsf3 cDNA- for pAFW backbone with C eGFP-Fwd	agtgtggtggaattcttaatATGCAGTGGCTTACACTTATTT	3
Tsf3 cDNA-for pAFW backbone with C eGFP-Rev	tcgcccttgctcaccatgatctaCTTGTCATCGTCATCCTTGTAATC	3
Evi5 cDNA- for pAFW backbone with C mCherry-Fwd	agtgtggtggaattcttaatATGACCCTGACCACAACG	3
Evi5 cDNA-for pAFW backbone with C mCherry-Rev	tcgcccttgctcaccatgatctaGCTTATCCATTTCCACGGCT	3
Evi5 cDNA- for pAFW backbone with C 3XFlag-Fwd	agtccagtgtggtggaattcgccaccatggccATGACCCTGACCACAACG	3
Evi5 cDNA-for pAFW backbone with C 3XFlag-Rev	gggttagggataggcttaccGCTTATCCATTTCCACGGCT	3
Hsp22 cDNA for pAFW backbone C 3XFlag-Fwd	ggttattgtctcatgagcgggccaccatggccATGCGTTCCTTACCGATGTTTTG	4

Hsp22 cDNA for pAFW backbone C 3XFlag-Rev	tcatggtctttgtagtcgccCTGACTGGCGGCTTTGTC	4
Hsp70 cDNA for pAFW backbone C 3XFlag-Fwd	ggttattgtctcatgagcgggccaccATGGCCCCTGCTATTGGA	4
Hsp70 cDNA forpAFW backbone C 3XFlag-Rev	tcatggtctttgtagtcgccGTCGACCTCCTCGACTGT	4
Fer1HCH cDNA for general Backbone with C 5XMyc-Fwd	tctcatgagcggtgatGccaccATGGTGAAACTAATTGCTAGCC	4
Fer1HCH cDNA for general Backbone with C 5XMyc-Rev	ggcggagcttctgatCAGGGTCTTGTCGAACAG	4
RFeSP cDNA for Gb general Backbone with C 5XMyc Fwd	tctcatgagcggtgatgccaccatggccATGATGAACGCCGTGTCG	4
RFeSP cDNA for general Backbone with C 5XMyc Rev	ggcggagcttctgatGCCGACCACGAGAAGAC	4
mAcon1 cDNA for general Backbone with C 5XMyc Fwd	tctcatgagcggtgatgccaccATGGCTGCGAGATTGATGAACG	4
mAcon1 cDNA for general Backbone with C 5XMyc Rev	ggcggagcttctgatCTGGGCCAGCTCCTTCATG	4
Hsp22-cFLAG cDNA for Ac5-STABLE1-neo Backbone1 and 2 Fwd	gtgtggtggaattcGCCACCATGGCCATGCGT	4
Hsp22-cFLAG cDNA for Ac5-STABLE1-neo Backbone1 and2 Rev	catgtctggatcccCTACTTGTCATCGTCATCCTTGTAATCG	4
Hsp70-cFLAG cDNA for Ac5-STABLE1-neo Backbone1 and2 Fwd	gtgtggtggaattcGCCACCATGGCCCCTG	4

Hsp70-cFLAG cDNA for Ac5-STABLE1-neo Backbone1 and2 Rev	catgtctggatcccCTACTTGTCATCGTCATCCTTGTAATCG	4
T2A-Hsp22-cFLAG cDNA for Ac5-STABLE1-neo Backbone1 and2 Fwd	gtgtggtggaattcGATATCATGAGCGGTGAAGGACGC	4
T2A-Hsp22-cFLAG cDNA for Ac5-STABLE1-neo Backbone1 and2 Rev	catgtctggatcccCTACTTGTCATCGTCATCCTTGTAATCG	4
Fer1HCH-5XMyc cDNA for T2A-Hsp22-cFLAG Backbone for Fwd	ccggatcggggtacGCCACCATGGTGAAACTAATTG	4
Fer1HCH-5XMyc cDNA for T2A-Hsp22-cFLAG Backbone for Rev	cttcaccgctcatgatGCTCTCCATTTCATTCAAGTCCT	4
RFeSP-5XMyc cDNA for T2A-Hsp22-cFLAG Backbone for Fwd	ccggatcggggtacCTCATGAGCGGTGATGCC	4
RFeSP-5XMyc cDNA for T2A-Hsp22-cFLAG Backbone for Rev	cttcaccgctcatgatGCTCTCCATTTCATTCAAGTCCT	4
mAcon1-5XMyc cDNA for T2A-Hsp22-cFLAG Backbone for Fwd	ccggatcggggtacTCATGAGCGGTGATGCC	4
mAcon1-5XMyc cDNA for T2A-Hsp22-cFLAG Backbone for Rev	cttcaccgctcatgatGCTCTCCATTTCATTCAAGTCCT	4
Backbone for C 3XFlag sequencing Fwd	GCGACACGGAAATGTTGAATAC	3,4
Backbone for C 3XFlag sequencing Rev	CCTTTTGCTCACATGTTCTTTCC	3,4
Backbone for C 5XMyc sequencing Rev	ATGGTGAGGTCGCCCAAGCTC	3,4

Tsf1 cDNA sequencing-Fwd	AAGAACTCGGACAGCGAC	3
Tsf2 cDNA sequencing-Fwd	AATCCAACCGGCCAAGCTG	3
Tsf3 cDNA sequencing-Fwd	TTCGGGATCACAAGTCTTCG	3
All pAFW backbone sequencing-Rev	GTGGTTTGTCCAAACTCATCAATG	3,4
Hsp22 cDNA sequencing Fwd	ATGCGTTCCTTACCGATGTTTTG	4
Hsp70 cDNA sequencing Fwd	CAAAGTTGTAAGCGACGGCG	4
Hsp70 cDNA sequencing Rev	CGCCGTCGCTTACAACTTTG	4
Hsp70 cDNA sequencing Fwd	GTGGAGAAGGCCCTCAACG	4
Hsp70 cDNA sequencing Fwd	GAACTCCGTCCTGGACAAGTG	4
Fer1HCH cDNA sequencing Fwd	CAAGGTGACCAAGTCCATCC	4
mAcon1 cDNA sequencing Fwd	TTCTGGAAGCCAGGCAGCGG	4
mAcon1 cDNA sequencing Fwd	ATGAGCCATGGCCTCAAGTCG	4
mAcon1 cDNA sequencing Fwd	ATCAAGAACCAACGCAACGG	4
RFeSP cDNA sequencing Fwd	AAATGTGCCCACATCCACGC	4

[A] primers are listed as the Forward (Fwd) and Reverse (Rev) pairs.

[B] lowercase sequence in primers indicates overlap sequences of the Gibson assembly reaction.

Chapter 3 Ecotropic viral integration site 5 (Evi5) controls vesicular iron trafficking in PG cells

3.1 Introduction

3.1.1 From iron to heme to ecdysone hormone

Iron is a critical trace element in biology that is strictly regulated to avoid its toxic effects on cells. It participates in a wide range of biological processes as a cofactor in form of a single atom, iron-sulfur clusters and heme. Steroid hormone biosynthesis is one of the highly iron-dependent metabolic processes, as it requires iron in the form of heme cofactors and Fe-S clusters. Steroids are master regulators of distinct developmental and biological processes. The pulses of steroids regulate cellular metabolism, sexual puberty, inflammation, and stress responses [73–76].

Research in *Drosophila* has dramatically advanced our knowledge about the link between iron and steroids. As described in chapter one, during larval stages, the prothoracic gland (PG), which represents the largest part of an endocrine tissue called the ring gland (RG), releases pulses of ecdysone into the hemolymph [71,79,113]. Like steroids hormones in humans, ecdysone tightly regulates the biological processes and developmental transitions in *Drosophila* [72]. For example, a major pulse of ecdysone at the end of larval life promotes metamorphosis, and a series of minor pulses during the L3 stage regulates physiological and behavioral changes such as the termination of feeding and the commitment to a pupal fate [79,114]. The insect enzymes that produce ecdysone are named Halloween enzymes [79,80]. These enzymes convert dietary cholesterol to the prohormone α-ecdysone. Once the prohormone is taken up into target tissues, the last Halloween enzyme converts it to a biologically active form called 20-Hydroxyecdysone (20E) [79,84,115]. The Halloween genes encode six cytochrome P450 enzymes (P450s), a single short-chain dehydrogenase/reductase, and a Rieske electron oxygenase [79,81,82]. All P450s require heme, and the Rieske electron oxygenase enzyme (Neverland) requires an Fe-S cluster as the cofactors. Furthermore, the mature heme is a porphyrin ring with a ferrous iron at its core [87,88]. Thus, heme and iron are essential components of ecdysone biosynthesis.

3.1.2 Prothoracic gland is a unique tissue to study iron delivery

The ecdysteroidogenic genes are expressed at very high levels in PG cells, comparable to ribosomal gene expression levels. These mass-produced enzymes ensure the peak production of ecdysone (an ecdysone pulse) required for developmental transitions. Consistent with this notion, a microarray analysis indicated that the expression of P450 genes is remarkably high at the end of

the 3rd instar larval stage [84]. This demonstrates that PG cells require a substantial amount of iron for heme biosynthesis. On the other hand, heme is a cytotoxic and hydrophobic molecule that cannot be stored as such. Therefore, iron delivery and heme production have to be synchronized in accordance with the ecdysone production in PG cells. Therefore, cellular iron's dynamic changes for heme production make the PG a remarkable tissue for studying iron delivery and iron homeostasis.

3.1.3 Vesicle trafficking and iron import into the cells

Despite their high demand for iron, the exact mechanism by which PG cells acquire iron is unknown. Iron acquisition likely varies between cells. While some cells use iron importers such as divalent metal transporter 1 (DMT1), others may receive iron from oxidative cleavage of heme or importing iron via transferrin and transferrin receptor process [24,35,116]. Other non-canonical iron-import systems such as iron delivery via secretory ferritin have not been characterized yet. Here I am focusing on the vesicle-mediated iron import into the cells [117]. The small GTPases Rab proteins act as the main components of intracellular vesicle trafficking and protein secretion [14]. Vertebrate Rab5 and Rab11 are considered to be critical for iron delivery [117,118], where they cooperate with transferrin proteins (Tsfs) to import iron into the cells [117]. In the extracellular space, two ferric iron ion [119] bind to apo-Tsf to form the holo-Tsf (also known as the Tsf-Fe(III)). The internalization of the holo-Tsf initiates via binding to a transferrin receptor (TfR) at the cell surface. The uptake is then continued with the formation of early endosomes. Rab5 is recruited to early endosomes to mediate this process. After internalization, Fe(III) is released from the Tsf-TfR into the vesicles and transported to the cytosol via endomembrane iron transporters in the form of ferrous iron[120]. Finally, the apo-Tsf-TfR complex is then recycled back into the plasma membrane. Rab11 has a pivotal role in the trafficking of recycling vesicles to the plasma membrane via microtubules [117]. However, this process has not been demonstrated in *Drosophila* due to lack of a TfR ortholog, despite having three Tsf paralogs (Tsf1, Tsf2, and Tsf3). *Drosophila* Tsf proteins harbor putative iron-binding lobes, but some authors have suggested that they function as antibiotic agents, vitellogenin precursor and juvenile hormone-regulated protein [62]. Studies on *Drosophila* and other insects demonstrated that Tsf proteins are upregulated upon microbial infections to sequester iron from invasive pathogens and function as the immune system protein [62,121]. Besides, insect Tsf proteins have been identified in oocytes and testes and classified as the vitellogenin iron-binding

proteins [62,122]. The insect juvenile hormone further has been shown to reduce Tsfs expression [62,123]. However, whether this hormonal regulation is linked to Tsf proteins iron transport is remained unclear.

Additionally, in *Drosophila* and other insects, Tsf levels increase in the fat body and the hemolymph (insects' blood) under stress conditions such as heat stress, wounding, light and oxidative stresses [62,124]. This suggests that the insect fat body, an equivalent tissue to the liver, synthesizes Tsf proteins and releases them into the hemolymph. Studies on Tsf1 demonstrated that it sequesters iron in the hemolymph upon bacterial infection [61]. Tsf2, on the other hand, resembles mammalian melanotransferrin and has a hydrophobic GPI region that suggests it may be anchored to the membrane and import iron via endocytosis [63,65]. The 3rd paralog, Tsf3, has not been characterized yet.

Another protein that cells use to regulate cellular iron levels is ferritin. Ferritin is an iron 24-subunit nano-cage composed of 12 heavy chains (H) and 12 light chains (L) subunits [64]. In both insects and mammalian cells, the H and L chains are encoded by two different genes [66]. It is predominantly considered that ferritin is a cytosolic protein for iron storage (storing on average 2000 ferric iron atoms, but up to 4500 per cage). However, *Drosophila,* and to a lesser extent, human ferritins, are secreted to the extracellular space via vesicle trafficking [40,116,125]. In *Drosophila*, both H chains and L chains contain the classic secretion signal peptide (SP) required for the ER to Golgi to plasma membrane secretion route. However, mammalian ferritin enter the non-canonical lysosomal secretion path due to the lack of a SP.

Interestingly, the circulatory ferritin is thought to play a decisive role in iron homeostasis [39]. Under normal and iron deficiency conditions, ferritin is believed to be imported into the cells and delivered to the lysosome [48,125]. In insect and vertebrates cells, lysosomal degradation or autophagy is a critical process for protein turnover and degradation [126,127]. The vesicular delivery of proteins to lysosomes occurs via two different processes. Some proteins are engulfed in the vesicles formed in the cytosol and they are then transferred to lysosomes via vesicle fusion [128]. But other proteins are trapped into vesicles that are created with lysosomal membrane invagination upon interaction with endomembrane proteins [128]. It has been shown that the mammalian nuclear receptor coactivator 4 (NCOA4) is the vesicular autophagy receptor of ferritin [129], however, there is no *Drosophila* ortholog of NCOA4. In the lysosome, ferritin is degraded, and then iron is

released. This process is called ferritinophagy, which results in an elevated amount of available cellular iron [49,129]. The ferritinophagy pathway is a branch of autophagy that has not been fully characterized. It is not clear which membrane proteins are recruited to the vesicles to participate in ferritinophagy. However, similar to humans, *Drosophila* Rab11 has a role in autophagosome formation and maturation. Rab11 regulates the transport of recycling vesicles to phagophore, and it has been shown that the fusion of mature autophagosomes to lysosomes is further facilitated with Rab11 [130,131]. Therefore, ferritinophagy may occur in *Drosophila* cells by different proteins.

3.1.4 The link between Evi5 and iron import into PG cells

The Ecotropic viral integration site 5 (Evi5) was originally identified on the 5th chromosome of the mouse as an integration site for Ecotropic viruses [132]. There are two orthologs in humans (hEvi5 and hEvi5-like) and one in *Drosophila* (Evi5), with ~ 59% and 64% protein sequence similarity (Figure 3.1A). Evi5 has two conserved membrane-related domains: a TBC domain and a coiled-coil domain, and has divergent roles in cell cycle regulation, cytokinesis, and vesicle trafficking [132–136]. In human cells, Evi5 is considered an proto-oncogene because of its functions during the cell cycle. hEvi5 has been demonstrated to be a centrosomal protein with a nuclear and cytosolic localization (close to the nuclear envelope) [134,135]. It co-localizes with alpha and gamma tubulins and functions as a component of pericentriolar material [134]. Evi5 further is associated with spindles during mitosis anaphase and remains within the midbody during cytokinesis. The coiled-coil domain facilitates the localization of Evi5 to centrosomes during mitosis and cytokinesis [133]. Therefore, knocking down Evi5 blocks cytokinesis and results in a multinucleated phenotype. *Drosophila* Evi5, in contrast, is a cytosolic protein. It has been shown that Evi5 is an essential effector protein for Rab11 during the migration of border cells in oocytes, and that abolishing *evi5* function blocks border cell migration [136].

It is well established that in vertebrates and Drosophila, Evi5 physically interacts with Rab11 via its TBC domain [132,133,136]. Rab proteins alternate between an active GTP-bound and an inactive GDP-bound form to fulfill their roles in vesicle trafficking. The exchange of GDP with GTP is catalyzed by guanine nucleotide exchange factors (GEFs) [137]. While the GTPase-activating proteins (GAPs) accelerate the Rab proteins' low intrinsic ability to hydrolyze GTP to GDP [137]. The switch between GTP and GDP forms is a prominent feature of all GTPase proteins. Remarkably, ~15% of human cancers are associated with mutations in GEF and GAP proteins [138].

Approximately 173 human genes and 64 *Drosophila* genes encode (~ 0.5 % of all genes) GAP proteins found to function for GTPase proteins of the Ras superfamily (i.e., the Arf, Rab, Ran, Rap, Ras, Rho, and Sar families). However, 51 and 27 genes in humans and *Drosophila* are Rab-specific GAP proteins, since they harbor TBC domains [136,138]. The TBC domain has an arginine residue (IXXDXXR) responsible for the GAP activity and was named after identifying the human Tre-2 oncogene, the yeast Bub2p and Cdc16 spindle checkpoint proteins, which were recognized to contain homologous domains [139].

The interaction between Evi5 and Rab11 indicates a potential link between Evi5 and iron homeostasis. However, no studies have linked Evi5 to steroid hormone production or heme/iron pathways. Interestingly, Evi5 is a high-risk locus for multiple sclerosis (MS). Genome-wide association studies (GWAS) in 38589 subjects have linked intronic and exonic SNPs of the Evi5 locus to MS [135,140–147]. This is potentially intriguing because some researchers have proposed a causal link between iron and MS [148].

Here, I showed that Evi5 is a novel regulator of iron-transporting vesicles in the *Drosophila* prothoracic gland. PG-specific loss of *Evi5* function substantially affects the number, size and morphology of cellular vesicles and blocks secretion of newly synthesized or recycling transferrins. Furthermore, I demonstrated that Evi5 physically interacts with ferritin heavy chain (Fer1HCH) and positive autophagy regulators. Lastly, I will present data suggesting that Evi5 may participate in iron delivery via ferritinophagy.

3.2 Material and methods

3.2.1 Fly stocks and medium supplementation analysis

The flies that I used in this project were either ordered from the stock centers or created in Dr. Kirst King-Jones' lab. To generate knockout allele for Evi5 and Tsf transgenic lines, I used CRISPR/Cas9 and PhiC31 systems, respectively. In all experiments, w^{1118} (#3605) flies were used as controls. Further, *phm22-GAL4* was a gift from Micheal O'Connor's lab. The *phm22-GAL4* is a PG-specific GAL4 driver, and in the text "*PG>"* stands for *phm22-Gal4*.

The list of flies that were created or ordered from the stock centers (Bloomington *Drosophila* stock center, Kyoto Stock center and Vienna *Drosophila* Resource center) is presented in Table 2.1 (Chapter 2, Section 2.1).

A cornmeal standard food was used for expanding fly populaitons, stock maintenance, and setting up crosses to generate desired genotypes. On the other hand, the standard Nutri-Fly food (DGRC) was used for nutrient supplementation studies (*e.g.,* adding iron or iron chelators). A list of used compounds and their concentrations is listed in Table 2.2.

3.2.2 Other experimental procedures

All details regarding protocols for the survival and developmental studies, microscopy analysis, in vivo and ex vivo antibody immunostaining, TEM microscopy, CRISPR/Cas9 Evi5^{FRT}, UAS-Tsf1-3XFLAG, UAS-Tsf2-3XFLAG and UAS-Tsf3-3XFLAG PhiC31 plasmid generation, cloning and bacteria work, S2 cells culture and transfection, immunoprecipitation Mass-spectrometry and PCR and qPCR experiments are described in Chapter 2.

3.2.3 Ongoing experiments and future directions.

A list of experiments that can be carried out as follow-up studies are described in the section 3.5 All the protocols needed for this section are described in chapter 2.

3.3 Results

3.3.1 Loss of Evi5 function in PG cells causes porphyria-like phenotypes and developmental delays

Heme production in animals occurs through eight highly conserved enzymes (Figure 1.4 and Figure 3.3A) [87]. These enzymes first convert Succinyl-CoA and glycine to cyclic structures called porphyrin rings (step 4, 5, 6 and 7 in the pathway). Porphyrins are then converted to heme by the incorporation of a ferrous iron into protoporphyrin IX at the last step in pathway [87,88]. Production of porphyrin rings is essential for life, but they are also highly toxic if they accumulate in cells. Under normal conditions these heme precursors are short-lived thanks to rapid turnover to the next metabolic step. Protoporphyrins emit red autofluorescent light when excited by UV light in the presence of oxygen [90–92]. Red autofluorescence is commonly observed in a group of heme-related disorders known as the porphyrias (chapter 1, section 1.2.3). When the Evi5 expression was impaired with a PG-specific RNAi (UAS-Evi5-RNAi^{VDRC}), I also observed a red autofluorescence phenotype in the PG cells (Figure 3.1D). Furthermore, the ring gland size of RNAi animals was significantly enlarged compared to the control ring glands. This phenotype was similar to what reported for the heme genes *Updo* and *PPOX* (Figure 3.1D) [70].

Evi5 encodes a GTPase activating protein that regulates vesicle trafficking and cell cycle. However, there are no reports showing that Evi5 is involved in the heme biosynthesis process. Therefore, I tried to confirm this phenotype with another non-overlapping RNAi (UAS-Evi5-RNAi^{TRIP}, Figure 3.1B). The 2nd RNAi confirmed the Evi5-RNAi^{VDRC} phenotype. However, the red autofluorescence and ring gland was not comparable to the first RNAi line. The red intensity and RG size of the Evi5-RNAi^{TRIP} were less intense and smaller, respectively (Figure 3.1D).

I further validated these results by creating a conditional mutant line for *Evi5* using the CRISPR/Cas9 system. The FLP/FRT system (Flippase/ Flippase Recombinase Target site) was used to generate the *Evi5* conditional mutant line (*Evi5^{FRT}*). I replaced the endogenous *Evi5* locus with a copy that is flanked with FRT sites. Further, I added sequences encoding three FLAG epitopes at C-terminus and before the stop codon of Evi5 (Figure 3.1C). I then excised the *Evi5* transcription unit with PG-specific expression of FLP. This strategy resulted in red autofluorescening PGs, thus validating the original findings with seen with PG-specific Evi5 depletion via RNAi. The observed phenotype was significantly stronger than the two RNAi lines (Figure 3.1D). Also, this result ruled out the possibility that the autofluorescence was caused by off-target effects, a common problem encountered when using RNAi lines.

In addition to the red autofluorescence, I observed that both PG-specific knockdown and conditional excision of *Evi5* led to a developmental retardation during the late 3rd instar larval (L3) stage. The L3 larvae continued to feed for a longer period before puparium formation (Figure 3.2A). This developmental delay resulted in larger larvae, pupae and adults compared to the control animals (Figure 3.2C and D). The *Evi5^{FRT}* and *Evi5-RNAi^{VDRC}* animals demonstrated stronger developmental lag, ~ 120 hours compared to the control. However, the delayed larvae of the *Evi5-RNAi^{TRIP}* line had approximately 65-70 hours prolonged feeding period before wandering behavior. Furthermore, I observed that in all Evi5-loss-of-function lines, a proportion of larvae attempted puparium formation, but formed abnormal pupae in the process (Figure 3.2C). Approximately 45, 30 and 20 percent of pupae failed to survive to adult flies in the Evi5^{FRT}, Evi5-RNAi^{VDRC} and Evi5-RNAi^{TRIP} lines, respectively (Figure 3.2B).

These results indicated that the Evi5^{FRT} and Evi5-RNAi^{VDRC} lines display a stronger penetrance than the TRIP RNAi line. Therefore, I used these two lines for the majority of the

subsequent experiments. Furthermore, these phenotypes are unique to PG depletion of *Evi5*, and I did not observe similar results for other Rab-GAP proteins in the PG (section 3.3.4, Figure 3.7).

3.3.2 Loss of Evi5 in PG cells induces ALAS expression and reduces expression of Halloween genes

Heme is an essential molecule for the normal function of nearly all cells, as it is a fundamental cofactor for hemoproteins, including the ecdysone cytochrome P450 enzymes (Figure 3.3A) [78,80,149]. When there is a defect in the heme biosynthetic pathway, heme precursors accumulate in all tissues, but with a higher level in tissues with high demand for heme. Indeed, the precursors accumulate due to a negative feedback regulation of the first and rate-limiting enzyme of the heme pathway called Aminolevulinate synthase enzyme (ALAS) [89]. Since PG cells require high amounts of heme to secret the ecdysone pulses, I reasoned that PG-specific loss of *Evi5* function reduces cellular heme levels, and that this in turn induces *Alas* expression. If the heme biosynthetic pathway is blocked downstream of Alas enzyme, the expectation is that this induces ALAS expression which further accelerates the accumulation of protoporphyrins, thus resulting in strong red autofluorescence in PG cells [70]. Further, low levels of heme should impair ecdysone production in PG cells, which would explain the developmental lag of *Evi5*-loss-of-function lines. To test this, the PG-specific expression of Alas was measured in the Evi5-loss-of-function lines via qPCR analysis. I observed 28-, 22- and 8-fold upregulation of *Alas* in PG cells of Evi5-RNAi^{VDRC}, Evi5^{FRT}, and Evi5-RNAi^{TRIP} animals, respectively (Figure 3.3B), suggesting that loss of Evi5 function causes a drop in heme biosynthesis. Furthermore, qPCR analysis indicated that the expression of Halloween genes is significantly reduced when the *Evi5* gene is knocked down or knocked out (Figure 3.3C). In brief, the expression of *Phm* (*phantom*), *Dib* (*disembodied*), *Shd* (*shade*), *Spo* (*spook*), and *Sad* (*shadow*) genes was lowered in the *PG>Evi5-RNAi^{VDRC}* and the *PG>Evi5^{FRT}* animals compared to the control. However, the downregulation of *Phm*, *Dib* and *Shd* genes was more dramatic in the Evi5-RNAi^{VDRC} line than the Evi5^{FRT} line.

The qPCR analysis of *Alas* and the Halloween genes suggests that Evi5 function is required for heme biosynthesis and ecdysone production of the PG cells. Thus, PG-specific loss of *Evi5* function would cause an ecdysone-deficient phenotype since all the cytochrome P450 enzymes (P450) in the ecdysone biosynthesis pathway require heme as a cofactor.

3.3.3 20E and hemin rescue porphyria-like phenotypes and developmental delays of PG-specific loss of *Evi5* function

Reductions in cellular heme and ecdysone production can lead to developmental defects in flies. This happens when the ecdysone concentrations that trigger developmental transitions would be lower than normal, or if a pulse is delayed. I hypothesized that retarded mutant Evi5 populations could be rescued by administering heme and ecdysone. This was tested by adding 20E (20-hydroxyecdysone) or hemin to the diet of mutant $Evi5^{FRT}$ delayed larvae and evaluating the time of developmental progression to pupae and adults (Figure 3.4). Surprisingly, the red autofluorescence of mutant $Evi5^{FRT}$ animals was considerably diminished after 20E feeding, but it nearly disappeared in animals fed with hemin (Figure 3.4A). In agreement with that, adding 20E and hemin to the animals' diet suppressed the *Alas* induction at least four-fold. Specifically, *Alas* expression of $PG>Evi5^{FRT}$ was reduced from 22-fold to 3- and 6-fold in the hemin- and 20E-supplemented media, respectively (Figure 3.4B). The developmental delay of mutant $Evi5^{FRT}$ animals was lowered from ~120 to ~24 and~32 hours upon rearing on the 20E and Hemin-supplemented media (Figure 3.4D). In addition, I observed that 20E-feeding resulted in an approximate ~20% increase in the adult enclosure of the $Evi5^{FRT}$ lines with ~55% in normal food to ~75% in 20E-enriched food. On the other hand, 82 % normal-adult flies appeared (~26% increase) when the delayed $Evi5^{FRT}$ larvae received hemin (Figure 3.4E). This suggests that the pupal lethality is caused by insufficient heme and ecdysone levels.

The diminished porphyria phenotype, *Alas* repression and hemin rescue data led to an intriguing suggestion that the heme deprivation of PG-specific depletion of Evi5 is the reason for the observed ecdysone defect phenotype. This raises two possibilities: A) Evi5 regulates the activity of one or more heme biosynthetic enzymes or its genes; or B) Evi5 has a role in providing iron for heme biosynthesis. Ecdysone synthesis, heme production and iron homeostasis are tightly linked and both processes are regulated dynamically in PG cells. Indeed, dietary iron absorption and then systemic transport and cellular deposition of iron in the PG are coordinated with heme and ecdysone production [70]. I carried out another media analysis to test this hypothesis. I fed the delayed $PG>Evi5^{FRT}$ animals with zinc-protoporphyrin IX (ZnPP). The ZnPP is an analog to heme that has a zinc atom in protoporphyrin IX (PPIX) instead of iron. In normal conditions, the ferrochelatase (FeCH) enzyme, which catalyzes the last step of the heme pathway, incorporates a ferrous iron atom into the PPIX to produce heme (Figure 3.3A). On the other hand, the ZnPP is

produced when the iron levels are insufficient and this acts as the heme oxygenase inhibitor. However, when the iron level is normal, the FeCH enzyme substitutes the zinc atom with a ferrous iron [150–153]. Therefore, ZnPP feeding would result in two possible consequences: 1st if the delayed *PG>Evi5^{FRT}* animals form pupae at the same time as the control animals, it suggests that Evi5 function may be critical for the heme pathway. 2nd if the ZnPP feeding fails to rescue the developmental delay phenotype, it suggests that PG cells' reduced heme levels are caused through iron deficiency. In fact, the ZnPP supplementation neither rescued the delay nor the red autofluorescence (Figure 3.4A). Delayed mutant animals of Evi5^{FRT} line initiated the wandering behavior at 120 ± 5 hours after molting to the L3 stage (Figure 3.4D). Therefore, this suggests that in *PG>Evi5^{FRT}* have reduced heme biosynthesis because of reduced iron levels.

I used *PG>PPOX-RNAi* as the experimental control to ensure that the hemin and ZnPP compounds are effective to analyze the cellular heme content. PPOX catalyzes the formation of PPXI, which is the substrate for the FeCH enzyme (Figure 3.3A). PG loss of PPOX function disrupts the heme production and causes porphyria phenotype (Figure 3.1D), and consequently, results in reduced ecdysone production and larval arrest (Figure 3.4C). Therefore, hemin and ZnPP administration would rescue the *PG>PPOX*-RNAi arrested larvae to the adult stage. The ZnPP supplantation recovered 25% of the *PG*>PPOX-RNAi arrested L3 larvae and upon rearing on the hemin supplemented diet, 46% of the arrested *PG>PPOX-RNAi* animals developed into adult flies (Figure 3.4C).

Lastly, I tested iron feeding on the delayed Evi5^{FRT} animals (Figure 3.4). I reasoned that elevated iron levels in the diet would compensate for the PG iron deficiency and thus rescue the delay and red autofluorescence phenotypes. In contrast, the dietary iron feeding partially decreased (25-30 hours) the observed lag phenotype (120 hours), and animals formed pupae after ~85-90 hours from L3 molting (Figure 3.3D). Furthermore, I observed 20% more pupae after iron administration but the red autofluorescence was still present in the PG (Figure 3.4A and E). Although iron rescued the delay of PG loss of *Evi5* partly, it does not rule out the possibility that Evi5 participates in the iron delivery for heme production of PG cells. Indeed, if the PG loss of Evi5 blocks iron intake or delivery, reduced cellular iron level would not be increased by adding extra iron in the animals' diet.

3.3.4 PG loss of function of Rab5 and Rab11 results in porphyria-like and ecdysone deficient phenotypes

The Evi5 protein contains an N-terminus TBC domain with a GTPase-activating protein (GAP) role [133,136]. The TBC domain of GAP proteins stimulates the intrinsic GTPase function of small Rab proteins to inactivate them during vesicle trafficking (Figure 3.5A). Evi5 physically interacts with Rab11 and acts as a GAP-GTPase for the Rab11 [132,133,136]. In vertebrates, Rab5 and Rab11 proteins are engaged in the systemic iron delivery via endocytosis and exocytosis processes (Figure 3.5A). I examined whether the loss of function of *Evi5* in PG affects vesicle trafficking mediated by Rab5 and Rab11. The depletion of Evi5 in PG cells would elevate the Rab11-GTP fraction as it accelerates the conversion of Rab11-GTP to Rab11-GDP. Therefore, expressing the constitutively active form of Rab11 ($Rab11^{CA}$) in PG cells should mimic $PG>Evi5^{FRT}$ and $PG>Evi5\text{-}RNAi^{VDRC}$ phenotypes. For this I tested $PG>Rab11^{CA}$ animals' developmental progression and the RG phenotype. Interestingly, PG overexpression of $Rab11^{CA}$ caused ~32 hours developmental delay (Figure 3.6). However, I did not observe any red autofluorescence in the RG of $PG>Rab11^{CA}$ animals under UV light. Next, I measured the expression of Rab5 and Rab11 in the RG of Evi5-$RNAi^{VDRC}$ animals via qPCR (Figure 3.5B). The Rab11 expression was significantly lowered in the Evi5-$RNAi^{VDRC}$ but Rab5 expression was unaffected.

Next, I wondered whether knocking down of *Rab5* and *Rab11* genes in the PG would affect the heme and ecdysone pathways. The PG loss of Rab5 function resulted in ~30 hours retardation in the pupae formation (Figure 3.5 C). In *PG>Rab11-RNAi* animals, however, nearly five percent of arrested larvae formed pupae, but all arrested larvae and formed pupae failed to develop into adults (Figure 3.5D). According to a genome-wide RNAi screen conducted by the King-Jones labs and others [154] (Appendix A.1), none of the *PG>Rab5-RNAi* and *PG>Rab11-RNAi* animals had the desired red autofluorescence RG phenotype. It was reported that they have relatively normal RG at the time that enlarged or red autofluorescence RGs are observable in other lines (such Evi5-RNAi at~40-44 hours of L3 stage). However, when I dissected the delayed larvae of *PG>Rab5-RNAi* at the end of the delay period (~65-70 hours from beginning of L3 stage) and the arrested *PG>Rab11-RNAi* larvae when they were 4 days old L3 larvae, the PG porphyria phenotype was detectable under UV light (Figure 3.5E). This result is intriguing because it suggests that in PG cells, Evi5, Rab5 and Rab11 proteins function in the same vesicular trafficking pathway that is essential for sustaining heme and ecdysone biosynthesis. Furthermore, it demonstrated that the

heme precursors accumulate to a lower extent in some RNAi lines with ecdysone deficiency phenotype. In these cases, expanding the time of sample collection might result in a more intense red signal. This result was further confirmed with a qPCR analysis of *Alas* expression in PG loss of *Rab5* and Rab11 animals. Alas was upregulated by 2 and 4 folds in *PG>Rab5-RNAi* and *PG>Rab11-RNAi* animals, respectively (Figure 3.5F).

To further pursue the vesicle trafficking pathway, I carried out two mini-RNAi screens. The first screen was to evaluate the function of all *Rab* genes in the PG cells. In *Drosophila* there are 27 Rab proteins that have a mammalian ortholog and six RabX proteins which have different sequences compared to other Rabs [155,156]. Only one of the RabX proteins (RabX5) has a human ortholog, but the other are only present in *Drosophila* [155]. Out of the 33 Rab lines that were previously covered in our genome-wide RNAi screen only *PG>Rab5-RNAi* and *PG>Rab11-RNAi* exhibited ecdysone deficiency phenotypes (inferred from the genome wide RNAi screening [154], Appendix A.1). On the other hand, depletion of none of *Rab* genes was reported to have enlarged ring gland morphology or porphyria phenotypes at the 2nd round of the screening (carried out by Kirst King-Jones' Lab, Appendix A.1). I attempted to repeat this screening to knock down all 33 *Rab* genes via using RNAi lines from other stock centers that I had not yet tested in the lab (Figure 3.6). The purpose of this mini screen was to evaluate the previous results via examining Rab-RNAi lines that target different regions of mRNA than previous lines (if available). Furthermore, I aimed to knock down the remaining four untested *Rab* genes with new Rab-RNAi lines. Overall, the results of the examined 33 RNAi lines were comparable with the original RNAi screen. In brief, PG-specific depletion of 29 *Rab* genes caused a minor developmental delay (~8 to 16 hours) at the L3 stage, except the *PG>Rab5-RNAi*, which resulted in ~32 hours retardation in puparium formation (Figure 3.6). In addition, *PG>Rab11-RNAi*, *PG>Rab40-RNAi* and *PG>RabX6-RNAi* resulted in the L3 arrested animals that continued to feed and died after approximately ten days (similar to Rab11-RNAi). Taken together this data demonstrated that the function of Rab5 and Rab11 is linked to ecdysone biosynthesis.

In a second RNAi screen, I used the same strategy to knock down all the Rab-GAPs and other effector proteins of Rab5 and Rab11 (GEF proteins) in *Drosophila* (Figure 3.7). The purpose of this RNAi screen was to test whether i) Evi5 is the only GAP protein associated with heme and ecdysone deficiency phenotypes, and ii), the PG-specific depletion of other *Rab5* and *Rab11* effectors (GEF proteins) would result in the red autofluorescence. In *Drosophila*, there are 27

known Rab-GAPs (including characterized proteins such as Evi5 and potential uncharacterized proteins), and five and three GEF proteins for Rab5 and Rab11, respectively. Consistent with the original screen, PG-depletion of 26 GAP-encoding genes neither caused red autofluorescence nor developmental phenotype (Figure 3.7). Msp300 was the only Rab-GAP that, similar to Evi5, exhibited ~50 hours developmental retardation when knocked down in the PG (Figure 3.7). The *Msp300* (Muscle-specific protein 300 kDa) encodes a predicted Rab2-GAP protein that functions in positioning of cellular organelles such as mitochondria within the muscle cells [136,155].

Furthermore, except for *PG > Crag-RNAi* animals, which codes a Rab11 GEF, interfering with the function of all Rab5 GEFs and other Rab11 GEF proteins caused no significant phenotype. Crag is a Calmodulin-binding protein with an N-terminus DENN domain, which governs the nucleotide exchange [157]. *Crag* function contrasts with Evi5's role for Rab11, as it physically interacts with GDP-Rab11 to exchange the GDP to GTP and activates Rab11. The *PG>Crag-RNAi* animals displayed ~60 hours delay at the L3 stage and ~20 percent lethality at the pupa stage, but unlike Evi5, they had no red autofluorescing ring glands (Figure 3.7).

Therefore, this further demonstrates that Rab5, Rab11 and Evi5 function in the same pathway, and they participate in the heme synthesis of PG cells, possibly via iron delivery.

3.3.5 Loss of Evi5 function in PG cells entraps vesicles and increases the vesicle number

I then addressed whether the loss of Evi5 function affects endocytosis and exocytosis in the PG cells. Rab11 is shown to have a pivotal role during the recycling process of vesicles [130,158]. Indeed, in vertebrates Rab5 mediates the internalization of cargos such as holo-Tsf (Tsf-Fe^{3+}) in early endosomes (EE), and Rab11 governs the externalization of the recycling cargos (apo-Tsf) in recycling endosomes (RE) to the plasma membrane [117,118]. I speculated that in PG cells, vesicle trafficking is blocked when Evi5 is impaired. This is because the loss of function of *Evi5* in PG cells has an adverse effect on the Rab11 expression (Figure 3.5B). The blocked recycling process would result in entrapped vesicles in the PG cells and cause a decline in the iron content required for heme and ecdysone synthesis. To test this, I sought to identify a marker for the EE in *Drosophila* cells and conducted an immunofluorescence staining for the hepatocyte-responsive serum phosphoprotein (Hrs). Hrs coordinates the endocytosis process, and it has been demonstrated that it colocalizes extensively with the Rab5 effector protein Early Endosomal Autoantigen 1 (EEA1, also known as Rabenosyn-5) on EE vesicles. Therefore, the Hrs signal can

be used as an EEs marker in PG cells. Hrs immunolocalization indicated an extensive signal in *PG>Evi5*^{FRT} and *PG>Evi5RNAi*^{VDRC} compared to the control (Figure 3.8A). I further supported this by converting the gray-scale image of immunostained RGs to a binary black and white image using ImageJ software (the brain tissues were not included). In a binary-RG image, the black dots represent the Hrs signal in the EE vesicles. I quantified the signals in control, *PG>Evi5*^{FRT} and *PG>Evi5RNAi*^{VDRC} lines (see method section) by dividing the number of black dots in each RG to the area of the RG. This created an index for the EEs in the RG, and I named it the EE-per-RG index. This was approximately six times higher in the *PG>Evi5*^{FRT} and *PG>Evi5RNAi*^{VDRC} RG (Figure 3.8B). Given the increased signal of Hrs, I counted the number of cells in the RG to ensure that the intensified EE-per-RG index is not due to an increase in the number of PG cells. I observed no significant difference between the number of RG cells in PG>*Evi5*^{FRT} and *PG>Evi5RNAi*^{VDRC} animals and control (Figure 3.8C).

Next, I conducted Transmission Electron Microscopy (TEM) to analyze vesicle trafficking in mutant Evi5^{FRT} PG cells and controls (Figure 3.9). The TEM technique was quite challenging as nearly all RG parts were covered under the mesh of the TEM grids. However, I was able to image the PG cells with high magnifications (0.5 to 2 µm). I observed a remarkably high number of entrapped vesicles in the mutant PG cells. In addition to high numbers, the morphology of the vesicles was affected in the mutant cells. Nearly all vesicles in *Evi5*^{FRT} PG cells had a larger size than those in controls. Furthermore, I observed abnormal vesicles with low density lumen, and vesicles with a dark halo around or inside of the lumen (Figure 3.9, image B, D and F). These abnormal dark vesicles resemble the electron-dense iron-containing lysosomes (see section 3.3.10 for more information, Figure 3.14). The TEM analysis also confirmed the increased size of PG cells after knocking out of the Evi5. Lastly, as the second control, I performed TEM analysis on brain cells of the control and mutant *PG>Evi5*^{FRT} animals to ensure that the abnormal vesicles are only present in the *Evi5* mutant PG cells. I observed no difference between control and mutant Evi5^{FRT} brain cells (Figure 3.9, image G and H).

The Hrs immunostaining and TEM microscopy revealed that the vesicle trafficking is severely impaired in the enlarged Evi5 mutant PG cells.

3.3.6 Loss of Evi5 entraps Transferrin proteins in the PG cells

I then addressed whether intercellular iron delivery is affected in the PG cells of mutant Evi5. To test this hypothesis, I used transferrin protein as a tool to check the systemic iron delivery process in PG cells. In the vertebrate cells, Transferrin (Tsf) and Transferrin-Receptor (TfR) are the major players of systemic iron delivery [29–31]. While Rab5 facilitates the endocytosis of holo-Tsf, Rab11 recycles apo-Tsf back to the plasma membrane [117,118]. Despite the absence of the TfR in *Drosophila*, there are three paralogous transferrin proteins in flies (Tsf1, Tsf2, and Tsf3). Evidence in insects suggests that Tsf1 is expressed in the fat body and released into the hemolymph as an immune responsive protein [61,62,159]. In the hemolymph, Tsf1 functions as an antimicrobial protein that limits iron for pathogens [121]. However, it has not been demonstrated whether Tsf1, Tsf2, and Tsf3 enter/leave the cell via endocytosis and exocytosis. Therefore, I examined whether vesicles observed in the PG>$Evi5^{FRT}$ larvae contain Tsf proteins. For this, I created transgenic lines for Tsf proteins with three N-terminus FLAG tags (UAS-3XFLAG-Tsf1, UAS-3XFLAG-Tsf2 and UAS-3XFLAG-Tsf3). I had generated them originally to express the transgenes in the PG cells (see the method section) since the endogenous PG-expression of Tsf1, Tsf2, and Tsf3 is low, and there are no antibodies available to recognize them. However, I could not detect transgenic proteins with either the FLAG immunostaining or the western blot analysis despite being transcriptionally expressed. A search on Tsf protein sequences revealed that all three proteins possess a secretory signal peptide (SP) at the N-terminus (Figure 3.10A). The signal peptide is approximately 20-30 amino acids (AA) and is cleaved off from the N-terminal part of the peptides [160,161]. This cleavage process is critical for the entry of newly synthesized proteins into the secretory pathway [160,161]. This indeed explains why transgenic Tsf proteins were undetectable as they had N-terminus 3XFLAG tags that were cleaved off. I further proved this by conducting an ex vivo assay using S2 Schneider cells (Figure 3.10B and C). I created three S2 cell transfection constructs for Tsf1. I added three FLAG epitope tags to the N-terminus and an eGFP to the C-terminus of the wild-type Tsf1 (named it Tsf^{WT}*). Additionally, I made two mutant constructs by removing the secretory signal-peptide (first 30 AAs between) and tagging the N-terminus of one them with 3XFLAG ($Tsf1^{\Delta SP1}$) and the C-terminus of the other one with eGFP ($Tsf1^{\Delta SP2}$). Upon immunostaining the transfected S2 cells, I observed that the Tsf1 protein is strongly recognizable when the signal peptide is removed (Figure 3.10C).

Therefore, I created C-terminally FLAG tag transgenic lines (UAS-Tsf1-3XFLAG, UAS-Tsf2-3XFLAG and UAS-Tsf3-3XFLAG) to test the function of Evi5 in the intercellular iron delivery.

I next sought to combine all three transgenic lines with the $Evi5^{FRT}$ line since approximately 46% of delayed *PG>Evi5^{FRT}* larvae develop into adults (knockout adults $Evi5^{KO}$). I used the $Evi5^{KO}$ flies to create $Evi5^{K}$; UAS-Tsf-3XFLAG and $Evi5^{K}$; phm22-GAL4 flies. These flies were crossed, and their progenies were used as the experimental samples. As controls, the progenies of phm22-GAL4 and UAS-Tsf123-3XFLAG cross were used (i.e., *PG>Tsf123-3XFLAG*). Next, I collected BRGC and hemolymph from the experimental and control animals. The BRGC samples were subjected to FLAG immunostaining, and the hemolymph samples were used for the Western blot analysis. The results strongly supported that in the $Evi5^{FRT}$ animals Tsf proteins are predominantly entrapped in vesicles of the PG (Figure 3.11A). In the control samples proteins were not detectable in the PG cells, which demonstrated that they were secreted into the hemolymph (Figure 3.11A). However, in the Western blot analysis, I identified Tsf proteins in the hemolymph of control and not in the *Evi5* mutant PG cells. In the hemolymph Western blot analysis, I further identified multiple protein bands for Tsf1 and Tsf3 (Figure 3.11B). According to Flybase, the protein size of Tsf1 and Tsf3 are 71.8 kDa and 81.1 kDa, respectively. There were two bands for Tsf1-3XFLAG; an intense protein band with an approximately 35 kDa and a 70.1 kDa band. But, I found an approximately 10 kDa and 81.1 kDa protein bands for the *PG> Tsf3-3XFLAG* animals (Figure 3.11B). The cleavage of Tsf proteins in the hemolymph suggests that Tsf1 and Tsf3 probably undergo the post-translational modifications.

These data suggest that Evi5 is recruited to Tsf protein-containing vesicles in the PG and loss of Evi5 function disrupts secretion and recycling of Tsf proteins (Figure 3.11C). It further demonstrates a paramount role for Evi5 in regulating iron delivery coupled with heme and ecdysone biosynthesis in the PG cells.

3.3.7 Evi5 is recruited to the vesicles that contains Tsf1, Tsf2, and Tsf3

I then addressed whether Evi5 colocalizes with newly synthesized Tsf proteins in cells to function in the iron transport. As mentioned in the previous section, *Drosophila* Tsf proteins harbor a secretion signal peptide that facilitates protein release to the extracellular space. Secretory proteins are translated, modified and folded in the ER and then transported to the Golgi for further

modifications. The proteins are finally released to the extracellular space via secretory vesicles [162]. Furthermore, none of the *Drosophila* Tsf proteins has been studied in detail, and whether they are entering the classical secretory pathway mediated by the ER and Golgi is unclear. Therefore, studying the subcellular localization of Tsf proteins is an extensive challenge because they are not easily detectable in the cytoplasm (as shown in the control PG cells in Figure 3.11A).

I carried out an in-vivo co-transfection assay to study the colocalization of Evi5 with Tsf1, Tsf2 and Tsf3. I created an S2 cell transfected construct for Evi5 by tagging the cDNA with a mCherry tag at the C-terminus part (Evi5-mCherry). However, for the Tsf proteins, I first deleted the signal peptide from the cDNA sequences, and then I tagged the proteins' C-terminus with an eGFP tag (Tsf1$^{\Delta SP}$-eGFP, Tsf2$^{\Delta SP}$-eGFP and Tsf3$^{\Delta SP}$-eGFP). I further included the eGFP protein as a control to ensure that the possible colocalizations are not a false positive due to the high expression of proteins.

Interestingly and in agreement with previous results, when I co-expressed the Evi5-mCherry transgene with each Tsf$^{\Delta SP}$-eGFP protein in S2 cells, Evi5 was predominantly recruited to Tsf-positive vesicles (Figure 3.12). Both Evi5 and Tsf proteins have cytoplasmic and vesicular distributions with a punctuated pattern. However, I observed that Evi5 colocalizes with Tsf1 considerably stronger than the Tsf2 and Tsf3 proteins. Further, it seems that the colocalization of Evi5 and Tsf3 is stronger compared to the Evi5 and Tsf2 colocalization. On the other hand, despite the predominant cytosolic presence of eGFP, I observed no co-localization for Evi5-mCherry and control eGFP (Figure 3.12). Therefore, this data suggests that Evi5 regulates the vesicle-trafficking required for iron import to the PG cells.

3.3.8 Evi5 Interacts with Fer1HCH

To further investigate the function of Evi5, I carried out immunoprecipitation with *in vivo* and *ex vivo* samples followed by MALDI-TOF Mass-spectrometry (IP-MS). I sought to identify the proteins that would interact with Evi5 to shed light on the function of Evi5 in iron transport. For this, I used the anti-FLAG affinity beads to immunoprecipitate the knocked-in protein in the Evi5^{FRT} larvae (40-44 hours L3 larvae) and the protein overexpressed in the S2 cells. As controls, I used the wild-type flies with no FLAG-tagged protein for the in vivo assay, but I used the eGFP protein C-terminally tagged with FLAG as the control for in vivo experiment. I analyzed the results in parallel to identify the ex vivo- and in vivo-specific proteins as well as to find proteins that are

common between the two assays. In both experiments, I removed all proteins that were identified in the control samples to remove the false positives. I identified 105 and 75 interacting proteins via the in vivo and the *ex vivo* assays with 18 proteins in common (Figure 3.13A). In this section, I will focus only on the high MS score proteins (top ten proteins) and proteins with known or plausible links to iron biology.

In general, and consistent with previous reports, proteins involved in vesicle trafficking, cell cycle regulation, border follicle cell migration, and microtubule-cytoskeleton organization were present in the Evi5 interactome (Table 3.1). Moreover, the presence of proteins that were reported to interact with Evi5 further supported the IP-MS experiments. Lastly, a gene ontology analysis of the two datasets demonstrated that the protein hits are highly enriched for GO terms relevant to the function of Evi5 (Figure 3.13C). In brief, the ten high-scoring interacting proteins of the *in vivo* experiment were Cindr, Pzg, Evi5 (as expected), Chc, CCT5, CG8036, Hsc70-4, Unk, Dap160 and CG34417 (Figure 3.13B). Among this set, Cindr is a member of the CD2AP/CIN85 family, and similar to Evi5, it has a function in the border follicle cell migration in oocytes. In addition, and in agreement with Evi5 function in vesicle trafficking, Chc (Clathrin heavy chain) and Hsc70-4 (Heat shock protein cognate-4) have a role in the organization of secretory granules from the Golgi [163,164]. Chc and Hsc70-4 are components used for autophagy. While Chc is required for autophagosome formation, Hsc70-4 targets proteins to lysosomes [165,166]. These data suggest that Evi5 may have a role during autophagy (see section 3.5).

CCT5 is also a member of the chaperonin coating protein family that binds to Hsp60 and functions in the organization of myosin-containing myofibrils [167]. However, the Dap160 protein is a Dynamin-associated protein and mediates synaptic vesicle transport in a Clathrin-dependent manner to import calcium into presynaptic cells [168]. As to the cell cycle function of Evi5, the Pzg (Putzig) is a nuclear protein that localizes on polytene chromosomes to regulate the expression of genes involved in the endocytosis of receptor-mediated signaling pathways such as JAK-STAT signaling. [169]. The uncharacterized CG8036 protein is also suggested to regulate chromatin silencing. Furthermore, human Evi5 physically interacts with cytoskeleton components with GTP binding ability, such as α and γ Tubulins [134]. Similarly, the CG34417, which is an uncharacterized protein and is predicted to have a role in the actin cytoskeleton organization of *Drosophila* cells (inferred from the Flybase database).

On the other hand, the top ten high score proteins that were pulled down in the ex vivo experiments are Zip, Evi5, β-tubulin, Jar, Hsc70-1, CG1737, CG8038, CG34417, CTT5 and Akap200 (Figure 3.13B and Table 3.2). The CCT5, CG8038 and CG34417 proteins were present in the high score proteins of the S2 cells experiment. The Zipper protein (Zip) binds to the myosin light chain in the cytoskeleton and positively regulates the follicle border cell migration [167,170]. β-tubulin is predicted to be a GTP-binding protein, and this suggests that Evi5 possibly functions as GAP protein upon the incorporation of β-tubulin into microtubules. Furthermore, Zip, Jar, and Akap200 regulate actin cytoskeleton organization, but Jar was further inferred to regulate vesicle trafficking across the actin filaments. The Hsc70-1 is predicted to be involved in protein folding and vesicle trafficking. There is no information for the CG1737 protein.

It is well established that the conversion of Rab11-GTP to Rab11-GDP is facilitated via physical interaction of Evi5 with Rab11 on the vesicle surface [132,136]. Rab11 is a pivotal Rab protein for various biological processes, including border cell migration, cytokinesis, endocytosis and exocytosis vesicle trafficking. To do this, it localizes to recycling endosomes, the Golgi apparatus, microtubules, centrosomes, the nuclear envelope and the plasma membrane [158,171]. I also observed the Rab11 protein in the original Evi5 interactome data sets. However, Rab11 was identified in the ex-vivo control and therefore was removed from the Evi5-specific hits. Moreover, Rab11 appeared not to be a high scoring protein in the interactome list. This could be possibly explained by the fact that Evi5 interacts only with the GTP-Rab11 form.

There were five proteins of the top ten high score proteins in the overlap subgroup (Akap200, Unk, CCT5, CG8036 and CG34417 proteins). Furthermore and surprisingly, in this subgroup I identified that Evi5 specifically precipitates Fer1HCH, but it was not in the list of top score proteins (Table 3.1 and Table 3.2). *Fer1HCH* encodes one of the two subunits of Ferritin protein that catalyzes the Fe^{2+} to Fe^{3+} conversion upon iron storage in the ferritin protein [43,172]. Interestingly, similar to mammalian ferritin that is secreted to the serum, *Drosophila* ferritin is secreted to the hemolymph [67]. It is worth mentioning the mammalian ferritin is predominantly existing in the cytoplasm and stores iron [67]. However, it has been proposed that the secretory ferritin may function as an immune response protein to sequester iron from pathogens or may function as an iron transporter [67]. The identification of Fer1HCH in two independent IP-Spec experiments provides additional evidence that Evi5 is recruited for iron transport. More

interestingly, I identified the small GTPase Rab14 (Table 3.1). As reported previously, the Rab14 has been demonstrated that interacts with Evi5 [155]. Rab14 has a high sequence similarity to Rab11 and functions in the defense response to bacteria, recycling and Golgi-to-endosome vesicle transport [173]. Furthermore, mammalian Rab14 functions in the transferrin recycling pathway similar to Rab11 [173]. Moreover, I found Snap29, tral and Gel proteins in the overlap hits (Table 3.1 and Table 3.2). Like the CG34417, all these proteins function in the exocytosis and microtubule-cytoskeleton organization [174].

Furthermore, the interactome data is consistent with the idea that Evi5 governs various aspects of vesicle trafficking. And consistent with the colocalization of Evi5 and Tsf proteins, the finding that Evi5 interacts with Fer1HCH supports the notion that Evi5 is recruited to vesicles that contain iron proteins.

3.3.9 Identifying the transferrin receptor in *Drosophila*

Tsf proteins are glycoproteins with two identical iron-binding domains that carry two ferric irons (Fe^{3+}) [29,30]. Upon the release of apo-Tsf proteins to the extracellular spaces via exocytosis, they bind and deliver iron (holo-Tsf) to various cells by binding to their specific cell surface receptor (TfR) [33,34]. The presence of TfR is a necessity for holo-Tsfs iron delivery as it facilitates the endocytosis into early endosomes. While transferrins are present in *Drosophila*, whether *Drosophila* has a non-canonical transferrin receptor remains a mystery. Since Evi5 colocalizes with vesicles that carry Tsf proteins for secretion, I hypothesize Evi5 further participates in recycling an unknown Tsf receptor to the plasma membrane. Therefore, I sought to identify the putative receptor/receptors and test whether they can colocalize or interact with Evi5. To do this, I used the UAS-Tsf1-3XFLAG, UAS-Tsf2-3XFLAG and UAS-Tsf3-3XFLAG transgenic lines and overexpressed the proteins ubiquitously. I then collected 40-44 hours L3 larvae and conducted an IP-MS experiment, and similar to the Evi5 in vivo assay, I used larvae with no transgene as the control. After removing the proteins present in the control samples from experimental protein lists, I found 85 and 63 interacting proteins for Tsf1 and Tsf3, respectively. Unfortunately, my experiment failed to pull down Tsf2. I will repeat this experiment as described in the future direction.

Next, I investigated the Tsf interactome data sets to identify cell surface receptor proteins or proteins involved in the endocytosis process. In the Tsf1 pulled down proteins, I identified

Cindr, Eps-15, and GCS2β proteins. Cindr and Eps-15 have a significantly high MS score (Table 3.3). Surprisingly, Cindr was coimmunoprecipitated in the Evi5 in vivo IP-MS experiment (see section 3.3.8). The Cindr protein is not a receptor, but it is an adaptor cell surface protein that binds to actin and is required for the cytoskeleton organization [175]. However, Cindr functions in the synaptic vesicle endocytosis and *cindr* mutant cells exhibit endocytosis defects [175]. This suggests that Cindr might be required for the endocytosis of Tsf1 as well. Likewise, the Eps-15 (Epidermal growth factor receptor pathway substrate clone 15) is an adaptor cell surface protein that interacts with Dynamin and Dynamin-associated protein 160 (Dap160) to form the presynaptic endocytosis complex [168,176]. Eps-15 is indeed an essential component of endocytosis, and mutant flies for Eps-15 demonstrated impaired vesicle endocytosis [168]. Surprisingly, mammalian Eps-15 is predicted to interact with Transferrin and disruption of its function blocks the internalization of Tsf into the cells [R38]. Therefore, this indicates an essential role for the Eps-15 during the endocytosis of Tsf protein. Surprisingly, the Eps-15 partner, Dap160, was precipitated according to the Evi5 in vivo IP-MS data (Table 3.3), even though I did not find Eps-15 itself in the interactome data.

On the other hand, the Glucosidase 2 β subunit (GCS2β) has a Low-density lipoprotein receptor class A domain (inferred from the InterPro database) and is predicted to be a member of the glucosidase II complex. This further supports the vesicular colocalization of Evi5 and Tsf proteins. The glucosidase II complex is an ER complex that removes glucose residues from newly synthesized glycoproteins like Tsf proteins [177]. Therefore, I hypothesize that GCS2β may be involved in the ER Tsf modification rather than acting as a receptor.

Finally, I found the Eps-15 in the Tsf3 interactome with the highest score in the list (Table 3.4). This indicates Eps-15 cooperates in the vesicle-mediated endocytosis of Drosophila Tsf proteins. Interestingly, I identified two transmembrane related proteins; Vap33 and CG13887 (Table 3.4). The Vap33 is a vesicle membrane-associated protein that localizes to the ER, Golgi and the lateral edge of the plasma membrane [178]. It has been shown that Vap33 is required for the quality control of newly synthesized secretory proteins in the ER [178]. CG13887, however, is an uncharacterized protein that is inferred to mediate the ER to Golgi vesicle transport due to having an ER membrane domain (Flybase). This protein was present in the in vivo protein list of Evi5 and further confirmed the colocalization of Evi5 and Tsf3 analysis. Interestingly, CG13887 is the

ortholog of the human B-cell receptor-associated protein 31 (BCAP31), which is a member of the B-cell receptor associated protein superfamily. The BCAP31 encodes a multi-pass transmembrane protein and is localized in the endoplasmic reticulum and plasma membrane [179].

These data identified the endomembrane proteins that interact with Tsf proteins, particularly those required for protein maturation and transport from the ER to Golgi and to the Plasma membrane. Notably, the interaction of Tsf1 and Tsf2 proteins with Eps-15, a critical component of the endocytosis process, suggests that this interaction is fundamental for iron import via transferrin.

3.3.10 Evi5 may facilitate iron release via ferritin autophagy

Here, I will present only preliminary data about the function of Evi5 in this process. However, I will plan to conduct further experiments to pursue this goal (see future directions).

TEM analysis of control and *Evi5*^{FRT} mutant cells revealed that there are many electron-dense vesicles in PG cells. While these homogeneously dense structures are highly uniform in the control, they are abnormally dispersed in the cytosol of mutant cells and have variable densities (Figure 3.9). By looking more closely at mutant cells, these structures have a larger size than control and show heterogeneous density. They vary from almost light (not dense) to remarkably high electron-dense structures. Using a TEM microscope, I demonstrated that the electron-dense vesicles resemble lysosomes in size and shape with residual bodies that probably arose from autophagosomes and secondary lysosomes (Figure 3.14). Interestingly, these electron-dense lysosomes are similar to the lysosomal ferritin that are termed siderosomes [180,181]. Siderosomes have an acidic lysosomal lumen that contains undigested holo-ferritin, hemosiderin (completely digested ferritin) and iron-containing compounds [181]. This is in line with the interaction of Evi5 with ferritin.

Siderosome and hemosiderin are terms describing different aspects of ferritin autophagy (ferritinophagy) during iron depletion. Indeed, electron microscopy analyses suggested that iron-loaded holoferritin could be transferred into lysosomes via ferritinophagy process [182]. In mammalian cells ferritin is shown to enter lysosomes via binding to NCOA4, a lysosomal receptor [48]. Studies in mice demonstrated that mutations in NCOA4 impairs systemic iron homeostasis and induces anemia [183]. This suggests that ferritinophagy can occur in the normal and iron-depleted

conditions. However, the underlying mechanism of ferritin iron recovery in these conditions is yet unknown.

Ferritin autophagy has not been described in *Drosophila,* but may very well exist. The interaction of Evi5 with Chc, Hsc70-4 and Fer1HCH is intriguing because it provides evidence for the Evi5-mediated ferritinophagy in *Drosophila*. Both Chc and Hsc70-4 interact with Evi5 via a remarkably high MS score (Figure 3R.16). The *chc* encodes the heavy chain of Clathrin, which is a major player in the endocytosis machinery. Clathrin, along with other cytoskeleton components such as dynamin, participates in protein lysosomal degradation [165]. The Clathrin and dynamin are shown to regulate the initiation of autophagosome formation and their fusion to primary lysosomes [165]. Surprisingly, I found dynamin (encoded by *Drosophila shibire* or short *shi*) in the interactome data set, but its MS score was not as high as that of Chc. Furthermore, Hsc70-4 is a cochaperone that localizes in the endosomes and functions in the generation of multivesicular bodies that are targeted to lysosomes [166]. Consistent with this, Rab11 has also been demonstrated to orchestrate the endosomal trafficking between autophagy and the recycling process [131].

All these data support the idea that Evi5 further plays a regulatory role in PG cells' iron release via ferritinophagy. I hypothesized that the developmental defect and porphyria phenotypes of PG loss of *Evi5* is caused by a defect in the lysosomal degradation of ferritin. Notably, ferritinophagy releases a large amount of iron into the cells under different conditions [47], as iron saturated ferritin harbor ~4500 iron atoms. Since at certain times PG cells need substantial iron amounts for heme and ecdysone biosynthesis, the lysosomal degradation of ferritin probably provides a large volume of iron for PG. It is plausible that Evi5 directs the holo-ferritin to lysosomes in order to restore iron into the cytosol prior to the ecdysone production surges (see section 3.4.2).

3.3.10.1 Ferritinophagy may be required for PG cells

Selective autophagy is a routine cellular process for protein turnover. In brief, first, a membrane structure, termed phagophore, is formed to engulf proteins. The phagophore is then progressed into double-membrane vesicles called the autophagosome. The autophagosomes are non-acidic vesicular structures that carry cargos for lysosomal degradation. Lastly, the autophagosomes are fused to primary lysosomes and form autolysosomes. The proteins that are

delivered for degradation are hydrolyzed within the acidic environment of lysosomes. The resulting components such as iron can be reused for different biosynthetic pathways [184–187].

To test for ferritinophagy, I first asked if autophagy and ferritin functions are required for PG cells. The *Fer1HCH* and *Fer2LCH* encode heavy chain and light chain subunits of ferritin. According to the genome-wide RNAi screening [154] (appendix A.1 section), knocking down Fer1HCH in PG cells causes L2 developmental arrest and a strong ecdysone deficiency phenotype. But PG knockdown of Fer2LCH causes no phenotype. Furthermore, in *Drosophila*, there are 17 autophagy-related proteins (Atg) that are key components of the autophagic machinery. They regulate the initial formation and elongation of phagophores, and further, they participate in autophagosome generation [184]. Out of 17 genes, PG-specific RNAi targeting *Atg7*, *Atg8a*, and *Atg14* results in pupal lethality, L2 arrest (similar to PG depletion of *Fer1HCH*), and L3 arrest, respectively [154]. Interestingly, Atg8a is a key player of selective autophagy [188] and its human ortholog GABARAP physically interacts with lysosomal ferritin receptor NCOA4 [129]. In agreement with these data, *PG>Chc-RNAi* animals show L3 developmental delay and pupal lethality, but *PG>Hsc70-4-RNAi* animals are L2 arrested (according to the RNAi screening).

I have evidence that Hsc70-4 interacts with ferritin indirectly. I conducted an ex vivo IP-MS experiment for two iron-responsive heat shock proteins, Hsp22 and Hsp70, and I found that they interact with Fer1HCH (See section 4.3.4 in chapter 4). Hsp22 and Hsp70 form a complex and have a role in transferring the Fe-S cluster to other proteins [53,189,190]. Furthermore, they are involved in protein turnover through chaperone-mediated autophagy [127,128]. I found that Hsp22 interacts with Fer1HCH and further confirmed the interaction via co-IP assay (Figure 4.5). Surprisingly, the Hsc70-4 physically interacts with Hsp22 and Hsp70 with a significant MS score (Figure 4.5).

These data suggest that Evi5 plays a central role during ferritinophagy via interacting with ferritin and proteins involved in autophagy.

3.3.10.2 Iron deficiency may induce ferritinophagy in PG cells

Autophagy is mainly activated when cells experience nutrient starvations to provide nutrients by turning over dysfunctional proteins and organelles [191]. Therefore, autophagy plays a critical role in cellular nutrient homeostasis [191]. I hypothesized that iron starvation drives ferritin

to the lysosomes in PG cells to utilize stored iron in the ferritin cages. Several studies in mammalian cells indicated that ferritin is degraded within lysosomes under iron chelation treatments [47,192]. Consistently, I have rudimentary data suggesting that induced iron deficiency via iron chelator affects PG cells' ferritin level. As it is explained in chapter 4 (dietary iron RNA-sequencing project), I used a Fer1HCH GFP-trap allele, Fer1HCH^{G188} [193], to observe ferritin response to dietary iron manipulation (Figure 4.9). I reared Fer1HCH^{G18} flies in the iron-depleted medium (BPS food, see method) for five generations and transferred animals in high iron level (FAC medium), and imaged their BRGC (See section 4.3.8.3 in Chapter4). The brain's GFP signal did not change significantly, but I observed a slightly stronger signal in the RG cells upon iron feeding (Figure 4.9, Figure 3.15A). The elevated GFP signal indicates ferritin is expressed in the RG when the iron level is high. However, the reduced GFP signal in the low iron condition barely supports ferritinophagy as it should be comparable to the GFP signal in normal food. Unfortunately, I did not evaluate the Fer1HCH^{G18} flies in basal iron conditions due to the RNA-sequencing experimental design (see section 4.3.8.3 Chapter 4). However, studies on GFP signal indicated that the GFP signal is depleted in the acidic environments [194]. This is in agreement with the acidic lumen of lysosomes and suggests that Fer1HCH-GFP is targeted to lysosomes in the BPs medium, but it should be studied with further details (see section 3.5.2).

Iron deficiency also exacerbates the developmental delay and pupae lethality of the *PG> Evi5-RNAi^{VDRC}* animals. I tested *Evi5-RNAi* animals similar to what I did for the control flies in the RNA-seq experiment (chapter 4). I raised the *Evi5-RNAi* flies in a low iron diet, and after each generation, I evaluated the PG loss of *Evi5*. After three generations of iron deficiency, the puparation rate of *PG>Evi5-RNAi* dropped from ~85% to ~30%, and the adult survival rate decreased from ~71% to 12% (Figure 3.15C). I was able to recover the lethality of *PG>Evi5-RNAi* animals upon iron and hemin supplementation. However, the rescued animals still exhibited developmental delays (Figure 3.15B). These were curiosity-driven experiments as the RNA-Seq project had no link to the Evi5. It is worth mentioning that wild type flies further exhibit developmental delay and lethality after being reared in the low iron diet for five generations (Figure 4.1). This suggests that depletion of Evi5 in PG cells enhances the susceptibility of iron scarcity in flies.

3.4 Discussion

3.4.1 Evi5 a novel regulator of cellular iron homeostasis

Previous studies demonstrated various functions for the Evi5-Rab11 complex during the cell cycle, cytokinesis and follicle border cell migration [132–136]. In this study, I identified novel and critical functions for Evi5 in systemic iron homeostasis. Evi5 is the only TBC RAB GAP whose dysfunction causes heme precursors accumulation and a porphyria phenotype. I demonstrated that Evi5 is predominantly recruited to the secretory vesicles of the ER-Golgi-plasma membrane path that contains transferrin proteins. Furthermore, I indicated that abolishing Evi5 blocks the secretion and recycling routes and results in an abundant number of engulfed vesicles. This decreases the intracellular iron level in the Evi5 PG cells and progresses in the heme and ecdysone deficiency phenotypes. The mutant phenotypes can be rescued significantly with hemin administration and partially with iron feeding, which further supports the impaired intracellular iron homeostasis of mutant cells.

The entrapped vesicles with abnormal dark regions in Evi5 mutants are identical to the electron-dense iron-containing lysosomes called siderosomes. The siderosomes are insoluble ferritin/iron-rich lysosomal vesicles that are mainly formed under iron overloaded conditions. I showed that Evi5 interacts with ferritin and loss of its function in PG, a tissue with high iron demand, resulting in engulfing insoluble iron-rich vesicles. In agreement with this, my results provided molecular insights into the Evi5 mediated iron recovery via ferritin autophagy. This idea is supported by the interaction of Evi5 with Clathrin, dynamin and co-chaperone Hsc70-4 that regulate vesicle trafficking required for protein lysosomal degradation. In line with this, Hsc70-4 interacts with ferritin via its cognate iron-responsive chaperone proteins, Hsp22 and Hsp70. On the basis of these findings, Evi5 may regulate the cross-talk between protein recycling to the plasma membrane and ferritin iron turn-over in PG cells. The interaction of Tsf1 and Tsf3 with Eps-15 further supports this model. Eps-15 is a plasma membrane protein that interacts with different endocytic proteins and recycles back to the plasma membrane [168]. Identifying the interaction of Eps-15 dynamin associated partner, Dap160, with Evi5 further supports the role of Evi5 in vesicular iron import via endocytosis and exocytosis.

The interaction of *Drosophila* Tsf proteins with Eps-15 also provides new evidence about the unknown endocytic process of Tsf proteins. Unlike mammalian cells, the *Drosophila*

transferrin receptor is yet unidentified, and Eps-15 may be the hitherto receptor. Future studies will be needed to address this hypothesis.

Evi5 is considered a high-risk gene for multiple sclerosis disease (MS). MS is a neuroinflammatory disease that has an adverse effect on oligodendrocyte and myelin [195]. MS patients have elevated ferritin levels (hyperferritinemia) in the cerebrospinal fluid and also display iron accumulation around the plaques [195,196]. Interestingly, there are numerous iron-loaded ovoid structures around the lesion of myelinated white matter in MS patients that resemble the engulfed vesicles I observed in the Evi5 mutant PG cells. Therefore, this study may open new insights into the link between iron accumulation and MS disease.

3.4.2 A proposed model for Evi5 role in Ferritin autophagy

The proteins found in the interactome data of Evi5 and Tsf proteins enabled me to propose two non-mutually exclusive models for the function of Evi5 in PG cells (Figure 3.16). During the 3rd instar larval feeding phase, Evi5 participates in iron import by governing the secretion and recycling of transferrin. The Eps-15/Dap160 endocytic complex facilitates internalization of holo-Tsf proteins in early endosomes. Next, Rab5 acts in regulating early endosome trafficking and sorting. The acidic environment inside endosomes advances iron release form holo-Tsf into the cytosol. The vesicular Eps-15/Dap160/Tsf complex is then recycled to the plasma membrane. Rab11 and Evi5 are recruited to these vesicles, and interaction of Evi5 with Rab11 and Dap160 is essential for the trafficking of the recycling vesicles. In this period, PG cells do not require abundant amounts of iron as the ecdysone pulse occurs at the end of the L3 stage. Imported iron in the cytosol is then utilized for different cellular iron requirements, and further is stored in ferritin (Figure 3.16A). In contrast to mammalian ferritin that is predominantly a cytosolic protein, the insect ferritin is mainly secreted to the extracellular space [67]. Therefore, the cytosolic ferritin in PG cells should be imported into the cells. It is also possible that there is also cytosolic ferritin outside the ER, but there is no evidence for this yet.

I hypothesize that prior to a major ecdysone pulse, ferritin is targeted to lysosomes to release the stored iron for heme synthesis. Ferritin is either imported into newly formed vesicles or entrapped into the endosomal vesicles. These vesicles are then targeted to primary lysosomes, and interaction of Evi5 with ferritin, Clathrin and Hsc70-4 are critical for the autophagy pathway. Given the fact that transferrins only bind to two ferric ions and ferritin binds to ~4500 ferric irons,

the ferritinophagy route would release substantial amounts of iron for heme synthesis (Figure 3.16A).

Another possible model is that ferritin itself functions in the systemic iron delivery for PG cells (Figure 3.16B). There is evidence that ferritin may function in extracellular iron trafficking. The mammalian and *Drosophila* ferritins are secreted to the extracellular spaces, and it has been shown that secretory ferritins are elevated in response to iron or pathogens [40,67,125]. However, the mechanism underlying ferritin iron trafficking is not characterized yet, as the endocytic pathway is still unknown. It is possible that PG cells synthesize and secrete holo-ferritin to the extracellular space, which may occur in iron-replete conditions. Holo-ferritin is then entered into the cells via an unknown mechanism, possibly through a receptor mediated endocytosis in the early endosomes. Next, the vesicles are directed to lysosomes for iron utilization, and Evi5 and Rab11 are required for this specific autophagy route.

The PG loss of function of Evi5 affects the vesicle trafficking of both models adversely. It results in the accumulation of engulfed vesicles that are not targeted to their cognitive pathway efficiently, and further promotes the formation of abnormal lysosomes. This would reduce the iron level and impair heme and ecdysone production. Therefore, mutant Evi5 animals develop very slowly and display a porphyria phenotype in the PG.

3.5 Future directions

This section's main objective is to describe experiments that I will carry out to pursue the function of Evi5 in ferritin autophagy.

3.5.1 Validating protein-protein interactions

I carried out several IP-MS experiments to identify protein partners of specific proteins. To further confirm protein-protein interactions, first, I will generate Schneider S2 cell transfecting plasmids to conduct the co-immunoprecipitation assay (CO-IP). The CO-IP protocol is described in chapter 2, section 2.20. I will be verifying whether Evi5 interacts with Fer1HCH, Chc and Hsc70-4 regardless of identifying Fer1HCH via the in vivo and ex vivo evi5 interactome protein lists. This will further support if Evi5 functions in the lysosomal degradation of ferritin.

In addition to this, I will repeat the IP-MS assay for Tsf2 to test whether Eps-15 is interacting with Tsf2. I will further verify the interaction of Tsf1 and Tsf3 with Eps-15 and the

interaction of Evi5 with Dap-160. These data will provide novel evidence for the endocytosis of Tsf proteins in *Drosophila* and further the role of Evi5 in this iron delivery pathway.

3.5.2 Evaluating the link between Evi5 and ferritinophagy in PG cells

To test whether autophagy occurs in the PG cells, I will use a double-tagged transgenic line for Atg8a. The USA-GFP-mCherry-Atg8a transgene is an excellent genetic tool to study autophagy. The line benefits from the quenching ability of the GFP protein in acidic environments [197]. In nonacidic structures such as autophagosomes, GFP-mCherry-Atg8a positive cells exhibit yellow signal (green merged with red) for Atg8a. However, when autolysosomes are formed, and autophagy is occurring, a red signal forms in the GFP-mCherry-Atg8a positive cells. This line would be a valuable tool to study the PG cells' autophagic process as depletion of Atg8a in PG cells results in an L2 Larval developmental arrest. First, I will rear the animals in the normal, BPS, and iron-supplemented foods, and then I will test the yellow and red fluorescence signals in PG cells. This test would allow me to check the autophagic flux in PG cells and whether it is activated via dietary iron manipulation.

Furthermore, I will use the GFP signal of the Fer1HCH^{G18} allele to analyze the ferritinophagy in the PG cells. To test this, I will raise the Fer1HCH^{G188} flies in the normal, BPS, and iron-supplemented foods and conduct a quantitative fluorescent western Blot. I will collect ring-gland samples and an anti-GFP antibody to detect ferritin in the blot. This will enable me to examine whether ferritin level changes in the PG cells upon dietary iron manipulations. I will further carry out this experiment by maintaining the Fer1HCH^{G188} flies in the BPS food for five generations and conduct the quantitative western blot analysis. In parallel to this, I will conduct the same strategy for Evi5^{VDRC}; Fer1HCH^{G188} flies to check whether the PG knockdown of Evi5 affects the ferritinophagy in the PG cells. I have combined the Evi5-RNAi ^{VDRC} flies with the Fer1HCH^{G18} flies. The Evi5^{VDRC}; Fer1HCH^{G188} flies will allow me to check the role of Evi5 in the PG cells' autophagy and whether the PG loss of *Evi5* affects ferritinophagy.

3.5.3 Food supplementation survival analysis of PG loss of function of Atg8a, Hsc70-4 and Fer1HCH

The main object of this experiment is to additionally examine whether PG ferritinophagic flux is required for iron homeostasis. The PG cells ultimately demand iron to produce heme, and one of the key components that can be used to bypass the ferritinophagy iron utilization would be

the hemin. As described in section 3.3.3, hemin feeding is an effective supplement to rescue the arrested larvae of *PG>PPOX-RNAi* (heme gene) and delayed *PG>Evi5^{FRT}* animals.

Here, I will use Fer1HCH-RNAi, Atg8a-RNAi and Hsc70-4-RNAi lines to knockdown Fer1HCH, *Atg8a* and *Hsc70-4* genes in the PG cells. As mentioned, according to the genome-wide RNAi screen, all progenies of these three crosses would result in an L2 larval developmental delay. However, I will raise the animals in normal, iron-, BPS-, ZnPP- and hemin-supplemented media and analyze whether the arrested L2 larvae can be rescued to the adult stage. I will further include *PG>PPOX-RNAi* as the control since they can rescue with hemin feeding. This experiment will confirm the initial results of the RNAi screen. By comparing the hemin and ZnPP administration, I will provide further evidence for the hypothesis that the ferritin iron is released and utilized for heme and ecdysone synthesis in PG cells.

3.5.4 Conclusion

My experiments indicate a novel and central function for Evi5 in regulating vesicle trafficking of heme/iron homeostasis. Furthermore, the potential function of Evi5 in iron release from ferritin will shed light on an unknown process in iron biology. These findings further have implications in the hitherto unknown role of Evi5 during multiple sclerosis disease.

3.5.6 Figures

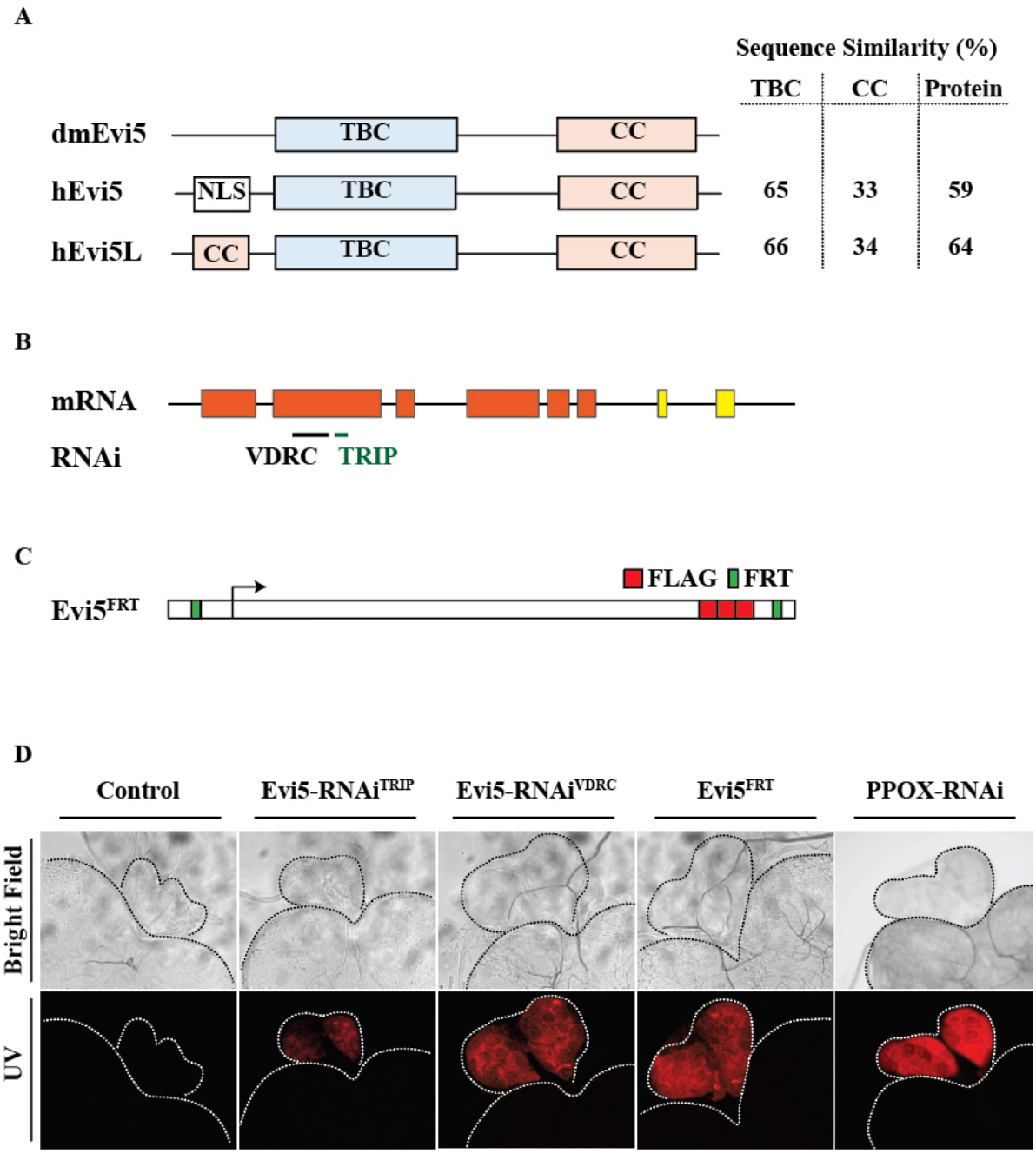
A
Sequence Similarity (%)
TBC
CC
Protein
dmEvi5
TBC
CC
hEvi5
NLS
TBC
CC
65
33
59
hEvi5L
CC
TBC
CC
66
34
64
B
mRNA
RNAi
VDRC
TRIP
C
Evi5FRT
FLAG
FRT
D
Control
Evi5-RNAiTRIP
Evi5-RNAiVDRC
Evi5FRT
PPOX-RNAi
Bright Field
UV

Figure 3. 1 PG depletion of Rab GAP protein Evi5 causes porphyria-like phenotype

A) Protein structure of *Drosophila* Evi5 and its orthologs human Evi5 (hEvi5) and human Evi5-like (hEvi5L). The percentage of sequence similarity between the TBC domain, the CC domain and the entire protein sequence for *Drosophila* Evi5 orthologs is presented. **B)** Schematic representation of *Drosophila* Evi5 mRNA and target sites of tested VDRC and TRIP RNAi lines. Orange boxes indicate exons present in all transcript variants, while yellow boxes are specific to some transcript variants. **C)** A schematic representation of the genomic locus of *Drosophila* $Evi5^{FRT}$ allele. The endogenous Evi5 is replaced with an allele that is flanked with FRT sites (green boxes) and carries 3XFLAG epitope tags (red boxes). The *Evi5* locus in the $Evi5^{FRT}$ allele can be removed by tissue-specific expression of flippase. **D)** The porphyria-like phenotype of PG loss of function of *Evi5* and PPOX. The Brain-ring gland complexes of Evi5-$RNAi^{TRIP}$ and Evi5-$RNAi^{VDRC}$, $Evi5^{FRT}$ allele and PPOX-RNAi lines exposed to UV light. Dotted lines indicate brain and ring gland areas.

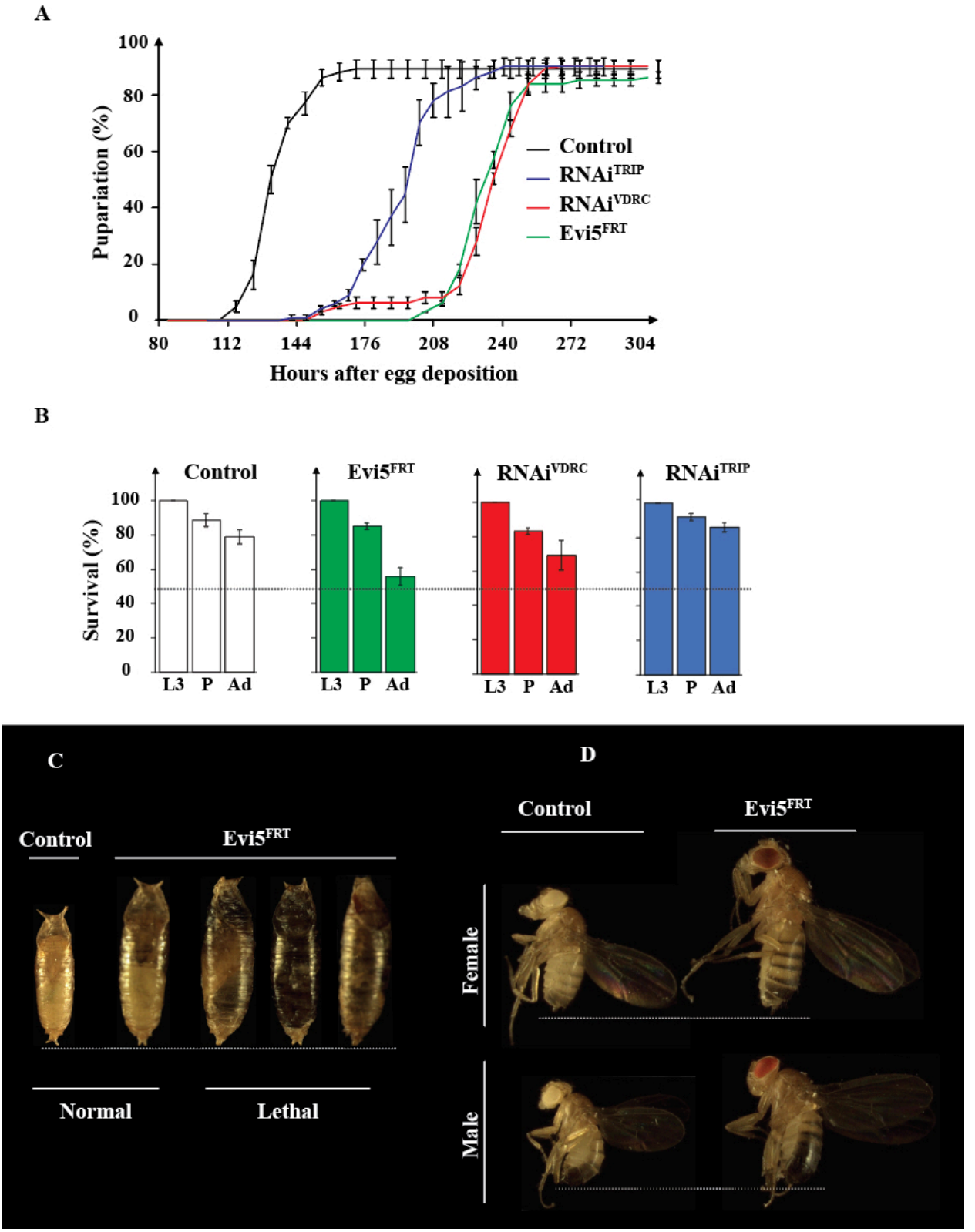
A
Pupariation (%)
100
80
60
40
20
0
80
112
144
176
208
240
272
304
Hours after egg deposition
Control
RNAi^TRIP
RNAi^VDRC
Evi5^FRT
B
Survival (%)
Control
Evi5^FRT
RNAi^VDRC
RNAi^TRIP
L3
P
Ad
C
Control
Evi5^FRT
Normal
Lethal
D
Control
Evi5^FRT
Female
Male

Figure 3. 2 PG depletion of *Evi5* causes developmental defects

A) The line graph depicts the timing of pupal development in Evi5-RNAi^{TRIP} (Blue line) and Evi5-RNAi^{VDRC} (Red line), Evi5^{FRT} (Green line) and control (Black line). PG loss of *Evi5* results in prolonged L3 stage and delay in pupae formation. Error bars represent the standard errors (SE) among three replicates of each time point. **B)** Survival analysis of 3rd instar larval (L3), pupae (P) and adults (Ad) upon PG depletion of *Evi5* compared to control animals. The error bars are SE among three replicates. The dotted line indicates 50% survival. **C)** and **D)** Pupal and adult size increase in Evi5^{FRT}. The developmental delay of mutant animals results in enlarged normal pupae and enlarged lethal pupae compared to control. Adult mutants further indicate enlarged body size than controls.

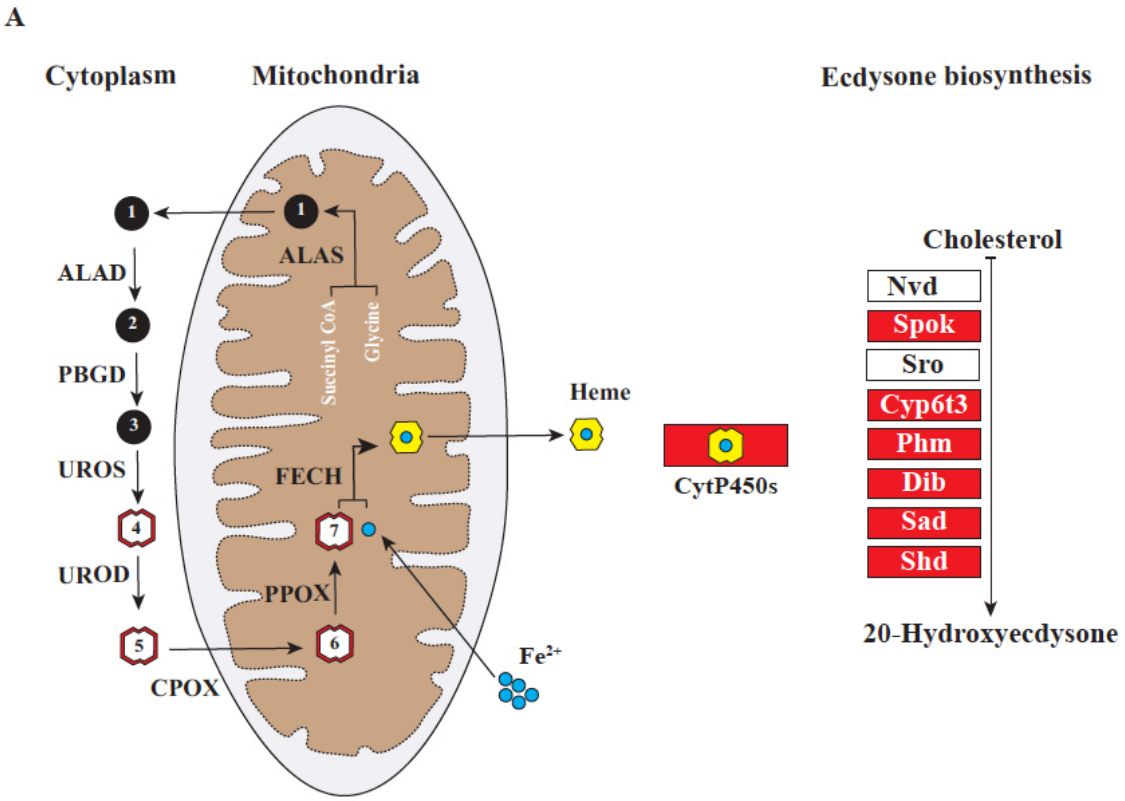
A
Cytoplasm
Mitochondria
Ecdysone biosynthesis
ALAD
PBGD
UROS
UROD
CPOX
ALAS
Succinyl CoA
Glycine
FECH
PPOX
Heme
CytP450s
Fe2+
Cholesterol
Nvd
Spok
Sro
Cyp6t3
Phm
Dib
Sad
Shd
20-Hydroxyecdysone

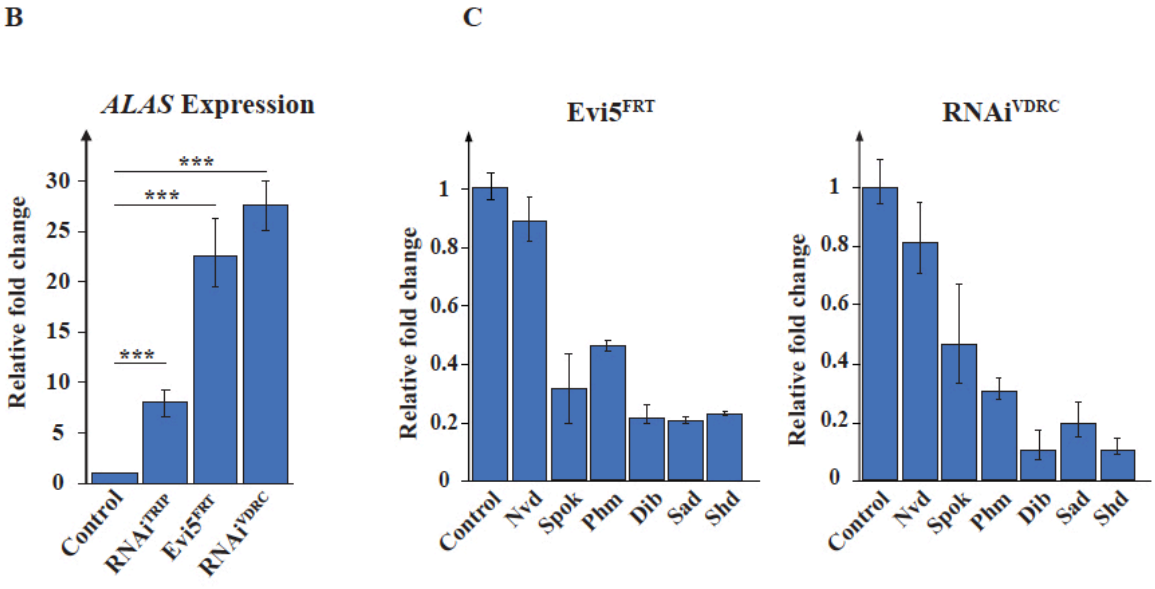
B
ALAS Expression
Relative fold change
Control
RNAiTRIP
Evi5FRT
RNAiVDRC
C
Evi5FRT
RNAiVDRC
Nvd
Spok
Phm
Dib
Sad
Shd

Figure 3. 3 PG loss of Evi5 function induces *ALAS* expression and reduces the expression of Halloween genes

A) Schematic overview of the heme and ecdysone biosynthesis pathways. Heme is a cofactor in hemoproteins such as cytochrome P450 enzymes in the ecdysone biosynthetic pathway (shown in red boxes). Red precursors in the heme biosynthetic pathway (4-7) are protoporphyrin rings that are autofluorescing red when exposed to UV light and air. In heme pathway: ALAS: Aminolevulinate synthase, ALAD: aminolevulinic acid dehydratase, PBGD: porphobilinogen deaminase, UROS: uroporphyrinogen III synthase, UROD: uroporphyrinogen decarboxylase, CPOX: coproporphyrinogen III oxidase, PPOX: protoporphyrinogen IX oxidase, FECH: ferrochelatase. In ecdysone pathway: Nvd: neverland, Spok: spookier, Sro: shroud, Phm: phantom, Dib: disembodied, Sad: shadow, Shd: shade. **B)** qPCR analysis of ALAS expression in Evi5-RNAi^{TRIP}, Evi5-RNAi^{VDRC} and Evi5^{FRT} lines and **C)** qPCR analysis of Halloween genes in Evi5-RNAi^{VDRC} and Evi5^{FRT} animals. Error bars are 95% confidence intervals among the replicates. Asterisks denote the student's t-test P-values (*$p < 0.05$ and ***$p < 0.001$).

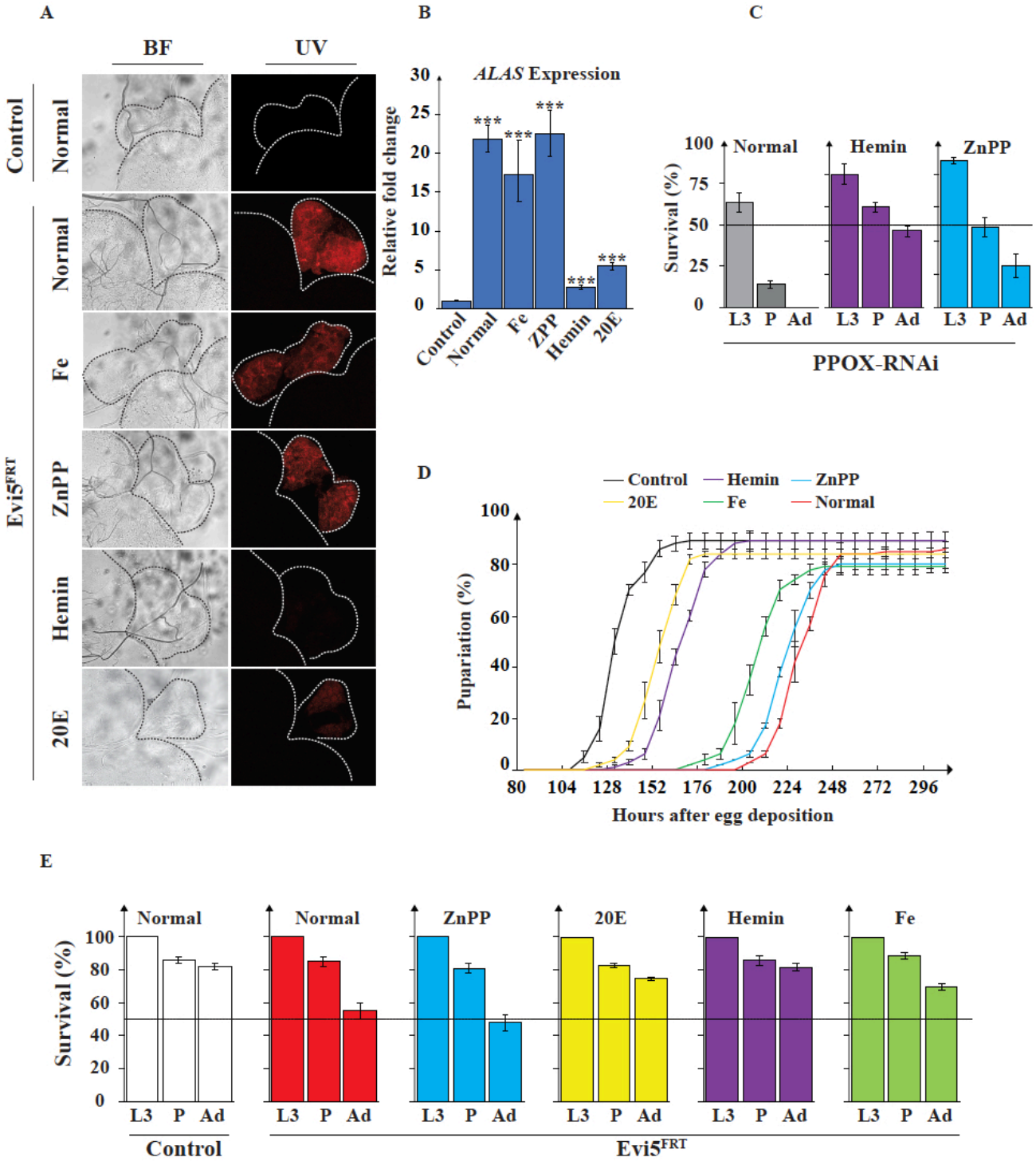
A
BF
UV
Control
Normal
Evi5FRT
Normal
Fe
ZnPP
Hemin
20E
B
ALAS Expression
Relative fold change
30
25
20
15
10
5
0
***
Control
Normal
Fe
ZPP
Hemin
20E
C
Survival (%)
100
75
50
25
0
Normal
Hemin
ZnPP
L3 P Ad L3 P Ad L3 P Ad
PPOX-RNAi
D
Control
Hemin
ZnPP
20E
Fe
Normal
Pupariation (%)
100
80
60
40
20
0
80 104 128 152 176 200 224 248 272 296
Hours after egg deposition
E
Survival (%)
100
80
60
40
20
0
Normal
Normal
ZnPP
20E
Hemin
Fe
L3 P Ad
Control
Evi5FRT

Figure 3. 4 Media supplementation effects on developmental defects of Evi5 mutants

A) Protoporphyrin accumulation in the PG cells of $Evi5^{FRT}$ mutant animals reared on normal, iron (Fe), zinc-protoporphyrin IX (ZnPP), hemin and 20-hydroxyecdysone (20E) supplemented media. The dotted lines show brain and ring gland areas in the Bright field (BF) and UV light. **B)** Relative expression analysis of ALAS in $Evi5^{FRT}$ mutants after raising animals in normal food, or iron-, ZnPP-, hemin- and 20E-enriched media. Error bars denotes 95% confidence intervals among the replicates and asterisks represents the P-value of the student's t-test analysis (*$p < 0.05$ and ***$p < 0.001$). **C)** survival analysis of PPOX-RNAi animals in normal, hemin and ZnPP supplemented media. **D)** and **E)** Pupariation timing and survival analysis of mutant $Evi5^{FRT}$ animals in different media. The error bars in the timing analysis line graph and survival bar graphs represent the replicates' standard error. L3: 3rd instar larvae, P: pupae, Ad: adults.

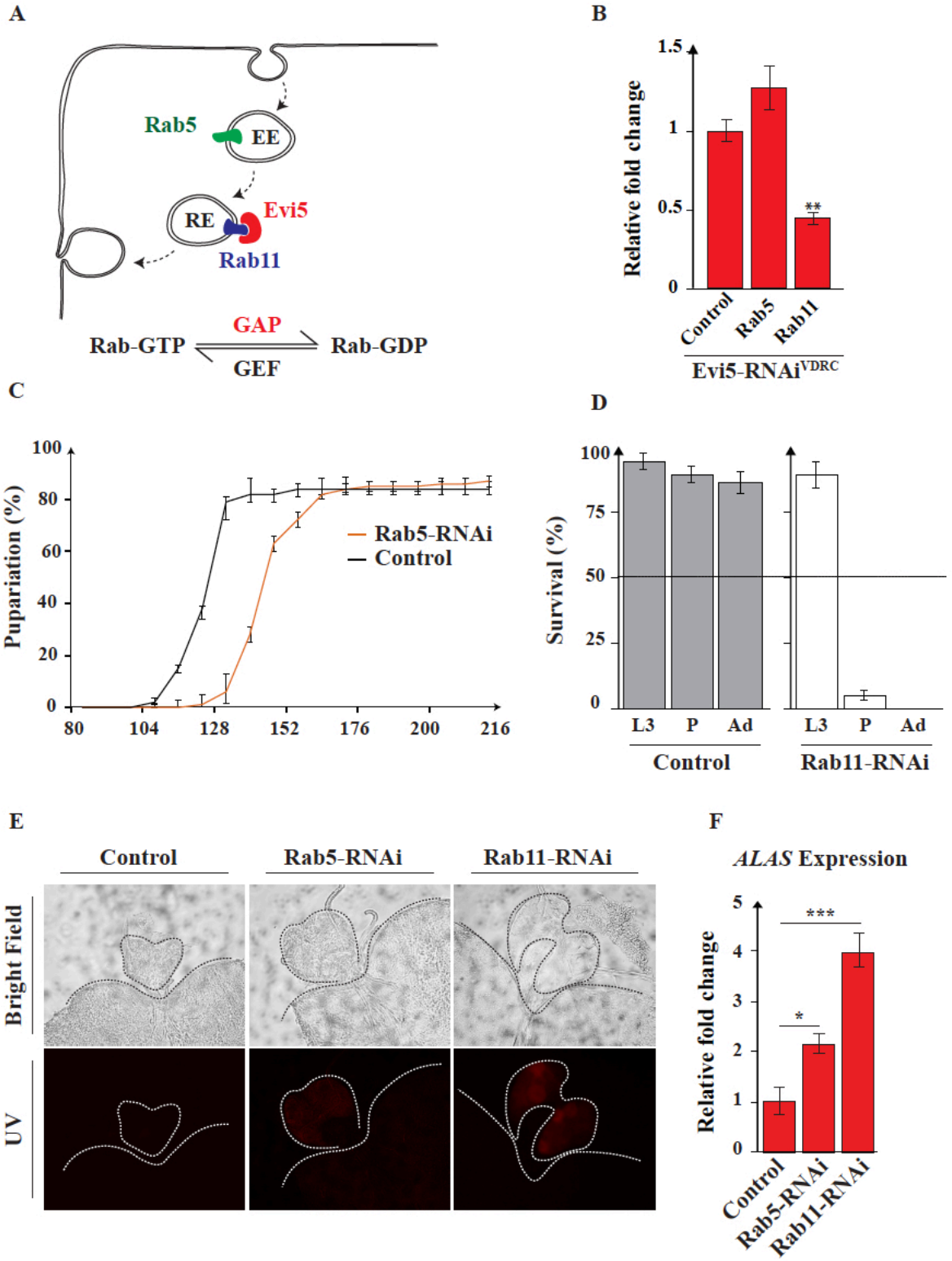
A
Rab5
EE
RE
Evi5
Rab11
GAP
Rab-GTP
Rab-GDP
GEF
B
Relative fold change
1.5
1
0.5
0
**
Control
Rab5
Rab11
Evi5-RNAiVDRC
C
Pupariation (%)
100
80
60
40
20
0
80
104
128
152
176
200
216
Rab5-RNAi
Control
D
Survival (%)
100
75
50
25
0
L3
P
Ad
L3
P
Ad
Control
Rab11-RNAi
E
Control
Rab5-RNAi
Rab11-RNAi
Bright Field
UV
F
ALAS Expression
Relative fold change
5
4
3
2
1
0
***
*
Control
Rab5-RNAi
Rab11-RNAi

Figure 3. 5 Rab5 and Rab11 function are critical in PG cells

A) Schematic overview of the function of Rab5 and Rab11 during endocytosis and exocytosis processes and function of Evi5 as the Rab-GAP for Rab11. Rab5 and Rab11 are predominantly localized in early endosomes (EE) and recycling endosomes (RE). Rab proteins cycle between Rab-GTP and Rab-GDP forms by guanine nucleotide exchange factors (GEF) and GTPase-activating proteins (GAPs). **B)** Expression of Rab5 and Rab11 in Evi5-RNai^{VDRC} animals by qPCR analysis. **C)** and **D)** pupariation timing and survival analyses of *PG>Rab5-RNAi* and PG>*Rab11-RNAi* animals. Error bars are standard errors. L3: 3rd instar larvae, P: pupae, Ad: adults. **E)** Red autofluorescence analysis of ring gland cells in *PG>Rab5-RNAi* and PG>*Rab11-RNAi* animals compared to control. UV is ultraviolet light, and BR is the bright field. **F)** Expression analysis of the *ALAS* gene in the ring glands of *PG>Rab5-RNAi* and PG>*Rab11-RNAi* animals. Error bars denote 95% confidence intervals among the replicates, and asterisks determine the P-value of the student's t-test analysis (*$p < 0.05$ and ***$p < 0.001$).

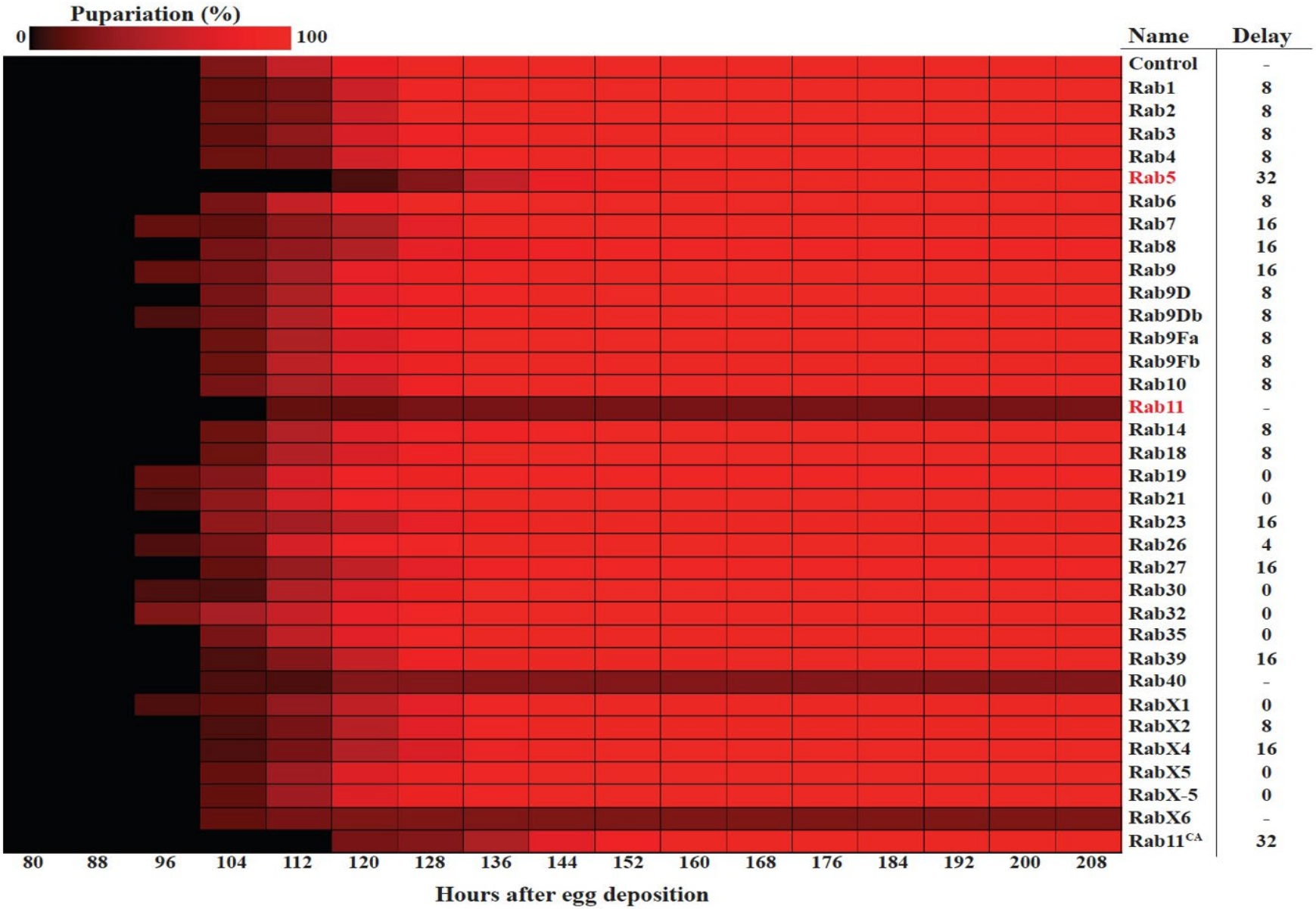
Pupariation (%)
0
100
Name
Delay
Control -
Rab1 8
Rab2 8
Rab3 8
Rab4 8
Rab5 32
Rab6 8
Rab7 16
Rab8 16
Rab9 16
Rab9D 8
Rab9Db 8
Rab9Fa 8
Rab9Fb 8
Rab10 8
Rab11 -
Rab14 8
Rab18 8
Rab19 0
Rab21 0
Rab23 16
Rab26 4
Rab27 16
Rab30 0
Rab32 0
Rab35 0
Rab39 16
Rab40 -
RabX1 0
RabX2 8
RabX4 16
RabX5 0
RabX-5 0
RabX6 -
Rab11CA 32
80 88 96 104 112 120 128 136 144 152 160 168 176 184 192 200 208
Hours after egg deposition

Figure 3. 6 PG-specific RNAi screen of Rab genes

Heatmap demonstrates the timing of the *PG>Rab-RNAi* screen. Scale bar denotes the percentage of pupariation where black is zero percent and red represents 100% pupae. Red names (*Rab5* and *Rab11*) are genes with red autofluorescent ring glands. The hyphen in the delay column (except control) shows L3 arrested genes. $Rab11^{CA}$ is catalytically active Rab11.

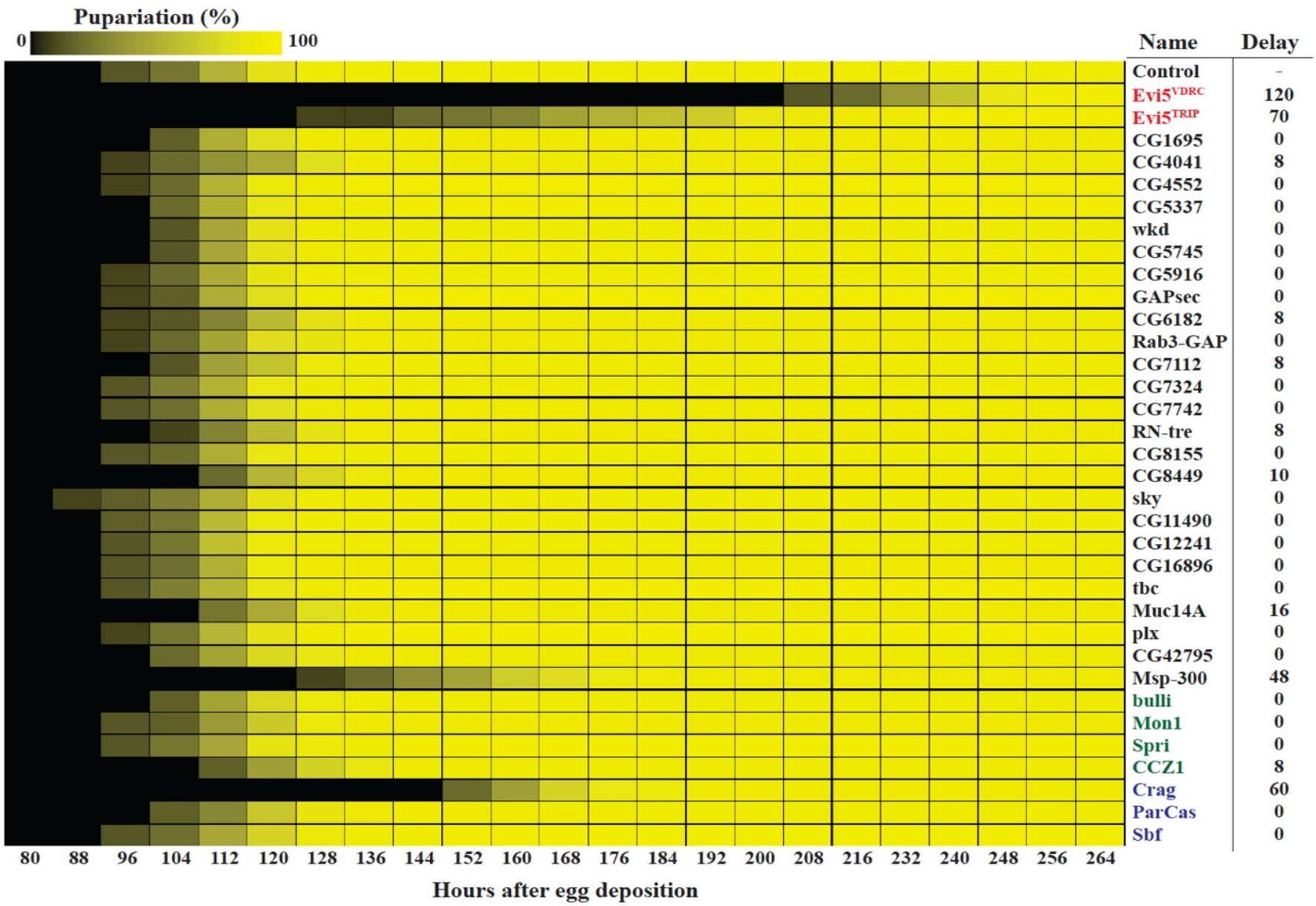
Pupariation (%)
0
100
Name
Delay
Control -
Evi5VDRC 120
Evi5TRIP 70
CG1695 0
CG4041 8
CG4552 0
CG5337 0
wkd 0
CG5745 0
CG5916 0
GAPsec 0
CG6182 8
Rab3-GAP 0
CG7112 8
CG7324 0
CG7742 0
RN-tre 8
CG8155 0
CG8449 10
sky 0
CG11490 0
CG12241 0
CG16896 0
tbc 0
Muc14A 16
plx 0
CG42795 0
Msp-300 48
bulli 0
Mon1 0
Spri 0
CCZ1 8
Crag 60
ParCas 0
Sbf 0
80 88 96 104 112 120 128 136 144 152 160 168 176 184 192 200 208 216 232 240 248 256 264
Hours after egg deposition

Figure 3. 7 PG RNAi screening of Rab-GAP, Rab5-GEF and Rab11-GEF genes

Heatmap demonstrates the timing of *PG>Rab-GAP-RNAi* and *PG>Rab-GEF-RNAi* screen. Scale bar denotes the percentage of pupariation where black is zero percent and yellow is 100% pupae. Red names are Evi5-RNAi^{TRIP} (Evi5^{TRIP}) and Evi5-RNAi^{VDRC} (Evi5^{VDRC}), which causes autofluorescence in ring glands. Green genes are Rab5-GEF (nucleotide exchange factors), and Blue are Rab11-GEF genes.

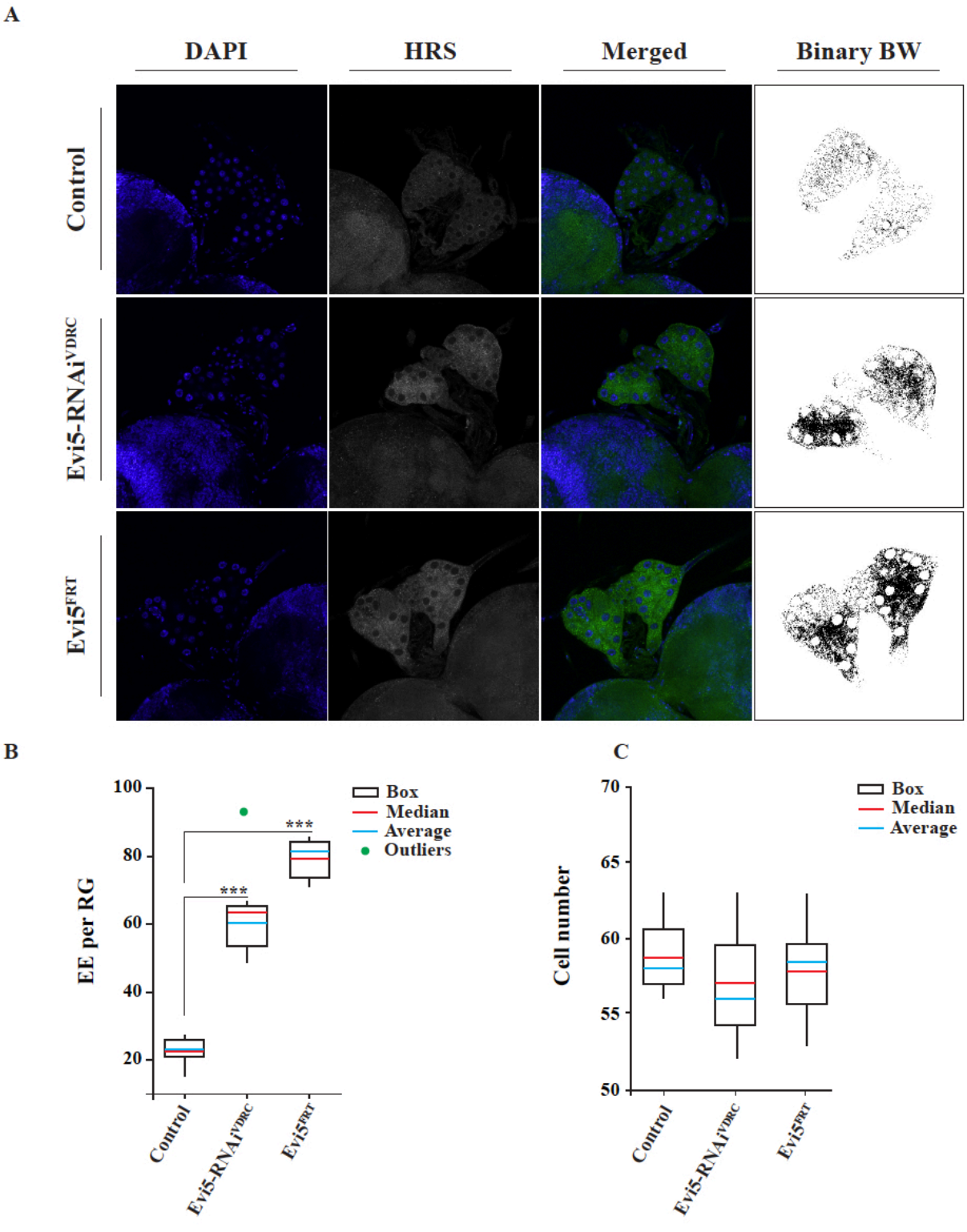
A
DAPI
HRS
Merged
Binary BW
Control
Evi5-RNAi^VDRC
Evi5^FRT
B
EE per RG
100
80
60
40
20
***
***
Box
Median
Average
Outliers
Control
Evi5-RNAi^VDRC
Evi5^FRT
C
Cell number
70
65
60
55
50
Box
Median
Average
Control
Evi5-RNAi^VDRC
Evi5^FRT

Figure 3. 8 Loss of Evi5 function increases early endosomes in PG cells

A) Immunofluorescent staining of hepatocyte responsive serum phosphoprotein (Hrs) in PG cells of control, Evi5-RANi^{VDRC} and Evi5^{FRT} animals. Blue channel is DNA/Nuclei stain DAPI, and Green channel is Hrs. Binary Black and White images denote the Hrs signal (black dots) in animals' ring glands. **B)** and **C)** Box plot of early endosome percentage (Hrs signal) and the number of cells in ring glands (RG) of control, Evi5-RANi^{VDRC} and Evi5^{FRT} animals. Red and blue lines indicate the average and the median of samples. Green dots are outliers. Asterisks are P-values in the student's t-test analysis (*$p < 0.05$ and ***$p < 0.01$).

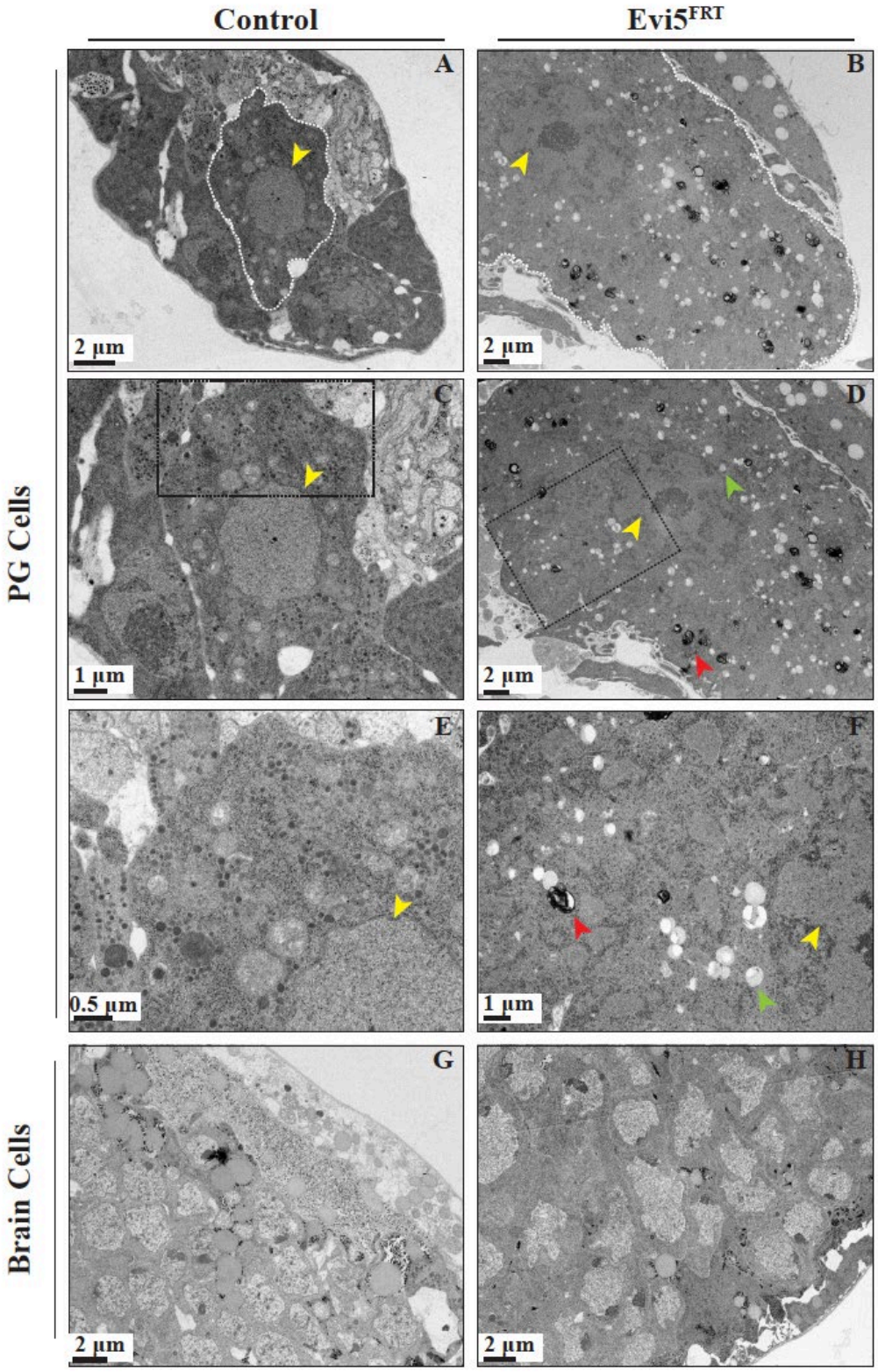
Control
Evi5FRT
A
B
C
D
E
F
G
H
2 µm
2 µm
1 µm
2 µm
0.5 µm
1 µm
2 µm
2 µm
PG Cells
Brain Cells

Figure 3. 9 Transmission Electron Microscopy analysis of Evi5^{FRT} Prothoracic gland cells (PG)

Bright field TEM analysis of PG (A-F) and Brain cells (G-H) in Control and Evi5^{FRT}. White dotted lines in A and B show the plasma membrane in the prothoracic glands. Dotted black boxes in C and D depict images with larger magnification in E and F. Yellow arrows in A-E images indicate the same nuclear membrane in the images with different magnifications. Red and green arrows in D and F point at high and low electron-dense vesicles within the mutant PG cells of Evi5^{FRT}. Scale bars are in micrometers (μm).

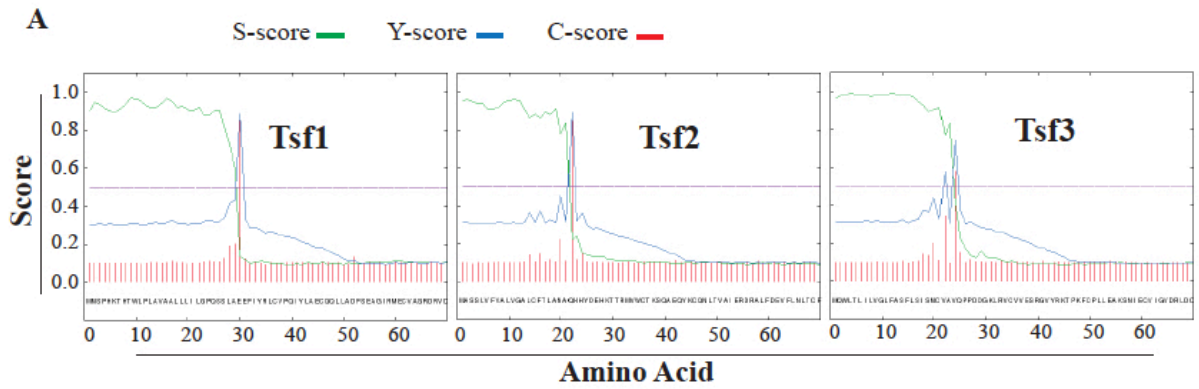
A
S-score
Y-score
C-score
Score
1.0
0.8
0.6
0.4
0.2
0.0
Tsf1
Tsf2
Tsf3
0 10 20 30 40 50 60
Amino Acid

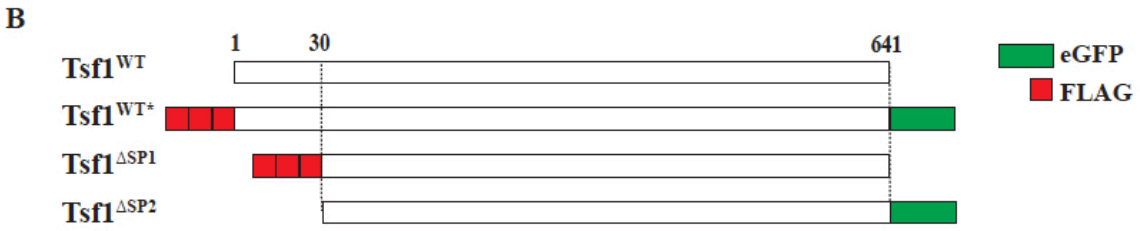
B
1
30
641
Tsf1WT
Tsf1WT*
Tsf1ΔSP1
Tsf1ΔSP2
eGFP
FLAG

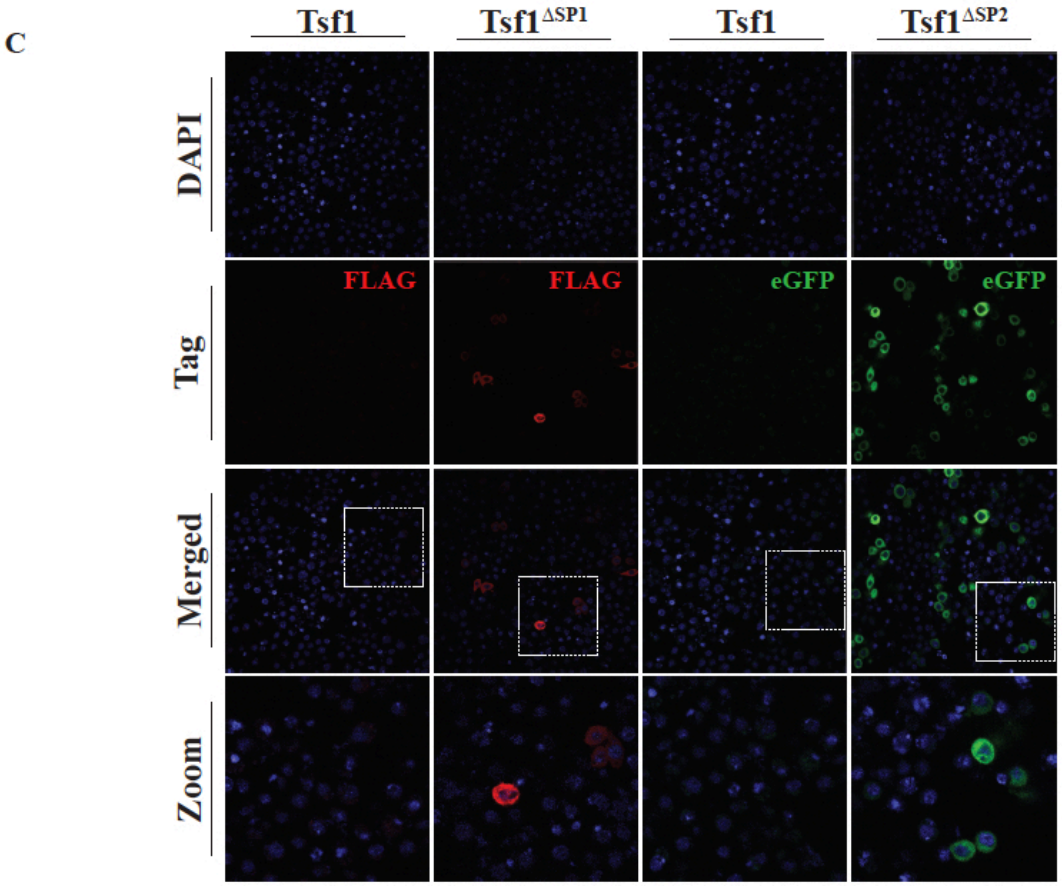
C
Tsf1
Tsf1ΔSP1
Tsf1
Tsf1ΔSP2
DAPI
Tag
Merged
Zoom
FLAG
FLAG
eGFP
eGFP

Figure 3. 10 Tsf proteins contain N-terminal secretion signal

A) Signal-P analysis of Tsf1, Tsf2 and Tsf3 proteins. S-score indicates secretion score (Green line), Y-score shows signal peptide from non-signal peptide (Blue line), and C-score represents the cut site score (Red line). Y-axis is the probability number of S, Y and C scores and, X-axis is protein sequence (letters at the bottom are the amino acid sequence and numbers refer to the amino acid location). **B)** S2 cell transfection plasmid design for Tsf1 protein. $Tsf1^{WT*}$ plasmid contains wild-type Tsf1 cDNA protein tagged with three N-terminus FLAG epitopes (red boxes) and a C-terminus eGFP protein. $Tsf1^{\Delta SP}$ plasmid lacks secretion signal peptide (1- 30 amino acids) and tagged with three N-terminus FLAG epitopes ($Tsf1^{\Delta SP1}$) and a C-terminus eGFP ($Tsf1^{\Delta SP2}$). **C)** S2 cells transfected with wild-type ($Tsf1^{WT}$) and mutant ($Tsf1^{\Delta SP}$) Tsf1. The blue channel is DNA/Nuclei stain DAPI, but red and green channels are FLAG and eGFP, respectively. Zoom panel is the area that is indicated by white boxes in the merge images.

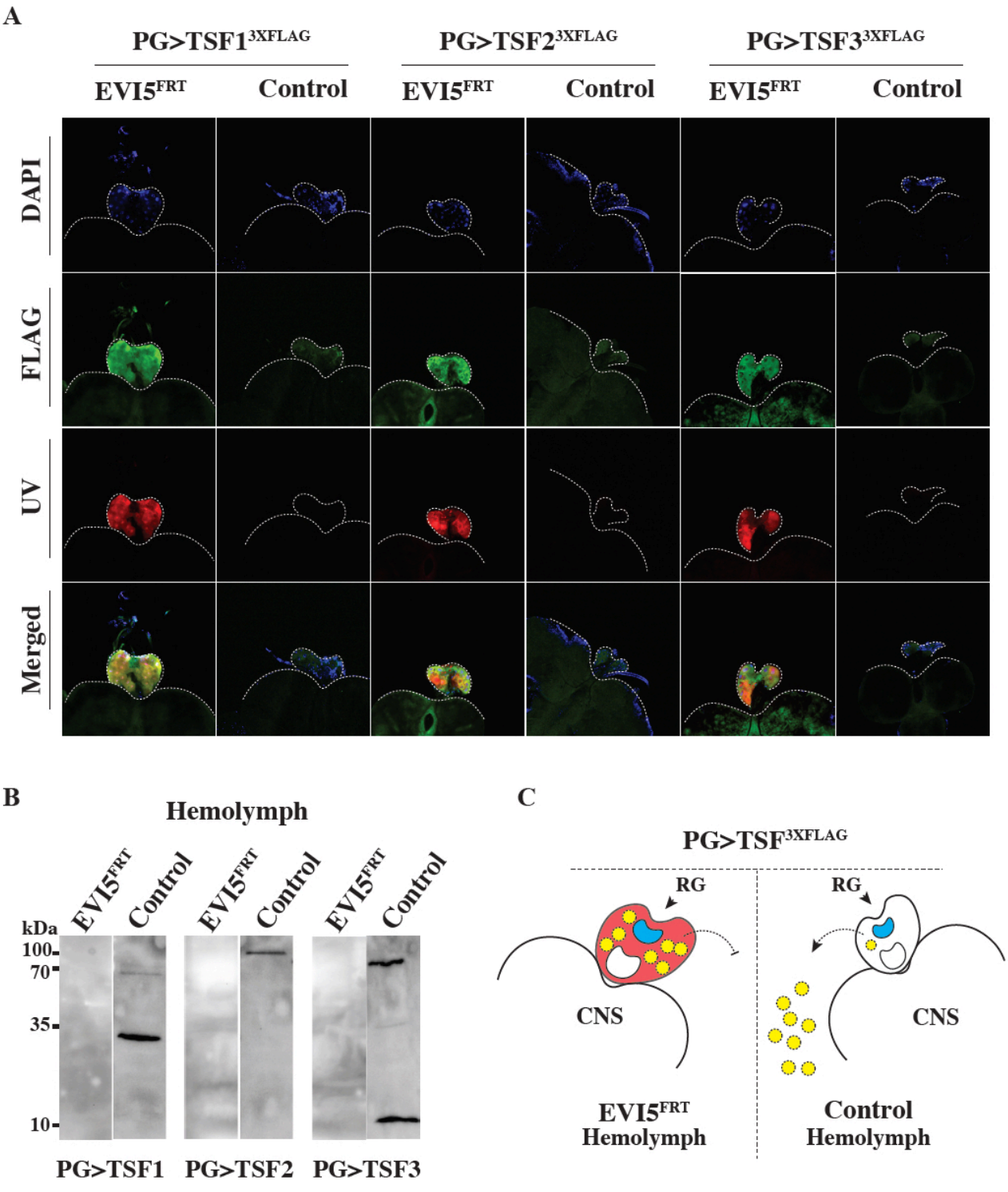
A
PG>TSF1^3XFLAG
PG>TSF2^3XFLAG
PG>TSF3^3XFLAG
EVI5^FRT
Control
DAPI
FLAG
UV
Merged
B
Hemolymph
kDa
100
70
35
10
PG>TSF1
PG>TSF2
PG>TSF3
C
PG>TSF^3XFLAG
RG
CNS
EVI5^FRT Hemolymph
Control Hemolymph

Figure 3. 11 PG-specific depletion of *Evi5* blocks secretion of Tsf proteins into hemolymph

A) Immunofluorescent labelling of FLAG-tagged Tsf1, Tsf2 and Tsf3 (Green) in Evi5 mutant ($Evi5^{FRT}$) and control backgrounds. The blue channel is DAPI (DNA/Nuclei stain), and the red channel (UV) is the autofluorescence of PG cells in $Evi5^{FRT}$ and control. **B)** Western blot analysis of FLAG-tagged Tsf1, Tsf2 and Tsf3 in Evi5 mutant ($Evi5^{FRT}$) and control hemolymph samples. **C)** A model for Evi5 function in Tsf proteins secretion and trafficking in the PG cells. PG loss of *Evi5* blocks secretion of Tsf proteins into the hemolymph and causes porphyria/autofluorescence phenotype.

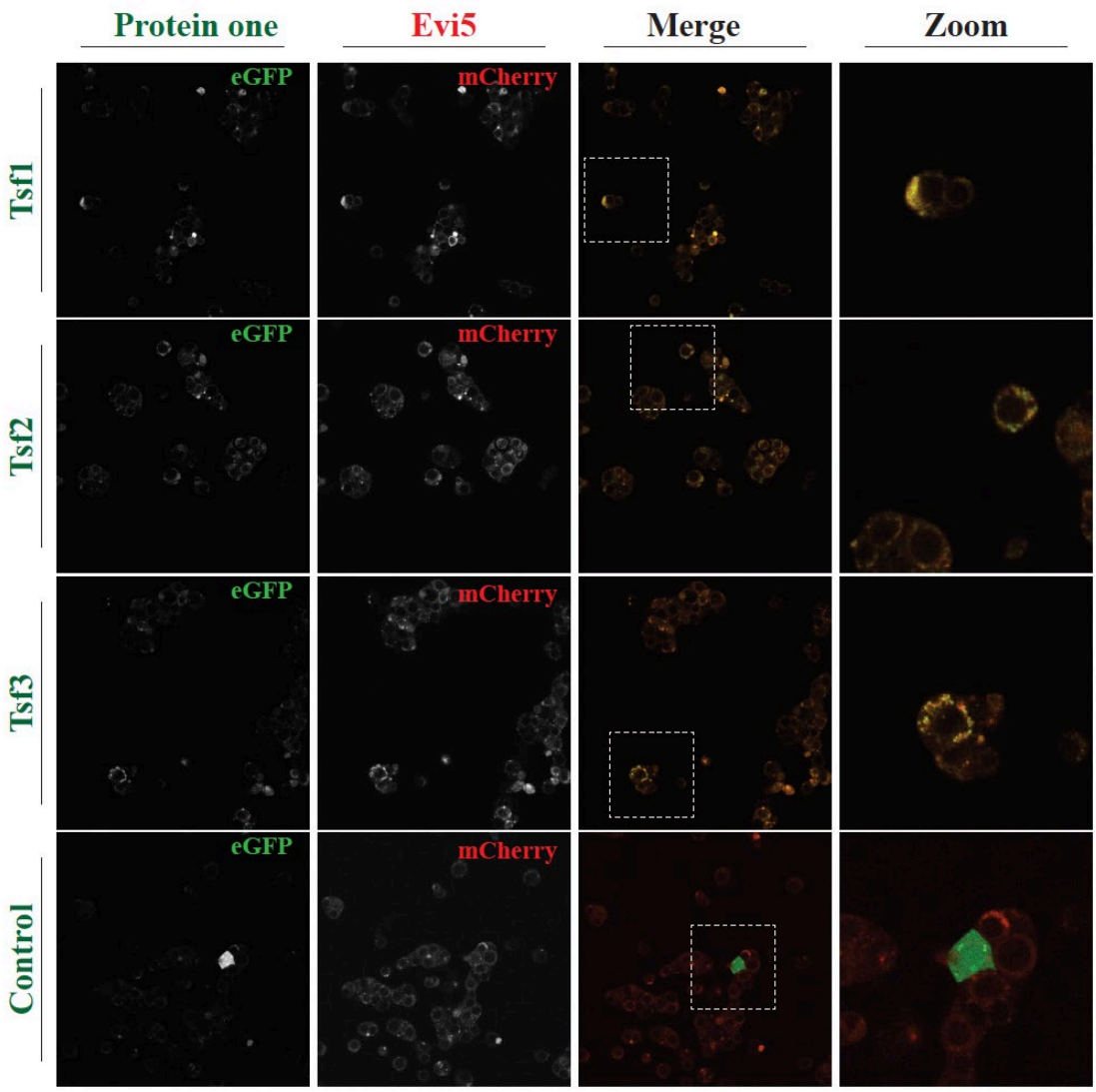

Figure 3. 12 Evi5 colocalizes with Tsf1, Tsf2, and Tsf3

Images of S2 cells co-transfected with Evi5-mCherry and Tsf1-eGFP, Tsf2-eGFP, Tsf3-eGFP and eGFP. Evi5 is expressed in its wild-type form tagged with mCherry. The secretion signals of Tsf1, Tsf2 and Tsf3 were removed and tagged with eGFP to entrap proteins in cells. Images in the red and green channels are shown in the grayscale, but a merged image has been shown in color to visualize co-localized proteins. White boxes indicate the zoomed area in the merged images.

A

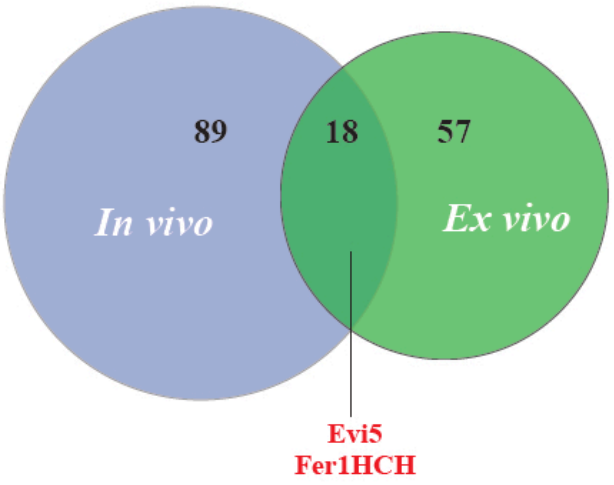

B

In vivo	*Ex vivo*
Cindr	Zip
Pzg	Evi5
Evi5	β-tubulin
Chc	Jar
CCT5	Hsc70-1
CG8036	CG1737
Hsc70-4	CG8038
Unk	CG34417
Dap160	CTT5
CG34417	Akap200

C

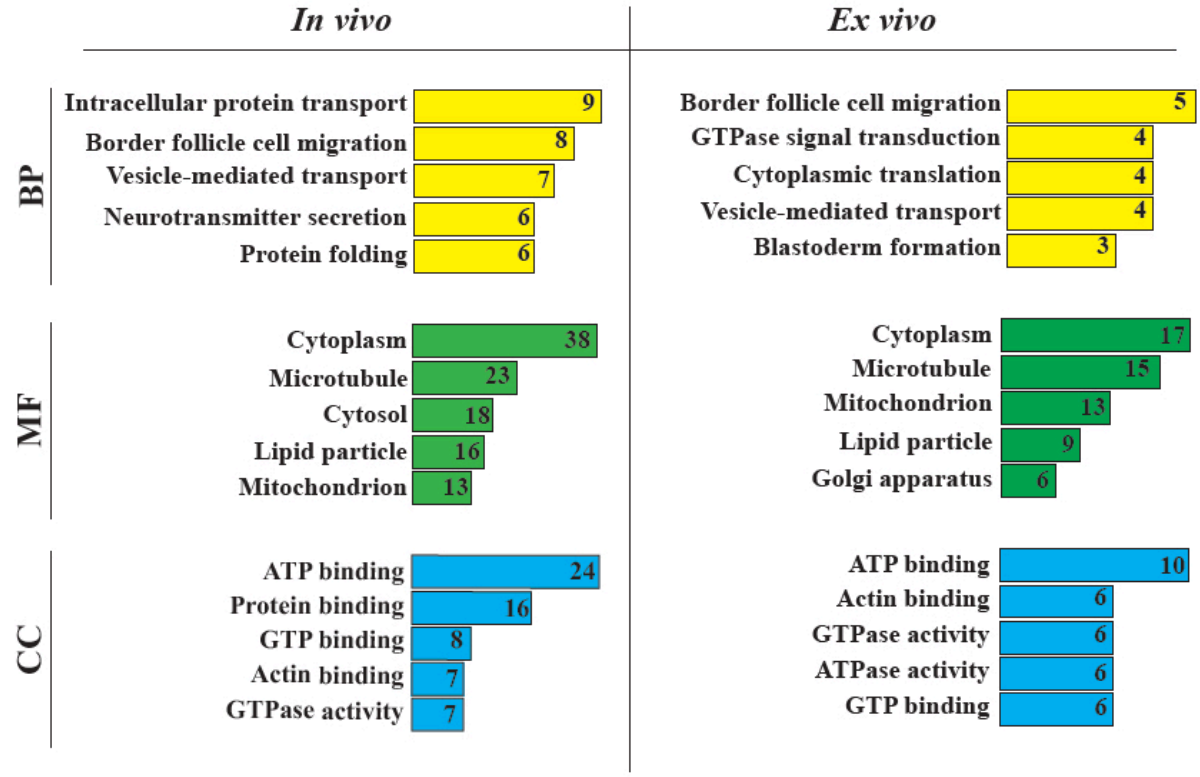

Figure 3. 13 Evi5 interacts with Ferritin heavy chain subunit

A) Venn diagram depicts the overlapping and non-overlapping proteins of in vivo and ex vivo immunoprecipitation assays. In the overlapping subset, there are Evi5 and ferritin heavy chain subunits (Fer1HCH). The in vivo assay was conducted by endogenously FLAG tagged Evi5 using $Evi5^{FRT}$ line, but the ex vivo assay was carried out by transfecting S2 Schneider cells with FLAG-tagged Evi5. **B)** The list of ten proteins (overlap and non-overlap) with the highest Mass-spectrometry score (the ion scores of all identified peptides) in each assay. Clathrin heavy chain (Chc) and Heat shock protein cognate-4 (Hsc70-4) are proteins with putative functions in the Ferritinophagy (shown in green). **C)** Gene ontology analysis of the immunoprecipitated proteins. Numbers indicate the number of genes in each category. BP: Biological Process, MF: Molecular Function, and CC: Cellular Component.

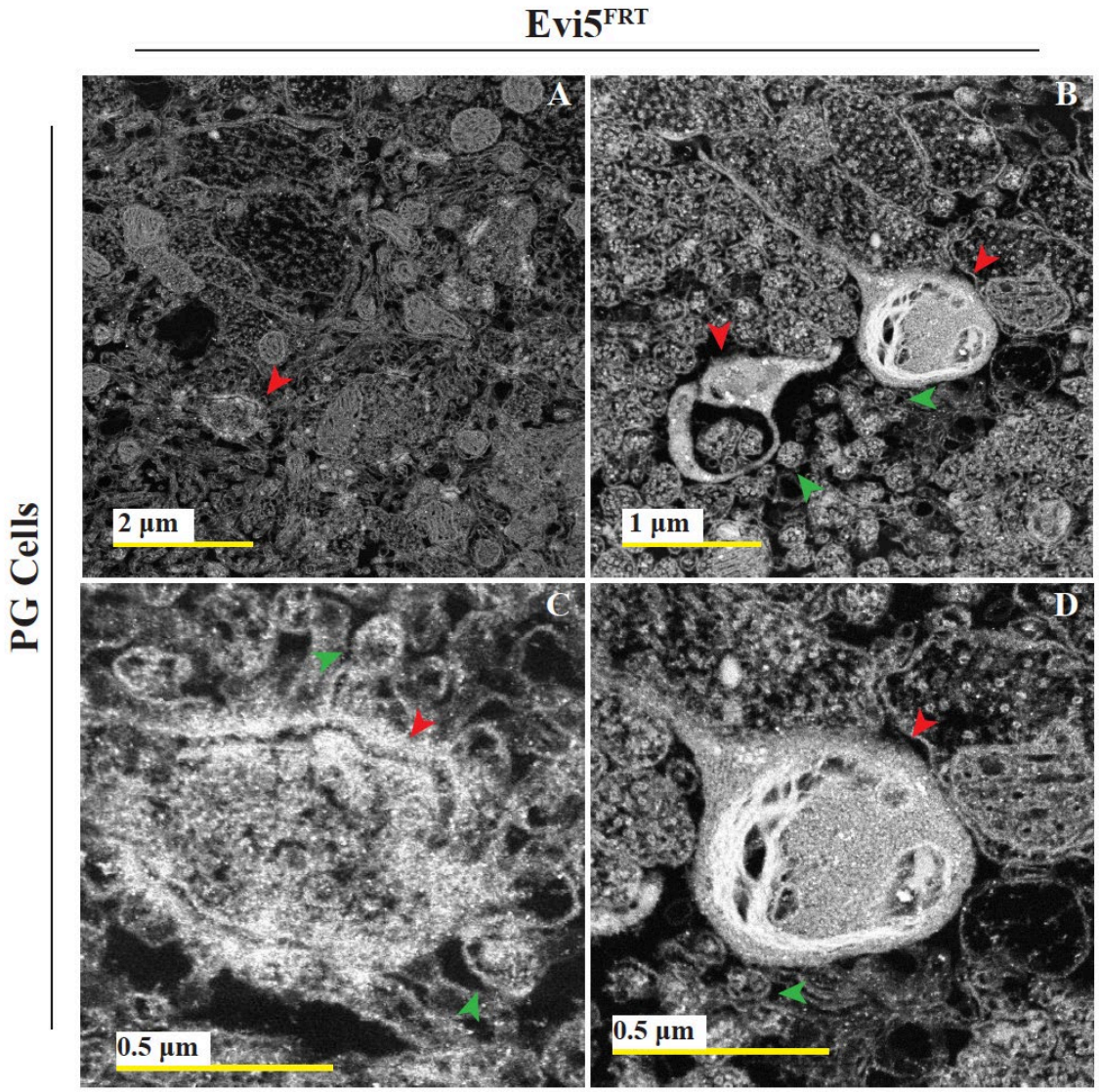

Figure 3. 14 Electron-dense vesicles in *Evi5^{FRT}* PG cells resembles lysosomes

Super resolution dark field TEM analysis of electron-dense vesicles in PG cells of Evi5^{FRT} animals. Red arrows in A-D point at vesicles with the white area that are electron dense vesicles. Green arrows in D and C depict lysosomal residual bodies. Scale bars are in micrometers (µm).

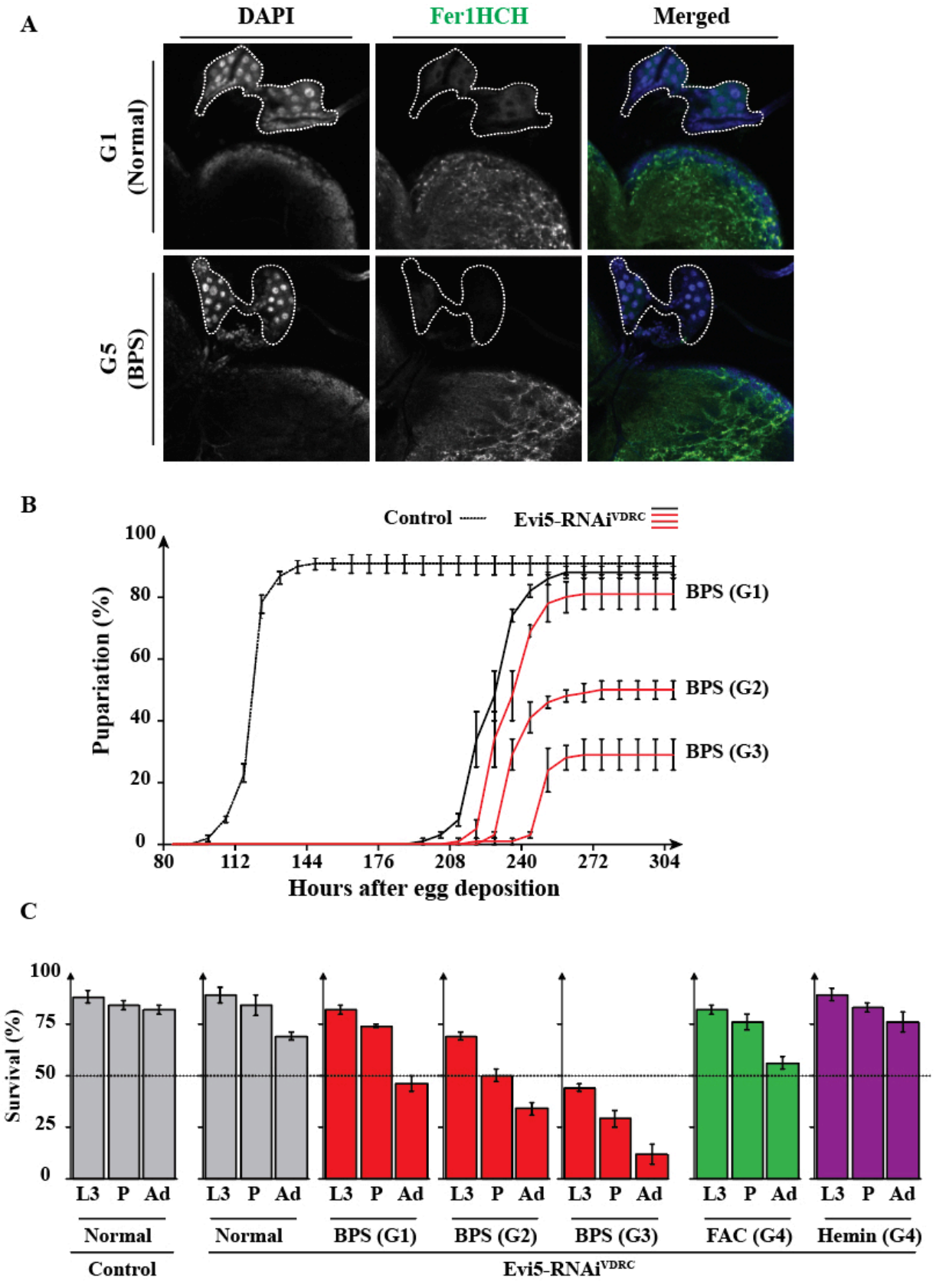
A
DAPI
Fer1HCH
Merged
G1 (Normal)
G5 (BPS)
B
Control
Evi5-RNAi^VDRC
Pupariation (%)
100
80
60
40
20
0
80
112
144
176
208
240
272
304
Hours after egg deposition
BPS (G1)
BPS (G2)
BPS (G3)
C
Survival (%)
100
75
50
25
0
L3 P Ad
Normal
Control
Normal
BPS (G1)
BPS (G2)
BPS (G3)
FAC (G4)
Hemin (G4)
Evi5-RNAi^VDRC

Figure 3. 15 Iron depletion reduces ferritin and exacerbate developmental defects of PG loss of *Evi5*

A) Ferritin level in PG cells of Fer1HCH-GFP^{G188} flies raised for five generations (G5) on iron chelator (BPS)-supplemented medium compared to animals in normal reference medium. The GFP channel demonstrates the intrinsic GFP signal in PG cells (no antibody staining). DAPI is **DNA**/Nuclei stain (Blue channel) **B)** Pupae developmental timing of Evi5-RNAi^{VDRC} animals in BPS food for three generations (G1-G3) compared to normal food. The black dotted line indicates control animals in normal food. **C)** Survival analysis of Evi5-RNAi^{VDRC} animals in food supplemented with BPS, iron (FAC), and Hemin. Evi5-RNAi^{VDRC} animals raised in BPS media for three generations (G1-G3) and the third-generation progenies (G4) were raised in FAC and hemin food. L3: 3rd instar larvae, P: pupae, Ad: adults. Error bars in B) and C) represent the standard errors.

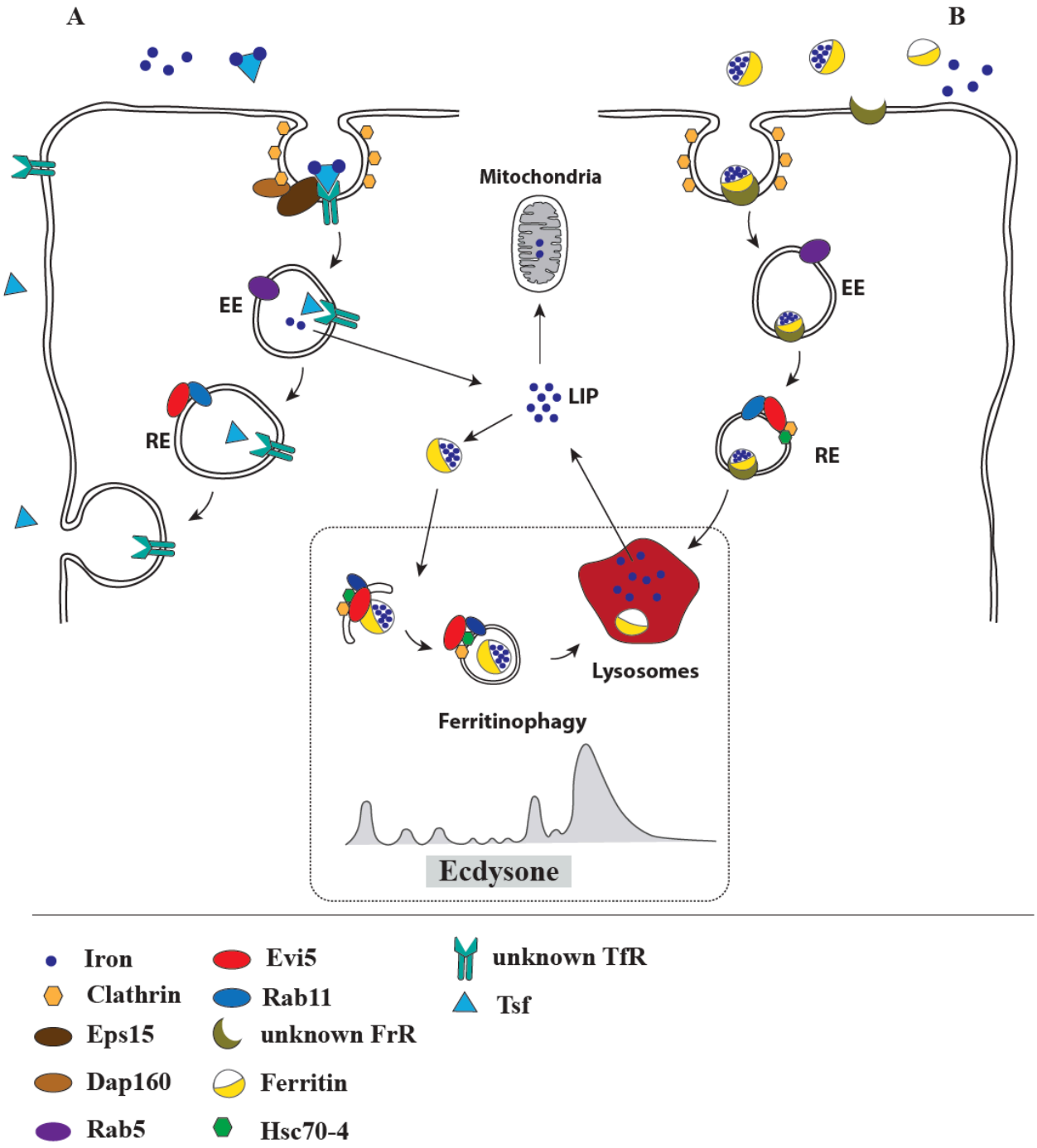
A
B
Mitochondria
EE
EE
LIP
RE
RE
Lysosomes
Ferritinophagy
Ecdysone
Iron
Clathrin
Eps15
Dap160
Rab5
Evi5
Rab11
unknown FrR
Ferritin
Hsc70-4
unknown TfR
Tsf

Figure 3. 16 A model for Evi5 function in iron homeostasis

In PG cells, iron is required for heme production prior to the production of ecdysone pulses. **A)** Transferrin (Tsf) mediated iron delivery. Holo-transferrin (= iron-loaded) is imported into cells via binding to an unknown receptor or Eps-15 (Epidermal growth factor receptor pathway substrate clone 15). This process is further facilitated by Dap160 (Dynamin associated protein 160) and Clathrin that form early endosomes (EE). Rab5 governs the entry of the holo-transferrin into EE. Inside the endosomes, iron is released and transported into the cytoplasm. Apo-transferrin (iron-free) is recycled to the plasma membrane in recycling endosomes which is regulated by Rab11. Evi5 governs Rab11 during the exocytosis of RE. The labile iron pool (LIP) is then used for cell demands such as heme and Fe-S cluster production in mitochondria or stored in ferritin. Ferritin-stored iron can be release at times of increased cellular iron demand by being targeted to the lysosomes. This process is termed ferritinophagy and facilitated by Evi5, Rab11, Clathrin and Hsc70-4 proteins. The lysosomal iron is then added to LIP in the cytoplasm. **B)** Ferritin-mediated iron delivery. Holo-ferritin entered into the EE via binding to its receptor (FrR) at the cell surface. The endocytosis process is probably mediated by Rab5. Next, the holo-ferritin is targeted to the lysosomes by endosomal vesicles to restore the iron. This process is regulated by Evi5, Rab11, Clathrin and Hsc70-4.

3.5.7 Tables

Table 3. 1 co-immunoprecipitated proteins in the Evi5 *in vivo* protein interactome.

Number[A]	Symbol	Name	Biological process[B]	IP-MS Score[C]
1	Cindr	CIN85 and CD2AP related	Receptor-mediated endocytosis, border follicle cell migration and actin filament organization	222.67
2	Pzg	Putzig	Ecdysone receptor-mediated signaling pathway, regulation of mitotic cell cycle and chromatin organization	206.9
3	Evi5	Ecotropic viral integration site 5	GTPase activator activity	128.3
4	Chc	Clathrin heavy chain	Endocytosis, Clathrin coat assembly, receptor-mediated endocytosis and positive regulation of autophagy	71.87
5	CCT5	Chaperonin containing TCP1 subunit 5	Protein folding	60.96
6	CG8036	-	Regulation of chromatin silencing	58.98
7	Hsc70-4	Heat shock protein cognate 4	Chaperone-mediated protein folding, late endosomal microautophagy and vesicle-mediated transport	57.56
8	Unk	unkempt	Neuron differentiation and compound eye development	40.66
9	Dap160	Dynamin associated protein 160	Clathrin-dependent synaptic vesicle endocytosis and endosomal transport	38.64
10	CG34417	-	Actin cytoskeleton organization	38.33
16	Rab11	Rab11	Endocytosis, exocytosis, Golgi to plasma membrane protein secretion and border follicle cell migration	24.09
20	Rab14	Rab14	Endocytic recycling, phagolysosome assembly and Golgi to endosome transport	21.55
49	Gel	Gelsolin	Actin cytoskeleton polymerization	9.65
54	Fer1HCH	Ferritin 1 heavy chain	Cellular iron ion homeostasis and iron ion import across plasma membrane	8.17
58	tral	trailer hitch	Actin cytoskeleton organization	7.69
102	Snap29	Synaptosomal-associated protein 29kDa	Autophagosome maturation and endocytosis	2.69

[A] Numbers represents the ranking of proteins based on IP-MS score.

[B] Biological process inferred from Flybase Database.

[C] IP-MS score is the sum of the ion scores of all the peptides that were identified in the MALDI-TOF Mass spectrometry.

Table 3. 2 Immunoprecipitated proteins in the Evi5 *ex vivo* proteome interactome.

Number[A]	Symbol	Name	Molecular Function[B]	IP-MS Score[C]
1	Zip	Zipper	Mitotic cytokinesis and border follicle cell migration	1037
2	Evi5	Ecotropic viral integration site 5	GTPase activator activity	232
3	β-Tub85D	beta-Tubulin at 85D	Mitotic cell cycle and microtubule cytoskeleton organization	186.26
4	Jar	Jaguar	Endocytosis, Cytoskeleton-dependent cytoplasmic transport, border follicle cell migration and actin cytoskeleton organization	82.56
5	Hsc70-1	Heat shock protein cognate 1	Vesicle-mediated transport and chaperone cofactor-dependent protein folding	78.32
6	CG1737	-	-	48.6
7	CG8036	-	Regulation of chromatin silencing	48.26
8	CG34417	-	Actin cytoskeleton organization	42.22
9	CCT5	Chaperonin containing TCP1 subunit 5	Protein folding	28.19
10	Akap200	A kinase anchor protein 200	Actin cytoskeleton organization and protein localization to membrane	24.02
14	Rab10	Rab10	Vesicle-mediated transport and exocytosis, basolateral protein secretion	21.94
18	Gel	Gelsolin	Actin cytoskeleton polymerization	14.83
23	tral	trailer hitch	Actin cytoskeleton organization	11.99
38	Fer1HCH	Ferritin 1 heavy chain	Cellular iron ion homeostasis and iron ion import across plasma membrane	7.58
69	Snap29	Synaptosomal-associated protein 29kDa	Autophagosome maturation and endocytosis	4.3

[A] Numbers represents the ranking of proteins based on IP-MS score.

[B] Biological process inferred from Flybase Database.

[C] IP-MS score is the sum of the ion scores of all the peptides that were identified in the MALDI-TOF Mass spectrometry.

Table 3. 3 Immunoprecipitated membrane-related proteins[A] in the Tsf1 proteome interactome.

Number	Symbol	Name	Biological process[B]	IP-MS Score[C]
1	Cindr	CIN85 and CD2AP related	Receptor-mediated endocytosis, border follicle cell migration and actin filament organization	171.16
2	Tsf1	Transferrin 1	Iron ion transport	103.44
3	Eps-15	Epidermal growth factor receptor pathway substrate clone 15	Endocytosis and endosomal transport	46.21
4	Dap160	Dynamin associated protein 160	Clathrin-dependent synaptic vesicle endocytosis and endosomal transport	11.73
5	GCS2β	Glucosidase 2 beta subunit	N-glycan processing	3.34

[A] proteins that are localized in plasma membrane and endomembrane compartments.

[B] Biological process inferred from the Flybase Database.

[C] IP-MS score is the sum of the ion scores of all the peptides that were identified in the MALDI-TOF Mass spectrometry.

Table 3. 4 Immunoprecipitated membrane related proteins in the Tsf3 proteome interactome.

Number	Symbol	Name	Biological process[1]	IP-MS Score[2]
	Eps-15	Epidermal growth factor receptor pathway substrate clone 15	Endocytosis and endosomal transport	72.74
	Tsf3	Transferrin 3	Iron ion transport	41.77
	Dap160	Dynamin associated protein 160	Clathrin-dependent synaptic vesicle endocytosis and endosomal transport	23.97
	Vap33	VAMP-associated protein 33kDa	Endoplasmic reticulum membrane organization and cytoplasmic microtubule organization	10.36
	CG13887	-	Endoplasmic reticulum to Golgi vesicle-mediated transport	6.32

[A] Biological process inferred from the Flybase Database.

[B] IP-MS score is the sum of the ion scores of all the peptides that were identified in the MALDI-TOF Mass spectrometry.

Chapter 4 Evaluating the transcriptome responses to dietary iron manipulations in *Drosophila*

4.1 Introduction

4.1.1 Iron Regulation in cells

Iron is a double-edged sword in the biological processes. On the one hand, iron is the principal electron donor in almost all biological and molecular processes. On the other hand, iron is potentially toxic because of the Fenton reaction and the generation of ROS [1,198,199]. Iron accelerates the conversion of H_2O_2 to the free radical HO^0 ion that can damage cellular membranes, proteins, and DNA molecules [1]. However, all organisms utilize abundant energy sources to acquire enough iron supplies and make iron bioavailable for biological processes. Proteins involved in respiration, electron transport, nucleic acids synthesis, steroid hormones production, carbohydrate, and lipid metabolisms bind to iron frequently in the form of the heme and iron-sulfur (Fe-S) clusters to fulfill their functions [3–8,70,149,200]. Iron must be under tight homeostatic regulation to ensure that cells have adequate iron levels. However, at the same time, the toxicity and reactivity of iron to cells must be limited [201–204]. Thus, the distribution and sequestering of iron is a cellular challenge in different tissues.

Duodenal enterocytes are the first site of the iron regulation as they govern iron uptake and then release it into the plasma and hemolymph [21,61,120]. Iron traverses apical and basolateral membranes of enterocytes to gain access to circulatory processes [116,120]. Once iron is in systemic circulation, it is mainly bound to the transferrin protein (Tsf). The Tsf proteins are iron transporters that are taken up by cells expressing transferrin receptor (TfR) [30,35]. The blood-brain barrier is another regulatory example that tightly governs iron acquisition into brain cells [205,206].

Furthermore, cells have adopted divergent cellular mechanisms to regulate iron homeostasis and iron import in response to different stimuli. The Iron Regulatory Proteins 1 & 2 (IRP1 and IRP2) are at the center of cellular iron regulation. In normal conditions, IRP is an aconitase enzyme that harbors an Fe-S cluster [52,207–210]. However, during iron scarcity, IRP loses the Fe-S cluster and becomes an mRNA-binding protein. The IRP regulates iron homeostasis via binding to the iron-responsive elements (IREs) within specific target mRNAs (typically located in the UTRs) of genes involved in the iron uptake, storage and distribution [52,207,210].

4.1.2 Iron misregulation and diseases

Misregulation of iron-modulating proteins disrupts the cellular iron balance and causes disorders associated with iron deficiency and iron overloaded [211–214]. Conditions in which iron levels do not meet the cellular demand will cause iron deficiency. Prolonged iron deficiency can result in infertility, embryonic lethality, and anemia [211,214–217]. On the other hand, when the iron level exceeds its cellular capacity, it may result in hemochromatosis and other iron overload disorders. Aceruloplasminemia and Hallervorden-Spatz disease are genetic disorders that result in iron overload, and conversely, iron overload is a risk factor for developing diabetes and pancreatic cancer [211,218–221]. Moreover, mutations in iron-related genes have been associated with neurodegenerative diseases such as Parkinson's disease and Alzheimer's disease [214,222–224].

Iron deficiency and iron overload further increase the cellular susceptibility to pathogens, and they can trigger different immune responses [225,226]. It has been demonstrated that the perturbation of iron homeostasis promotes the proliferation of immune cells. Consistently, iron misregulation alters the production and release of cytokines such as interleukins and tumor necrosis factors in cells that enhance host resistance to infections [226].

4.1.3 RNA sequencing to determine the iron transcriptome

Despite our growing knowledge of biological responses to iron, our grasp of homeostatic regulation and genome-wide responses to iron in different tissues remains rudimentary. Several comprehensive microarray studies have been conducted in various model organisms and cell lines. The ultimate objective of these studies was to address central underlying cellular responses to either iron deficiency or iron overload [227–236]. However, the microarray technique has a significant limitation in identifying novel genes because it is based on designing and hybridizing probes to the predefined genes [237,238]. Therefore, evaluating the comprehensive genomic response to a stimulus is not feasible.

In recent years, sequencing the total cellular RNA content has become the mainstream high-throughput technique that enables transcripts' identification and quantification simultaneously [239,240]. However, the results of RNA-sequencing (RNA-seq) are not unbiased and ready to interpret. It generates datasets that inherit various errors during different steps. Thus,

identifying the differentially expressed genes (DEGs) with RNA-Seq needs a precise data-mining and data analysis approach [240–243].

I used a complex RNA-Seq approach to investigate transcript profiles of different tissues in *Drosophila* larvae in response to dietary iron manipulations. The *Drosophila* is an excellent model to study underlying genetic and molecular mechanisms of iron homeostasis. While there are absent or altered molecular processes in *Drosophila*, intriguing similar iron homeostatic mechanisms exist between humans and *Drosophila* [61,64,159]. In both organisms, dietary iron is absorbed with metal transporters in the intestinal enterocytes. Iron is then stored in ferritin or transported to other tissues via circulatory Tsf proteins [61]. However, the lack of the hepcidin hormone, the transferrin receptor, ferroportin, and the different subcellular localization of ferritin are notable differences between *Drosophila* and humans [61,244,245]. Therefore, investigating molecular aspects of iron metabolism in *Drosophila* would improve our knowledge about hitherto unidentified iron homeostasis players in *Drosophila*, which may lead to similar findings in other organisms.

Here I present the results of a high throughput genome-wide screening in *Drosophila* larvae using tissue-specific RNA-seq and computational data analysis approaches via edgeR and Deseq2 methods. My work unveiled detailed transcriptional responses of larval brain ring gland complex (BRGC), gut, and whole larval body (WB) to various dietary iron levels. To study the iron transcript profile, I manipulated iron levels of *Drosophila* food via the iron chelator BPS and the iron salt Ferric ammonium citrate (FAC). A key difference to other studies was that I starved larvae on iron-depleted media for several generations, which resulted in a stronger transcriptional response to iron. The RNA-seq analysis was not only analyzing different tissues (brain ring gland complex, gut, and whole body), but also tested each of these tissues at four time points after the experimental group was switched to an iron-rich food source (controls were left on iron-depleted medium). Subsequent genetic loss of function analysis, protein-protein interactions, and iron staining identified genes with hitherto unknown links to iron biology. Thus, this study provides a genome-wide resource for further research in the iron area.

4.2 Material and methods

4.2.1 Fly stocks and food supplementation

The list of flies and their stock centers that I ordered for this project is presented in Table 2.1. (Bathophenanthrolinedisulfonic acid disodium salt hydrate) and FAC (Ferric Ammonium iron(III) citrate) media were prepared according to the description in section 2.1 and table 2.2 in chapter 2.

4.2.2 RNA sequencing and verification experiments

For this project, I used w^{1118} flies (control strain) and I raised them in the BPS and FAC media (Table 2.2). The Brain Ring Gland Complex (BRGC), gut and whole larval body (WB) sample collection, RNA isolation and cDNA generation are described in section 2.13, 2.14, and 2.16 in chapter2.

As explained in section 2.16, I used the Ovation *Drosophila* RNA-seq system 1-16 kit to generate the RNA-seq libraries. I then mapped the raw FastQ data to the *Drosophila* reference genome and counted the reads for genes. Next, the raw reads were analyzed with different strategies (as described in section 2.17 in chapter 2) to identify responsive genes in the iron deficient and the iron overload conditions (Differentially Expressed Genes: DEGs).

To verify the identified DEGs, the qPCR analysis, Prussian blue staining, ex vivo IP-MS experiment and CO-IP assay were performed. They are described in details in the 2.15, 2.8, 2.21 and 2.20 sections of chapter 2, respectively. The list of primers, plasmids and generated cDNAs constructs are presented in Table 2.3, Table 2.4 and Table 2.5.

4.2.3 Downstream RNA-seq data analysis

To further analyze the DEGs, I carried out term enrichment, HHpred and SignalP analyses. Gene ontology term enrichment analysis was performed with the PANTHER database (www.pantherdb.org/panther/goslim.jsp).

I used the HHpred tools to perform a structural-based homolog analysis. Then protein sequences were collected from the Flybase database and then subjected for alignment with the HHpred tool (MPI Bioinformatics Toolkit, https://toolkit.tuebingen.mpg.de/tools/hhpred). Lastly, I used the SignalP software to identify the secretion signal peptide within the protein sequences of the DEGs (version 5.0, http://www.cbs.dtu.dk/services/SignalP/).

4.3 Results

4.3.1 *Drosophila* 3rd instar larvae as a model for studying iron homeostasis

Drosophila at the 3rd instar larvae stage (L3) requires substantial amounts of nutrients to develop into the next stage (prepupae) [246]. Therefore, I reasoned that the application of the L3 for studying iron biology would create robust gene sets and provide new insights into iron biology studies. To achieve a comprehensive genomic response to dietary iron, I performed a three-step approach. First, I manipulated the iron level of the medium to sensitize animals' development to the iron deficiency. Next, I generated the gene expression profiles for three different tissues: BRGC, gut and WB via RNA sequencing. Lastly, I performed downstream computational analysis and confirmed the differentially expressed genes (DEGs) in each tissue.

To alter the dietary iron levels, I used BPS (an iron chelator) to deplete iron and FAC (a source of ferric iron) to increase iron in the food (see method section). Our primary goal was to compare animals' transcriptome in iron-replete and iron-depleted conditions. How long can flies survive on an iron-depleted diet? Interestingly, I observed no developmental effect in larvae raised for one generation (G1) on BPS-supplemented medium (Figure 4.1A and B). This was further supported via a qPCR analysis for *IRP1A*, *Fer1HCh* and *Tsf1* (known iron-responsive genes) that indicated no transcriptional response in G1 BPS-administrated animals (Figure 4.2). Because of the potential toxicity, I did not test higher concentrations of BPS (>120 μM) in the diet. However, I decided to rear animals for additional generations in BPS-enriched food and monitor their development.

Animals started to form pupae with ~8 hours developmental delay after the 2nd generation (G2) of using BPS-supplemented media. Until the 4th generation (G1 to G4), there were no remarkable differences between animals' survival in control and BPS-enriched food. However, animals exhibited longer developmental lag after being raised in the low iron diet (Figure 4.1A). In the 5th generation (G5), animals were significantly susceptible to lack of dietary iron, and they had ~32 hours retardation in forming pupae. Further, in the G5, I observed that only 42% of embryos grew into adult flies (Figure 4.1B), indicating a significant drop in survival rates. The G5 animals could recover fully after adding back FAC into their diet (data not shown). Therefore, I used the iron-susceptible G5 flies to carry out the RNA-Seq experiment.

4.3.2 Dietary iron RNA sequencing of G5 flies

To carry out RNA-Seq analysis, I staged G6 larvae (progenies of the G5 flies) developmentally until the initiation of L3 stage in the PBS medium. I then divided newly hatched L3 larvae into two groups, one group continued to feed on the BPS medium, but the second group was reared on the FAC medium. Next, I collected the WB, BRGC and gut samples at 4, 8, 12, and 16 hours of feeding in the BPS and FAC media (Figure 4.1C). The RNA samples were then isolated and applied for the sequencing. Upon RNA sequencing, I obtained ~22 million paired-end reads per sample (total number of samples = 48). Out of this data set, ~95% of the reads were mapped to the *Drosophila* genome via the HISAT2 software. In total, I was able to map 14557 genes with at least one read per gene. Any ambiguous reads that aligned to multiple genes were trimmed off and not included in subsequent analysis (Figure 4.1D). Lastly, I performed two computational analyses on raw reads to identify DEGs. First, a media type analysis that compared transcripts in BPS medium versus FAC medium and identified 119 DEGs in response to diet (regardless of time points). Second, a time-course analysis that analyzed tissues at 4 and 16 hours to find genes that respond to iron temporally. It is noticeable that all the DEGs were identified in response to low and high iron levels in the food. Therefore, genes are either upregulated or downregulated after the switch to iron-rich food. I categorized the DEGs into two groups: the genes that are BPS-upregulated (downregulated genes after the switch to iron-rich food) and genes that are FAC-upregulated.

I used the edgeR and DESEq2 R-packages to find the DEGs and calculate expression fold changes (FC) in both analyses [247–249]. These methods distinguish the DEGs with negative binomial distribution algorithms and generate statistical support for each DEG (an adjusted p*-value via normalization of raw reads). However, the edgeR and DESEq2 normalize the data differently and select different genes. Further, it has been shown that the DESEq2 is not suitable for finding genes with a small number of reads [248]. Therefore, to achieve higher confidence results, I used both packages in parallel to find packages specific (edgeR- or Deseq2-specific DEGs) and those DEGs that overlap between the two methods (I called them common genes). Finally, I used a P-value of 0.05 as a cut-off threshold in both edgeR and Deseq2 methods to identify DEGs (Figure 4.3).

4.3.3 DEGs found in BRGC samples

Upon BRGC transcript analysis, I identified 50 DEGs with a P-value ≤ 0.05, of which 13 transcripts were found via Deseq2, 44 with the edgeR. There were seven overlapping DEGs between the two methods (Table 4.1). Out of 50 DEGs, 15 genes were FAC-upregulated, and 35 were BPS-upregulated genes (Figure 4.3A).

4.3.3.1 BRGC: FAC-upregulated genes

In the FAC-responsive group, I identified eight heat-shock encoding genes (*Hsp* genes) with ~1.5 to 2.5 fold change (FC) induction (Table 1.4). Seven Hsp genes were common between the two methods, and the last one was edgeR-specific DEG (Figure 4.3A). Of these, two genes encode small chaperone proteins; the *hsp22* and *hsp26*, and six genes encode members of the Hsp70 family; the *hsp68*, *hsp70Aa*, *hsp70Ab*, *hsp70Ba*, *hsp70BBb*, and *hsp70Bc* (Table 4.1). All these different *hsp70* genes encode identical protein isoforms (similar amino acid sequence), and previous studies suggest that they have evolved from duplication of two ancient *hsp70* genes [250,251]. Interestingly, Hsp22 and hsp70 are protein partners that function in transporting the Fe-S clusters to recipient proteins [53,189,190].

I further found a putative carbohydrate-binding protein named lectin-22c with 49.87 FC induction (Table 4.1). The lectin-22c is predicted to be a galactose binding protein and is an ortholog to human protein COLEC11. The collectin COLEC11 is an innate immune lectin protein with a carbohydrate-binding domain and plays a role in recognizing carbohydrates [252]. Consistently, high iron plays a critical role in the development of type2 diabetes, which is characterized by increased glucose levels in the blood [253]. Additionally, there were two protease enzymes, the Rpt3, a proteasomal ATPase, and CG33128, with an aspartic-endopeptidase InterPro domain. This might be due to enhanced protein aggregation and protein insolubility in the presence of dietary iron [254]. Finally, I identified a chemoreceptor (*Gr58b*) and three non-annotated genes with significantly high fold changes. Two genes were unknown (*CG13721* and *CG14095*), but *CG6295* codes a polypeptide with a lipase-like domain (Table 4.1).

4.3.3.1 BRGC: BPS-upregulated genes

On the other hand, in the BPS responsive genes, I found two transmembrane transporters *Mco4* and *dmGlut* (Figure 4.3A and Table 4.1). The *Drosophila* multicopper oxidase 4 (*Mco4*)

gene is essentially uncharacterized, but the yeast ortholog, the ferroxidase Fet3p, is a high affinity iron importer and used when iron levels are low. No high-affinity iron importer has been described in higher eukaryotes. Mco4 and Fet3p are members of the multicopper ferroxidase family [255]. The induction of *Mco4* with 42.22 FC in animals reared on BPS-medium (= low iron) is consistent with the role of Fet3p, as it imports iron with a high affinity [255]. The next DEG was dmGlut, which is a sodium-dependent phosphate transporter with a high affinity to L-glutamate. The induction of dmGlut in the BPS media (FC=1.29) is also consistent with the previous findings. It is indicated that the glutamate level of the brain is significantly diminished under iron scarcity [256].

Surprisingly, I noticed that 23 out of 35 DEGs of the BPS group are highly upregulated, and they are transcripts involved in divergent metabolic processes (Figure 4.3A and Table 4.1). For example, glutathione S transferase GstE6, protease inhibitor Kaz-m1, a putative serine endopeptidase CG10405, a lipid-binding sensory protein CheB93b, a putative inositol monophosphatase CG17028 and glycosyltransferase Ugt302K1. Furthermore, 17 genes are categorized under "amino-polysaccharide chitin metabolic process". The presence of metabolic genes in the DEG set suggests that applied iron deprivation imbalanced cellular metabolisms in the BRGC (Table 4.7). Indeed, it is well-known that iron starvation can contribute in progression of metabolic disorders, and altered levels of lipid, carbohydrate, and amino acids are reported in anemia [257–260]. The induction of GstE6 further suggests that iron deprivation induced the generation of free radicals, consistent with the notion that iron deficiency induces lipid peroxidation, which results in ROS formation [261].

Furthermore, chitin (UDP-N-acetylglucosamine) is the main polysaccharide of the insect cuticle, but the link between chitin synthesis and iron homeostasis hitherto is unknown. It is indicated that the first enzyme in the chitin pathway, the UDP-N-acetylglucosamine diphosphorylase (also known as the mummy), is required for the proper organization of axon tracts in the CNS [262–264]. This suggests that BPS supplementation had an adverse effect on neuronal development in the brain. Moreover, it is worth mentioning that the Ugt302K1 is a UDP-glycosyltransferase that suggests it may function in the chitin metabolism.

I also identified two reproductive-related genes; an unclassified peptide sex-hormone called "Ductus ejaculatorius peptide 99B" (Dup99B) and "Antigen 5-related" (Ag5r) with FCs equal to 82.14 and 5.05 (Table 4.1). Ag5r is a CAP superfamily member (also known as sperm-

coating proteins) and is needed for male reproductivity. Interestingly, iron is required for normal spermatogenesis, particularly for sperm ejaculate thinning [9,265], and disruption of *Drosophila* mitoferrin causes male sterility [68]. This raises the question of whether iron deficiency induces signal molecules in the BRGC that may contribute to spermatogenesis.

Finally, I found eight uncharacterized genes, seven of which had insufficient annotation data (Figure 4.3A, Table 4.1). But the CG6244, which was significantly upregulated (FC=22.16), is orthologous to human elongation factor ELOF1 and anticipated to function in transcription via binding to RNA polymerase II complex [266].

4.3.4 Hsp22 and Hsp70 physically interact with Ferritin and Fe-S containing proteins

Next, I sought to study the Hsp22 and Hsp70 chaperone proteins since they were significantly upregulated after FAC supplementation. I chose to carry out an *ex vivo* Immunoprecipitation followed by MALDI-TOF mass-spectrometry (IP-MS) experiment in S2 Schneider cell by manipulating the media's iron level (using FAC and BPS). For this, I expressed Hsp22-3XFLAG, Hsp70-3XFLAG, and GFP-3XFLAG proteins in the S2 cells treated with FAC and BPS. The Flag-tagged GFP was used as the control to remove all the false-positive interactions in the experimental samples.

In brief, the IP-MS of Hsp22 resulted in 177 and 128 proteins in the FAC and BPS media (Figure 4.4A), respectively. There were 88 overlapping proteins and 129 medium-specific proteins between the two treatments (89 for the FAC- media and 40 for the BPS media). Hsp70, however, had a smaller interactome network. I found 35 and 13 proteins pulled-down proteins under FAC and BPS treatment, respectively. There were 12 overlaps and 24 non-overlap among the hits (Figure 4.4B). As reported previously, the Hsp22 and Hsp70 physically interact with each other to fulfill their common functions. Similarly, in the Hsp22 data sets, I further identified Hsp70 protein and vice versa. Furthermore, the PANTHER GO analysis of Hsp22 and Hsp70 interactome data sets identified BP, MF, and CC terms relevant to the heat shock proteins (data not shown). All these data support that the MT-IP assay was enabled to precipitate interacting proteins of Hsp22 and Hsp70 under the iron manipulation.

Surprisingly, I found that Hsp22 interacts with some key iron biology proteins. Upon FAC treatment, I identified the mitochondrial Cysteine Desulfurase (Nsf1), a critical component of the Fe-S cluster biosynthesis machinery, and ferritin heavy chain subunit (Fer1HCH). Furthermore,

mAcon1 (Mitochondrial aconitase 1), Cyp12a4 (an oxidoreductase) and RFeSP (Rieske iron-sulfur protein) were detected in the FAC interactome of Hsp22. The Fe-S-related-proteins in the interactome data sets are in agreement with the function of the Hsp22/Hsp70 complex in transporting the Fe-S clusters to recipient proteins [53,189,190]. The interaction of Hsp22 with Fer1HCH, mAcon1 and RFeSP was confirmed via a co-IP assay (Figure 4.4C). I co-transfected the S2 cells with plasmids encoding Hsp22-3XFLAG and mAcon1-5XMyc, RFeSP-5XMyc or Fer1HCH-5XMyc simultaneously. I then used Hsp22-3XFLAG as bait and immunoprecipitated proteins using the anti-FLAG bead. This suggests that the *Drosophila* Hsp22/Hsp70 complex also has a role in transporting the Fe-S clusters to proteins. Furthermore, the interaction with Fer1HCH indicates that the Hsp22/Hsp70 complex may facilitate ferritin folding or ferritin autophagy (see section 3.3.10 and 3.3.11).

Finally, I wondered if the Hsp proteins function is critical for brain cells or Ring-gland cells. To determine this, I first measured the expression of *Hsp22* and all *Hsp70s* in the RG and the brain separately. I then knocked-down their expression in each tissue individually. I found that all the Heat-shock genes are highly enriched in the RG, with > 8-fold expression (P-value < 0.0001). This was in agreement with the PG>RNAi-knockdown analysis (Figure 4.5A). I used a Prothoracic gland (PG)-specific Gal4 driver (phm22-Gal4) and a brain-specific Gal4 driver (Insc-Gal4) to deplete Hsp22 and Hsp70 the PG or the brain cells. The PG is the major part of the RG and requires abundant amounts of iron for ecdysone production [70,80,81]. Out of all tested *Hsp* genes, PG depletion of *Hsp22*, *Hsp70Ba* and *Hsp70Bbb* genes resulted in a significant developmental defect (Figure 4.5B). The PG loss of *Hsp22* and *Hsp70Ba* caused a prolonged feeding time (developmental delay) during the 3rd instar larvae larval stage (L3) with ~32 and ~24 hours, respectively. The *PG>Hsp70Bbb-RNAi* showed 69 % lethality during the 2nd and 3rd instar larvae (Figure 4.5B). On the other hand, I observed no significant developmental defects upon RNAi knockdown of *Hsp* genes in the brain cells (data not shown).

4.3.5 DEGs of Gut media analysis

In the gut dataset, I identified 26 and 40 DEGs via Deseq2 and edgeR, respectively. There were 18 overlapping DEGs between the two approaches. Among all the gut DEGs, 23 transcripts were FAC-upregulated, and 25 were BPS-upregulated (Figure 4.3B and Table 4.2).

4.3.5.1 Gut FAC upregulated genes

I identified ten metal-related genes among the FAC-upregulated genes. The ferritin subunits (the *Fer1HCH* and *Fer2LCH*), *Zip89B*, *Zip99C* (also known as *dZip13*), *galla-1* and an uncharacterized transcript; *CG17376* that codes for a 4Fe-4S binding protein (Table 4.2). Ferritin is an inducible iron protein that stores the excess iron. Our result indicated *Fer1HCH* and *Fer2LCH* expression induced for ~4 FC upon the media switch. This is consistent with reports that demonstrated iron induces ferritin in the *Drosophila* gut cells [66]. The Zip89B (FC=2.91) and Zip99C (Deseq2 FC= 2.06, edgeR FC=3.71) are zinc/iron permease of solute carrier family 39 (SLC39). The Zip89B is speculated to be an iron transporter, but the Zip99C functions in *Drosophila* iron homeostasis via loading iron into ferritin inside the ER [267]. Further, it is indicated that loss-of-Zip89B causes iron absorption defects in midgut cells [267].

Galla-1 is the homolog of human Iron-sulfur assembly component 2A (CIA2A, also known as FAM96A). The CIA2A, along with CIAO1, transfers 4Fe-4S to the iron regulatory protein (IRP1) and facilitates aconitase activity of IRP1 (also named holo-IRP) [268,269]. As mentioned in section 1.1.5, the apo-IRP1 enhances or blocks the translation of iron proteins through binding to iron-responsive elements (IRE) in the UTRs of mRNAs. For example, IRP1 binds to IREs in the 5'-UTR of Fer1HCH and blocks ferritin translation under low iron [209]. Although it has not been experimentally proven that *Drosophila* IRP1 (IRP1A) blocks translation of Fer1HCH mRNA under iron deprivation, induction of galla-1 in the iron overload condition (Deseq2 FC= 2.19, edgeR FC=5.82) suggests that it may contribute to the ferritin iron loading by converting IRP1 to aconitase.

Moreover, five additional metal coding genes, *MtnA*, *MtnB*, *MtnE*, *Ctr1B*, and *CG10505*, were upregulated after FAC supplementation (Table 4.2). The *MtnA*, *MtnB*, and *MtnE* were induced for approximately 2-6 FC and they belong to the metallothionein family and bind to copper. The Ctr1B (Deseq2 FC= 2.16, edgeR FC=3.53) is also a copper transporter that uptakes Cu in the intestine cells, but CG10505 (FC=5.98) is an ABC-transporter and responds to copper and zinc. This data provides further evidence for the interplay between iron, zinc, and copper metabolism.

Furthermore, there were genes encoding a water channel (Drip), a predicted Ca^{2+} dependent C-type lectin (CG7763), and a ribosomal gene (RpS5b) that were induced with FAC. The CG7763,

which has 2.16 Deseq2 FC and 5.39 edgeR FC, possess a C-type (Ca2+dependent) lectin like domain that has a carbohydrate-binding activity (Flybase). Many pathogens bind to the cell surface glycans of the host cells, and lectin proteins block this process via binding to carbohydrates [253]. The upregulation of *CG7763* in the FAC medium indicates that the gene may contribute to the immunity via carbohydrates binding. I also found a trans-splicing variant of mod(mdg4) locus named pre-mod(mdg4)-N with a remarkably high FC (FC=369.65, Table 4.2) . The *mod(mdg4)* locus encodes different proteins from both DNA strands of this locus. The trans-splicing mechanism generates diverse proteins by combining transcripts composed of 5′-exons with transcripts that are encoded by 3′-exons [270]. The Mod(mdg4) protein have an N-terminal BTB/POZ domain, and act as a transcription factor that governs chromatin structure [271,272]. This significant induction suggests that the mod(mdg4) locus may contribute to the regulation of iron genes in the gut. The rest of the FAC-up genes (8 genes) were uncharacterized genes (Table 4.2).

4.3.5.1 Gut BPS upregulated genes

Among the BPS upregulated genes, I further found iron-related genes (Figure 4.3B, and Table 4.2). The expression of membrane iron importer Malvolio (*Mvl*) and three putative heme-binding cytochromes: *CG5157*, *CG13077*, and *CG13078*, were significantly enhanced (~2-25 FC). *Mvl* is expressed in the midgut and plays a key role in the systemic iron homeostasis via iron import [273–275]. CG5157 induced for is orthologous to human CYB5B, which localizes in the outer mitochondrial membrane and functions in progesterone metabolism [276]. CG13077 and CG13078 are cytochrome b561 proteins. They are inferred to act as transmembrane ferric reductases due to a high homology to human CYB561D1 and CYB561D1 proteins.

Furthermore, there was a predicted trimeric intracellular cation membrane channel (CG33061) and a riboflavin transporter (Rift). Interestingly, studies on plants under iron-deprived conditions also demonstrated changes in riboflavin transport [119]. Consistently, administering riboflavin and iron to patients with iron-deficiency anemia has been shown to reduce the disease prevalence significantly [277]. Moreover, I identified a protein with a putative function in peroxisome biogenesis (CG33474). CG33474 is an ortholog to human PEX11G that regulates the size and number of peroxisomes in cells. Peroxisomes are enriched for copper and iron and can release metals under specific conditions [278]. This suggests that the BPS derives iron release from protein degradation in the peroxisomes.

Similar to BRGC, the gut cells isolated from animals reared on the iron depleted media further increased the transcriptional level of metabolic-related genes significantly (~ 1.5 – 30 FC, Table 4.2). In summary, I found CG18179, an uncharacterized putative serine-type endopeptidase and Ugt37A1 and Ugt302E1 that are glycosyltransferase enzymes (Table 4.2). The presence of glycosyltransferring enzymes suggests that chitin metabolism is also activated in the gut cells. Indeed, the peritrophic membrane layer of the insect midgut contains chitin and functions as a defense barrier against toxins and pathogens [279]. Interestingly, iron starvation has been associated with increased immunity to infection in both humans and insects [280,281]. I further observed an increase in the expression of antimicrobial immune molecule IM4 with a 127.12 FC in the low iron diet. This illustrates that the IM4 may participate in the innate iron immune response in *Drosophila*, as the IM4 level is elevated upon bacterial infection [282]. Desi (Desiccate) is another immune/stress-related protein in this list. It is a signaling protein with SH2, PDZ and cAMP-dependent protein kinase phosphorylation domains. It has been demonstrated that Desi is involved in the desiccation stress resistance [283]. It is worth noting that desiccation stress is associated with an increase in the chitin level of insect cuticle [284]. All this evidence strongly indicates that chitin-triggered immunity is induced under iron starvation.

Furthermore, I found a significant high BPS transcriptional response for Ng3 (new glue 3, FC= 147.03), which is an ecdysone-regulated intermoult puff gene (Table 4.2). Ecdysone is the key steroid in *Drosophila* that regulates gene expression of salivary gland polytene chromosomes in these puffs (= decondensed chromatin regions indicative of gene activity). Genes in the early puffs are induced directly by the ecdysone and encode proteins that activate secondary responsive genes [285,286]. As mentioned before, the steroid hormone production in the PG is considerably dependent on iron for heme production [70,95,149]. This indicates ecdysone may directly regulate the gene expression of midgut and hindgut polytene chromosomes in response to iron deficiency.

Additionally, Superoxide dismutase 3 (Sod3), which converts oxygen free radicals to hydrogen peroxide, was among the 25 BPS-up genes with 1.58 FC (Table 4.2). *Drosophila* has three *Sod* genes (*Sod1*, *Sod2* and *Sod3*) that encode Cu, Zn and Mn metal binding proteins involved in free radical defense mechanism [287–289]. Interestingly, the SOD enzyme has also been induced in plants under severe iron deficiency to protect cells from superoxide radicals [290]. This suggests Sod3 plays a similar role in *Drosophila* cells and may contribute to redox balance via iron-binding

activity. Finally, and surprisingly, I identified three trans-splicing variants of the mod(mdg4) locus in the gut; the pre-mod(mdg4)-I, pre-mod(mdg4)-V and pre-mod(mdg4)-z with 670.92, 252.48 and 138.14 FC upon BPS supplementation, respectively (Table 4.2). The significant induction of these transcripts , along with FAC-upregulated pre-mod(mdg4)-N, provide substantial evidence that mod(mdg4) locus coding transcription factors that regulate iron homeostasis in the midgut.

4.3.6 DEGs of WB Media analysis

I analyzed the WB-specific transcripts with the same strategy as the BRGC and gut. In total, I found 21 DEGs with eight overlaps between the edgeR and Deseq2 methods. Of which, 15 genes were Deseq2-specific, and 14 genes were edgeR-specific hits (Figure 4.3C and Table 4.3).

The 13 genes of 21 DEGs were FAC up-regulated (With six overlaps), and eight transcripts were induced with BPS supplementation (with two overlaps). Moreover, I identified that 13 DEGs of WB (62%) are further present in the gut data set (Figure 4.3C and D). One explanation for this is that the gut represents a large volume of the whole larval body. However, investigating the other genes allows us to identify iron-responsive genes in the other tissues. Therefore, I focused only on the eight WB-specific genes and used the FlyAtlas RNA-seq data to check their tissue-specific expression in the larval [291].

4.3.6.1 WB FAC upregulated genes

I found six FAC responsive genes: the *dgt2*, *Lk*, *CG3732*, *CG8745*, *CG14989*, and *CG7720* with moderate expression level (~1.3 to 1.8 FC, Table 4.3). The Dgt2 is a microtubule-binding peptide from the augmin complex expressed in the Larval CNS and trachea. It governs the localization of γ-tubulin into the microtubules [292,293]. The link between microtubule polymerization/depolymerization and iron has not been established yet. But, preliminary studies suggested that iron affects microtubule polymerization [294], and increased blood platelet counts in the iron deficiency anemia is a consequence of decreased tubulin expression [295]. I also identified Leucokinin (*LK*) neuropeptide that is expressed in the innervated neurons of the corpus cardiacum gland, the CNS, and the trachea of larvae [296]. The LK participates in the homeostatic regulation of ions such as Ca^{2+} via adjusting the motility of the Malpighian tubes and hindgut [297]. Our data also proposes an iron homeostasis role for the Leucokinin in *Drosophila* that needs further experimental validation.

Furthermore, the CG7720 is a non-annotated membrane sodium/glucose cotransporter. The CG7720 is predicted to be a member of the solute carrier family (SLC) because of high homology to the human SLC5A5, SLC5A8 and SLC5A12 proteins. According to the FlyAtlas, *CG7720* is highly expressed in the larvae gut, but it also has moderate expression in the Malpighian tubules, salivary gland, trachea, and carcass. Identification of this metal transporter in the WB samples and not the gut samples (Deseq2 FC= 1.83, edgeR FC= 231, Table 4.3) suggests that it might be required for iron import in other tissues.

Finally, two of the three remaining FAC upregulated genes encode peptides with putative metabolic functions (Table 4.3). The *CG3732,* which has a 1.31 FC, is moderately expressed in the CNS and trachea. It is inferred that the CG3732 is a nuclear lipopolysaccharide-binding protein with a zinc finger motif (found in RanBP2). The zinc fingers are common protein motifs in nuclear proteins, but they further have lipid and protein binding abilities [298]. It is worth noting that the lipopolysaccharides enhance inflammatory responses by increasing the mitochondrial superoxide production, and iron has been indicated to elevate this process [299]. The *CG8745*, however, encodes a putative transaminases enzyme with significantly high level in the larval fat body. The fat body is the insect liver, and the induction of *CG8745* (FC= 1.48) under iron overload is consistent with the observation in the humans[300 300]. It is demonstrated that high iron level in liver cells enhances the transaminases activity [300]. The molecular function of CG14989 is still unknown, but it is classified as a nuclear protein (inferred from Flybase).

4.3.6.2 WB BPS: upregulated genes

Two DEGs of WB-specific hits (CG14205 and CG17580) were BPS-inducible genes (Table 4.3). The *CG14205* FC is included for 2.75 and is inferred to encode an acyltransferase-3. The acetyl group is a type of acyl groups that induce physical resistance of chitin [263,264]. This is consistent with the induction of chitin-related genes in other tissues and further supports the idea that chitin pathways are activated during iron depletion. Moreover, the *CG14205* has a significant expression in the larval and adults' midgut, according to the FlyAtlas RNA-seq data. Our data suggests that the *CG14205* is expressed in other tissues upon iron depletion. On the other hand, *CG17580* encodes an unknown nuclear protein with a relatively moderate expression in the fat body, imaginal disc and testis. However, its expression was significantly high in this cohort, with

a 148.06 FC (Table 4.3). This suggests CG17580 may have a regulatory function in the nucleus during iron depletion.

4.3.7 Time course analysis of DEGs

I next asked which genes have a temporal response to the iron level. I narrowed our analysis to 4- and 16-time points to distinguish the genes with an early (4 hours) and late response (16 hours) to dietary iron. The temporal analysis enabled us to identify a large number of DEGs at these time points. The results are summarized in Figure 4.6A.

Additionally, I performed a principal component analysis (PCA) to examine which tissue has higher variance in the four and 16 hour timepoints (Figure 4.6A) [110]. The high variance in a dataset demonstrates that the more genes have responded to the media treatment. Therefore, this can be inferred as a higher number of genes with divergent expression patterns or a higher number of DEGs. The PCA indicated that gut transcripts form the most discrete group among other samples at both time points, but they had the highest variation and positive correlation at the four hour time point. The PCA further showed that the BRGC and WB had high variance at 16 hours, and they were distinct from the gut samples at this time point. Consistently, I further identified more genes in BRGC and WB in the late analysis. However, I found more genes in the gut tissue's early response (Figure 4.6A). The PCA analysis, therefore, indicated that the gut is the primary tissue that responds to FAC immediately after the media switch (as expected). On the other hand, for the internal tissues such as BRGC iron has to be systemically delivered to be sensed. Thus, BRGC responds to the dietary FAC at the later time point of the experiment.

4.3.7.1 Temporal profile of DEGs in BRGC samples

In the early responding group of BRGC transcripts, I identified 43 (31 FAC-UP and 12 BPS-UP) and 46 (with 13 FAC-up and 33 BPS-up) genes with the Deseq2 and the edgeR, respectively (Figure 4.6B and Table 4.4). Among these genes were 22 FAC and 8 BPS upregulated overlaps. However, in the late analysis, there were 377 Deseq2 and 193 edgeR DEGs. There were 31 overlap genes between the outputs. Furthermore, there were 268 FAC-up genes (Deseq2: 248 DEGs and edgeR=20 DEGs) and 302 BPS-up genes (Deseq2: 129 DEGs and edgeR=173 DEGs) in total.

4.3.7.2 Temporal profile of DEGs in gut samples

In the gut early response analysis, the Deseq2 resulted in 1461 hits, of which 262 genes were upregulated in the FAC media, and 1199 genes were upregulated in the BPS media. On the other hand, the edgeR found 614 DEGs that 188 were FAC-up and 426 were BPS-up genes. There were 155 FAC- and 404 BPS-upregulated overlaps (in total, 559 genes, Figure 4.6B and Table 4.5).

In the gut late-analysis, I found 481, 211, and 143 hits for the Deseq2, edgeR, and overlap genes, respectively. Among the DEGs of late analysis, there were 336 responsive genes to FAC (Deseq2 =194, edgeR =142 and overlap=93 genes) and 356 responsive genes to BPS (Deseq2 287, edgeR =69 and overlap =50 genes).

4.3.7.1 Temporal profile of DEGs in WB samples

Finally, for the WB, I identified 534 and 310 genes with the Deseq2 and edgeR in the quick analysis. The number of FAC and BPS-upregulated genes of the Deseq2 hits was 160 and 137, but the DEGs numbers for the edgeR were 88 and 222 genes (Figure 4.6B and Table 4.6). I also found 252 overlapping transcripts between the two methods (FAC-up= 79 and BPS-up=173 genes). In the WB-late response set, there were 589, 391, and 307 genes for the Deseq2, edgeR, and overlaps, respectively. Of which 303, 189, and 150 DEGs were FAC-up, but 286, 202 and 157 DEGs were BPS-up, respectively.

4.3.8 Confirming identified DEGs with different assays

To further validate the identified DEGs in this study, I performed three different experiments. First, I measured the expression level of a subset of selected genes via the quantitative real-time PCR (qPCR). Second, I carried out a Prussian-blue staining to detect iron in the midgut of 3rd instar larvae after knocking down a group of selected genes. The selection was a cherry-picking strategy to check whether these genes' function is essential for iron absorption in the gut cells. However, I tried to select genes with already known functions in iron homeostasis and genes with unknown function that were found by my analysis. This would allow a better comparison between the selected genes. Lastly, I used a GFP-tap allele of ferritin heavy chain protein, the Fer1HCHG[188] allele, to explore the endogenous expression pattern of Fer1HCH in the BRGC and gut upon iron manipulation.

4.3.8.1 qPCR validation of DEGs

To verify the expression of genes identified by Deseq2 and edgeR, I selected a subset of genes from each tissue's overlap groups. In order to carry out qPCR, I used the remaining RNA samples of the RNA-seq. I selected the *Hsp22*, *Hsp68*, *Hsp70Ab*, and *Hsp70Bbb* genes for the BRGC. In the gut genes, the *Fer1HCH*, *Fer2LCH*, *galla-1*, and *Mvl* were selected. The *CG5157 Fer1HCH*, *Fer2LCH*, and *galla-1* were picked from the WB set to perform qPCR (Figure 4.7). Furthermore, I used the Ribosomal protein RP-49 as the endogenous control. I generated 72 data points for each gene (three biological replicates run in triplet for two types of media, and four tested time points, 3 x 3 x 2 x 4= 72). I then calculated the delta-delta CT (ΔΔ CT) value of each gene based on the CT values in FAC and BPS media (in relation to the expression of Rp49). Finally, I plotted the results based on the media in which a gene has a higher expression level in each time-point. Therefore, graphs show upregulation of genes in BPS-supplemented media compared to the FAC media and vice versa. The qPCR expression analysis of selected genes was in agreement with the RNA-Seq data (Figure 4.7).

4.3.8.2 Prussian-blue staining

I next sought to test whether the gut DEGs are functionally critical for the iron absorption or transport (Figure 4.8). Since there was a large number of genes, I hand-picked 24 genes from both FAC- and BPS-upregulated genes. These were mostly genes that appeared promising based on their strong transcriptional response, their protein domains or the predicted functions. I also included genes that were already known to function in the iron homeostasis in this subset. The *Fer1HCH*, *Fer2LCH*, and *Zip99C* genes were selected for this assay to test the Prussian blue staining's sensitivity. To interfere with the function of selected genes in the gut cells, I crossed a midgut Gal4 driver (*NP3084-Gal4*) that expresses Gal4 predominantly in the whole midgut with RNAi lines of 24 genes. As the control, I conducted the same cross for the wild-type flies (*NP3084-Gal4>W^{1118}*). I next fed the progeny of the *NP3084-Gal4>RNAi* crosses with FAC- and BPS-enriched food until the late L3 stage. Finally, the guts were dissected and stained with Prussian Blue to detect iron-rich cells. I repeated the staining up to five times to compare the blue signal between control and RNAi larvae. I only focused on results of the FAC medium as I did not detect intensive blue/iron signal in the BPS media (Figure 4.8A). In control animals raised in the FAC media, I detected the blue signal in the anterior and posterior midgut with an intense signal in the middle midgut iron region. However, I observed four blue signal patterns in the experimental

group compared to the control (Figure 4.8B). First, a no-effect pattern (similar to the control), second, a no or weak blue signal in the midgut, third, a similar ferritin pattern with an intense signal only in the iron region and fourth, a stronger positive signal in the midgut.

I found three upregulated genes in the FAC subset and two in the BPS subset that did not affect iron signal or transport in the midgut (Figure 4.8B). There were three transporters in the second group: the *Zip99C* (FAC-upregulated gene), *Ugt302E1* and *ABCA* (two BPS-up-regulated genes). The loss of function of these genes in gut cells exhibited no or a weak iron signal. As mentioned earlier, the Zip99C codes a member of the ZIP transporter family that functions in the iron transport of gut cells [301,302]. Consistently, the staining indicated that the gut loss of function of Zip99C blocks iron transport into the iron-secretory pathway. The ABCA is a membrane ATPase lipid transporter, and the Ugt302E1 is a chitin-related enzyme (UDP-glycosyltransferase). Their transcripts are up-regulated in iron-deficient conditions, but their ablation in the midgut cells dramatically decreases iron signal after FAC administration. This suggests they may be invp;ved in iron import during iron scarcity.

In the third group (similar to ferritin staining pattern), nine genes showed only a blue stain in the iron cell region (Figure 4.8B). This is similar to what has been reported for the loss of *Fer1HCH* and *Fer2LCH* in midgut [67]. Drip, which codes an aquaporin water channel, heat shock protein Hsp68, and ribosomal protein Rps5b are FAC upregulated genes in this group. Interestingly, analogous iron accumulation of midgut-specific knockdown of Hsp68 and Rps5b to Fer1HCH provides evidence that heat-shock proteins (particularly Hsp22 and Hsp70s) along with ribosomal proteins function in iron homeostasis by regulating the folding of ferritin. The other six genes of the BPS-upregulated gene cohort are non-annotated and have unknown functions. Among them, there were a putative cation transporter (CG33061) and a predicted peroxisomal biogenesis factor (CG33474). This also indicates that these uncharacterized genes may be iron importer during the iron deficiency.

Finally, I found two genes, the *CG14626* and *galla-1*, that, when targeted via RNAi, resulted in iron accumulation in midgut cells. *CG14626* gene is not characterized yet. However, the iron accumulation of gut loss of function of *galla-1* is consistent with the findings that indicated mutations in genes involved in Fe-S cluster assembly, such as Frataxin, cause iron accumulation in cells [303].

4.3.8.3 Fer1HCH expression pattern

Ferritin is an evolutionarily conserved iron storage protein composed of two subunits: a heavy-chain subunit and a light-chain subunit [43]. Under iron overload conditions, the expression of ferritin encoding genes is governed by two distinct mechanisms. First, it is regulated by elevation in the expression of subunit encoding genes, and second, their mRNA stability is controlled by the IRE/IRP system [209].

Consistent with previous observations, I also detected a significant induction in *Fer1HCH* and *Fer2LCH* expression in the gut and WB samples (up to a six-fold change, Figure 4.7), but not in the BRGC samples. However, In the BRGC, I found that the protein encoded by *Hsp22*, a highly expressed gene in the ring gland (RG), physically interacts with Fer1HCH. This suggests that ferritin is either imported into RG cells or is regulated at the protein level (see section 3.3.10 and 3.3.11).

Given the induction of ferritin genes, I wondered whether this up-regulation is detectable at the protein level. I used the GFP-tagged Fer1HCH allele ($Fer1HCH^{G188}$) that has been used to investigate the tissue-specific expression of ferritin in *Drosophila* [193]. For this, I mimicked the same iron manipulation that I did for the RNA-seq experiment. I reared the $Fer1HCH^{G188}$ flies in BPS-media for five generations and then transferred the 6th generation into the FAC supplemented food. As expected in the iron overload and iron-depleted conditions, I did not observe a significant difference between the brain's Fer1HCH expression (Figure 4.9). However, I observed a slight increase in the GFP signal of the RG cells after FAC supplementation.

On the other hand, in the midgut of animals raised in the BPS food, the GFP-Fer1HCH signal was restricted to the iron region cells. But, upon FAC administration, I observed a large number of midgut cells (including the iron region) that express GFP-Fer1HCH. The fluorescence in the anterior midgut cells was weaker than the signal in the posterior midgut cells (Figure 4.9). This data is also in agreement with the RNA-Seq results.

4.3.9 HHpred and GO enrichment analysis of DEGs

I next sought to perform gene ontology/ term enrichment statistics using PANTHER GO-Slim [304] to investigate patterns among DEGs (Table 4.7). Furthermore, I performed the HHpred analysis to identify distal homologous proteins in the other species. The HHpred uses a hidden

Markov model to find homolog proteins based on sequence alignment and secondary structure similarity [305]. It creates a Homology Probability score (HP) by analyzing the secondary structures within the proteins. The higher the score, the more structurally similar two proteins are. Therefore, this allows us to identify iron proteins' orthologs that have not been identified in *Drosophila* because of the protein sequence discrepancies. I looked for homologs with a link to metals in the outputs and categorized them into three groups based on the metals type: iron-, copper- and other metal-proteins (Table 4.14). However, here I only focused on the *Drosophila* unknown proteins linked to iron homeostasis and had an HP score > 50.

4.3.9.1 BRGC DEGs analysis

In the FAC-upregulated genes of BRGC, all the BP and MF terms referred to the heat-shock genes. The "response to heat" and the "heat-shock protein binding" were the top BP and MF terms, respectively. Furthermore, the "cytosol" and "plasma membrane or extracellular" and "nucleus" were the overrepresented CC-terms. This is in agreement with the subcellular localization of hsp70 proteins in the cytosol and nucleus [306]. However, I did not identify any GO slim terms with statistical significance for the BPS upregulated gene cohort (Table 4.7).

Next, I wondered why most of the DEGs in this tissue are predicted to act as extracellular proteins (Table 4.17). Therefore, I used the SignalP-5 server to identify if they harbor a signal peptide required for protein secretion to extracellular space [160]. Intriguingly, the analysis demonstrated that 72% of responsive transcripts (36 genes out of 50) encode a statistically confident signal peptide required for protein import to the extracellular space.

Lastly, I performed the HHpred analysis to identify distal homologs for the BRGC genes (Table 4.14). I found four iron-related proteins in the first group, of which two proteins were similar to the iron transporters and two proteins were identical to the Fe-S proteins. dmGlut and Mco4 had an HP score of 100 to the iron transporter ferroportin in Bdellovibrio bacteriovorus and FET3 in yeast. Recall that ferroportin is an iron exporter in duodenal enterocytes that releases iron into the circulation [307], and that ferroportin has not yet been identified in *Drosophila*. The *CG6244* and *Ugt302K1* further encode proteins with 87.17 and 68.4 HP to Rubredoxin-1 of Desulfovibrio desulfuricans (an Fe^{3+}-binding electron transfer protein) and in *Clostridium pasteurianum's* NIFH1 (an 4Fe-4S binding oxidoreductase), respectively. The Rubredoxin-1 is predicted to be involved in the redox processes but the NIFH1 is a nitrogenase iron protein that is involved in

nitrogen fixation process [308]. The similarity of Ugt302K1 with the NIFH1 further suggests that enzymes in the chitin biosynthesis pathway may require an Fe-S cluster as the cofactor.

4.3.9.2 Gut DEGs analysis

The GO enrichment analysis of the gut FAC-up DEG set detected BP and MF categories relevant to the metal homeostasis. It was due to the presence of *Zip89B*, *Zip99C*, *Ctr1B*, *Fer1HCH* and *Fer2LCH* genes in this set. However, for the BPS-up transcripts, I did not find GO terms with statistical confidence with either PANTHER or PANTHER GO slim analysis (Table 4.7). However, I could not identify significant GO-CC terms for all the gut DEGs (FAC and BPS genes). But, when I carried out the SignalP-5 analysis, 17 genes (11 BPS-up and 6 FAC-up genes) had a significant value for the secretion signal peptide (Table 4.18).

Next, I conducted the same HHpred procedure as the BRGC to find orthologs of the gut DEGs (Table 4.15). I identified 15 iron-related genes via the gut's HHpred analysis, but only eight DEGs had a significant ortholog to an iron-related protein. The HHpred indicated that the modifier of mdg4 (mod(mdg4)) proteins are highly similar to the yeast iron regulatory transcription factor ATF2. A standard BLAST search misses this. The pre-mod(mdg4)-Z, pre-mod(mdg4)-I, pre-mod(mdg4)-V and pre-mod(mdg4)-N had 89.76, 89.75, 74.16 and 73.24 HP scores to the yeast ATF2, respectively. Interestingly, when the iron is deficient, ATF2 upregulates the expression of vacuolar and mitochondrial NRAMP iron transporters (*SMF3* and *MRS4*) in yeast [309]. Moreover, I found that the CG14014, a transcript in the BPS-up cohort, is a structurally similar to the human c-Myb transcription factor (96.27 HP score). Interestingly, the c-Myb transcription factor participates in iron homeostasis by regulating the duodenal enterocytes' ferroportin expression [307].

I further found that the CG5157 is similar to the humans' Cytochrome b5 reductase SUOX with a 99.58 HP score, and the CG13078 and CG13077 are orthologs of human's Cytochrome b reductase CYBRD1 with 99.89 and 99.86 HP score. The Cytochromes are oxido-reductive proteins that bind iron in the form of a heme prosthetic group [86].

4.3.9.3 WB DEGs analysis

The enrichment analysis of WB FAC-up transcripts demonstrated that the BP and MF terms were highly enriched for the metal-iron related terms (Table 4.7), similar to the terms in the gut DEGs. On the other hand, I did not identify any terms for the BPS-up genes because of the

limited number of genes. Furthermore, I could not detect any GO-CC slim terms for both FAC- and BPS-DEGs. This was consistent with the SignalP-5 analysis that I found only five secretory proteins (Table 4.19).

The HHpred server further identified 11 metal-relevant orthologs for the WB genes (Table 4.16). Of which, five genes were the known proteins of iron homeostasis, and three genes were overlapped to the gut DEGs. However, the other two genes are orthologs to the cytochrome proteins. The CG17580 is identical to cytochrome C oxidase CTADII in *Paracoccus denitrificans* with a 72.57 HP score, and the CG14205 is similar to the CYBRD1 with a 79.8 HP.

4.3.10 GO analysis of the temporal DEGs

I next performed the Panther GO-slim enrichment analysis for the quick and late DEGs. There were overlap terms among the upregulated sets, but I only focused on the highly enriched biological process (BP) and molecular function (MF) terms since they are the most characterized GO terms.

4.3.10.1 BRGC GO analysis

In the BRGC quick FAC upregulated genes, I did not find any significant GO terms due to a small number of DEGs (Table 4.8). However, in the late analysis, the BP and MF-GO terms of the FAC upregulated DEGs (Deseq2 and edgeR) were relevant to heat shock proteins. The "response to heat", "cellular response to heat" and "response to unfolded proteins" were the top statistically enriched terms (Table 4.8).

On the other hand, in the early response BPS-up group, I further found heat-shock-related BP and MF terms in the Deseq2 and edgeR DEGs (Table 4.9). In the late BPS-up genes, I did not find overrepresented BP and MF terms for Deseq2 genes. However, in the edgeR set, the DNA catabolic, apoptosis and metabolic processes terms were the top three BP GO categories. But, the nuclease activity- and endopeptidase activity-terms were the top MF enriched GO terms.

4.3.10.2 Gut GO analysis

In the gut tissue, the "zinc ion transport" and "glutathione metabolic process" were frequently BP-detected terms in both quick and late FAC-upregulated transcripts (Table 4.10). This is consistent with the previous studies that demonstrated iron-responsive genes are further expressed in Zinc deficiency and zinc overload conditions [234,310,311]. Furthermore, glutathione S-

transferase enzymes, particularly the Delta and Epsilon classes, are well-known detoxifying enzymes that protect cells from oxidative damages [261]. Expression of GST genes (such as *GstD* and *GstE*) upon FAC administration indicates oxidative damages protective processes have been activated in the gut cells.

In the quick BPS upregulated genes, I found that terms relevant to lipid metabolism, such as "lipid homeostasis" and "lipid localization" are highly enriched among the gut transcripts (Table 4.11). Interestingly, it has been demonstrated that iron deficiency stimulates lipid metabolism in vertebrates [257]. This suggests that *Drosophila* may share identical responses to iron restriction. On the other hand, I could only find the heat shock-relevant BP and MF terms in the late BPS-up of the edgeR set.

4.3.10.3 WB GO analysis

Because of the large number of shared genes between gut and WB, I observed similar BP and MF terms in the quick WB FAC-upregulated DEGs (Table 4.12). The terms relevant to iron/metals such as "zinc ion transport", "transition metal ion transport" and "glutathione transferase activity" were prevalent BP-terms among the Deseq2, edgeR, and overlap sets. However, "alkyltransferase activity" was the only enriched MF term for the quick WB FAC-upregulated DEGs.

I observed similar metal-relevant terms in the late edgeR DEGs. However, the metabolic processes terms such as amino acid metabolism, carboxylic acid metabolism, and carbohydrate metabolism appeared significantly in the late Deseq2 PB terms. This is because of the genes linked to lipid metabolism (*Lsp1 α*, *Lsp1 β*, *LSp1 γ*, *Lsp2*, *Npc2d*, and *Npc2g*) and carbohydrate metabolism (*GlyP*, *Mal-A1*, *Pfk*, *Gapdh1&2*, *Ldh*, *Tpi*, and *GCS2 β*). The link between the iron level and metabolic status is still unclear. However, iron increases lipid peroxidation and advances insulin resistance syndrome [312,313]. Furthermore, The GO analysis detected only "drug binding" MF term for the late FAC-up in the Deseq2 set.

Finally, I observed metabolism-related BP- and MF terms in all quick and late analyses BPS upregulated sets (Figure 4.13).

4.5 Discussion

4.5.1 Experimental procedures

The imbalanced iron levels are associated with a wide range of disorders such as hereditary hemochromatosis, iron-loaded induced anemia and iron-deficiency induced anemia [212,217–220,314,315]. My work has demonstrated that *Drosophila* larvae are an excellent model to study biological responses to iron. To investigate and compare transcriptional responses to changes in dietary iron, I reared flies for five generations in BPS-supplemented diet. The iron chelator BPS has a high affinity to the absorbable iron (ferrous) and reduces cellular iron levels. Our decision to use 5th generation of flies was not arbitrary, as BPS had no or minor developmental effects on the G1 flies. This was presumably due to maternal iron stores or the induction of iron deficiency mediated iron turnover [216,316]. In G5, on the other hand, animals showed a dramatic prolonged larval stage and lethality (Figure 4.1A and B), but yet there was a reasonable number of surviving larvae to carry out experiment.

Our approach was not successful to find all genes involved in iron homeostasis such as the transferrin receptor (TfR), which is the major player of the mammalian systemic iron delivery [33]. However, identifying the known iron homeostasis genes in our experiment (*Fer1HCH*, *Fer2LCH*, *Mvl*, *galla-1*, and *Zip99C*) demonstrated that our experimental and computational approaches successfully found documented iron-responsive genes. I designed our experiment with two replicates because of the large number of samples. To identify DEGs, I used the Deseq2 and edgeR platforms as they are designed to find DEGs with a limited number of reads and biological replicates [247–249]. To avoid false positives, Deseq2 calculates a modified mean over all samples to re-estimate adjusted P-value for all genes [247,248]. Therefore, it replaces the outliers with the predicted value, resulting in a conservative way to find target genes [247,249]. edgeR, on the other hand, is less conservative in the finding of DEGs. The primary assumption in edgeR is based on the reads' abundance per each transcript, and the statistical significance (P-value) of each gene is calculated across the samples (experimental vs. control) [247,317]. Therefore, the two methods' overlapping genes result in the differentially expressed genes with significantly high confidence.

4.5.2 Heat shock proteins and iron

A critical finding of this study was identifying *Drosophila* heat-shock genes. I found *Drosophila* Hsp22 and members of the Hsp70 family respond to dietary iron manipulation. Hsp22 is a small chaperone that binds to protein oligomers to block the protein aggregation during stress [318–321]. However, the release of protein from the Hsp22 requires Hsp70 protein [318–321]. Indeed, the Hsp22/Hsp70 complex is the central machinery for protein folding of newly synthesized polypeptides and refolding of misfolded aggregated proteins [320,322]. The Hsp22/Hsp70 complex is known to have a role in the Fe-S clusters corporation into proteins [53,189,190]. My study further found that the Hsp22/Hsp70 complex in *Drosophila* interacts with the core component of 2Fe-2S cluster biosynthesis machinery, NFS1, and recipients proteins such as SDHA, mAcon1 and RFeSP (Figure 4.5A and B).

Furthermore, I noticed that Hsp22 and all Hsp70s are highly expressed in the PG and depletion of their functions results in developmental defects associated with ecdysone deficiency (Figure 4.4) [81]. Interestingly, the PG cells express a class of steroidogenic enzymes named Halloween enzymes that require substantial amounts of heme and Fe-S clusters [81]. The Halloween enzymes produce massive pulses of ecdysone hormone to govern developmental and biological processes [79,84,113]. Intriguingly, one of the Halloween enzymes (Neverland) is a Rieske iron-sulfur cluster protein that harbors Fe-S cofactor [82]. The physical interaction of Hsp22 with RFeSP suggests Hsp22 and Hsp70 proteins may contribute to steroid hormone production via transferring Fe-S cofactors to Neverland.

Lastly, I identified a novel role for the Hsp22/Hsp70 complex in the regulation of ferritin. The Hsp22/Hsp70 complex physically interacts with the holo-ferritin. This is to possibly regulate protein subunits folding and refolding, a process required for iron incorporation or targeting ferritin to the lysosomes (Section 3.3.10 and 3.3.11).

4.5.3 Iron and immunity

Another hallmark of this study was to identify genes with direct functions in immunity. The competition of higher organisms with their invading pathogens for iron resources, has been indicated to trigger both innate and adaptive immune responses [323–325]. Surprisingly, I found that *Drosophila* larvae express the lectin genes in response to FAC and the antimicrobial immune IM4

gene in response to BPS. The lectins are the principal component of the defense mechanism that destroys pathogens directly or via macrophages [211–213]. But, the IM4 is an immune protein that contributes to the defense system against injuries and pathogen infections [282]. These distinct defense responses are, in part, due to the increased risk of infection after iron modification that triggers iron immunity.

Additionally, I found evidence that immune responses triggered by low-iron is probably associated with the chitin metabolism. The chitin is the major component of the insect cuticular layer, which is the first defense line against risk factors [263,264]. Besides, chitin is an integral part of the peritrophic midgut membrane that protects epithelial cells from physical damages, toxins, and pathogens [279]. Under the low iron condition, I identified secretory proteins with a chitin-binding domain (Table 1). Furthermore, I found that the glycosyl- and acetyltransferase enzymes (Ugt302K1, Ugt37A1, Ugt302E1, and CG14205) are induced in the BPS media, suggesting they increase the chitin's physical properties, as the acyl groups are shown to elevate the physical resistance of chitin [263,264]. All these data indicate that chitin immunity would create a physical barrier against pathogens under iron depletion.

4.5.4 Iron regulatory transcription factors

Finally, our study in gut tissue identified orthologs of transcription factors with known roles in iron homeostasis. Interestingly, I identified four transcript isoforms of the modifier of mdg4 gene (three transcripts: Pre-mod(mdg4)-I, V, and Z in BPS food and the Pre-mod(mdg4)-N in FAC food) that respond to dietary iron manipulation. The HHpred analysis further indicated that all four isoforms have structural similarity with yeast iron-transcription factor ATF2 (Table 2). The modifier of mdg4 is a component of a gypsy insulator complex that, along with Su(Hw) (suppressor of Hairy wing insulator), modulates enhancer activity by physically attaching chromatin fibers to the nuclear membrane [271,272]. The mod(mdg4) gene has coding exons on its antiparallel DNA strands, and undergoes a complex trans-splicing process to form at least 31 isoforms with divergent roles [326]. This suggests that different isoforms of the mod(mdg4) facilitate the expression pattern of iron genes to coordinate the iron status. Whether these isoforms govern the iron regulatory enhancers to participate in iron homeostasis is an interesting question to address.

The HHpred analysis further identified the CG14014 (gut, BPS-up) as a homolog to the human c-Myb proto-oncogene transcription factor (Table 4.15). The c-Myb protein modulates the Myeloid zinc-finger 1 (MZF-1) activity, which induces the expression of ferroportin iron exporter [307]. However, whether elevation of CG14014 transcript in the iron-deficient food activates or suppresses iron transporter in *Drosophila* midgut cells is still a mystery.

4.6 Conclusion

In summary, this study identified previously known and novel iron-responsive genes that function in biological aspects of iron homeostasis. Our screening found candidates for some of the hitherto missing genes in *Drosophila*. But, it was inefficient to discover all the unidentified genes. Furthermore, our results revealed that there are overlapping cellular responses to iron deviancy and iron overload between *Drosophila* and humans. Therefore, this indicates *Drosophila* is an excellent model to study iron-related diseases.

4.7 Figures

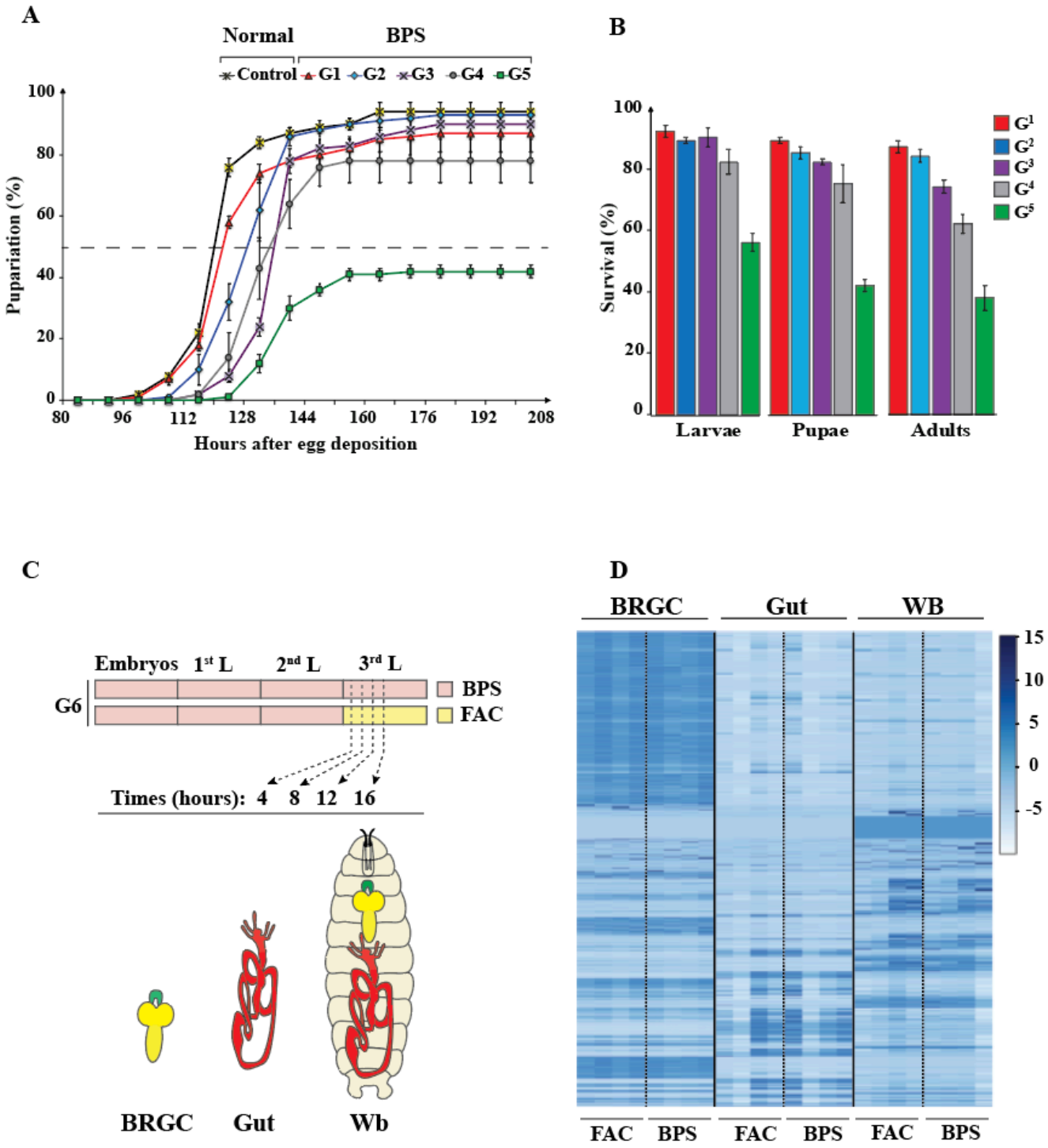
A
Normal
BPS
Control
G1
G2
G3
G4
G5
Pupariation (%)
Hours after egg deposition
B
Survival (%)
Larvae
Pupae
Adults
C
Embryos
1st L
2nd L
3rd L
G6
BPS
FAC
Times (hours): 4 8 12 16
BRGC
Gut
Wb
D
BRGC
Gut
WB
FAC
BPS

Figure 4. 1 Dietary Iron manipulation RNA-Seq experimental workflow

A) The timing of control flies pupae development for five generations (G1-G5, solid-colored lines) in BPS-supplemented media compared to control flies on normal food (black line). The dotted line indicates 50% of the larvae that have developed into the pupae. **B)** Percent survival of L3 larvae, pupae, and adults for generations G1 to G5, when reared on BPS food. Error bars represent the standard deviation among biological replicates. **C)** A schematic cartoon depicts the sample collection and time points of RNA-seq experiments. G6 eggs were carefully staged until the initiation of the 3rd instar larvae in the BPS food. Half of the population transferred into the FAC medium, and the other half reared in the BPS medium. After 4, 8, 12, and 16 hours, the BRGC (Brain Ring-Gland Complex), gut, and WB (Whole larval Body) samples were collected for carrying out the RNA-seq experiment. **D)** Heatmap of all transcripts (14557) in BRGC, Gut, and Wb samples. Solid lines separate transcripts within each tissue, and dotted lines separate transcripts in FAC and BPS supplemented media.

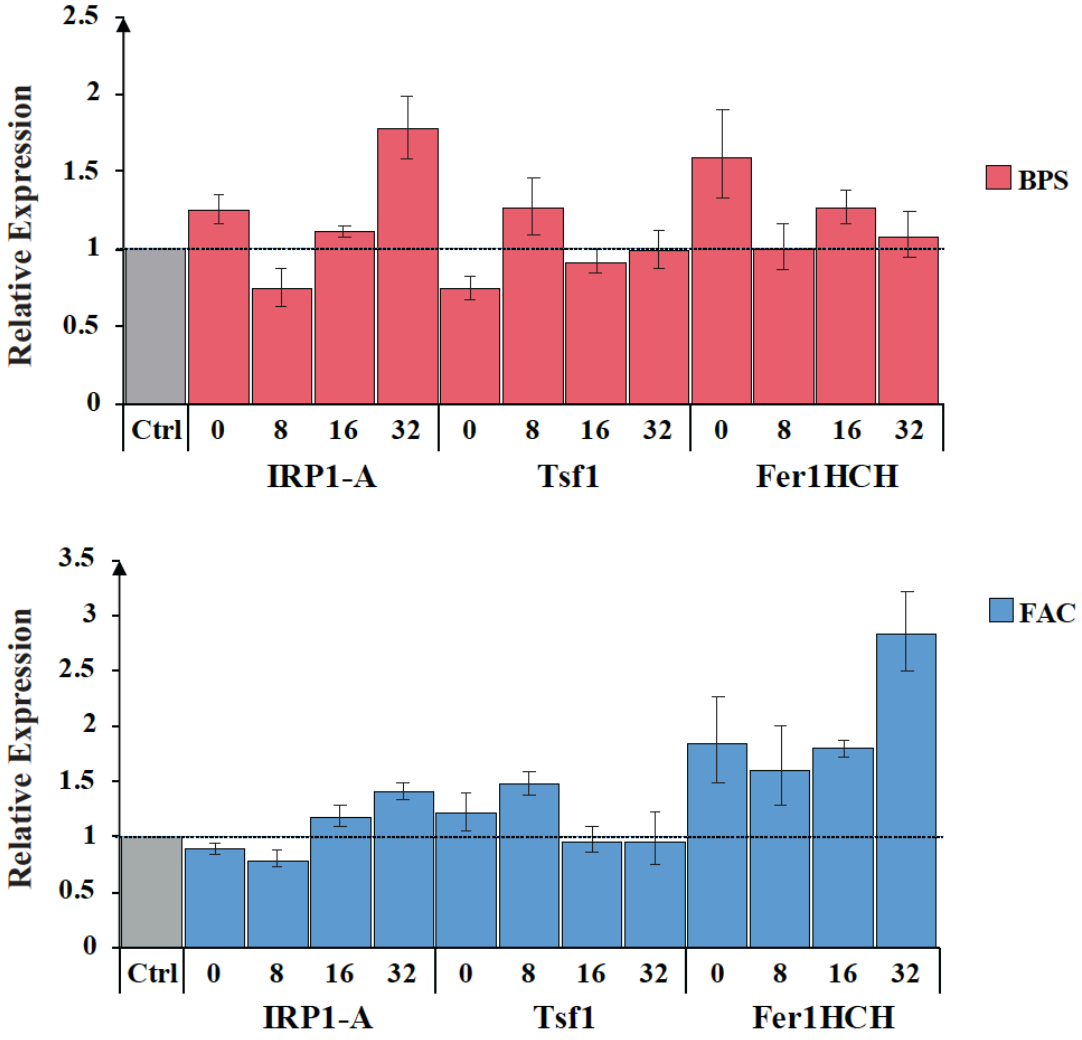

Figure 4. 2 qPCR analysis of iron-related genes in G1 control animals

The expression of ferritin 1 heavy chain subunit (Fer1HCH), transferrin 1 (Tsf1) and Iron-regulatory protein 1A (IRP-1A) in control whole larval body (WB). Animals were reared in media supplemented with BPS or FAC. Gene expression was normalized to rp49 levels and is shown as a relative fold change compared to the gene in larvae reared on normal food. The X-axis indicates sample collection time (0, 8, 16, and 32 hours after L2/L3 molt). The dotted line shows the control (Ctrl) expression level. Three biological replicates were used to perform the qPCRs. Error bars represent 95% confidence intervals among the replicates.

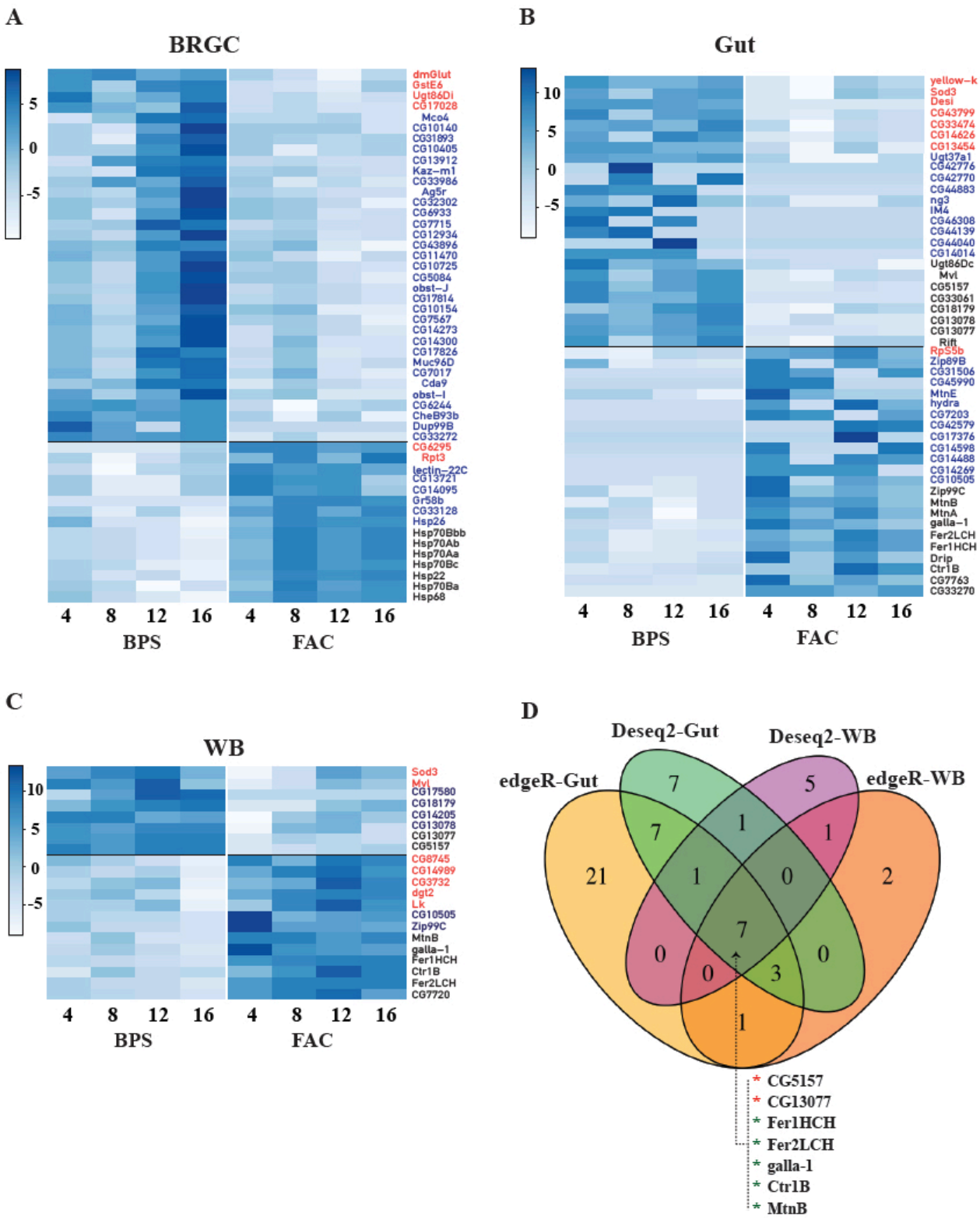
A
BRGC
5
0
-5
dmGlut
GstE6
Ugt86Di
CG17028
Mco4
CG10140
CG31893
CG10405
CG13912
Kaz-m1
CG33986
Ag5r
CG32302
CG6933
CG7715
CG12934
CG43896
CG11470
CG10725
CG5084
obst-J
CG17814
CG10154
CG7567
CG14273
CG14300
CG17826
Muc96D
CG7017
Cda9
obst-I
CG6244
CheB93b
Dup99B
CG33272
CG6295
Rpt3
lectin-22C
CG13721
CG14095
Gr58b
CG33128
Hsp26
Hsp70Bbb
Hsp70Ab
Hsp70Aa
Hsp70Bc
Hsp22
Hsp70Ba
Hsp68
4 8 12 16 4 8 12 16
BPS
FAC
B
Gut
10
5
0
-5
yellow-k
Sod3
Desi
CG43799
CG33474
CG14626
CG13454
Ugt37a1
CG42776
CG42770
CG44883
ng3
IM4
CG46308
CG44139
CG44040
CG14014
Ugt86Dc
Myl
CG5157
CG33061
CG18179
CG13078
CG13077
Rift
Rp59b
Zip89B
CG31506
CG45990
MtnE
hydra
CG7203
CG42579
CG17376
CG14598
CG14488
CG14269
CG10505
Zip99C
MtnB
MtnA
galla-1
Fer2LCH
Fer1HCH
Drip
Ctr1B
CG7763
CG33270
4 8 12 16 4 8 12 16
BPS
FAC
C
WB
10
5
0
-5
Sod3
Myl
CG17580
CG18179
CG14205
CG13078
CG13077
CG5157
CG8745
CG14989
CG3732
dgt2
Lk
CG10505
Zip99C
MtnB
galla-1
Fer1HCH
Ctr1B
Fer2LCH
CG7720
4 8 12 16 4 8 12 16
BPS
FAC
D
Deseq2-Gut
Deseq2-WB
edgeR-Gut
edgeR-WB
7
5
7
1
1
21
1
0
2
7
0
0
3
0
1
* CG5157
* CG13077
* Fer1HCH
* Fer2LCH
* galla-1
* Ctr1B
* MtnB

Figure 4. 3 Media analysis differentially expressed genes

A), **B)** and **C)** are heatmaps of differentially expressed genes (DEGs) in BRGC, gut, and WB. The heatmaps' raw names are DEGs names. Genes are color-coded: red indicates Deseq2-specific hits while blue is edgeR-specific hits. The black names show overlap hits between the two methods. The horizontal solid lines in the heatmaps separate BPS- upregulated (top) and FAC-up (bottom) transcripts. The scale bars show the range of Log2 fold Changes. Column labels indicate the time points in the BPS and FAC supplemented media. **D)** Venn diagram represents overlaps between the gut and WB transcripts. The red asterisks show genes from the BPS- upregulated group: (*CG5157*, *CG13077*), and green asterisks show FAC-up genes, including Ferritin 1 heavy chain 1 (*Fer1HCH*), Ferritin 2 light chain (*Fer2LCH*) *galla-1*, Copper transporter 1B (*Ctr1B*) and Metallothionein B (*MtnB*).

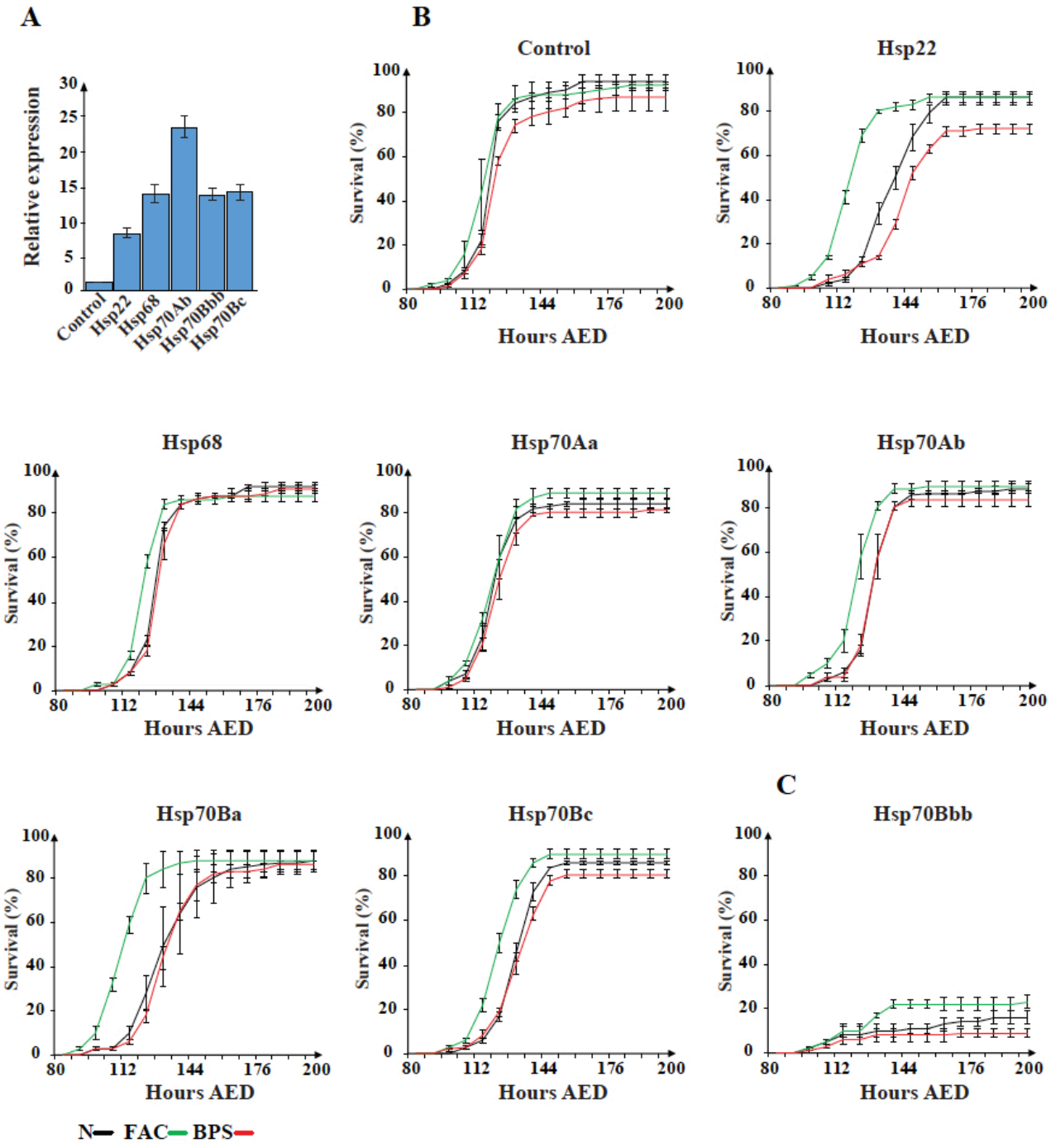
A
Relative expression
30
25
20
15
10
5
0
Control
Hsp22
Hsp68
Hsp70Ab
Hsp70Bbb
Hsp70Bc
B
Control
Hsp22
Hsp68
Hsp70Aa
Hsp70Ab
Hsp70Ba
Hsp70Bc
C
Hsp70Bbb
Survival (%)
100
80
60
40
20
0
80
112
144
176
200
Hours AED
N
FAC
BPS

Figure 4. 4 Heat-shock proteins function in the PG cells

A) qPCR analysis of Heat-shock protein (*Hsp*) genes in the RG relative to their expression in the brain cells. RGs were isolated from *PG>Hsp-RNAi* animals, and brains were isolated from brain>Hsp-RNAi flies. Error bars are 95% confidence intervals and asterisks represent the P-values in the student's t-test (*$p < 0.05$ and ***$p < 0.01$). **B)** The developmental timing of control and *PG>Hsp-RNAi* animals pupae. Black lines show animals in normal (black lines), BPS (red lines), and FAC (green lines) supplemented media. Y-axis denotes the percentage of pupariation, and X-axis shows hours after the egg deposition. **C)** Pupae developmental timing of *PG> Hsp70Bbb-RNAi* animals. The *PG> Hsp70Bbb-RNAi* animals are L3 arrested, and few larvae are formed pupae. Error bars in B and C represent the replicates' standard deviation errors.

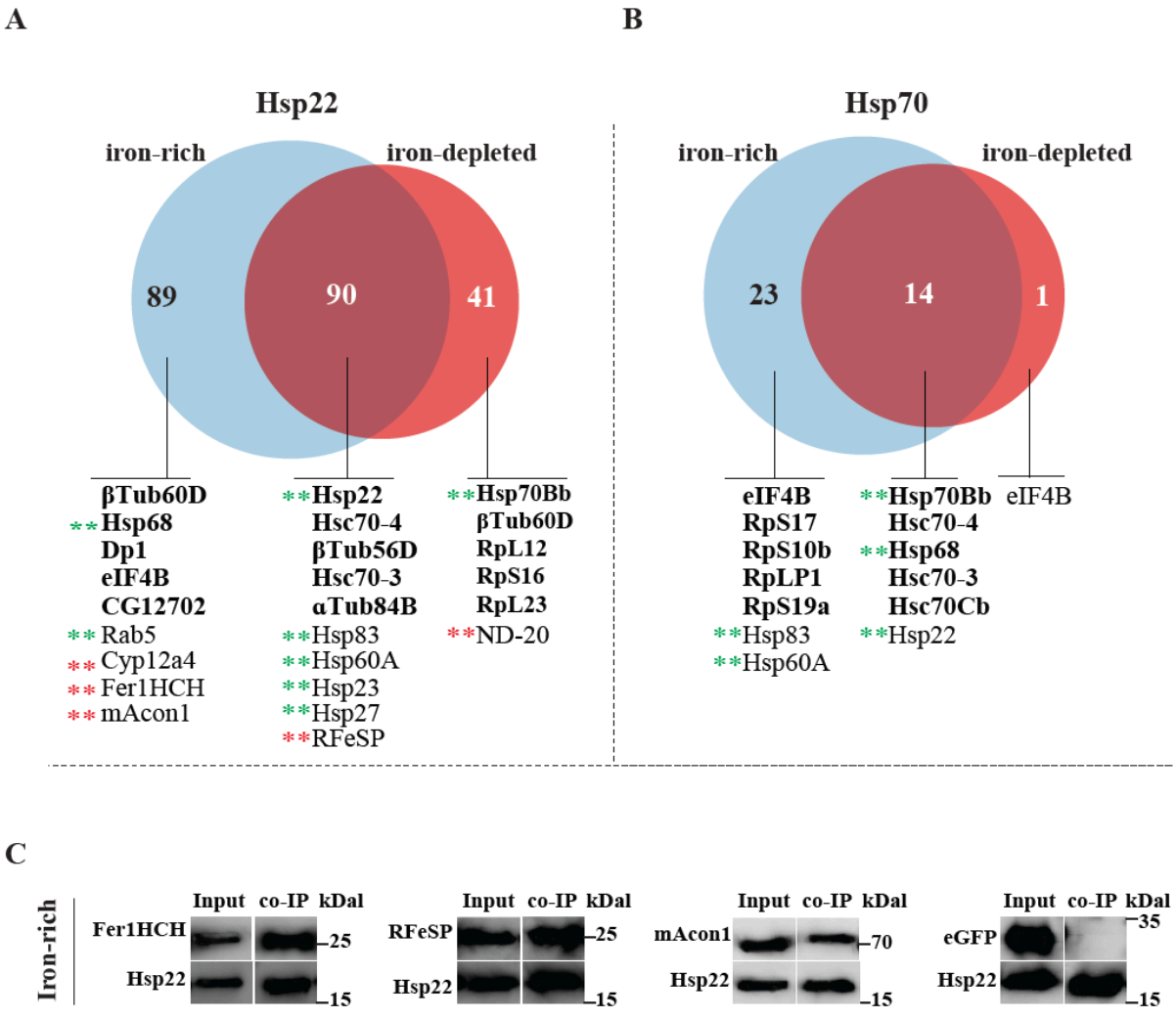

Figure 4. 5 Hsp22 and Hsp70 protein-protein interaction.

A) and **B)** Venn diagrams of Hsp22 and Hsp70 ex vivo proteome interactomes in iron-rich (blue) and iron-depleted media (red). The proteins shown in bold are the top five high score proteins in each category. Red asterisks indicate proteins that are directly iron-linked proteins and green asterisks are indirectly iron linked-proteins. **C)** CO-IP Western Blot analysis of co-transfected S2 cells with plasmids encoding Hsp22-3XFLAG and Myc-tagged Fer1HCH, RFeSP, mAcon1, and eGFP. 50 % of the sample served as the input (Input), and the rest was used for the co-IP assay. Proteins were detected with anti-FLAG and anti-Myc antibodies.

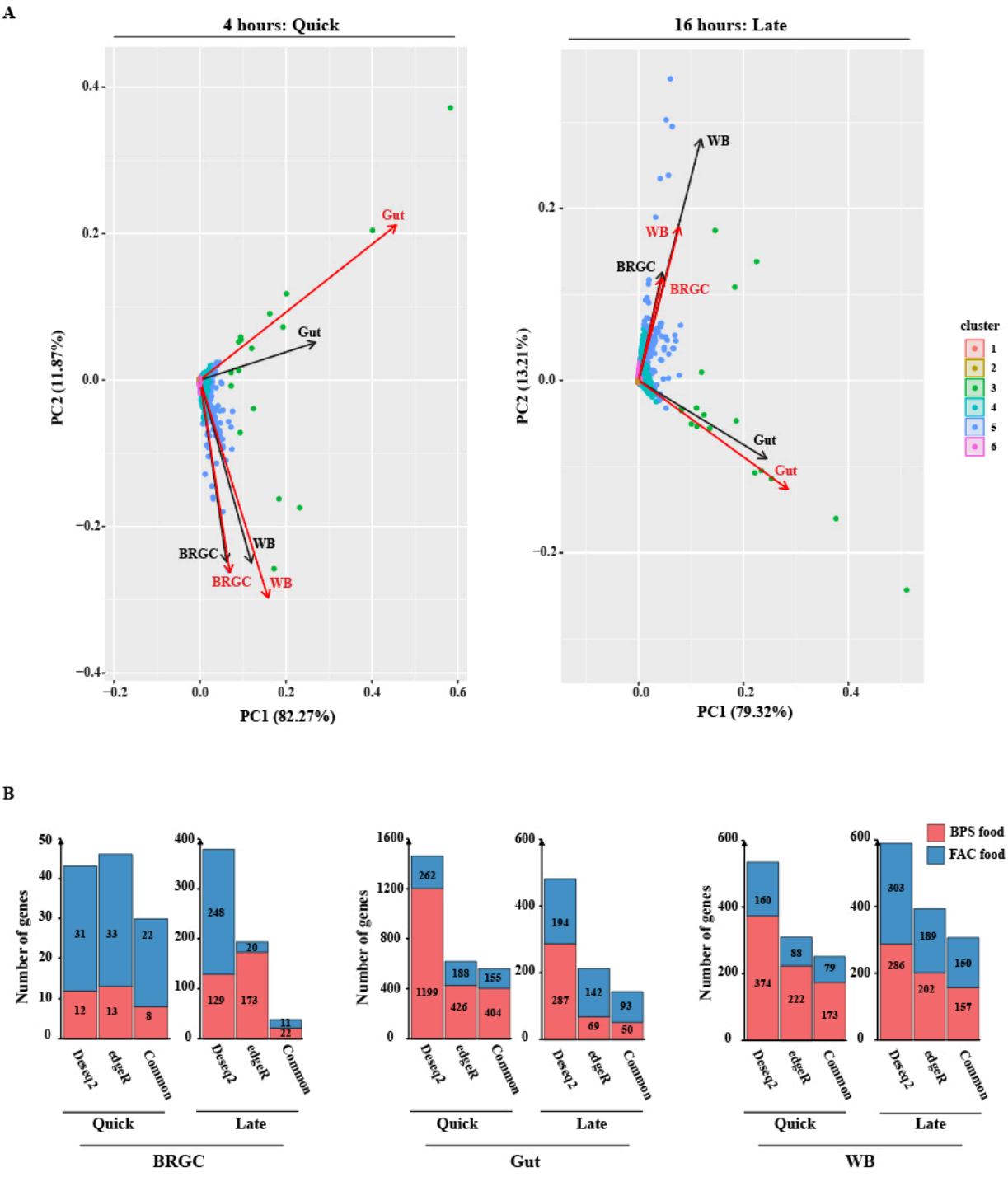
A
4 hours: Quick
16 hours: Late
PC2 (11.87%)
PC1 (82.27%)
PC2 (13.21%)
PC1 (79.32%)
Gut
WB
BRGC
cluster
1
2
3
4
5
6
B
Number of genes
BPS food
FAC food
Deseq2
edgeR
Common
Quick
Late
BRGC
Gut
WB

Figure 4. 6 Principal Component Analysis (PCA) and DEGs number in early and late responses

A) Principal component analysis of BRGC, gut and WB transcripts in 4-hour (early) and 16-hour (late) samples. The PC1 and PC2 in each graph represent the top two principal components of analyzed time points. All genes were grouped in six clusters (1 to 6) via K-means analysis. **B)** The number of identified DGE transcripts in BRGC, Gut, and WB tissues via edgeR and Deseq2. The red bars indicate the number of DEGs in BPS and the blue bars show DEGs in FAC supplemented media. The common bars are the overlapping DEGs between edgeR and Deseq2 analyses.

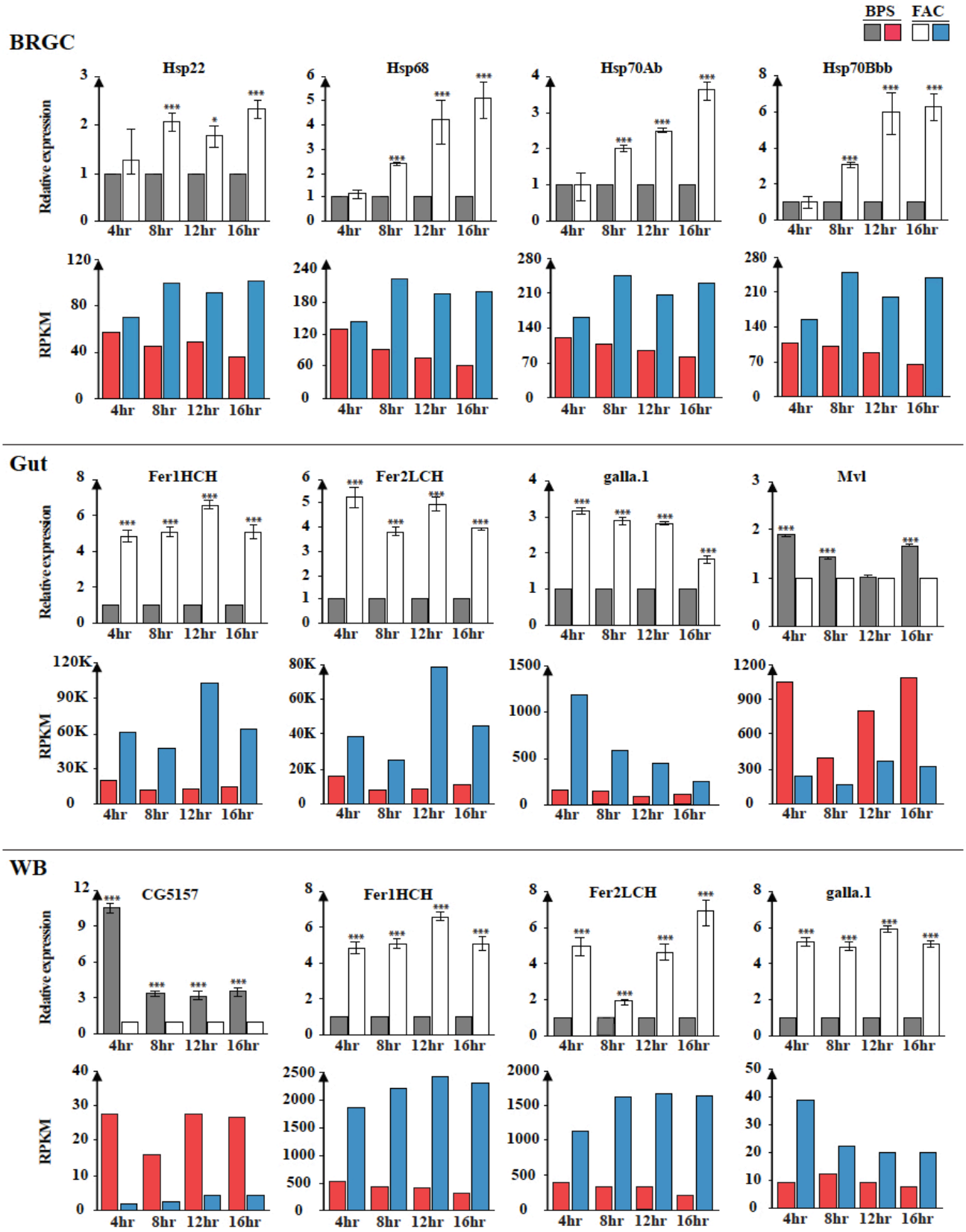
BPS
FAC
BRGC
Hsp22
Hsp68
Hsp70Ab
Hsp70Bbb
Relative expression
RPKM
4hr
8hr
12hr
16hr
Gut
Fer1HCH
Fer2LCH
galla.1
Mvl
WB
CG5157

Figure 4. 7 Time course qPCR analysis of DEGs in BRGC, gut and WB

qPCR expression analysis of selected DEGs in BRGC, gut and WB compared to their RNA-seq RPKMs (Reads Per Kilobase of transcript per Million mapped reads). The expression of selected genes were measured in the BPS (gray and red), and FAC (white and blue) supplemented media, relative to Rp-49 expression. The RPKM graphs indicate linear RPKM of the gene in the BPS media vs. FAC media. The *Hsp22*, *Hsp68*, *Hsp70Ab*, and *Hsp70Bbb* genes were selected from the BRGC transcripts. In the gut DEGs, the *Fer1HCH*, *Fer2LCH*, *galla-1*, and *Mvl* genes were analyzed, but the *CG5157*, *Fer1HCH*, *Fer2LCH*, and *galla-1* genes analyzed for the WB transcripts. Three biological replicates were used to perform the qPCRs. Error bars indicate the 95% confidence intervals. Asterisks are P-values of the student's t-test (*$p < 0.05$ and ***$p < 0.001$).

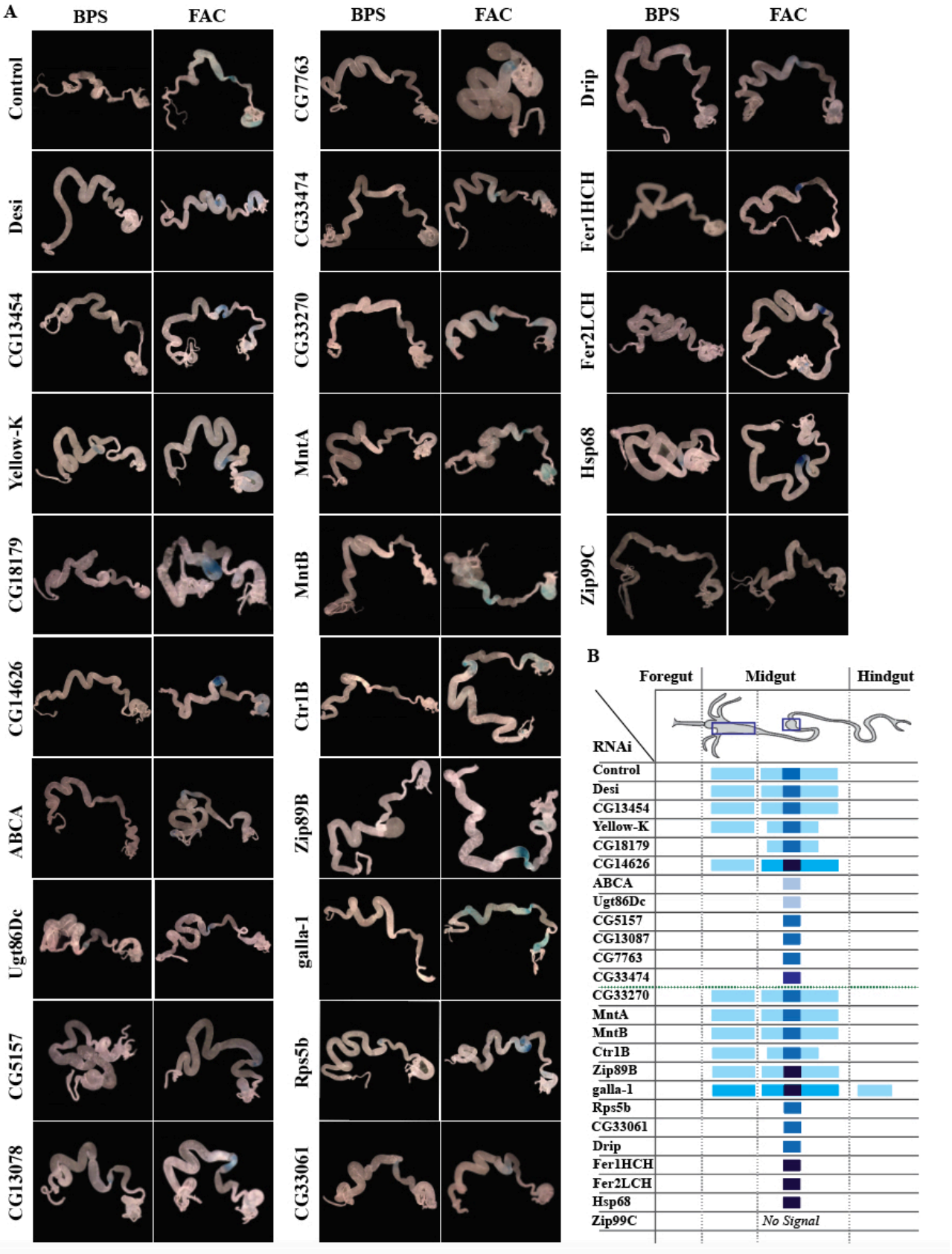
A
BPS
FAC
Control
Desi
CG13454
Yellow-K
CG18179
CG14626
ABCA
Ugt86Dc
CG5157
CG13078
CG7763
CG33474
CG33270
MntA
MntB
Ctr1B
Zip89B
galla-1
Rps5b
CG33061
Drip
Fer1HCH
Fer2LCH
Hsp68
Zip99C
B
Foregut
Midgut
Hindgut
RNAi
Control
Desi
CG13454
Yellow-K
CG18179
CG14626
ABCA
Ugt86Dc
CG5157
CG13087
CG7763
CG33474
CG33270
MntA
MntB
Ctr1B
Zip89B
galla-1
Rps5b
CG33061
Drip
Fer1HCH
Fer2LCH
Hsp68
Zip99C
No Signal

Figure 4. 8 Intestinal iron staining of gut-specific DEGs

A) Visualizing iron containing cells in the whole larval gut using Prussian blue staining. Whole guts were isolated from *NP3084-GAL4>DEGs-RNAi* and control animals that were reared on BPS and FAC foods. The whole guts of L3 larvae were collected and stained with the Prussian blue stain (ferrocyanide). The blue color indicates the midgut cells where ferric iron is accumulated. **B)** Schematic of Prussian-blue results for each DEG-RNAi line reared in the FAC-supplemented media. The blue color intensity was based on ten stained guts, and indicates the iron signal level in the gut regions. The green dotted line separates the BPS upregulated transcripts (above the green lines), FAC upregulated transcripts (below the green line).

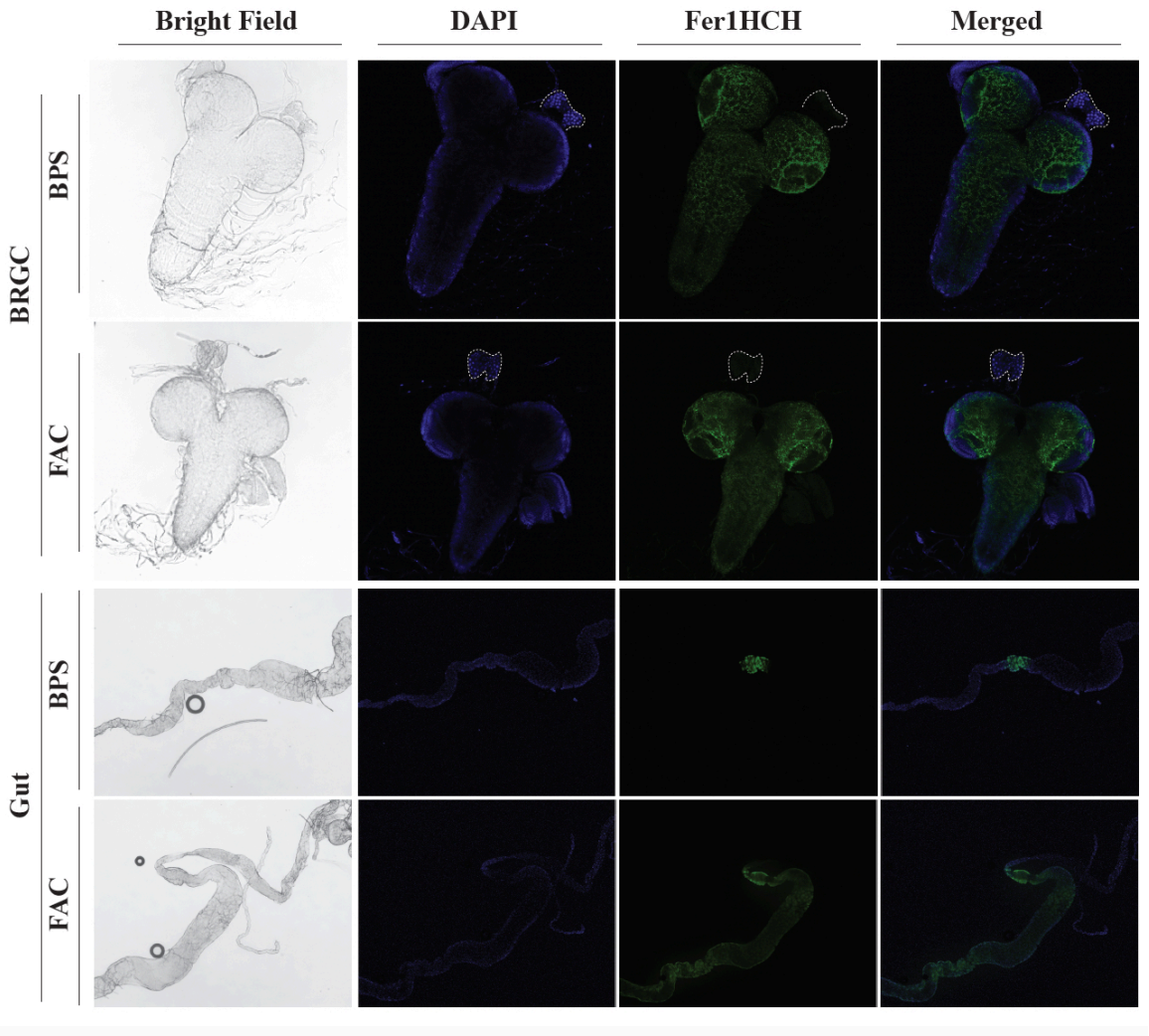

Figure 4. 9 Ferritin level in BRGC and gut cells.

Brain ring gland complex (BRGC) and gut of the Fer1HCH-GFP^{G188} animals. Samples were collected from animals raised on BPS food for six generations. Larvae were staged carefully until the beginning of the L3 stage, and then divided into two groups. One group continued to feed on BPS food, whereas the second group was transferred to FAC-containing food. The BRGC and gut samples were isolated at 40 hours L3 larvae. DAPI is the nuclei/DNA stain. The green channel indicates intrinsic GFP signals (Fer1HCH level) of the Fer1HCH-GFP^{G188} animals.

4.8 Tables

Table 4. 1 Brain and Ring gland complex (BRGC) DEGs identified in Media analysis

Analysis	Symbol	Name	Deseq2 P-value[A]	edgeR P-value[B]	Deseq2 FC[C]	edgeR FC[D]
Deseq2 BPS-upregulated	dmGlut	Dietary and metabolic glutamate transporter	3.39E-04	-	1.29	-
	CG17028	-	4.70E-02	-	1.26	-
	GstE6	Glutathione S transferase E6	3.89E-02	-	1.21	-
	Ugt302K1	UDP-glycosyltransferase family 302 member K1	2.72E-04	-	1.2	-
edgeR BPS-upregulated	Peritrophin-15b	Peritrophin-15b	-	6.38E-07	-	374.81
	CG10140	-	-	2.42E-05	-	154.34
	obst-I	obstructor-I	-	1.09E-05	-	101.83
	Dup99B	Ductus ejaculatorius peptide 99B	-	7.66E-05	-	82.14
	CG33272	-	-	3.04E-07	-	81.57
	CG33986	-	-	2.67E-05	-	62.25
	Mco4	Multicopper oxidase 4	-	2.62E-05	-	42.22
	CG10154	-	-	1.10E-04	-	31.78
	CG10725	-	-	2.75E-06	-	27.28
	CheB93b	Chemosensory protein B 93b	-	7.73E-05	-	26.72
	CG6244	-	-	1.70E-05	-	22.16
	CG12934	-	-	3.66E-06	-	21.56
	CG10405	-	-	5.97E-05	-	21.41
	Peritrophin-15a	Peritrophin-15a	-	7.91E-07	-	20.82
	CG5084	-	-	3.77E-06	-	17.88
	CG13912	-	-	9.54E-05	-	17.39
	CG7017	-	-	6.69E-05	-	13.93
	CG17826	-	-	2.92E-07	-	12.04
	Muc96D	Mucin 96D	-	7.85E-07	-	10.93

	CG6933	-	-	3.93E-05	-	10.78
	Cda9	Chitin deacetylase-like 9	-	1.36E-06	-	10.63
	CG7567	-	-	7.78E-06	-	9.78
	Kaz-m1	Kazal-type protease inhibitor m1	-	7.93E-05	-	9.32
	CG43896	-	-	1.21E-04	-	8.34
	CG14300	-	-	4.78E-05	-	7.73
	CG32302	-	-	1.25E-04	-	7.73
	obst-J	obstructor-J	-	5.58E-06	-	7.21
	CG14273	-	-	7.13E-05	-	6.59
	CG11470	-	-	1.93E-05	-	6.5
	CG7715	-	-	1.57E-06	-	5.13
	Ag5r	Antigen 5-related	-	8.45E-05	-	5.06
Deseq2 FAC-upregulated	CG6295	-	3.57E-06	-	1.35	-
	Rpt3	Regulatory particle triple-A ATPase 3	4.13E-02	-	1.11	-
edgeR FAC-upregulated	Gr58b	Gustatory receptor 58b	-	4.80E-05	-	50.21
	lectin-22C	lectin-22C	-	2.91E-09	-	49.87
	CG13721	-	-	9.74E-05	-	31.56
	CG33128	-	-	6.11E-05	-	28.64
	CG14095	-	-	1.49E-04	-	27.28
	Hsp26	Heat shock protein 26	-	2.43E-05	-	1.55
Common FAC-upregulated	Hsp22	Heat shock protein 22	3.57E-06	3.58E-09	1.42	1.88
	Hsp68	Heat shock protein 68	3.39E-04	1.93E-08	1.35	2.08
	Hsp70Aa	Heat-shock-protein-70Aa	5.17E-08	2.85E-12	1.49	2.01
	Hsp70Ab	Heat-shock-protein-70Ab	5.17E-08	2.86E-12	1.49	2.01
	Hsp70Ba	Heat-shock-protein-70Ba	1.49E-02	2.96E-05	1.26	2.28
	Hsp70Bc	Heat-shock-protein-70Bc	1.02E-05	1.62E-10	1.41	2.07
	Hsp70Bbb	Hsp70Bbb	5.17E-08	6.15E-13	1.49	2.27

[A and B] P-values represent adjusted P values in the Deseq2 and edgeR analyses.

[C and D] Calculated Fold changes (FC) in the Deseq2 and edgeR analyses. Analysis-specific genes are sorted according to FCs, but common genes are ranked based on gene names.

Table 4. 2 differentially expressed genes (DEGs) in gut samples identified by media analysis

Analysis	Symbol	Name	Deseq2 P-value[A]	edgeR P-value[B]	Deseq2 FC[C]	edgeR FC[D]
Deseq2 BPS-upregulated	CG33474	-	9.76E-04	-	2.11	-
	Desi	Desiccate	2.53E-04	-	2.07	-
	yellow-k	yellow-k	2.55E-03	-	2.03	-
	CG13454	-	2.10E-03	-	1.99	-
	CG14626	-	8.81E-03	-	1.93	-
	CG43799	-	7.97E-04	-	1.72	-
	Sod3	Superoxide dismutase 3	2.47E-02	-	1.58	-
edgeR BPS-upregulated	pre-mod(mdg4)-I	-	-	1.17E-10	-	670.92
	CG44040	-	-	2.85E-05	-	364.56
	pre-mod(mdg4)-V	-	-	7.63E-05	-	252.48
	ng3	new glue 3	-	4.87E-06	-	147.03
	CG46308	-	-	6.22E-05	-	140.07
	pre-mod(mdg4)-Z	-	-	6.78E-05	-	138.14
	IM4	Daisho1	-	8.78E-05	-	127.12
	CG44139	-	-	1.15E-04	-	125.37
	CG14014	-	-	2.16E-05	-	109.9
	Ugt37a1	UDP-glycosyltransferase family 37 member A1	-	2.93E-05	-	29.86
Common BPS-upregulated	CG13077	-	3.35E-34	2.61E-36	6.68	22.01
	CG13078	-	1.21E-07	1.58E-16	2.68	24.93
	CG18179	-	4.89E-03	1.43E-07	1.99	3.76
	CG33061	-	2.55E-03	8.18E-06	1.84	95.01
	CG5157	-	4.38E-24	4.37E-25	4.79	10.63
	Mvl	Malvolio	6.04E-07	7.16E-08	2.22	2.73
	Rift	Riboflavin transporter	2.55E-03	1.23E-05	1.87	2.31

	Ugt302E1	UDP-glycosyltransferase family 302 member E1	5.20E-03	2.36E-06	1.96	5.5
Deseq2 FAC-upregulated	RpS5b	Ribosomal protein S5b	5.87E-03	-	1.92	-
edgeR FAC-upregulated	tRNA:Leu-TAA-1-1	transfer RNA:Leucine-TAA 1-1	-	2.52E-08	-	410.15
	pre-mod(mdg4)-N	-	-	2.31E-06	-	369.65
	CG17376	-	-	6.32E-05	-	249
	CG14269	-	-	1.68E-06	-	188.71
	CG14488	-	-	4.06E-06	-	151.17
	CG42579	-	-	4.35E-05	-	149.09
	CG14598	-	-	8.89E-05	-	123.64
	hydra	Hydra	-	1.22E-04	-	83.87
	CG7203	-	-	1.01E-04	-	83.29
	CG10505	-	-	1.04E-07	-	5.98
	MtnE	Metallothionein E	-	7.40E-05	-	5.98
	Zip89B	Zinc/iron regulated transporter-related protein 89B	-	1.36E-04	-	2.91
Common FAC-upregulated	CG33270	-	7.82E-04	8.75E-06	1.95	94.35
	CG7763	-	7.10E-04	8.30E-08	2.16	5.39
	Ctr1B	Copper transporter 1B	3.83E-04	7.17E-09	2.16	3.53
	Drip	Drip	9.76E-04	1.05E-07	2.1	3.97
	Fer1HCH	Ferritin 1 heavy chain homologue	5.69E-61	3.32E-43	4.26	4.92
	Fer2LCH	Ferritin 2 light chain homologue	1.07E-28	2.26E-29	3.66	4.63
	galla-1	galla-1	4.47E-04	7.39E-09	2.19	5.82
	MtnA	Metallothionein A	2.90E-02	1.54E-06	1.75	2.22
	MtnB	Metallothionein B	8.67E-05	5.82E-10	2.31	6.63
	Zip99C	Zinc/iron regulated transporter-related protein 99C	1.93E-03	2.00E-07	2.06	3.71

[A and B] P-values represent adjusted P values in the Deseq2 and edgeR analyses.

[C and D] Calculated Fold changes (FC) in the Deseq2 and edgeR analyses. Analysis-specific genes are sorted according to FCs, but common genes are ranked based on gene names.

Table 4. 3 Whole larval body (WB) deferentially expressed genes (DEGs) identified by media analysis.

Analysis	Symbol	Name	Deseq2 P-value[A]	edgeR P-value[B]	Deseq2 FC[C]	edgeR FC[D]
Deseq2 BPs-upregulated	Mvl	Malvolio	7.93E-07	-	1.57	-
	Sod3	Superoxide dismutase 3	3.28E-02	-	1.34	-
edgeR BPS-upregulated	CG17580	-	-	3.50E-06	-	148.06
	CG13078	-	-	3.28E-06	-	23.43
	CG18179	-	-	1.10E-05	-	3.32
	CG14205	-	-	2.65E-05	-	2.75
Common BPS-upregulated	CG13077	-	7.98E-13	6.15E-16	2.17	4.72
	CG5157	-	1.26E-18	1.44E-25	2.5	8.34
Deseq2 FAC-upregulated	CG14989	-	6.16E-11	-	1.6	-
	CG8745	-	1.36E-02	-	1.48	-
	Lk	Leucokinin	1.92E-02	-	1.36	-
	CG3732	-	1.66E-03	-	1.31	-
	dgt2	dim gamma-tubulin 2	3.68E-02	-	1.31	-
edgeR FAC-upregulated	CG10505	-	-	1.55E-08	-	7.57
	Zip99C	Zinc/iron regulated transporter-related protein 99C	-	1.21E-05	-	3.25
Common FAC-upregulated	CG7720	-	6.75E-10	1.26E-08	1.83	2.31
	Ctr1B	Copper transporter 1B	9.27E-05	8.66E-09	1.65	3.68
	Fer1HCH	Ferritin 1 heavy chain homologue	4.23E-71	3.72E-39	3.68	4.86

	Fer2LCH	Ferritin 2 light chain homologue	1.54E-48	3.76E-31	3.29	4.66
	galla-1	galla-1	6.69E-03	1.23E-06	1.53	2.66
	MtnB	Metallothionein B	2.74E-09	2.52E-15	1.94	5.1

[A and B] P-values represent adjusted P values in the Deseq2 and edgeR analyses.

[C and D] Calculated Fold changes (FC) in the Deseq2 and edgeR analyses. Analysis-specific genes are sorted according to FCs, but common genes are ranked based on gene names.

Table 4. 4 DEGs of the brain ring gland complex (BRGC) time course analysis

BRGC[A]							
Q-Deseq2	**Q-Common**	CG5707	Sad	Sps1	snRNP-U1-70K	CG12934	CG10650
CG12984	CG43056	Hn	Dib	Nnp-1	Prosalpha4	Cda9	Acbp6
CG15357	ng2	Yuri	CG6310	CCT7	Snf	CG14300	CG4562
CG15784	Muc96D	Sgsh	mRpL52	Prosalpha2	Hsp60A	CG42460	CG15347
Hsp70Bb	mt:ND6	Lfg	Acbp3	Srl	La	CG9920	Tsp42Ed
Muc26B	Thor	a10	Cpr67Fa2	CCT5	Nap1	Peritrophin-15b	regucalcin
CG14397	Hsp70Bb	Vdup1	mRpS25	CG9246	Bic	Sid	CG9672
Thor	CG15357	CG33939	r-l	CG10286	Rpt6	CG7567	CG32249
CR14798	CG12984	SPARC	CG12909	Cdk1	PCNA	CG4318	IM33
mt:ND6	**Q-Common***	CG43630	CG14544	CG11089	Tudor-SN	Peritrophin-15a	CG2233
Muc96D	LysS	TpnC25D	Pbp45	Tsr1	CG3760	Ubc84D	CG14302
ng2	Et	Lcp3	CG31198	CG9253	Hrb98DE	CG3528	CG31313
CG43056	Karl	CG3588	Tll	CG14186	Bel	CG32726	CG17108
Q-Deseq2*	Tep4	Mlp84B	nudC	SpdS	Ref1	CG14957	Lcp65Ac
LysS	He	CG17919	CG43222	CSN6	SmD2	CG32302	CG9757
Et	mthl6	Capu	eEF1delta	Eip71CD	Rcc1	CG13806	PPO1
Karl	CG33460	MP1	mRpL51	CCT3	eIF2beta	CG15153	deltaTry
Tep4	CG11131	Hexo1	Sptr	CCT6	Uba1	CG8560	gammaTry
He	Muc55B	CG8740	CG2972	Nop56	CNBP	CG17636	CG30031
mthl6	CG13545	CG18538	CG4866	CCT2	eRF1	CG6933	PPO2
CG33460	CG7203	Ugt302C1	Nopp140	Mge	Pp1-87B	CG10405	CG7299
CG11131	Cpr31A	NKCC	CG8785	Sirt1	B52	PH4alphaPV	Thor
Muc55B	CG32237	CG14835	Hsp67Bc	Prosalpha6	Df31	CG5399	Cyp9c1

CG13545	Hml	Tspo	CG2260	CG13096	His2Av	CG30025	
CG7203	CG5532	CG10365	Tgt	Peng	MFS3	CG12115	**L-edgeR***
CG4259	CG15422	CG34190	Stv	CG4806	Sqd	CG7715	Acbp3
Cpr31A	Mag	CG9672	mRpL20	mRpL39	Prps	CG4563	CG18662
CG32237	CG34446	CG32368	CG8492	Fkbp59	eIF1	CG34452	CG14346
Hml	CG13041	Mlc2	His1:CG33801	CG10576	Pnut	CG13810	CG3604
CG10912	CG7290	CG46320	Hsp23	Ran	Sf3b3	CG10814	CG15357
CG33465	CG44242	CG10559	Sgt1	Fkbp39	Porin	Jon65Aiii	CG15605
Rdh	SclA	CG4847	CG15386	Ahcy	Nacalpha	CG13324	CG14932
CG5532	**L-Deseq2**	Ms	Fabp	Pfdn4	Cyp1	Pebp1	CG18132
CG15422	att-ORFB	CG34291	CG42455	CG6937	Ubi-p63E	Pgant4	CG33795
Mag	deltaTry	Ana	CG18600	CCT4	eEF1beta	obst-J	CG33128
CG42694	gammaTry	CG13375	CG32409	Cyt-c-p	**L-edgeR**	CG7714	LManVI
CG34446	CG30031	Cyp6a17	CG10361	CG18662	CG11672	Jon25Bi	TwdlO
Mal-A8	CG32249	CG9123	Tko	Acbp1	CG10140	CG11470	Lsp2
CG13041	Thor	Nepl3	CG10973	p23	CG6403	Jon65Aiv	Hsp70Bbb
Nplp4	CG31337	CG34028	CG4069	CG6218	CG9988	Acbp4	Hsp68
CG7290	CG9757	CG6845	l(3)07882	Prosbeta1	att-ORFB	Jon25Bii	Hsp70Bc
CG15399	CG7299	CG13369	CG18178	Pomp	obst-I	Phae2	Hsp70Aa
CG44242	CG15461	Path	CG9922	mRpL44	CG31464	CG5506	Hsp70Ab
SclA	CG14830	Fas3	nop5	alphaTub84B	CG33985	CG17145	Hsp22
Q-edgeR	GstE5	CG43781	Spok	CG1416	CG13102	CG14273	CG34132
CG15357	Ple	CG13227	Ns1	CG33853	CG33986	Tgy	**L-Common***
Obp47a	CG13403	Nazo	CG8939	CG33856	CG43896	obst-H	CG34268
CG12984	Irc	CG6299	CG8545	CG33859	CG15213	CG31789	CG15282
Hsp70Bb	CG15579	CG15098	Stip1	RpI1	CG42728	CG15818	Ntf-2r
CG9928	Cys	dmGlut	l(2)k09848	Prosbeta3	CG42714	Mco1	CG13488

Cpr35B	CAH9	CG43693	CG7182	Usp14	CG34291	CG15043	Nazo
CG13021	Wnt2	GstE11	CG30349	ND-24	CG7017	yip7	CG34028
CG33272	CG33189	CG2698	CG5290	Alien	CG45061	Ag5r	CG34291
CG43056	CG17549	CG13067	Hsp27	vig2	Cpr49Ae	CG7953	CG9672
Muc96D	l(3)neo43	CG13488	CG7137	Nup35	CG13511	CG17147	CG33939
ng2	CG17028	miple2	CG4338	Droj2	CG34236	CG10910	Hn
mt:ND6	Tsp68C	Ntf-2r	Pfdn5	Kra	Muc26B	Obp56h	CG31313
Thor	obst-B	CG15282	CG5033	Cyt-b5	Nazo	LysB	CG17108
Q-edgeR*	Gfat2	Spn27A	Mtr3	Paics	obst-F	CG4830	Cyp9c1
SclA	Drm	CG34268	mRpL3	mRpS30	CG7252	CG10962	CG7299
CG15422	Dpy	CG44243	CG13097	Nup50	CG10154	CG13323	CG9757
IM18	Ser	Non1	CG40439	Eff	CG17290	LysS	Thor
CG43895	Cyp9c1	Pdcd4	Hsc70Cb	CG1622	PIG-Wb	Npc2e	CG32249
Lcp65Ag3	Hui	Lk6	CG8490	Prosbeta2	CG34268	CG6839	deltaTry
CG13465	CG12963	Ilp2	Pit	Rpt1	CG33939	betaTry	gammaTry
Mst87F	CG32523	CG12239	CG1542	Prosbeta5	CG5172	CG42729	CG30031
CG43107	CG14265	Ed	Dim1	CG4038	CG17826	alphaTry	att-ORFB
CG8299	Pio	Crc	NHP2	Nop60B	CG14160	CG8997	**L-Common***
CG14495	CG13827	**L-Deseq2***	Ance	CG9281	CG34028	LysD	Hsp68
Dpy-30L2	CG33099	Hsp68	Ppan	Pen	Dup99B	Myo28B1	Hsp22
CG7290	CG33978	Hsp22	CG12975	SF2	CG15282	CG5966	Hsp70Aa
LysS	CG17108	Hsp70Aa	LManVI	Men	CG10725	CG3106	Hsp70Ab
CG13041	CG10877	Hsp70Ab	CG11980	Art1	Drsl5	Tsp29Fb	CG34132
Mag	Dgp-1	Hsp26	ND-B14.7	Nlp	CG34451	Cyp9b2	Hsp70Bc
Et	Ucp4C	CG34132	CG32243	Rpn6	Phae1	CG8664	TwdlO
CG33460	Hh	Hsp70Bc	l(1)G0020	CG14207	Ntf-2r	CG30457	Hsp70Bbb
mthl6	GstT4	alphaTub85E	CCT1	EMC3	CG5084	CG7298	Acbp3
CG8157	Fiz	TwdlO	mRpL16	Bnb	CG30411	CG13321	LManVI

He	GstE8	CG17278	Mod	Sod1	CG11192	CG8952	CG18662
Karl	CG42649	CG4456	Tim23	Rump	CG13488	Hn	
CG11131	CG6770	DnaJ-1	CG3071	Rpn13	CG13712	CG15482	
Muc55B	Lcp4	Hsp70Ba	Icln	Obp99a	CG34282	Qua	
CG7203	CG43103	CG5955	Aay	Awd	Mco4	CG3819	
CG13545	CG43330	Mag	Viaf	Naa15-16	Andorra	Obp99b	
Tep4	CG30440	CG17571	RpLP0-like	Hsc70-4	CG14628	CG34251	
CG32237	CG9782	CG42445	SmF	betaTub56D	CG43773	Jon74E	
Hml	CG42740	Hsp83	CG12321	Rpt2	Mst57Db	LysE	
Cpr31A	CG9691	Hsp70Bbb	Nsun5	CG10565	Muc96D	Tsp29Fa	
Ppn	CG31313	mRpL33	CG10340	RpL38	BomT2	CG4928	
CG5532	CG13984	CG1124	Mgr	dUTPase	obst-G	CG31775	
CG34446	CG13117	CG8461	mRpL54	MFS9	Kaz-m1	CG42586	
CG44242	CG31437	Nmdmc	mRpS10	CG18815	CG6870	CG2556	

[A] DEGs of each group are separated by gray cells in the table. Q- and L- stand for quick and late analysis and asterisk represents FAC-upregulated analysis.

Table 4. 5 DEGs of the gut time course analysis

Gut[A]								
Q-Deseq2	Akap200	Pex5	BomS2	ATPsynD	UQCR-Q	CG12728	Hph	CG5590
CG13078	CG31635	CG7916	CG42323	RpS13	Jon99Fii	CG11837	DOR	CG8306
ninaD	CG9119	CG6726	CG46308	Fabp	ATPsynD	Ugt49C1	Lmpt	CG11912
CG13077	CG8562	Grasp65	NimC3	CG15093	RpS13	CG15096	Bun	sut1
CG5157	Slif	CG3902	CG46318	RpL14	CG15093	Zip48C	Cue	CG5773
CG31089	Atpalpha	Mf	CG30161	RpL37a	Fabp	mt:CoII	CG15255	su(r)
CG42662	Lab	CG33170	BomS1	Jon99Ciii	RpL14	mt:ATPase8	CG6295	RpL10Ab
CG34316	RYBP	Aldh7A1	SclA	Porin	Porin	Ku80	Tank	Nlp
Ugt302E1	CG3603	CG17896	GNBP-like3	LysD	RpL37a	mt:srRNA	Jon99Ciii	CG17597
CG10081	Hyccin	GATAe	NimB5	Kdn	Jon99Ciii	CG42319	Jon99Cii	ScpX
CG1394	Lasp	RpL14	Sfp33A4	Jon99Cii	Kdn	CG14907	CG10939	PMP34
CG14205	CG42837	CG4053	CG13606	Jon25Bii	LysD	CG12171	CG7025	CG13315
CG12643	GEFmeso	CG11162	IMPPP	CG13078	Jon99Cii	mt:ND4	CG32485	**L-edegR***
Lsm10	CG6424	Faf	CG33470	ninaD	Jon25Bii	CG32512	CG9304	CG9877
CG16727	Roq	Sea	CG46321	CG13077	CG10505	CG4797	Jon65Aiii	CG15282
CG5892	Men-b	Syx5	CG33189	CG5157	MtnB	RpA-70	CG10353	Lcp65Ag2
CG15309	CG33099	TfIIA-L	lin-28	CG31089	GstD4	CG15027	SdhB	pre-mod(mdg4)-G
CG2187	CG43773	Slik	CG18598	CG42662	MtnE	GstS1	Emp	CG17764
CG10621	Sec16	Eaf	CG13116	CG34316	galla-1	Mdr49	His3.3A	Gbp3
Oat	Aop	CG17036	CG15641	Ugt302E1	CG2065	mt:ND6	Ero1L	CG7059
CG1139	Syp	CG30479	RYa-R	CG10081	Drip	Cyp28a5	Cyp28d2	CG33946
CG10560	CG8093	drongo	CG13049	CG1394	CG7763	CG31974	Desat1	VepD
CG45087	Drpr	ND-ACP	CG5928	CG14205	CG16898	Damm	Fmo-2	CG34227
CG7370	CG5789	porin	CG34453	CG12643	Zip99C	CG6769	CG4562	Psh
CG5973	CG31145	sdt	CG18371	Lsm10	CR40454	CG15096	CG5835	CR14798
MFS12	Tina-1	Vamp7	CG42512	CG16727	CR45854	Zip48C	CAP	CG15605

Adh	CG13607	COX7C	Acp53Ea	CG5892	CG33301	CG11837	Pepck2	asRNA:CR43885
CG33181	Mim	Tao	PGRP-SA	CG15309	CR45863	Ugt49B1	Cib	CG14451
MFS1	NKCC	CG6901	Andorra	CG2187	CG12224	CG31549	CG42249	CG42392
Drsl5	Ugt35E1	Pdk	CG42759	CG10621	CG42810	puml	CG9471	CG14445
Mag	CG14715	atl	CG33061	Oat	Fer1HCH	mt:ND3	CG12945	CG30288
Ste:CG33247	PAPLA1	CG33096	CG13949	CG1139	Dhd	SmB	Tina-1	CG34443
Alp9	Rogdi	rgn	CG31741	CG10560	Cyp6d2	CIAPIN1	Diddum	cid
Brk	Galk	Df31	Hs3st-B	CG45087	CG31546	CG5958	Sgl	CG14598
CG32407	Seipin	RpL37a	CG15742	CG7370	5CR45857	ClC-a	CG44250	Lcp65Ae
Acbp5	CG4586	CG9399	CG33775	CG5973	CR33363	Prip	CG4199	TwdlP
Mvl	CG9003	ScpX	Rtnl2	MFS12	Mal	Mocs2A	Alt	Cpr49Af
Cyt-b5-r	SdhB	CG6013	CG13078	Adh	Rdog	CG10463	LamC	l(3)mbn
Cyp28d2	CG32280	Syx1A	ninaD	CG33181	CR41609	CG1575	Rl	Lsp2
Sfp33A4	mRpS24	nrv3	Ste:CG33247	MFS1	CG4607	Nle	betaggt-I	TwdlO
Hph	CG13252	PCB	CG13077	Drsl5	Fer2LCH	SelG	Efr	Lcp1
CG30161	nonA	CG8788	CG42822	Mag	CR45862	mt:ATPase6	Khc	CG12607
CG13631	Ace	Pka-C1	Ste:CG33238	Ste:CG33247	Naam	Myc	Rtnl1	Lcp4
SclA	PGRP-SC2	CG9018	CG5157	Alp9	CR40741	ZnT63C	P5cr-2	Lcp65Ag1
CG44242	CG5447	CG7630	CG31089	Brk	CG6996	l(3)72Dn	Arl8	CG13705
Mipp1	Hnf4	Sfxn1-3	Ste12DOR	CG32407	CR45859	Ssrp	CG7470	Lcp3
CG9416	Eglp4	Jon99Ciii	CG7370	Acbp5	CG7720	GstD7	alpha-Est7	Lcp65Ab1
Paip2	CRAT	CG3907	CG34316	Mvl	GstD6	GstE3	Alp12	Lcp65Ab2
CG10365	Pak	Ocrl	Ugt302E1	Cyt-b5-r	Gcn5	CG8675	Moe	Lcp2
Reg-2	ACXD	yrt	CG5892	Cyp28d2	CG2064	eIF6	Vps26	CG11350
CG34198	CG16953	CG4603	CG14205	Sfp33A4	CG2909	CG5728	fa2h	Vajk3

Tim17b1	Fatp3	CG7564	CG6770	Hph	CG9945	CG10182	CG44008	Cpr65Ax1
Uro	CG32564	COX8	CG45087	CG30161	Zip89B	Act42A	OtopLb	Cpr65Ax2
GstT4	MED6	Sec24AB	CG12643	**Q-Common**	GstD3	Nop60B	CG44001	CG6910
Rift	CG12338	svr	CG10621	CG13631	GstE1	Srl	CG2938	Vajk2
Ste:CG33238	Hr39	Pgant9	CG10560	SclA	**Q-Deseq2***	mt:lrRNA	Rab6	Scp2
Agpat2	Sirup	Fsn	Drsl5	CG44242	CG34054	CG7298	Ccm3	CG18095
CG11892	CG10863	kdn	CG16727	Mipp1	CG31525	Jafrac1	l(2)37Cc	CG32241
AANATL6	How	CG14407	CG13631	CG9416	Zip42C.2	Arc1	Rala	CG32603
Ste12DOR	CG17928	Tapdelta	CG1139	Paip2	CG31288	Trxr-1	Cpb	CG16743
alpha-Est2	CG5828	Tab2	CG13312	CG10365	CG14906	Akr1B	GstO2	His1:CG33834
JhI-26	CG15343	CG15611	CG2187	Reg-2	CG31694	CG10505	Inx2	CG13731
CG13312	Ben	Dap160	Oat	CG34198	CG1840	MtnB	Pbgs	CG13177
CG14218	Ggamma1	chinmo	MFS12	Uro	Ctr1B	GstD4	Vps4	CG13218
Mfrn	Hsp83	CG17681	MFS1	GstT4	CG44142	MtnE	CG6218	Obp83g
CG32266	Px	Cpsf100	CG5973	Rift	GstE7	galla-1	AspRS	CG14963
Roh	CG13392	Galt	CG33181	CG33238	CG17814	CG2065	Coprox	Lsp1alpha
CG14957	Naa60	Vha36-1	Paip2	Agpat2	CG6928	Drip	CG1486	CG42807
CG17724	Dnc	wkd	Brk	CG11892	Obp84a	CG7763	Clic	AttD
Fok	TpnC73F	CG9132	Adh	AANATL6	CG30148	CG16898	CG4301	CG30016
smp-30	For	CG11889	CG13325	Ste12DOR	CR45860	Zip99C	CG7992	Fer1HCH
Fpps	GstZ1	scyl	CG14219	alpha-Est2	Out	CR40454	l(2)k05819	CG34043
Cer	CG6409	Ubc2	Alp9	JhI-26	GstD8	CR45854	CG18747	Fer2LCH
CG9452	Gish	jvl	Mag	CG13312	CG14269	CG33301	Kcc	MtnE
CG42494	CG17597	CG3091	Cyt-b5-r	Mfrn	GstD1	CR45863	betaTub56D	fon
CG33655	Gdap2	LysD	Cer	CG32266	CG18540	CG12224	Svil	Lsp1beta
CG12896	Glut1	Pdha	CG34446	Roh	CG13460	CG42810	CG3662	Muc11A
CG6287	CG34417	spin	Cyp28d2	CG14957	MtnA	Fer1HCH	Slik	CG42586
CG4306	CG5835	oys	CG43348	CG17724	MRP	Dhd	Pld3	CG31775
CG13116	CG13585	mRpL12	Mvl	Fok	Arc2	Cyp6d2	CG17167	Ctr1B
CG13606	Shn	VhaPPA1-1	CG32407	smp-30	Mocs1	CG31546	l(2)gl	CG2233

CG14688	Lamp1	CG46280	Acbp5	Fpps	Cks85A	CR45857	ergic53	Zip89B
CG18598	CG7968	CG32369	CG46309	Cer	Wun	CR33363	CG13220	CG8837
CG45081	CG44245	P5cr	GstT4	CG42494	Hsp70Aa	Mal	LManII	CG7763
NimB5	PPP4R2r	Rac1	CG10365	CG33655	Hsp70Ab	rdog	Ctp	CG6125
CG32032	CG6178	CG2200	Hph	CG12896	AOX1	CR41609	Adh	CR33363
CG13928	Wts	Sar1	CG34198	CG6287	Tut	CG4607	14-3-3epsilon	CG3604
LysE	CG14615	CG32425	Uro	CG13116	CG14841	Fer2LCH	alpha-Est2	Amyrel
CG6277	Acox57D-p	milt	CG9416	CG13606	Hh	CR45862	Ox	MtnB
CG15641	CG44085	CG45076	Mipp1	CG14688	Cpr73D	Naam	PCB	CG5070
Arx	CG46319	CG9825	Reg-2	CG18598	CG13021	CR40741	Flr	AANATL6
CG11226	CG14630	Hmu	PGRP-SD	NimB5	mod(mdg4)-U	CG6996	Rpn6	swi2
RabX1	CG8223	CG3662	CG44242	LysE	Mdr50	CR45859	SkpA	Uro
Cpr65Av	Gug	Galphao	RabX1	CG6277	CR45855	CG7720	Csp	apolpp
Prx2540-2	Agpat3	Xe7	AANATL6	CG15641	1CR41602	GstD6	CG17029	CG10505
Eaat1	Tip60	Vps26	Mfrn	RabX1	Irbp	Gcn5	SdhA	salt
CG17167	CG17278	CG9436	CG32266	Cpr65Av	GstD10	CG2064	Idh	galla-1
CG8112	CG42375	CRIF	alpha-Est2	Prx2540-2	ng2	CG2909	Past1	Alp7
CG11151	CG7379	aux	CG12896	Eaat1	CG6808	CG9945	Ome	CG34426
Swip-1	Ush	Gabat	Fok	CG17167	RpS5b	Zip89B	CG9527	hui
Gk2	nrv1	CG32278	Rift	CG8112	CG10638	GstD3	**L-edgeR**	CG15155
AANATL3	LManVI	alt	CG11892	CG11151	mt:ND2	GstE1	Jon65Aiii	mino
MsR2	Fic	sw	Agpat2	Swip-1	MtnD	**Q-Common***	Jon99Cii	CG3690
MFS3	Ptpa	Jon99Cii	CG14688	Gk2	CG43094	CG34054	CG3902	Cyp4d14
CG43107	CG31710	Cdep	CG42494	AANATL3	Puml	CG31525	CG7298	CG14787
TfIIA-S	Slu7	CG17633	smp-30	MFS3	SmB	Zip42C.2	Jon74E	CNT2
Sbm	CG11149	TRAM	Roh	TfIIA-S	Mst	CG31288	Cyp6a2	CR40454
Nenya	CG6903	Kcmf1	CG17724	Sbm	CIAPIN1	CG14906	CG1532	CR45854
CG1208	Fkbp12	CG8929	Eaat1	CG1208	mt:ND3	CG31694	CG10182	Syt1
CG13325	Vha16-1	btz	Fpps	CG13325	ClC-a	CG1840	CG15784	CG46306

CG32276	Mpc1	l(2)efl	CG14957	CG32276	CG5958	Ctr1B	CG11370	CG16762
CG14502	Pug	Pak3	JhI-26	CG13315	CG31549	GstE7	thetaTry	CG1208
CG13315	kat80	wdb	LysE	Spi	Sol	Peritrophin-15a	AcCoAS	EbpIII
Spi	CG17751	RFeSP	Prx2540-2	Ox	CG6145	CG6928	CG33801	CG5697
Ox	CG13004	Sting	AANAT L3	CG43349	Prip	CG30148	CG7272	CG31248
CG13044	CG1143	egl	Pdcd4	JTBR	Mocs2A	CR45860	CG8206	MFS12
CG43349	CG6283	Ae2	Cpr65Av	Srr	MED10	Out	Nero	Zip48C
JTBR	AcCoAS	CG5149	CG13311	ATPsynE	CG3735	GstD8	Sug	CG8664
PGRP-LF	Atet	CG13510	CG6287	CG3270	CG18596	CG14269	Mal-A7	CG8620
Srr	Gclc	CG11771	CG16965	CG45092	CG10463	GstD1	Mfrn	l(3)87Df
ATPsynE	l(1)G0320	Ppcs	CG6277	RYa-R	CG1575	CG13460	CG46309	Fatp3
CG3270	Desat1	eIF4H1	Glec	CG43348	Wde	MtnA	Eaat1	CG7582
CG43965	CG33981	LManII	Prx2540-1	PGRP-SD	CG7246	MRP	CG14120	Alp8
CG45092	CG15879	spen	CG11151	CG42497	Nle	Arc2	CG45087	Zip99C
RYa-R	Smr	Mapmodulin	CG43349	CG13893	CG12321	Mocs1	CG5953	SLC22A
CG43348	CG33051	Lmpt	Ox	Zip71B	Myc	Wun	Rift	CG31075
PGRP-SD	Sccpdh1	mRpL50	Swip-1	Npc2d	CG3808	Hsp70Aa	Alp10	Npc2c
CG42497	Rtnl1	mbl	CG15221	CG9717	Ssrp	Hsp70Ab	CG6271	CG15096
CG13893	Hs6st	Mlf	CG13315	Glec	Ugt35C1	AOX1	CG4269	CG3270
GV1	Gbeta13F	Synd	Pirk	CG34453	SelG	CG14841	Nplp4	CR45863
Zip71B	Samuel	mRpS29	Spi	Dh31-R	l(3)72Dn	Hh	Mvl	Lsd-1
Npc2d	dnr1	Jon25Bii	TfIIA-S	Ndae1	mt:ATPase6	CG13021	CG5892	CG7953
CG9717	Ham	UQCR-6.4	CG17167	CG10600	CG32756	pre-mod(mdg4)-U	Thor	Drip
Glec	su(Hw)	Tom7	MFS3	Fatp1	GstD7	Mdr50	CG18179	CG3699
CG34453	Myo31DF	Tpi	CG8112	regucalcin	CG2875	CR45855	CG13678	Mcad

Dh31-R	Ps	CG15118	JTBR	ACC	CG10916	CR41602	Alp9	CR41609
Ndae1	CG10654	Patronin	Gk2	CG15221	CG10513	Irbp	Hsp68	CG32407
CG10600	GlyP	VhaAC45	Sbm	CG34446	GstE3	GstD10	Ugt302E1	MtnA
Fatp1	Su(Tpl)	NKAIN	CG8028	Mino	ZnT63C	CG10638	Hsp26	CG42806
Regucalcin	CG10343	hzg	CG1208	CG14219	eIF6	mt:ND2	Hsp22	Peritrophin-15b
ACC	Mdy	l(1)G0289	Dh31-R	CG46306	CG11710	MtnD	CG5157	CG4363
CG15221	CG4896	MYPT-75D	Srr	Ifc	CG8675	mt:ND4L	Hsp70Aa	CG8997
CG34446	CG34194	Vha26	Nplp4	CG16965	Act42A	E(spl)malpha-BFM	Hsp70Ab	CG7916
Mino	CG5767	CG3776	CG9717	Pirk	Nop60B	CG43376	Hsp70Bbb	mt:ND4L
CG14219	Dnd	aralar1	CG32276	AANATL2	CG5728	Fbp2	Ugt37A1	CR40741
CG46306	CG33965	Tsp42Eb	ATPsynE	CG13311	CG12766	CG6299	CG13077	Peritrophin-15a
Ifc	Act57B	CG30160	Zip71B	CG9664	CG10182	CG3008	CG13078	CR45855
Mos	Taf6	Cndp2	CG3270	CG46309	Srl	Ver	Hsp70Bc	mt:ND4
CG33919	NC2beta	fau	CG45092	Tkv	spn-A	CR45861	SdicC	CR45862
CG16965	PMP34	CG9471	AANAT L2	CG14877	SpdS	Cpr62Bb	Sfp33A2	CR45859
Pirk	BtbVII	Dredd	CG46306	ND-B14.5B	CG43896	CR45853	CG18628	Jon25Biii
Slbo	Dpy-30L1	Non2	Npc2d	CG34330	Mal-A7	Igl	CG9129	CR41602
yellow-k	Rdx	Mal-A3	CG14877	Fpgs	mt:lrRNA	CG11333	Rdh	mt:srRNA
AANATL2	Tango2	AP-2mu	CG13893	NimC3	Rtc1	CG15484	CG12725	**L-Common***
CG13311	CG33523	CG8207	Ndae1	Prx2540-1	Ugt37A2	Hsp68	CG6999	Lsp2
CG9664	CG34284	fa2h	CG42807	ABCA	RpI135	mt:CoII	Blanks	Fer1HCH
CG46309	Mlt	mtgo	CG10073	CG13049	CG15916	CG7203	CG42531	Fer2LCH
CG13950	Argk	Nipsnap	CG10600	PGRP-SA	NHP2	Ku80	COX4L	Zip89B
Tkv	Stas	CG5770	CG42497	DOR	Mat89Ba	CG42516	CG14346	MtnE
CG14877	Rab35	EloB	Smvt	Fiz	CG33786	mt:ATPase8	CG42364	CG13177
CG17707	Cyp6a21	CAH3	CG13051	CG8028	CG33217	CG12171	CG15357	Ctr1B
ND-B14.5B	Inc	PGRP-LB	Fatp1	CG6574	CG9286	CG13947	Tep5Psi	Lsp1alpha

CG34330	mRpL13	Pex13	CG34228	CG42759	CG10799	Sing	CG12310	CR33363
Fpgs	Spir	CG9672	Mino	Pdcd4	CG12926	CG14907	CG34161	AANATL6
NimC3	CG42455	UbcE2M	CG9664	Vnd	CG33158	CG13659	EbpII	CG31775
Prx2540-1	Dop	mRpL15	Regucalcin	CG42807	l(2)k09848	CG42319	Cpr78E	CG42586
CG14573	CG6012	Vha55	ACC	Chk	CG11123	CG14589	Cpr64Ab	galla-1
ABCA	Zasp66	Mob2	Vnd	CG31183	Stc	mt:srRNA	CG14974	CG10505
CG13049	CG42258	CAH7	Fpgs	Smvt	CG5800	CG32512	CG43965	swi2
PGRP-SA	Ssdp	CG7220	Tkv	CG44008	Jafrac1	GstS1	CG18853	MtnB
DOR	Chrac-14	chic	RpS29	P5cr-2	TTLL5	RpA-70	**L-Common**	CG30016
Fiz	Sgg	CG10467	Ifc	Fusl	CG1671	CG4797	CG13077	CR40454
CG8028	GlyS	Cnot4	Fusl	CG10073	CG31259	CG31974	CG13078	CR45854
CG7997	CG18180	CG1907	CG31183	CG34228	Pgant4	mt:ND4	CG5157	CG6910
CG6574	Pih1D1	ncm	ABCA	Fancl	U3-55K	Mdr49	CG18853	Amyrel
CG14245	Lk6	Tango5	DOR	CG5928	CG8064	CG6769	Hsp22	Alp7
CG42759	Btsz	CG7523	ND-B14.5B	CG42819	CG7637	mt:ND6	Alp9	CNT2
Pdcd4	CG9220	Khc-73	Fiz	CG30015	SmD3	CG15027	Hsp70Bbb	CG3604
CG9701	CPT2	NFAT	CG30015	Mondo	Arc1	Cyp28a5	CG18179	mino
Rcd6	fl(2)d	RpS28b	CG8665	Ncc69	Non3	Damm	CG5892	salt
Vnd	Pka-R2	Tim10	CG34330	CG14568	CG9555	Ugt49B1	Mvl	CG1208
CG42807	CG14767	Rab7	ATPCL	Cyp311a1	Trxr-1	CG11837	CG43965	CG14787
Chk	CG34445	GstO2	CG6574	Crq	CG14464	CG15096	Ugt302E1	pre-mod(mdg4)-G
CG31183	CG7029	Bacc	CG42819	ATPCL	Trx-2	Zip48C	Alp10	CG42807
CG3630	Naus	Nak	Chk	CG42512	nop5	puml	CG14974	Zip48C
Smvt	CG5823	Ubc10	Fancl	CG31741	l(2)k09022	SmB	Cpr78E	CG16743
CG44008	l(3)L1231	hebe	P5cr-2	CG43078	Prat	CIAPIN1	Rift	CG31248
P5cr-2	CG43783	Mur29B	CG44008	RpS29	Kz	mt:ND3	CG4269	AttD
Fusl	Rab8	Whamy	CG43078	CG18179	CG7627	ClC-a	CG14120	EbpIII

CG10073	Cyp6d5	mRpS2	CG14568	PAN3	Mekk1	CG5958	CG45087	CG16762
CG34228	Dic1	cN-IIIB	Cyp311a1	Alp10	PIG-Wb	CG31549	Mfrn	Fatp3
Andorra	Acsl	Sap47	Ncc69	Ringer	Akr1B	Prip	CG46309	CG5697
Fancl	CG32264	levy	PRAS40	PRAS40	CG7006	Mocs2A	Eaat1	CG3690
Run	CG8839	CG11050	CG5009	CG8665	CG12301	CG10463	CG5953	CG6125
CG5928	LysB	glob1	Cyp4d8	FASN1	CG11180	CG1575	Sug	CG7582
CG18765	upset	Fak	Mondo	CG2162	Elp1	Nle	Nero	Alp8
Amn	Gal	mRpS10	Crq	CG12512	GstE6	Myc	CG6271	Zip99C
CG42819	CG8034	PpV	ringer	Amy-p	Lfg	Ssrp	Mal-A7	CG13218
Fw	Ugt35A1	mxt	CG12512	CG5009	CG14777	SelG	CG8206	CG46306
CG30015	CG15237	rump	CG14795	EbpIII	CG2199	l(3)72Dn	CG34161	CG31075
Mondo	sens-2	Cyp4p1	Amy-p	CROT	Cyp305a1	mt:ATPase6	AcCoAS	CG34426
Syn1	Mbs	CG7149	PAN3	Cyp4d8	CG12499	GstD7	CG7272	CG17764
Ncc69	KrT95D	Csp	CG18179	CG18747	CG10910	GstE3	thetaTry	CG8664
CG14568	CG17191	Ubc6	FASN1	SecCl	CG1582	ZnT63C	CG33801	MFS12
Hgo	Swim	p130CAS	CROT	Rtnl2	Ubi-p63E	eIF6	CG11370	CG15096
Cyp311a1	MED31	CG12054	CG2162	Fst	CG15255	CG8675	Tep5Psi	CG14963
PPO2	Drep2	Rcc1	CG10418	CG10184	CG33785	Act42A	Cpr64Ab	CG7059
CG13679	Wmd	SNF4Agamma	Alp10	CG10623	Mtr4	Nop60B	SdicC	CG7763
Crq	Ada1-2	CSN3	Salt	Acp53Ea	CG15044	CG5728	CG10182	SLC22A
ATPCL	CG17233	CG10208	EbpIII	Fmo-2	l(3)07882	CG10182	CG1532	Drip
CG42512	CG3868	CG5854	CG18747	CG12384	CG6724	Srl	CG15357	hui
CG31741	CG8009	ZnT41F	CG10623	Kdm4B	CG15673	mt:lrRNA	COX4L	CG7953
CG43078	Chd64	CG9205	SecCl	CG1358	Nop56	Jafrac1	Cyp6a2	CG2233
RpS29	CG31550	Indy	CG10184	PGRP-SC1a	CG42806	Arc1	CG14346	CG3699
CG18179	Cype	CG2681	CG5506	Mnt	Fib	Trxr-1	Blanks	Npc2c
CG32107	Bnl	CG17834	CG1358	CG33169	Ugt37D1	Akr1B	CG12310	CG8620
PAN3	Jheh2	SerRS-m	SCCRO4	Eglp2	CG9799	**L-Deseq2**	Jon74E	l(3)87Df
Alp10	NitFhit	Tailor	Mnt	l(2)k09913	Kra	CG13077	CG3902	CG5070

Ringer	Letm1	CG34310	PGRP-SC1a	Axo	Sf3b3	CG13078	CG7298	Lsd-1
PRAS40	COX5B	Pisd	Axo	CG13051	CG9512	CG5157	Jon99Cii	Mcad
CG8665	Gasp	dod	Kdm4B	Dl	mbf1	CG18853	Jon65Aiii	CR45863
FASN1	CG10962	Mal-A6	CG15771	CG5506	CG14850	Hsp22	**L-Deseq2***	CG3270
Ugt49B2	CG32638	slmo	Atf3	Rab14	CG11300	Alp9	Lsp2	MtnA
CG2162	Prtp	Amacr	CG33169	Salt	CG32198	Hsp70Bbb	Fer1HCH	Gbp3
CG12512	Cyp4d1	Oatp33Ea	Eglp2	CG6295	att-ORFB	CG18179	Fer2LCH	CR43885
Amy-p	SREBP	CG34301	Fmo-2	CG15771	CG8087	CG5892	Zip89B	CR41609
CG5009	CG3655	Mdh2	CG12384	CG10418	Leu-TAA-1-1	Mvl	MtnE	CG42806
EbpIII	Jheh1	CG5028	Rab14	ATPsynF	mod(mdg4)-J	CG43965	CG13177	CG4363
CG10657	Aay	cdi	Fst	Gbs-70E	CG30148	Ugt302E1	Ctr1B	CG32407
CROT	Gs1	Mp20	Tara	Adf1	mod(mdg4)-N	Alp10	Lsp1alpha	CG8997
Cyp6t1	Hacl	CG13551	CG7860	Sec61beta	CG42810	CG14974	CR33363	CG15605
Cyp4d8	CG43897	AP-2alpha	Adf1	CG13784	Dhd	Cpr78E	AANATL6	CG33946
CG18747	Zasp52	kst	Muc68E	SCCRO4	CG43376	Rift	CG31775	psh
SecCl	Sply	Aps	CG6295	Atf3	Lcp65Ag3	CG4269	CG42586	Peritrophin-15b
Rtnl2	CG6665	sau	l(2)k09913	Hs3st-B	Oxp	CG14120	galla-1	CG42392
Fst	CAP	alpha-Est4	ATPsynF	CG7860	CG13947	CG45087	CG10505	CG14451
CG12490	SCOT	CG2915	RhoGAP68F	CG10939	CG34040	CG2812	swi2	CG30288
CG10184	CG3065	Neb-cGP	CG13784	CG14621	CG13021	mfrn	MtnB	CG7916
CG10623	mRpL46	CG7582	CG10939	CG32813	mod(mdg4)-U	CG46309	CG30016	Peritrophin-15a
Gb	Gdh	CG2246	App	CG13949	CG5402	CG43107	CR40454	CR40741
Acp53Ea	Coprox	CG32795	Cyp6a14	RhoGAP68F	CG11333	Eaat1	CR45854	mt:ND4L

Fmo-2	CG8312	CG17508	Bet1	Vsg	Igl	CG5953	CG6910	CR45855
Sox14	CG11737	CG11453	Jim	CG14795	CG15579	Sug	Amyrel	mt:ND4
CG12384	CG43736	nSMase	betaTry	Jim	CG31496	Nero	Alp7	CR45862
Kdm4B	RhoL	par-1	bc10	Gpdh1	CG14269	CG6271	CNT2	CR45859
CG1358	CG42825	Jheh3	CG14621	Muted	CG44622	CG9500	CG3604	
PGRP-SC1a	su(sable)	up	Gbs-70E	bc10	CG14841	Mal-A7	Mino	
Mnt	Echs1	Ass	Sec61beta	Gs2	CG15484	CG8329	Salt	
CG33169	ZAP3	Sec31	CG11659	Tara	E(spl)malpha-BFM	CG9416	CG1208	
Eglp2	CG33199	betaTub56D	CG32813	Cyp6a14	Djl	CG8206	CG14787	
l(2)k09913	HDAC6	eIF4E1	ReepA	CG13284	Sing	CG34161	CG43103	
Axo	CG9826	COX5A	Vsg	ReepA	Fbp2	AcCoAS	pre-mod(mdg4)-G	
CG13051	Gro	Arl1	Muted	CG6330	Cpr62Bb	CG7272	CG42807	
Dl	Cic	CG9663	Gs2	Dci	CG10918	thetaTry	Trf	
kek5	Ppa	CG15117	moody	CG33144	CG13022	CG10337	CG17108	
CG5506	Csk	Not1	mRpL33	Ugt37B1	Sfp51E	His1:CG33801	Zip48C	
Rab14	kin17	Jon25Biii	Chrb	Mal-A8	CG7203	Ugt302K1	CG16743	
Salt	CAH9	SsRbeta	CG6330	App	CG5888	Eip78C	CG31248	
CG13082	CG7536	Smurf	CG33144	Chrb	CG34057	Pol31	AttD	
Mrtf	mRpL27	ND-18	Gpdh1	CG31075	CG14589	Gb	EbpIII	
CG6295	JIL-1	CG44243	Dci	Fhos	Sfp26Ad	CG5059	CG43095	
Ric	UQCR-Q	CG14120	Fhos	Ugt302C1	dpr19	l(3)02640	CG16762	
CG15771	Grx1	Vha68-2	CG3604	CG11659	**Q-edegR***	CG11825	Fatp3	
CG34427	CG5381	Fkbp14	CG34325	CG7970	CG33641	CG11370	CG5697	
CG10418	Tko	E2f1	CG13284	moody	CG13258	NAAT1	CG11313	
ATPsynF	Myd88	SelR	CG31075	CG34325	CG14075	Tep5Psi	CG3690	
CG17544	Cyp4d14	GstT3	CG7970	CG13075	Det	RnrS	CG12116	
Gbs-70E	CG1637	shot	CG3829	mRpL33	CG9040	Srp	CG6125	
Adf1	CG13369	Kr-h2	CG6337	CG6337	MtnB	Hh	CG7582	

Sec61beta	Muc	Syx7	RpL36	ATPsynC	CG10505	Cpr64Ab	Alp8	
CG13784	Treh	CG31086	CG45089	CG45089	CR45857	CG5890	Zip99C	
SCCRO4	CG9674	Ran	Mef2	CG3829	MtnE	CG18540	CG9107	
Atf3	Chi	CG7920	Ugt37B1	CG1532	CG34054	CycE	CG13218	
Hs3st-B	CG14856	CG4598	Jon99Fi	Muc68E	Zip42C.2	lawc	CR45857	
Hiw	CG2765	Rab5	04-Sep	CG12848	CG7763	SdicC	CG46306	
CG7860	Axud1	lola	Mal-A8	Mef2	Muc68Ca	cutlet	CG31075	
CG15432	Qless	Dp1	Ugt302C 1	Bet1	GstD4	CG10433	CG34426	
Br	Nuf	Pgant6	CG13047	CG10672	galla-1	Damm	CG17764	
CG10939	TSG101	Ald1	AstA	CG1927	CG13460	Ugt49C1	CG8664	
CG14621	Mal-A4	Cisd2	CG4752	LRR	CG2065	upd3	CG14456	
Seq	CG7966	SdhD	CAH2	RpL36	CG16898	CG10182	MFS12	
CG32813	CG9981	alpha-Est1	CG12848	CG3604	Drip	AdoR	CG15096	
CG13949	CG7834	hts	CG1532	Vps20	CG12224	Ppn	CG14963	
RhoGAP68 F	Ars2	CG42354	CG13075	Herp	Zip99C	CG1532	CG7059	
Vsg	CG8176	CG16903	CG7778	betaTry	CR40454	CG9825	CG7763	
CG14795	CG7458	Mfe2	CG34376	Aldh-III	CR45854	CAH9	SLC22A	
Jim	Rox8	ND-B18	Acbp6	CAH2	CR33363	CG5246	Drip	
Gpdh1	CG7470	blw	CG1927	04-Sep	MtnD	CG43394	Hui	
Apt	IKKbeta	siz	LRR	AstA	CR45863	CG1943	CG7953	
Muted	HDAC4	ND-B14.5A	CG43773	CG34376	CG31546	CG15357	CG2233	
bc10	Cbs	Vha44	ATPsynC	Ugt303A1	Naam	Fax	ssp7	
Gs2	Usp2	CG31343	Herp	CG17776	Cyp6d2	CG16790	CG3699	
Su(z)2	CG9515	Syb	CG5704	CG17752	CG33301	CG33474	Npc2c	
Tara	FBXO11	Pdxk	CG17776	CG7778	Fer1HCH	CG5789	CG8620	
CG11034	CG32137	Mlc2	CG17752	WASp	CG2909	Ewg	l(3)87Df	
Cyp6a14	Jarid2	Aldh	CG10672	Lbk	GstD5	Sld5	CG12951	
Mub	RanBPM	lqfR	Aldh-III	CG4752	28SrRNA-Psi:CR41609	COX4L	CG5070	

CG13284	CG10300	CG17272	Vps20	Jon99Fi	Mal	Sod3	Lsd-1	
CG4269	CG1943	Pglym78	Lbk	Sod3	28SrRNA-Psi:CR45862	Odd	Mcad	
ReepA	Idh3a	SelT	Ugt303A1	CG5704	Rdog	Cyp6a2	CR45863	
CG6330	Cpr	COX7A	CG13220	Eas	CG7720	Syx13	CG3270	
Pinta	Bigmax	CG1640	bab2	CG1544	CG4607	Dcp-1	MtnA	
Dci	CG33228	ND-15	mab-21	CG9527	28SrRNA-Psi:CR40741	Pnt	CG43155	
CG33144	CG9171	Rap1	Sod3	LPCAT	28SrRNA-Psi:CR45859	Bnl	AANATL3	
Whd	CG31522	Phb2	LPCAT	RpS11	GstD6	Raw	CG8028	
Ugt37B1	Fra	eEF1beta	CG11594	bab2	Fer2LCH	msn	CG34256	
Pol32	Hep	CG4658	WASp	CG4239	CG6996	CG14346	CG18814	
Mal-A8	PRL-1	CG5618	Eas	mab-21	CG2064	blanks	Npc2g	
CG10948	IM33	CG8206	CG1544	AANATL4	Zip89B	Path	Gbp3	
App	ND-13B	eIF4G1	CG4239	CG8963	CG31525	CG11898	Ak6	
Luna	Sky	Alas	CG8963	Mcad	CG9945	CG34417	CR43885	
Chrb	Bgm	alpha-Cat	Mcad	Mlc1	GstE1	CG12310	CG30289	
CG31075	Cyp6a9	Rpb12	CG9119	Acbp6	Gcn5	Hydr1	CG4306	
Fhos	CG8661	CG8036	Amy-d	CG13220	GstD3	GluRS-m	CROT	
Ugt302C1	TpnC47D	eEF1delta	CG9527	Amy-d	CG1840	CG44014	CR41609	
CG11659	Taf4	Vha100-1	Lasp	CG11594	CG14906	Kr-h1	CG42806	
CG7970	His2Av	mRpS9	Acox57D-d	Acox57D-d	Hh	MFS1	Nemy	
Moody	Men	RhoGAP1A	RpS11	CG13047	CG31694	CG30043	GstE10	
Step	Jon99Fii	Jon99Ci	AANATL4	LSm1	CG6928	CG34325	CG4363	
CG34325	ND-B14	Acn	Seipin	UK114	CG31288	LpR1	CG14230	

CG13075	Gyc76C	Traf-like	Syp	Act87E	Ctr1B	Jon74E	CG32407	
mRpL33	CG11562	SkpA	Mlc1	Akap200	Arc2	CG33056	Nop56	
CG6337	CG7322	l(2)gl	Akap200	CG9119	CR45860	Fpgs	CG7460	
ATPsynC	Vap33	ScsbetaA	Slif	CG8562	Peritrophin-15a	CG30423	CG2680	
CG45089	Gcl	UQCR-C2	Atpalpha	Slif	GstE7	Tep4	Xpac	
CG34242	alpha-Est3	CG3719	UK114	Atpalpha	CG44014	CG3902	CG8997	
CG3829	CG34176	Dera	CG42837	CG3603	Ugt37A3	CG4829	CG7637	
CG1532	CG30069	betaCOP	Act87E	Lasp	MtnA	CG7298	betaTub60D	
Muc68E	CG42637	CG31248	Rogdi	CG42837	Out	mRpL33	CG18473	
CG12848	Strica	Nacalpha	Roq	GEFmeso	GstD1	Pst	CG11899	
Mef2	Arl5	Diap1	CG5828	CG6424	GstD8	CG3719	Cyp6a8	
DAAM	Fibp	CG17029	GEFmeso	Roq	Hsp70Aa	CG44286	CG5757	
CG16762	CG17119	CG18745	CG8562	CG43773	Hsp70Ab	CG33181	CG15605	
Bet1	CG42813	CG10877	CG6424	Sec16	MRP	Atf3	Pit	
CG10672	CG15773	mAcon1	CG14715	Syp	Mocs1	ref(2)P	CG33946	
CG1927	Twin	wal	CG3603	CG5789	Wun	CG4783	Psh	
CG10147	CG15155	mRpL53	CG5789	Tina-1	AOX1	CG5151	Peritrophin-15b	
LRR	Vha14-1	bic	nonA	Ugt35E1	18SrRNA-Psi:CR41602	Swim	CG42392	
AstC-R2	Tis11	Rpn8	Ugt35E1	CG14715	Mdr50	CoRest	CG11891	
CG4297	Wrd	CG7272	SdhB	PAPLA1	Ver	CG18417	CG17026	
l(1)G0469	Vrp1	Nedd4	Sec16	Rogdi	Irbp	Alas	Pkg21D	
CG2906	RhoGAP19D	ND-75	Fatp3	Galk	GstD10	Naa60	Tim9b	
RpL36	CG4538	CG11267	CRAT	Seipin	mt:ND4L	CG2765	CG14451	
Ptx1	ATPsynD	Dip-B	PAPLA1	SdhB	28SrRNA-Psi:CR45855	rho-7	CG30288	
CG3604	Mtd	eIF4B	Hnf4	CG32280	mt:ND2	Loco	Cln3	

Cf2	Cdc7	RpL28	CG5447	CG13252	CG10638	Dh31	Nau	
CG42488	Ldsdh1	RpL40	CG32280	nonA	Hsp68	CG31324	CG6330	
Vps20	Ctp	Jon66Cii	PGRP-SC2	PGRP-SC2	CR45853	SecCl	GstT3	
Herp	CG31751	GCS2beta	Tina-1	CG5447	CG6299	Chd64	Gba1a	
MESR3	Smox	Clc	CG13252	Hnf4	CG42516	CG33116	l(2)k09848	
betaTry	RpS13	Shmt	Pak	Eglp4	CG13659	ACC	mt:ATPase8	
l(3)neo43	Pde8	CG31673	CG13585	CRAT	CR45861	CG18585	CG6126	
Aldh-III	CG43954	HINT1	Galk	Pak	CG3008	CG42380	CG7916	
CAH2	Akt1	Arf79F	PPP4R2r	Fatp3	mt:ND4L	GlcT	CG31041	
04-Sep	Gr39a	CG3061	For	CG12338	CG14851	CG42379	Nha1	
AstA	Patr-1	Pax	CG14630	CG10863	CG10801	Sps2	Peritrophin-15a	
CG7785	CG8080	akirin	Ben	CG5828	CG43187	Kay	CR40741	
CG34376	Ck	p23	Eglp4	Ben	E(spl)mal pha-BFM	smash	CG17928	
Ugt303A1	Ppat-Dpck	CG8773	CG7968	Ggamma1	CG43376	p38c	mt:ND4L	
CG17776	CG33995	Scamp	CG17597	Hsp83	Fbp2	CG33995	CG8353	
Jet	CG3746	garz	AcCoAS	TpnC73F	CG6299	Btnd	CG7860	
CG17752	Drp1	Cam	CG6409	For	CG3008	CG14820	CG5011	
Tgo	CG17598	Alg11	CG46319	CG6409	Ver	CG42518	Adgf-A	
CG7778	CG9727	zetaTry	CG12338	Gish	CR45861	CG6424	Mal-A1	
WASp	Sd	ATP6AP2	CG10863	CG17597	Cpr62Bb	Pino	Inos	
Lbk	CG12213	Eno	Hsp83	Gdap2	CR45853	Dnk	Hacl	
CG4752	CG17271	Bsg	Ggamma 1	CG5835	Igl	Nhe2	PGRP-LB	
Oatp74D	CG31224	tzn	TpnC73F	CG13585	CG11333	Nub	CG14989	
CG11095	CG15093	RpL26	Gdap2	Lamp1	CG15484	MTF-1	AANATL4	
Jon99Fi	CG5946	eIF2gamma	CG5835	CG7968	Hsp68	CG13784	Ugt301D1	
Sod3	CG1607	14-3-3zeta	Gish	PPP4R2r	mt:CoII	CG13284	Tsp42Eg	
CG5704	CG7460	Pdhb	Agpat3	CG6178	CG7203	Dl	Est-Q	
Eas	aph-1	CG15347	CG8223	CG46319	Ku80	CG30344	CG11241	
CG1544	CG32066	Pp1-87B	Lamp1	CG14630	CG42516	Sbm	Pfdn4	

CG9527	mthl10	spidey	Vha16-1	CG8223	mt:ATPase8	Trbl	CR45855	
LPCAT	CG9034	mRpL9	CG6178	Agpat3	CG12171	MFS14	CG12115	
RpS11	Idi	Dip-C	nrv1	nrv1	CG13947	CG31917	CG15019	
CG18473	BBIP1	mge	Desat1	LManVI	Sing	CG12643	CG10300	
bab2	CG15706	Muc18B	LManVI	Fkbp12	CG1239	Ifc	CG7966	
CG4239	Osa	Tm1	Gclc	Vha16-1	CG14907	CG31323	RpLP0-like	
Vago	CG41128	Chchd2	CG5767	CG6283	CG13659	Chs2	CG16749	
Wgn	Mpcp1	CG3819	Fkbp12	AcCoAS	CG42319	CG5004	Npc2d	
mab-21	Graf	ATPsyndelta	l(1)G0320	Gclc	CG14589	Toll-9	Oscillin	
CG11367	CG5151	Cyt-c1	CG6283	l(1)G0320	mt:srRNA	CG7920	CG34330	
AANATL4	Sf3b6	CG11076	Rtnl1	Desat1	CG11103	Muted	mt:ND4	
CG8963	CG11791	CG10602	Cyp6a21	Rtnl1	CG32512	Jra	2CR45862	
Mcad	Dhit	CG8907	Su(Tpl)	Myo31DF	GstS1	CG8665	CG5009	
Cyp6a18	CG8516	colt	CG33965	GlyP	RpA-70	Cyp4ad1	smp-30	
Mlc1	Fabp	Rab11	Act57B	Su(Tpl)	CG4797	By	mRpL49	
Acbp6	CG6094	betaTub97EF	GlyP	CG5767	CG31974	CHES-1-like	l(2)k09913	
CG13220	beta4GalNAcTA	eEF1gamma	Argk	CG33965	mt:ND4	Gs1	ninaD	
Amy-d	Spn42Dc	**Q-edgeR**	Myo31DF	Act57B	Mdr49	Sec20	Acbp3	
CG11594	cdc14	BomS3	CG18180	Argk	CG15743	Swip-1	CG10910	
Acox57D-d	Pmp70	CG10081	LysB	Cyp6a21	CG6769	CG31343	Hexo1	
Ugt304A1	CG12375	CG15309	Acsl	CG18180	mt:ND6	alpha-Est3	CG9547	
CG13047	Tmod	pre-mod(mdg4)-I	Chd64	Acsl	CG15027	CG6484	CR45859	
LSm1	Gem	CG42662	COX5B	LysB	Drep1	CG13506	Cht9	
UK114	mRpL1	CG33655	CG3868	CG3868	Cyp28a5	CG12848	Ent2	
CG10543	CG15534	CG1394	Gdh	Chd64	Damm	CG15771	CG15126	

Spec2	Sima	Lsm10	Echs1	COX5B	CG31464	Pkn	alpha-Est10	
Kua	Faf2	BomBc1	Jon99Fii	Gdh	Ugt49B1	CG10116	MtnD	
Act87E	Sod1	Dro	UQCR-Q	Echs1	CG12728	Aay	GstE12	

[A] DEGs of each group are separated by gray cells in the table. Q- and L- stand for quick and late analysis and asterisk represents FAC-upregulated analysis.

Table 4. 6 DEGs of the whole larval body (WB) time course analysis.

WB[A]						
Q-Deseq2	Lsp1gamma	Ugt302C1	Ugt37A3	mt:ND4L	Cyt-b5-r	Zip89B
Mdh2	Srr	CG5770	GstE1	TwdlO	CG14701	Cyt-b5-r
Aldh	CG18179	ABCA	Gadd45	eIF4E3	Zip89B	CG31075
CG11961	CG3568	CG13679	CG8675	Lcp65Ae	CG34166	CG15673
Vha16-1	CG42819	CG16926	GstD10	Sun	Def	LysE
Men-b	CG45086	CG11151	CR45862	Prc	CG14974	CG7763
Gdh	CG13599	Fpps	CG7142	Mvl	CG14851	Drip
Gapdh1	CG42486	sinah	CG31694	Agpat2	CG7763	CG42807
Rtnl1	smp-30	vanin-like	Gcn5	CG4627	Edg78E	CG43315
Sply	CG5246	CG8664	Mdr50	CG16985	CG30108	CG33786
CG11350	CG13312	Npc2h	CG6299	CG33833	CG12725	CG31089
Tina-1	CG11892	Gk2	CG42319	CG33842	CG15673	CG8745
l(3)mbn	CG45087	Cyp4d1	CG31259	CG31613	Drip	CG42822
CG8997	CG5892	CG33704	CG7300	CG33839	Cpr65Au	galla-1
Pdxk	CG13077	Dpy-30L1	CG14191	CG33863	Cpr49Ac	CG32249
ATPCL	CG34316	CG11425	CG31974	CG33866	CG30430	Mal-A1
CG7920	CG16727	CG14957	MFS14	CG33851	Mal-A1	Cyp4d14
Hsp83	CG5157	CG15534	CG12171	CG33815	CG42807	Cpr49Ah
Lama	CG14205	CG9717	MtnB	CG33809	CG4830	CG6901
Jon25Bii	ninaD	CG10953	CG14237	CG33806	CG8745	CG4830
CG15093	CG13078	CG15706	Out	CG33854	E(spl)m2-BFM	CG11345

Jon99Fii	**Q-edgeR**	CG34446	Pym	CG33857	CG10621	CG8664
ND-19	Gpdh1	fusl	CG4607	CG33848	CG31089	CG10621
Vajk2	ATPsynC	Cyp6a21	Baf	CG33860	CG32276	CG30423
CG18180	LysB	AANATL4	ZnT63C	CG33803	CG32249	PGRP-LB
Sar1	CG32241	Acbp3	28SrRNA-Psi:CR45859	CG33836	CG16704	Sardh
ATPsynD	Lcp65Ab2	CG43349	Mocs1	CG33812	CG43773	CG7953
CG33307	Lcp65Ab1	Fst	CG11710	CG33845	CG30423	Jdp
Agpat3	Eip71CD	spirit	Zip42C.2	CG9922	CG46244	CG18003
Eglp4	Ndae1	CG11781	GstD1	CG13067	CG18003	CG42455
CG5773	LysD	Lcp65Ad	Peritrophin-15a	mt:ATPase8	Tra	CG34446
CG5946	Fabp	LysD	Wun	CR45861	Cpr49Ah	CG32276
mt:ND6	OtopLb	Cyp310a1	CG6769	CG34291	galla-1	Zip99C
VhaM9.7-b	Lcp3	Ugt303A1	CG3704	CG5246	CG7953	CG16704
Jon99Ci	Fst	salt	CG7298	CG32073	Zip99C	Cyp309a1
Cyp6d5	Acbp3	CG42764	CNT2	CG13912	Cyp4d14	CG12896
ND-18	CG9396	CG7906	CG15784	mRpL36	CG11668	CG8997
Ox	Cyp310a1	CG34426	CG15638	CG34117	CG43165	nAChRbeta3
COX5B	AANATL4	Drsl3	Arc1	SNRPG	CG8997	EndoU
CG5853	CG15534	Lcp3	CG43630	CG9877	Sox14	CROT
Myo31DF	Ugt303A1	CG13325	CG30054	CG33894	CG3565	CG5770
l(2)efl	CG34426	CG9396	CG7339	CG33898	CG30413	CG32603
Ldsdh1	CG33965	Ndae1	CG14995	CG33892	CG30380	PPO2
Ckd	Spirit	fabp	Jafrac1	CG33868	CG42455	GstD10
Pug	CG11151	yip3	**L-Deseq2**	CG33888	CG11345	Borr
Hydr2	AANATL2	CG33965	CG5157	CG33902	CG42255	CG13403
Jon25Bi	Gk2	Mst84Db	CG13077	CG33880	CG42822	CG15199
Aldh7A1	CG11425	AANATL2	CR45863	CG33890	PPO2	Pcp
Vajk3	CG15706	ND-B8	CG30065	CG33896	Cht4	Rab32
SdhB	Ugt302C1	OdsH	Alp10	CG33900	CG32603	Cyp28a5
Inx3	CG16926	Eip71CD	CG18179	CG33870	Jdp	Ank2

Nemy	CG11781	OtopLb	CG10598	CG33874	CG18557	Eip74EF
Fbp	Npc2g	Art6	Alp9	CG33882	CG8100	Br
Hn	Salt	Lcp65Ab2	CR45862	CG33886	Twz	CG8788
glob1	CG14688	Lcp65Ab1	28SrRNA-Psi:CR45859	CG33906	CG13403	CG4686
Fatp1	CG10953	CG34185	CG15126	CG33904	CG11029	Scp2
Mal-A4	CG9717	CG2574	CG14205	CG33910	Kni	PGRP-SC2
Indy	vanin-like	CG11052	CG5892	CG17949	CG43315	CG7720
CG2233	Fpps	CG14451	28SrRNA-Psi:CR45860	CG33872	Obp85a	Kr
CG9119	CG31775	CG30184	28SrRNA-Psi:CR40741	CG33878	CG33786	CG11563
Cyp4p1	CG42586	Ubc84D	CG14742	CG33884	Sardh	CG8661
CG7630	Fusl	CG32241	CG13228	CG33876	GstD10	Scamp
Pmp70	Cyp6a21	LysB	CG4269	CG33908	PGRP-SC1b	CG5767
CG8839	CG43349	Gpdh1	CG15296	Pfdn4	Br	lmgB
Ugt35A1	CG8664	ATPsynC	28SrRNA-Psi:CR41609	Sec61gamma	CG8661	CG4734
Efr	Dpy-30L1	**Q-Deseq2***	TrxT	Lcp65Ag1	Cyp309a1	CG4210
Pig1	CG34446	CG10505	Lcp65Af	Nero	CG34001	Lst
CG32603	Cyp28a5	MtnD	5.8SrRNA:CR40454	mt:ND3	lin-52	GstD9
Inos	CG5770	MtnE	5.8SrRNA-Psi:CR45854	CG18067	Cyp28a5	CG10361
Vha14-1	CG14957	CG2065	CG13325	CR45853	Cry	CG12926
cype	CG34215	Zip99C	CG42635	Phf5a	Scamp	Uck
FASN1	Galk	GstD4	CG42488	mRpL20	nAChRbeta3	LysD
UQCR-Q	ABCA	GstD2	primo-2	CR45855	CG5767	Pdgy
Sea	Cyp28d2	Fer1HCH	CG31050	Peritrophin-15a	CG8788	scramb2
CG7966	CG33099	galla-1	CG32457	CG17996	EndoU	Vrp1
CG9399	Npc2h	Ctr1B	Sdhaf3	CR41602	Scp2	AsnS
Jheh1	Cyp4d1	Fer2LCH	CG30033	Ssb-c31a	CG5770	AdenoK
Mlp60A	CG41128	Drip	CG43638	Tgy	Borr	Shop

COX8	AANATL6	CG16898	Drs	mRpL41	PGRP-LB	CG7970
Irp-1B	CG33267	MtnA	CG40813	HSPC300	LysD	Cf2
Roh	CG10621	CG6996	ATPsynepsilonL	CG32284	CROT	Bug22
mt:ND1	Alp10	CG31288	CG14120	CG44014	CG4686	Pxn
Gabat	CG3270	Arc2	CG32284	CG12730	CG12896	CG4306
QIL1	CG13066	Lcs	CG33669	CG13445	CG4734	fz2
Sfxn1-3	Ugt35C1	CG2064	CG4375	CR40454	AdenoK	CG34215
Argk	CG18747	CG8620	CG13445	CR45854	Kr	CG30457
CG42709	CG5506	CG33301	CG33552	CG14120	CG3690	CG4563
CG15083	CG9259	CG9759	CG12730	Sdhaf3	D	Spf45
TwdlP	CG10962	CG10474	Peritrophin-15a	ATPsynepsilonL	AsnS	Cat
Acbp2	Nepl10	Zip89B	CG43153	CR41609	Rab32	CG31705
ND-MWFE	Rift	Mal	Sdic4	CG13325	Eip74EF	CG3999
DnaJ-1	CG15741	Acp63F	Lcp65Ag3	TrxT	CG34222	CG11835
ND-MNLL	CG42562	CG7763	CG6870	Lcp65Af	Lst	CG1673
Men	CG6574	Rdog	HP6	HP6	CG12926	CG32248
Desat1	STUB1	CG14695	CG14036	CG13373	CG4884	CG5955
mRpL18	CG2187	GstD5	CG30447	CR40741	CG4210	Cpr78Cc
CG17508	CG13679	GstD8	CR41602	CG14205	scramb2	Nplp4
PGRP-SC2	Smvt	Qtzl	CR45855	CR45860	CG8750	CG13731
Jon99Fi	Acbp5	CG7720	mt:ND3	CG5892	CG5402	Lsp1beta
CG7778	CG15155	CG12868	CG4960	CG42488	CG7970	Fon
CG4830	CG8837	CG33986	CG17650	CR45859	PGRP-SC2	Muc68Ca
CG42837	CG9757	AOX1	CG42577	CG4982	Pcp	Act87E
CG31313	CG16704	Damm	CG32832	CR45862	CG34215	CG7465
Mpc1	Mvl	CG5550	CG14237	CG40813	Cat	Obp99c
Echs1	CG17167	Ugt37A3	CG4949	CG4269	Ank2	Lcp1
UK114	CG7860	GstE1	CG12126	CG15126	CG11563	Jon25Bi
Hph	CG32276	CG43204	CG44014	Lcp65Ag3	CG4563	Acbp5
CG12338	CG7968	Phu	Pex7	CG18179	Pdgy	Ldh
ATPsynC	Hsp68	Gadd45	mRpL41	CG15296	CG30457	CG7290

CG11752	Ugt301D1	Rev7	Tgy	CR45863	Pxn	Eglp4
LManVI	Pirk	Rpp21	Lcp65Ag1	CG13228	Cf2	CG32241
Gpdh1	Lcp2	CG8675	Ssb-c31a	Alp10	CG4306	Lcp9
CG7772	CG32073	GstD10	CG4982	CG42580	Shop	LysB
CG12896	GstT4	Cp110	CG31639	Drs	lmgB	CG10953
CG4968	CG31075	28SrRNA-Psi:CR45862	CG14327	CG13135	PpD6	CG11151
CG6834	Kr	CG7142	CR45853	CG13077	fz2	Idgf4
AcCoAS	CG13893	CG31694	CG9609	Alp9	CG31705	TpnC73F
CG9336	CG44242	Gcn5	CG9928	CG10598	Bug22	Ald1
LysB	Reg-2	CG12239	CG15124	CG5157	CG45154	Jon25Biii
PH4alphaPV	Pepck2	CG30495	Nero	CG30065	CG1673	Act57B
Cpr78Cc	CG9664	Mdr50	Odc1	Mtk	CG3999	Eno
CG3984	Mal-A6	CG6299	CG17996	CG13078	Vrp1	Gdh
heph	Ugt37B1	Ver	CG43237	CG3349	Cpr100A	CG11350
Yuri	Adh	CG42319	CG17580	CG14829	CG11835	Argk
LManV	CG34166	CG30062	CG16986	CG34040	Nplp4	**L-Common***
Sod3	Hsp26	CG31259	Sec61gamma	CG46026	Prp38	Fer2LCH
ssp7	Exu	CG7300	CG15375	CG34377	CG8320	Fer1HCH
CG43124	Fiz	CG14191	CG42580	CG10587	Spf45	Obp99b
Mondo	CG34330	CG31974	CG33868	CG43775	CG32248	CG10505
CG14818	CG1208	ETH	CG33870	Cpr72Eb	yellow-e	Lsp1gamma
Lamp1	alpha-Est2	CG14906	CG33872	BomS1	Cpr78Cc	CG17107
Mipp1	CG32751	CG10918	CG33874	Diedel2	EcR	Lsp1alpha
CG17059	Lcp1	MFS14	CG33876	CG42581	CG13731	Ctr1B
ATPsynE	CG11313	Snap25	CG33878	CG15368	Fon	CG45087
CG8560	CG17751	CG12171	CG33880	CG14086	Lsp1beta	CARPB
Aldh-III	CG10073	MtnB	CG33882	CG14069	Prx2540-2	CG14143
Lcp9	Srr	CG14237	CG33884	CG14631	CG5955	CG43816
PMP34	Cyp6g1	out	CG33886	CG12479	CG8475	CG42259
l(2)k09913	Alp9	Pym	CG33888	CG44476	Elal	CG31075

CG32241	CG32407	CG4607	CG33890	CG34169	Cindr	Lsp2
ABCD	CG18179	baf	CG33892	CG31230	DOR	LysE
Cyp6a23	CG11892	ZnT63C	CG33894	pre-mod(mdg4)-Z	CG42502	Acp95EF
CG34305	CG43114	28SrRNA-Psi:CR45859	CG33896	CG43982	CG10467	Cyt-b5-r
Ubc84D	smp-30	Mocs1	CG33898	CG13058	CG6415	CG14701
CG44774	CG13315	CG11710	CG33900	CG34298	CG5506	Zip89B
CG30184	CG42662	CG12766	CG33902	Os-C	Shmt	CG34166
CG14451	CG45087	Zip42C.2	CG33904	CG15480	CG1299	Def
Seipin	CG13230	GstD1	CG33906	CG43815	su(r)	CG14974
Aay	CG12493	Peritrophin-15a	CG33908	CG42716	CG5273	CG14851
CG11052	TotA	wun	CG33910	CG16964	Cyp9b2	CG7763
regucalcin	Mal-A8	CG6769	CG17949	Z600	Vsg	Edg78E
CG2574	CG17107	CG3704	CG34298	CG43237	Tis11	CG30108
ND-B14.5B	Cyp311a1	Pop1	mRpL20	CG14095	CG3603	CG15673
CG17752	Uro	CG7298	CG17195	CG14327	Act87E	Drip
CG34185	CG42819	CNT2	CG9877	CG15605	CG8534	Cpr65Au
Srp14	CG9928	CG15784	Phf5a	CG43221	Fus	Cpr49Ac
CG1544	CG13312	CG15638	CG34291	CG43230	Tsp42Ek	Mal-A1
Mdy	Lsp1beta	CG14292	Pfdn4	CG12995	CG2736	CG42807
CG17124	CG17134	Arc1	mt:ATPase8	pre-mod(mdg4)-U	Muc68Ca	CG4830
Lcp65Ab2	CG42486	CG43630	mRpL36	Sdic4	CG7465	CG8745
Lcp65Ab1	CG16727	CG10513	CG13067	pre-mod(mdg4)-L	Mur29B	CG10621
CG9527	CG13077	CG3224	CG13912	CG4960	Pgm2a	CG31089
Art6	CG34316	5.8SrRNA-Psi:CR45863	CR45861	CG17195	lectin-22C	CG32276
OtopLb	CG14219	sif	Lcp65Ae	CG34170	Fatp1	CG32249
Acbp6	CG5246	CG30054	CG32073	CG14659	Obp99c	CG16704

Eip71CD	CG5892	Alp7	Sun	pre-mod(mdg4)-H	Arl4	CG43773
CG4686	RpS19b	CG7339	Prc	CG17580	Reg-2	CG30423
OdsH	Mag	CG12963	Mvl	CG32457	CG13075	CG46244
Cyp9b2	Taf12L	Picot	CG9922	CG31050	Tsf1	CG18003
Tango2	CG32249	Mdr49	mt:ND4L	CG34204	Lcp1	Cpr49Ah
ND-B8	CG14205	CG14989	RpS14a	CG42635	Sf3b6	galla-1
AANATL2	Lsp1alpha	CG11417	CG5246	CG14742	CG4053	CG7953
Mst84Db	CG5157	CG10597	TwdlO	CG42577	How	Zip99C
CG33965	ninaD	Rbm13	CG34117	CG43271	PPO1	Cyp4d14
CG17633	CG31089	CG5645	CG18585	pre-mod(mdg4)-V	CG44243	CG8997
yip3	Fbp2	CG14995	CR33363	CG43137	Acbp5	CG30413
mfrn	CG13325	Ndg	Agpat2	pre-mod(mdg4)-W	Ldh	CG30380
CG8562	Lsp1gamma	CG1575	Z600	**L-Common**	CG9536	CG42455
Mur29B	Obp99b	CG13806	mRpL49	CG5157	Jon25Bi	CG11345
Fabp	CG30270	His1:CG33834	CG16985	CG13077	Pal1	CG42822
Axo	CG43168	Prip	CG31613	CR45863	CG13962	PPO2
mino	CG11588	CG6724	CG33803	CG30065	Rbp9	Cht4
Ndae1	Ubc84D	scf	CG33806	Alp10	CG13545	CG32603
CG9396	CG14451	Fib	CG33809	CG18179	CG32241	Jdp
CG18003	E(spl)m6-BFM	CG1671	CG33812	CG10598	CG7290	CG13403
CG6178	CG30184	mbm	CG33815	Alp9	Scaf	CG43315
Mgstl	CG16998	CG12825	CG33833	CR45862	Eglp4	Obp85a
CG42846	CG11052	betaggt-II	CG33836	CR45859	Mcad	CG33786
JhI-26	CG12679	CG12909	CG33839	CG15126	Reb	Sardh
CG13325	Cby	Jafrac1	CG33842	CG14205	Cht10	GstD10
Lcp3	CG11404	AnxB10	CG33845	CG5892	Irk1	Br
Drsl3	CG9875	puml	CG33848	CR45860	Npc2d	CG8661
LysE	CG34185	Gnmt	CG33851	CR40741	yip2	Cyp309a1
CG34426	SkpD	snRNP-U1-70K	CG33854	CG14742	Hui	Cyp28a5

CG6295	CG14070	su(w^{327})	CG33857	CG13228	Kcmf1	Cry
Ifc	CG2574	Nmd3	CG33860	CG4269	Fbp	Scamp
Oat	CG30099	Lfg	CG33863	CG15296	CG10184	nAChRbeta3
Ugt305A1	CG17375	CG3918	CG33866	CR41609	LysB	CG5767
CG7906	Drsl3	GstS1	CG14191	TrxT	CG11151	CG8788
CG6287	OdsH	CG11030	SNRPG	Lcp65Af	CG17271	EndoU
CG42764	CG7906	nop5	mt:ND2	CR40454	Arg	Scp2
CG34278	CG34253	obst-J	CG34169	CR45854	Lcp9	CG5770
Salt	CG15764	CG11672	CG4627	CG13325	CrebA	Borr
Ugt303A1	CG33704	CG9143	RNASEK	CG42635	Ben	PGRP-LB
Use1	CG8349	Trxr-1	SclA	CG42488	CG10953	LysD
Cyp310a1	ND-B8	Xrp1	eIF4E3	CG31050	Yip1d1	CROT
LysD	CG42460	GstE3	CG17734	CG32457	Osa	CG4686
Lcp65Ad	Reepl1	Usp16-45	CG10182	Sdhaf3	Pfk	CG12896
CG11781	CG12689	CG42806	Sod3	Drs	CG8547	CG4734
CG42807	Lcp65Ad	r-l	RpL18A	CG40813	CG31496	AdenoK
CG10184	CG13989	Ssrp	CG15255	ATPsynepsilonL	CG10910	Kr
spirit	Sfp65A	CG9877	CG13058	CG14120	CG9512	AsnS
CG9981	CG43077	CG17109	CG14631	CG32284	Cact	Rab32
Bet5	CG8197	MRP	mt:CoII	CG13445	betaCOP	Eip74EF
CG8665	CG5043	CG9205	Rbp1	CG12730	Idgf4	CG34222
Npc2d	Mst84Db	Dph5	CG1542	Peritrophin-15a	PAN3	Lst
CG7970	Sdic4	CG1703	CG13059	Sdic4	TpnC73F	CG12926
SecCl	CG15200	CG5867	CG14671	Lcp65Ag3	CG17597	CG4210
Fst	CG33463	ImpL2	mt:ND6	HP6	Tsp42Ec	scramb2
CG43349	CG14739	CG5162	Lcp65Ag2	CR41602	Obp44a	CG8750
CG13082	Art6	RpL22	Gs1l	CR45855	MFS3	CG7970
Acbp3	CG43071	CG4928	GstE9	mt:ND3	CG11313	PGRP-SC2
AANATL4	CG17105	Ahcy	mt:lrRNA	CG4960	CG3984	Pcp
Cyp6a21	CG42764	La	Membrin	CG42577	CG10939	CG34215
Fusl	Ocho	CNBP	RpS20	CG44014	Arm	Cat

CG34446	Sinah	CG43896	CG10570	mRpL41	Nmda1	Ank2
Cyt-c1L	pre-mod(mdg4)-L	**Q-edgeR***	mRpS6	Tgy	Ald1	CG11563
CG15706	Dic2	pre-mod(mdg4)-I	CG12868	Lcp65Ag1	Heph	CG4563
CG10953	VepD	CG12912	CG13319	Ssb-c31a	CG6910	Pdgy
CG9717	Mst84Da	pre-mod(mdg4)-O	CG5021	CG4982	Ubi-p5E	CG30457
CG15534	CG13380	CG43630	CG33818	CG14327	Lamp1	Pxn
CG14957	CG43210	CR34254	CG33821	CR45853	Exd	Cf2
CG11425	CG31230	CG15638	CG33824	Nero	Pdk	CG4306
Dpy-30L1	yip3	Drsl5	CG33827	CG17996	CG4962	Shop
CG33704	CG43449	CG30054	CG33830	CG43237	Larp	lmgB
CG42649	CG13599	E(spl)malpha-BFM	Spase12	CG17580	Act57B	PpD6
Cer	CG43348	CG13299	Mfrn	Sec61gamma	Sec24CD	fz2
Cyp4d1	CG31008	Zip42C.2	mt:srRNA	CG42580	CG7567	CG31705
Gk2	CG34178	CG10505	CG9921	CG33868	Peritrophin-A	Bug22
Npc2h	CG45086	MtnE	CG42806	CG33870	Eip55E	CG45154
CG8664	CG42500	CG2065	RpS21	CG33872	TRAM	CG1673
vanin-like	Lsp2	MtnB	SelG	CG33874	Got1	CG3999
sinah	CG13078	MtnD	mt:ND4	CG33876	26-29-p	Vrp1
Fpps	**Q-Common**	GstD4	RpL38	CG33878	Eno	CG11835
CG11151	CG13078	Zip99C	RpS14b	CG33880	Gdh	Nplp4
CG16926	ninaD	GstD2	Alp5	CG33882	Cher	Spf45
CG13679	CG14205	galla-1	CG1124	CG33884	Skeletor	CG32248
ABCA	CG5157	Fer1HCH	CG1532	CG33886	Mpcp1	Cpr78Cc
CG5770	CG16727	Ctr1B	CG31611	CG33888	CG10912	CG13731
Ugt302C1	CG34316	CG10474	CG33871	CG33890	CG18135	fon
CG14688	CG13077	Drip	CG33873	CG33892	Zasp66	Lsp1beta
Cyp28d2	CG5892	Fer2LCH	CG33875	CG33894	Idgf6	CG5955
CG33099	CG45087	CG16898	CG33883	CG33896	Roh	Act87E
CG2187	CG11892	Lcs	CG33885	CG33898	CtsB1	Muc68Ca
Alp10	CG13312	CG8620	CG33887	CG33900	CG13360	CG7465

CG33267	CG5246	CG9759	CG33889	CG33902	Tpi	Obp99c
CG18747	smp-30	MtnA	CG33901	CG33904	Zasp52	Lcp1
Cpr65Aw	CG42486	CG6996	CG33903	CG33906	OstDelta	Acbp5
Galk	CG13599	Arc2	CG33905	CG33908	CG11350	Ldh
Npc2g	CG45086	CG31288	CG33907	CG33910	Gel	Jon25Bi
CG8837	CG42819	CG33301	CG33909	CG17949	AdSS	CG32241
CG13989	CG18179	CG2064	CG15715	CG34298	CG1927	CG7290
CG9259	Srr	GstD5	Pfdn6	mRpL20	SdhB	Eglp4
CG31008	Lsp1gamma	mal	Rpp14a	CG17195	Argk	LysB
Ugt302E1	Alp9	GstD8	Est-6	CG9877	CG43897	CG11151
CG9928	CG14219	Zip89B	Ip259	Phf5a	Npc2g	Lcp9
Cyp6g1	CG31089	CG7763	UQCR-14	CG34291	Lig	CG10953
Nepl10	CG43449	rdog	CG9521	Pfdn4	Hmu	Idgf4
STUB1	CG32407	CG14695	CG7299	mt:ATPase8	GlyP	TpnC73F
CG12493	CG31230	CG12868	P32	mRpL36	CG10911	Ald1
Mal-A6	CG34330	Damm	CG31086	CG13067	CG1674	Act57B
Cyp28a5	Adh	Ugt37A3	CG12057	CG13912	CG4847	Eno
CG31775	CG17751	Gadd45	mRpL32	CR45861	Ubi-p63E	Gdh
CG42586	CG10073	CG7720	RnrS	Lcp65Ae	Echs1	CG11350
CG11842	RpS19b	CG7142	CG34330	CG32073	ND-75	Argk
CG31075	Mal-A8	CG5550	CG17931	Sun	Prosalpha2	
CG34039	CG32276	CR45862	CG33891	Prc	Gapdh2	
CG17107	Pepck2	CG32267	CG33893	Mvl	CG2233	
Ugt35C1	CG43114	CG42319	CG33895	CG9922	GCS2alpha	
CG15741	Ugt37B1	GstD10	CG33897	mt:ND4L	Gapdh1	
CG34215	CG34166	AOX1	CG33899	RpS14a	CG17826	
CG5506	CG32751	Gcn5	smt3	CG5246	Pax	
CG43175	CG43210	CG8675	CG13364	TwdlO	CG17896	
Mag	CG13315	CG4607	mRpL45	CG34117	Serp	
CG16965	Cyp311a1	GstE1	RpL36A	Agpat2	CG45076	
CG3270	CG44242	Mdr50	RpL27	Z600	**L-edgeR***	

Smvt	Hsp68	Pym	ND-24	CG16985	CG30380	
CG42662	CG1208	CG31259	Elm	CG31613	CG8750	
CG9664	Mvl	CG31694	ATPsynG	CG33803	CG30413	
CG10962	CG13893	CG7300	RpS30	CG33806	Edg78E	
CG10621	Reg-2	CG6299	Tom20	CG33809	Def	
CG15200	Acbp5	CG14191	CG15597	CG33812	pre-mod(mdg4)-O	
CG41128	Kr	out	Cys	CG33815	CG46244	
CG9757	GstT4	CG14237	CG12310	CG33833	CG5693	
CG11313	CG17167	baf	RpS18	CG33836	Obp85a	
CG15155	Pirk	28SrRNA-Psi:CR45859	RpL10	CG33839	CG34222	
CG42562	CG13380	CG31974	mRpS14	CG33842	CG17169	
CG7860	CG7968	CG11710	CG31618	CG33845	Cry	
CG16704	Taf12L	MFS14	CG33808	CG33848	CG34219	
Dic2	alpha-Est2	CG15784	CG33814	CG33851	CG45154	
CG13484	CG6574	CG14907	CG33817	CG33854	CG34323	
AANATL3	Fiz	CG12171	CG33820	CG33857	CG43308	
Ugt301D1	Ocho	Mocs1	CG33823	CG33860	PpD6	
TotA	Rift	wun	CG33826	CG33863	CG16741	
CG32073	CG32073	ZnT63C	CG33829	CG33866	CG42733	
Rift	TotA	CG6769	CG33832	SNRPG	CG14294	
CG14877	Ugt301D1	CG3704	CG33835	mt:ND2	BomBc1	
Ocho	Dic2	Peritrophin-15a	CG33838	CG34169	Him	
Yp3	CG16704	CNT2	CG33841	CG4627	robls54B	
Fiz	CG7860	GstD1	CG33844	RNASEK	CG34309	
CG6574	CG42562	CG7298	CG33847	eIF4E3	CG43083	
alpha-Est2	CG15155	CG7339	CG33850	CG17734	CG33919	
Taf12L	CG11313	Arc1	CG33862	RpL18A	CG42841	
Rca1	CG9757	CG14995	CG33865	CG15255	CG32712	
CG7968	CG41128	Jafrac1	RpL22	CG13058	Obp22a	
CG13380	CG15200	**Q-Common***	RpS25	CG14631	Trk	

Pirk	CG10621	CG10505	ND-B18	mt:CoII	CG17105	
CG17167	CG10962	MtnD	Pst	mt:ND6	Lsp2	
GstT4	CG9664	MtnE	ND-AGGG	mt:lrRNA	Lsp1gamma	
Kr	CG42662	CG2065	RpL29	RpS20	CG34166	
Acbp5	Smvt	Zip99C	RpL35	mt:srRNA	Acp95EF	
Reg-2	CG3270	GstD4	RpL10Ab	RpS21	Fer2LCH	
CG13893	Mag	GstD2	CG32633	mt:ND4	Obp99b	
Mvl	CG5506	Fer1HCH	CG15308	RpS14b	CG14974	
CG1208	CG34215	galla-1	RpL11	CG7299	Fbp2	
Hsp68	CG15741	Ctr1B	RpS27A	RpL36A	CG43816	
CG44242	Ugt35C1	Fer2LCH	RpS26	RpL27	Amy-p	
Cyp311a1	CG17107	Drip	**L-edgeR**	RpS30	CG10505	
CG13315	CG31075	CG16898	RpL22	CG15597	Fer1HCH	
CG43210	CG31775	MtnA	RpL10	CG12310	CG17107	
CG32751	CG42586	CG6996	RpS18	RpS18	CG14143	
CG34166	Cyp28a5	CG31288	CG12310	RpL10	CG8093	
Ugt37B1	Mal-A6	Arc2	CG15597	RpL22	CG17362	
CG43114	CG12493	Lcs	RpS30	**L-Deseq2***	Amy-d	
Pepck2	STUB1	CG2064	RpL27	Fer2LCH	CG14851	
CG7685	Nepl10	CG8620	RpL36A	Fer1HCH	MtnB	
CG32276	Cyp6g1	CG33301	CG7299	Obp99b	Lsp1alpha	
Mal-A8	CG9928	CG9759	RpS14b	CG10505	Cpr65Au	
CG13123	CG31008	CG10474	mt:ND4	Lsp1gamma	CG14701	
RpS19b	CG9259	Zip89B	mt:srRNA	CG17107	Ctr1B	
CG10073	CG13989	Mal	RpS21	Lsp1alpha	CG6277	
CG17751	CG8837	CG7763	RpS20	Ctr1B	Amyrel	
Adh	Npc2g	Rdog	mt:lrRNA	CG45087	CG45087	
CG34330	Galk	CG14695	mt:CoII	CARPB	Cpr49Ac	
CG31230	CG18747	GstD5	RpL18A	CG14143	CG42259	
CG10560	CG33267	GstD8	mt:ND6	CG43816	CARPB	
CG32407	Alp10	CG7720	CG15255	CG42259	CG8087	

CG43449	CG2187	CG12868	RNASEK	CG31075	CG30108	
CG31089	CG33099	AOX1	CG17734	Lsp2	Cht4	
CG14219	Cyp28d2	Damm	mt:ND2	LysE	CG43773	
Alp9	CG14688	CG5550	RpS14a	Acp95EF	CG30091	

[A] DEGs of each group are separated by gray cells in the table. Q- and L- stand for quick and late analysis and asterisk represents FAC-upregulated analysis.

Table 4. 7 Gene ontology analysis of media analysis-of BRGC, gut and WB.

Medium	Tissue	GO Category[A]	GO-Term[B]	REF[C]	List[D]	P-value[E]
FAC-upregulated	BRGC	BP	response to unfolded protein	26	7	2.55E-15
			cellular response to unfolded protein	26	7	2.55E-15
			cellular response to topologically incorrect protein	38	7	2.69E-14
			response to topologically incorrect protein	38	7	2.69E-14
			protein folding	76	7	2.41E-12
		MF	heat shock protein binding	24	7	1.57E-15
			ATP binding	25	7	2.01E-15
			unfolded protein binding	47	7	1.05E-13
			drug binding	69	7	1.28E-12
			purine ribonucleoside triphosphate binding	74	7	2.02E-12
		CC	Cytosol	409	8	6.78E-09
			plasma membrane	1264	8	3.34E-05
			cell periphery	1292	8	3.92E-05
			Membrane	1501	8	1.15E-04
			cytoplasmic part	1570	8	1.59E-04
	Gut	BP	cellular iron ion homeostasis	5	2	4.61E-05
			iron ion homeostasis	7	2	7.89E-05
			cellular transition metal ion homeostasis	14	4	1.20E-08
			transition metal ion homeostasis	16	4	1.89E-08
			zinc ion transport	10	2	1.44E-04

		MF	ferrous iron binding	5	2	4.61E-05
		CC	-			
	WB	BP	cellular iron ion homeostasis	5	2	1.72E-05
			iron ion homeostasis	7	2	2.94E-05
			cellular transition metal ion homeostasis	14	4	1.44E-09
			transition metal ion homeostasis	16	4	2.28E-09
			maintenance of location	21	2	2.05E-04
		MF	ferrous iron binding	5	2	1.72E-05
			iron ion binding	14	2	9.77E-05
		CC	-			
BPS-upregulated	BRGC	BP	chitin metabolic process	121	16	1.23E-23
			glucosamine-containing compound metabolic process	131	16	3.99E-23
			amino sugar metabolic process	135	16	6.25E-23
			aminoglycan metabolic process	146	16	2.01E-22
			drug metabolic process	265	16	1.61E-18
		MF	structural constituent of peritrophic membrane	2	2	3.73E-05
			chitin binding	126	16	2.24E-23
			drug binding	833	16	4.84E-11
			carbohydrate derivative binding	1008	16	7.82E-10
		CC	extracellular region	1215	17	1.23E-09
			Intracellular	6220	4	2.62E-05
			intracellular organelle	5104	2	2.92E-05
			Organelle	5285	2	1.47E-05
	Gut	BP	-			
		MF	-			
		CC	-			
	WB	BP	-			
		MF	tetrapyrrole binding	15	2	3.99E-05
			heme binding	15	2	3.99E-05
		CC	-			

[A] BP, MF, and CC indicate enriched Biological Process, Molecular Function, and Cellular Component groups in the GO Category.

[B] GO terms of the panther GO-slim analysis.

[C] REF is the number of genes within the *Drosophila* Reference genome.

[D] List represents the number of genes within the given query list.

[E] P-value represents the statistical significance of the GO terms (P-value < 0.05).

Table 4. 8 Gene ontology analysis of time course FAC upregulated BRGC genes

Medium	Tissue	GO Category[A]	GO-Term[B]	REF[C]	List[D]	P-value[E]
Deseq2	Quick	BP	-			
		MF	-			
		CC	-			
	Late	BP	chaperone-mediated protein folding	25	11	1.38E-11
			proteasome assembly	7	3	5.64E-04
			protein stabilization	7	3	5.64E-04
			response to unfolded protein	26	9	5.79E-09
			cellular response to unfolded protein	26	9	5.79E-09
		MF	heat shock protein binding	24	11	9.75E-12
			ATP binding	25	10	2.55E-10
			snoRNA binding	14	5	1.43E-05
			unfolded protein binding	47	15	1.12E-13
			purine ribonucleoside triphosphate binding	74	14	3.12E-10
		CC	chaperonin-containing T-complex	6	5	6.36E-07
			preribosome, large subunit precursor	20	9	8.99E-10
			small nucleolar ribonucleoprotein complex	12	5	7.82E-06
			preribosome, small subunit precursor	8	3	7.65E-04
			mitochondrial large ribosomal subunit	17	5	3.10E-05
edgeR	Quick	BP	-			
		MF	-			
		CC	-			

	Late	BP	chaperone-mediated protein folding	25	7	2.96E-14
			response to unfolded protein	26	7	3.76E-14
			cellular response to unfolded protein	26	7	3.76E-14
			cellular response to topologically incorrect protein	38	7	3.95E-13
			response to topologically incorrect protein	38	7	3.95E-13
		MF	heat shock protein binding	24	7	2.32E-14
			ATP binding	25	7	2.96E-14
			unfolded protein binding	47	7	1.53E-12
			drug binding	69	7	1.85E-11
			purine ribonucleoside triphosphate binding	74	7	2.92E-11
		CC	Cytosol	409	8	1.43E-07
Common	Quick	BP	-			
		MF	-			
		CC	-			
	Late	BP	chaperone-mediated protein folding	25	7	3.04E-16
			response to unfolded protein	26	7	3.86E-16
			cellular response to unfolded protein	26	7	3.86E-16
			cellular response to topologically incorrect protein	38	7	4.08E-15
			response to topologically incorrect protein	38	7	4.08E-15
		MF	heat shock protein binding	24	7	2.38E-16
			ATP binding	25	7	3.04E-16
			unfolded protein binding	47	7	1.59E-14
			drug binding	69	7	1.94E-13
			purine ribonucleoside triphosphate binding	74	7	3.08E-13
		CC	Cytosol	409	8	7.36E-10
			cytoplasmic part	1570	9	1.54E-06
			plasma membrane	1264	7	5.78E-05
			cell periphery	1292	7	6.66E-05
			Membrane	1501	7	1.74E-04

[A] BP, MF, and CC indicate enriched Biological Process, Molecular Function, and Cellular Component groups in the GO Category.

[B] GO terms of the panther GO-slim analysis.

[C] REF is the number of genes within the *Drosophila* Reference genome.

[D] List represents the number of genes within the given query list.

[E] P-value represents the statistical significance of the GO terms (P-value < 0.05).

Table 4. 9 Gene ontology analysis of time course BPS upregulated BRGC genes

Medium	Tissue	GO Category[A]	GO-Term[B]	REF[C]	List[D]	P-value[E]
Deseq2	Quick	BP	chaperone-mediated protein folding	25	3	0.00000269
			response to unfolded protein	26	3	2.99E-06
			cellular response to unfolded protein	26	3	2.99E-06
			cellular response to topologically incorrect protein	38	3	8.67E-06
			response to topologically incorrect protein	38	3	8.67E-06
		MF	heat shock protein binding	24	3	2.40E-06
			ATP binding	25	3	2.69E-06
			unfolded protein binding	47	3	1.59E-05
			drug binding	69	3	4.76E-05
			purine ribonucleoside triphosphate binding	74	3	5.82E-05
		CC	-			
	Late	BP	-			
		MF	-			
		CC	cellular_component	4618	20	2.07E-05
			cell part	4195	16	7.61E-06
			Cell	4195	16	7.61E-06
			intracellular part	3599	13	3.00E-05
			Intracellular	3607	13	3.03E-05
edgeR	Quick	BP	chaperone-mediated protein folding	25	3	3.35E-06

			response to unfolded protein	26	3	3.74E-06
			cellular response to unfolded protein	26	3	3.74E-06
			cellular response to topologically incorrect protein	38	3	1.08E-05
			response to topologically incorrect protein	38	3	1.08E-05
		MF	heat shock protein binding	24	3	2.99E-06
			ATP binding	25	3	3.35E-06
			unfolded protein binding	47	3	1.98E-05
			drug binding	69	3	5.93E-05
			purine ribonucleoside triphosphate binding	74	3	7.25E-05
		CC	-			
	Late	BP	DNA catabolic process, endonucleolytic	11	3	5.86E-04
			execution phase of apoptosis	12	3	7.26E-04
			organic substance metabolic process	2561	14	2.98E-04
			metabolic process	2645	14	1.11E-04
			nitrogen compound metabolic process	2298	12	3.68E-04
		MF	single-stranded DNA endodeoxyribonuclease activity	10	3	4.65E-04
			galactosyltransferase activity	11	3	5.86E-04
			serine-type endopeptidase activity	139	11	2.19E-06
			serine hydrolase activity	144	11	3.02E-06
			hydrolase activity, acting on acid phosphorus-nitrogen bonds	144	11	3.02E-06
		CC	cellular component	4618	21	3.93E-10
			cytoplasmic part	1570	7	1.39E-03
			Cytoplasm	2236	8	7.30E-06
			intracellular organelle part	1510	5	2.57E-04
			organelle part	1535	5	1.77E-04
Common	Quick	BP	chaperone-mediated protein folding	25	3	8.91E-07
			response to unfolded protein	26	3	9.93E-07

			cellular response to unfolded protein	26	3	9.93E-07
			cellular response to topologically incorrect protein	38	3	2.88E-06
			response to topologically incorrect protein	38	3	2.88E-06
		MF	heat shock protein binding	24	3	7.96E-07
			ATP binding	25	3	8.91E-07
			unfolded protein binding	47	3	5.29E-06
			drug binding	69	3	1.59E-05
			purine ribonucleoside triphosphate binding	74	3	1.95E-05
		CC	-			
	Late	BP	-			
		MF	-			
		CC	-			

[A] BP, MF, and CC indicate enriched Biological Process, Molecular Function, and Cellular Component groups in the GO Category.

[B] GO terms of the panther GO-slim analysis.

[C] REF is the number of genes within the *Drosophila* Reference genome.

[D] List represents the number of genes within the given query list.

[E] P-value represents the statistical significance of the GO terms (P-value < 0.05).

Table 4. 10 Gene ontology analysis of time course FAC upregulated gut genes.

Medium	Tissue	GO Category[A]	GO-Term[B]	REF[C]	List[D]	P-value[E]
Deseq2	Quick	BP	zinc ion transport	10	4	7.21E-05
			response to ionizing radiation	8	3	7.30E-04
			glutathione metabolic process	37	12	2.41E-11
			cellular transition metal ion homeostasis	14	4	2.09E-04
			transition metal ion homeostasis	16	4	3.22E-04
		MF	snoRNA binding	14	8	1.65E-09
			telomeric DNA binding	7	3	5.37E-04
			transferase activity, transferring alkyl or aryl (other than methyl) groups	42	12	8.33E-11
			ATPase-coupled transmembrane transporter activity	76	7	5.29E-04
			primary active transmembrane transporter activity	77	7	5.69E-04
		CC	Pwp2p-containing subcomplex of 90S preribosome	6	4	1.60E-05
			small-subunit processome	34	17	4.32E-18
			small nucleolar ribonucleoprotein complex	12	5	7.23E-06
			t-UTP complex	45	18	1.02E-17
			preribosome, small subunit precursor	8	3	7.30E-04
	Late	BP	cellular transition metal ion homeostasis	14	4	7.25E-05
			transition metal ion homeostasis	16	4	1.13E-04
			cellular macromolecule metabolic process	1595	4	5.73E-06
			regulation of biological process	1384	3	1.46E-05
			regulation of cellular process	1300	2	7.22E-06
		MF	-			
		CC	-			
edgeR	Quick	BP	zinc ion transport	10	4	1.77E-05
			glutathione metabolic process	37	12	3.41E-13
			cellular transition metal ion homeostasis	14	4	5.20E-05
			transition metal ion homeostasis	16	4	8.08E-05
			transition metal ion transport	16	4	8.08E-05

		MF	telomeric DNA binding	7	3	1.87E-04
			transferase activity, transferring alkyl or aryl (other than methyl) groups	42	12	1.21E-12
			ATPase-coupled transmembrane transporter activity	76	6	4.31E-04
			primary active transmembrane transporter activity	77	6	4.60E-04
			transmembrane transporter activity	376	14	2.36E-04
		CC	-			
	Late	BP	zinc ion transport	10	3	1.99E-04
			cellular transition metal ion homeostasis	14	4	1.84E-05
			transition metal ion homeostasis	16	4	2.87E-05
			Unclassified	9426	106	1.61E-04
			biological process	4355	21	1.61E-04
		MF	-			
		CC	cellular component	4618	22	6.26E-05
			cell part	4195	17	1.03E-05
			Cell	4195	17	1.03E-05
			intracellular part	3599	11	1.18E-06
			Intracellular	3607	11	1.17E-06
Common	Quick	BP	zinc ion transport	10	4	8.33E-06
			glutathione metabolic process	37	11	9.27E-13
			cellular transition metal ion homeostasis	14	4	2.47E-05
			transition metal ion homeostasis	16	4	3.85E-05
			transition metal ion transport	16	4	3.85E-05
		MF	telomeric DNA binding	7	3	1.06E-04
			transferase activity, transferring alkyl or aryl (other than methyl) groups	42	11	3.00E-12
			ATPase-coupled transmembrane transporter activity	76	6	1.55E-04
			primary active transmembrane transporter activity	77	6	1.65E-04
			active transmembrane transporter activity	142	7	6.75E-04
		CC	Preribosome	67	6	8.08E-05
	Late	BP	zinc ion transport	10	3	5.27E-05
			cellular transition metal ion homeostasis	14	4	3.11E-06

			transition metal ion homeostasis	16	4	4.88E-06
		MF	-			
		CC	intracellular part	3599	7	1.15E-04
			Intracellular	3607	7	1.14E-04
			intracellular membrane-bounded organelle	2469	2	3.11E-05
			membrane-bounded organelle	2477	2	3.09E-05
			intracellular organelle	2824	2	4.74E-06

[A] BP, MF, and CC indicate enriched Biological Process, Molecular Function, and Cellular Component groups in the GO Category.

[B] GO terms of the panther GO-slim analysis.

[C] REF is the number of genes within the *Drosophila* Reference genome.

[D] List represents the number of genes within the given query list.

[E] P-value represents the statistical significance of the GO terms (P-value < 0.05).

Table 4. 11 Gene ontology analysis of time course BPS upregulated gut genes.

Medium	Tissue	GO Category[A]	GO-Term[B]	REF[C]	List[D]	P-value[E]
Deseq2	Quick	BP	lipid homeostasis	13	7	5.92E-04
			fatty acid catabolic process	22	11	2.78E-05
			cellular lipid catabolic process	37	13	1.00E-04
			carboxylic acid catabolic process	49	16	3.41E-05
			organic acid catabolic process	49	16	3.41E-05
		MF	flavin adenine dinucleotide binding	16	9	7.56E-05
			electron transfer activity	24	9	8.01E-04
			cofactor binding	74	23	1.42E-06
			oxidoreductase activity, acting on the CH-OH group of donors, NAD or NADP as acceptor	51	13	1.31E-03
			proton transmembrane transporter activity	51	13	1.31E-03
		CC	mitochondrial inner membrane	110	23	3.09E-04
			organelle inner membrane	111	23	5.17E-04
			Mitochondrion	307	57	5.91E-07
			cytoplasmic part	1570	191	3.13E-06
			Cytoplasm	2236	266	1.00E-07
	Late	BP	-			
		MF	catalytic activity	2345	79	1.13E-05
		CC	-			
edgeR	Quick	BP	-			
		MF	oxidoreductase activity	260	22	3.12E-05
		CC	-			
	Late	BP	chaperone-mediated protein folding	25	7	2.09E-10
			response to unfolded protein	26	7	2.64E-10
			cellular response to unfolded protein	26	7	2.64E-10
			cellular response to topologically incorrect protein	38	7	2.67E-09
			response to topologically incorrect protein	38	7	2.67E-09
		MF	heat shock protein binding	24	7	1.64E-10

			ATP binding	25	7	2.09E-10
			unfolded protein binding	47	7	1.00E-08
			drug binding	69	7	1.13E-07
			purine ribonucleoside triphosphate binding	74	7	1.77E-07
		CC	-			
Common	Quick	BP	-			
		MF	oxidoreductase activity	260	22	1.56E-05
		CC	-			
	Late	BP	-			
		MF	-			
		CC	-			

[A] BP, MF, and CC indicate enriched Biological Process, Molecular Function, and Cellular Component groups in the GO Category.

[B] GO terms of the panther GO-slim analysis.

[C] REF is the number of genes within the *Drosophila* Reference genome.

[D] List represents the number of genes within the given query list.

[E] P-value represents the statistical significance of the GO terms (P-value < 0.05).

Table 4. 12 Gene ontology analysis of time course FAC upregulated WB genes

Medium	Tissue	GO Category[A]	GO-Term[B]	REF[C]	List[D]	P-value[E]
Deseq2	Quick	BP	zinc ion transport	10	3	3.49E-04
			cellular transition metal ion homeostasis	14	4	3.89E-05
			transition metal ion homeostasis	16	4	6.05E-05
			glutathione metabolic process	37	9	1.51E-09
			cellular modified amino acid metabolic process	59	11	2.59E-10
		MF	transferase activity, transferring alkyl or aryl (other than methyl) groups	42	10	2.15E-10
		CC	small nucleolar ribonucleoprotein complex	12	3	5.46E-04
			preribosome, large subunit precursor	20	4	1.28E-04
			Preribosome	67	9	1.47E-07
			t-UTP complex	45	6	1.97E-05
			nucleolar part	61	8	8.76E-07
	Late	BP	alpha-amino acid metabolic process	51	10	5.90E-07
			carboxylic acid catabolic process	49	9	3.51E-06
			organic acid catabolic process	49	9	3.51E-06
			small molecule catabolic process	86	13	1.79E-07
			cellular amino acid metabolic process	91	10	5.92E-05
		MF	drug binding	69	9	4.14E-05
		CC	-			
edgeR	Quick	BP	zinc ion transport	10	3	5.67E-05
			cellular transition metal ion homeostasis	14	4	3.43E-06
			transition metal ion homeostasis	16	4	5.38E-06
			glutathione metabolic process	37	7	6.83E-09
			transition metal ion transport	16	3	1.87E-04
		MF	transferase activity, transferring alkyl or aryl (other than methyl) groups	42	7	1.49E-08

		CC	-			
	Late	BP	cellular transition metal ion homeostasis	14	4	7.56E-05
			transition metal ion homeostasis	16	4	1.17E-04
			alpha-amino acid metabolic process	51	6	9.73E-05
			macromolecule metabolic process	2043	8	1.20E-05
			cellular macromolecule metabolic process	1595	6	9.75E-05
		MF	-			
		CC	intracellular part	3599	28	6.45E-04
			Intracellular	3607	28	6.45E-04
			cellular_component	4618	35	2.48E-05
			cell part	4195	31	4.49E-05
			Cell	4195	31	4.49E-05
Common	Quick	BP	zinc ion transport	10	3	4.36E-05
			cellular transition metal ion homeostasis	14	4	2.41E-06
			transition metal ion homeostasis	16	4	3.79E-06
			glutathione metabolic process	37	7	3.67E-09
			transition metal ion transport	16	3	1.44E-04
		MF	transferase activity, transferring alkyl or aryl (other than methyl) groups	42	7	8.04E-09
			transporter activity	416	10	1.06E-04
			transmembrane transporter activity	376	9	2.47E-04
		CC	-			
	Late	BP	cellular transition metal ion homeostasis	14	4	3.25E-05
			transition metal ion homeostasis	16	4	5.06E-05
			alpha-amino acid metabolic process	51	6	2.91E-05
		MF	-			
		CC	-			

[A] BP, MF, and CC indicate enriched Biological Process, Molecular Function, and Cellular Component groups in the GO Category.

[B] GO terms of the panther GO-slim analysis.

[C] REF is the number of genes within the *Drosophila* Reference genome.

[D] List represents the number of genes within the given query list.

[E] P-value represents the statistical significance of the GO terms (P-value < 0.05).

Table 4. 13 Gene ontology analysis of time course BPS upregulated WB genes

Medium	Tissue	GO Category[A]	GO-Term[B]	REF[C]	List[D]	P-value[E]
Deseq2	Quick	BP	triglyceride metabolic process	11	4	4.65E-04
			acylglycerol metabolic process	16	5	1.57E-04
			neutral lipid metabolic process	16	5	1.57E-04
			carbohydrate biosynthetic process	17	5	1.99E-04
			lipid localization	39	6	9.59E-04
		MF	oxidoreductase activity	260	23	1.12E-06
		CC	respiratory chain complex	35	7	8.61E-05
			Respirasome	38	7	1.36E-04
			oxidoreductase complex	33	6	4.37E-04
			mitochondrial respirasome	33	6	4.37E-04
			inner mitochondrial membrane protein complex	67	9	1.37E-04
	Late	BP	ribosomal large subunit biogenesis	55	7	1.95E-05
			ribosome biogenesis	170	12	6.82E-06
			ribonucleoprotein complex biogenesis	217	12	6.68E-05
		MF	structural constituent of ribosome	111	19	1.02E-14
			structural molecule activity	143	19	6.12E-13
		CC	cytosolic small ribosomal subunit	37	7	1.86E-06
			cytosolic ribosome	82	15	3.13E-12
			cytosolic large ribosomal subunit	45	8	5.10E-07
			mitochondrial large ribosomal subunit	17	3	2.34E-03
			small ribosomal subunit	52	9	1.19E-07
edgeR	Quick	BP	biological process	4355	37	2.57E-06

			cellular metabolic process	2431	19	3.87E-04
			cellular process	3571	26	1.23E-06
			nitrogen compound metabolic process	2298	14	1.68E-05
			macromolecule metabolic process	2043	10	3.67E-06
		MF	-			
		CC	intracellular part	3599	36	1.64E-03
			Intracellular	3607	36	1.29E-03
			cell part	4195	39	6.57E-05
			Cell	4195	39	6.57E-05
			cellular component	4618	42	7.71E-06
	Late	BP	-			
		MF	structural constituent of ribosome	111	10	3.28E-07
			structural molecule activity	143	10	2.85E-06
		CC	cytosolic small ribosomal subunit	37	5	5.64E-05
			small ribosomal subunit	52	6	2.26E-05
			cytosolic ribosome	82	9	2.80E-07
			ribosomal subunit	118	12	5.92E-09
			Ribosome	131	12	1.75E-08
Common	Quick	BP	biological process	4355	32	4.05E-04
			cellular process	3571	22	8.17E-05
			nitrogen compound metabolic process	2298	11	2.09E-04
			macromolecule metabolic process	2043	8	6.29E-05
			biological regulation	1573	4	3.59E-05
		MF	-			
		CC	cellular component	4618	35	4.92E-04
			intracellular organelle	2824	17	6.48E-04
			Organelle	2852	17	4.77E-04
			protein-containing complex	1582	6	5.15E-04
			intracellular organelle part	1510	5	2.50E-04
	Late	BP	-			
		MF	structural constituent of ribosome	111	10	1.88E-08

			structural molecule activity	143	10	1.76E-07
		CC	cytosolic small ribosomal subunit	37	5	1.33E-05
			small ribosomal subunit	52	6	4.03E-06
			cytosolic ribosome	82	9	2.08E-08
			ribosomal subunit	118	12	1.80E-10
			Ribosome	131	12	5.48E-10

[A] BP, MF, and CC indicate enriched Biological Process, Molecular Function, and Cellular Component groups in the GO Category.

[B] GO terms of the panther GO-slim analysis.

[C] REF is the number of genes within the *Drosophila* Reference genome.

[D] List represents the number of genes within the given query list.

[E] P-value represents the statistical significance of the GO terms (P-value < 0.05).

Table 4. 14 HHpred analysis of BRGC media analysis genes.

Analysis	Symbol	Name	Organism	Probability[A]
Deseq2 BPS-upregulated	CG17028	Inositol monophosphatase 2	Homo sapiens	100
	dmGlut	Solute carrier family 39, Iron-regulated(iron transporter ferroportin)	Bdellovibrio bacteriovorus	100
	GstE6	Glutathione S-transferase theta-2	Homo sapiens	99.95
	Ugt302K1	nitrogenase iron protein, iron-sulfur cluster, Oxidoreductase	Clostridium pasteurianum	68.4
edgeR BPS-upregulated	Cda9	Low-density lipoprotein receptor-related protein 5	Melipona quadrifasciata	100
	Mco4	Iron transport multicopper oxidase FET3, multicopper oxidase, Oxidoreductase	Saccharomyces cerevisiae	100
	Kaz-m1	Follistatin: Inhibin beta A chain	Homo sapiens	99.65
	CG14273	uPAR, Urokinase plasminogen activator surface receptor	Homo sapiens	95.72
	CG6933	CHIT1 - Chitotriosidase-1	Homo sapiens	95.24
	CG43896	Beta-nerve growth factor	Homo sapiens	94.8
	CG6244	Rubredoxins, electron-transfer, iron-sulfur proteins	Desulfovibrio desulfuricans	87.17
	CG7567	Nup155, Nuclear pore complex protein	Homo sapiens	76.05
	Dup99B	Cytochrome C, Cppper chaperone	Thioalkalivibrio paradoxus	74.89
	Peritrophin-15a	Cytochrome C, Cppper chaperone, multicopper oxidase	Pseudomonas fluorescens	49.47
	CG12934	Prostaglandin-H2 D-isomerase	Homo sapiens	49.19
	CG10405	CopC, metallochaperone, copper binding	Pseudomonas fluorescens	48.13
	CG10725	CopC, metallochaperone, copper binding	Pseudomonas fluorescens	47.53
	CG13912	BLM helicase, hydrolase	Homo sapiens	44.79
	Peritrophin-15b	Cytochrome C, Cppper chaperone, multicopper oxidase	Thioalkalivibrio paradoxus	42.27

	CG10154	CopC, metallochaperone, copper binding	Pseudomonas fluorescens	37.35
	CG7715	Putative hemin ABC transport system; metal-binding	Burkholderia cenocepacia	36.65
	Muc96D	Cytochrome C, Cppper chaperone, multicopper oxidase	Thioalkalivibrio paradoxus	36.07
	CG14300	Cytochrome C, Copper Chaperone	Thioalkalivibrio paradoxus	33.3
	CG11470	LTP1, Lipid transport, oxidoreductase	Saccharomyces cerevisiae	32.03
	CG33986	Cytochrome C, Copper Chaperone	Thioalkalivibrio paradoxus	31.72
	obst-J	CopC, metallochaperone, copper binding	Pseudomonas fluorescens	31.71
	obst-I	CopC, metallochaperone, copper binding	Pseudomonas fluorescens	29.67
	CG33272	CopC, metallochaperone, copper binding	Pseudomonas fluorescens	29.05
	CG7017	Cytochrome C, Cppper chaperone	Thioalkalivibrio paradoxus	27.65
	CheB93b	Glycoside Hydrolase Family 61, metal binding site	Phanerochaete chrysosporium	27.2
	CG17826	CopC, metallochaperone, copper binding	Pseudomonas fluorescens	26.31
	CG32302	CopC, metallochaperone, copper binding	Pseudomonas fluorescens	24.3
	CG5084	Cytochrome C, Copper Chaperone	Thioalkalivibrio paradoxus	22.72
	Ag5r	CopC, metallochaperone, copper binding	Pseudomonas fluorescens	21.54
	CG10140	CopC, metallochaperone, copper binding	Pseudomonas fluorescens	20.76
	CG6295	Lipoprotein lipase, Lipase	Homo sapiens	100

Deseq2 FAC-upregulated	Rpt3	TP-dependent zinc metalloprotease FtsH, zinc metalloprotease	Homo sapiens	99.81
edgeR FAC-upregulated	CG33128	Cathepsin D, Beta Amyloid Cleaving;	Rattus norvegicus	100
	Hsp26	Heat shock protein beta-1; Molecular Chaperone	Homo sapiens	99.79
	lectin-22C	Lectin, Metalloprotein	Rattus norvegicus	99.78
	Gr58b	Odorant receptor,Ion channel	Apocrypta bakeri	99.75
	CG13721	CopC, metallochaperone, copper binding	Pseudomonas fluorescens	53.05
	CG14095	extracellular globin-3, Hemoglobin Chain D1, Transport protein	Lumbricus terrestris	6.46
Common FAC-upregulated	Hsp68	Hsp70, heat shock related 70 KAD protein	Homo sapiens	100
	Hsp70Ba	Hsp70, heat shock related 70 KAD protein	Homo sapiens	100
	Hsp70Bc	Hsp70, heat shock related 70 KAD protein	Homo sapiens	100
	Hsp70Aa	Hsp70, heat shock related 70 KAD protein	Homo sapiens	100
	Hsp70Ab	Hsp70, heat shock related 70 KAD protein	Homo sapiens	100
	Hsp70Bbb	Hsp70, heat shock related 70 KAD protein	Homo sapiens	100
	Hsp22	Low molecular weight heat shock	Xylella fastidiosa	99.71

[A] Probability indicates relevant representations of significance of identified hit (Probability > 50 considered as a true positive hit).

Table 4. 15 HHpred analysis of gut media analysis genes.

Analysis	Symbol	Name	Organism	Probability[A]
Deseq2 BPS-upregulated	Sod3	Superoxide dismutase, oxidoreductase	Homo sapiens	100
	yellow-k	NHLRC2, NHL repeat-containing protein 2	Homo sapiens	99.34
	CG43799	Apolipoprotein C-I, lipoprotein	Homo sapiens	88.89
	CG13454	GTP Cyclohydrolase I	Listeria monocytogenes	66.72
	CG14626	Polyamine-modulated factor	Homo sapiens	57.56
	Desi	Microplusin preprotein, Antimicrobial peptide	Rhipicephalus microplus	44.3
	CG33474	Potential Copper transporting ATPase	Oryctolagus cuniculus	35.82
edgeR BPS-upregulated	Ugt37a1	Sterol 3-beta-glucosyltransferase	Saccharomyces cerevisiae	99.94
	CG14014	CAAT/enhancer-binding protein beta, MYB,Transciption Factor DNA Methylation	Homo sapiens	96.27
	IM4	Cytochrome C, Copper Chaperone	Thioalkalivibrio paradoxus	94.56
	pre-mod(mdg4)-Z	Iron-regulated transcriptional activator AFT2, transcription factor	Saccharomyces cerevisiae	89.76
	pre-mod(mdg4)-I	Iron-regulated transcriptional activator AFT2, transcription factor	Saccharomyces cerevisiae	86.75
	pre-mod(mdg4)-V	Iron-regulated transcriptional activator AFT2, transcription factor	Saccharomyces cerevisiae	74.16
	CG44040	laccase, multicopper oxidase, Oxidoreductase	Botrytis aclada	73.19
	ng3	Nitrate/TMAO reductases, membrane-bound tetraheme, cytochrome c3	Desulfovibrio desulfuricans	67.53
	CG44139	CDGSH iron sulfur domain-containing protein;	Homo sapiens	47.03
	CG46308	Consensus sequence based basic form; cell cycle	Homo sapiens	25.94
Common	Mvl	Divalent metal cation transporter MntH	Eremococcus coleocola	100

BPS-upregulated	CG18179	Hemoglobin subunit alpha	Sus scrofa	100
	Rift	Equilibrative nucleoside transporter 1, adenosine transport	Homo sapiens	100
	CG13078	Cytochrome b reductase 1,Oxidoreductase	Homo sapiens	99.89
	CG13077	Cytochrome b reductase 1,Oxidoreductase	Homo sapiens	99.86
	CG33061	Trimeric intracellular cation channel type	Gallus gallus	99.84
	Ugt302E1	UDP-glucuronosyltransferase 2B7	Homo sapiens	99.62
	CG5157	Cytochrome b5 reductase	Homo sapiens	99.58
Deseq2 FAC-upregulated	RpS5b	60S ribosomal protein L8	Homo sapiens	100
edgeR FAC-upregulated	tRNA:Leu-TAA-1-1	-	-	-
	CG10505	ABC transporter, anion channel	Homo sapiens	100
	Zip89B	transporter, zinc, cadmium	Bordetella bronchiseptica	99.95
	pre-mod(mdg4)-N	Iron-regulated transcriptional activator AFT2, transcription factor	Saccharomyces cerevisiae	73.24
	CG42579	cGMP-dependent protein kinase 1, small gtpase	Homo sapiens	72.45
	MtnE	CD-7 metallothionein	Homo sapiens	55.02
	hydra	STIP1 homology and U-box containing; U-box, Chaperone	Danio rerio	50.83
	CG14598	CopC, metallochaperone, copper binding	Pseudomonas fluorescens	30.42
	CG7203	Uteroglobin	Rattus norvegicus	28.4
	CG14488	Neuroendocrine convertase 1	Mus musculus	23.89
	CG14269	Apocytochrome f, Cytochrome b6	Chlamydomonas reinhardtii	13.79
	CG17376	insecticidal toxin, spider toxin, neurotoxin; NMR	Tegenaria agrestis	12.98
Common FAC-upregulated	Zip99C	transporter, zinc, cadmium	Bordetella bronchiseptica	100
	Fer2LCH	Ferritin light chain	Trichoplusia ni	100

	Drip	Aquaporin-2, water transport simulations, c-terminal	Homo sapiens	100
	Ctr1B	Ion transporters	Salmo salar	100
	Fer1HCH	Ferritin heavy chain; Oxidoreductase	Homo sapiens	99.83
	CG7763	lectin, metalloprotein	Rattus norvegicus	99.74
	MtnA	CD-7 metallothionein	Homo sapiens	94.09
	CG33270	ABC transporter solute binding protein	Botrytis aclada	77.18
	galla-1	NifU1, iron-sulfur cluster binding	Oryza sativa	72.69
	MtnB	CD-7 metallothionein	Homo sapiens	53.79

[A] Probability indicates relevant representations of significance of identified hit (Probability > 50 considered as a true positive hit).

Table 4. 16 HHpred analysis of WB media analysis genes.

Analysis	Symbol	Name	Organism	Probability[A]
Deseq2 BPS-upregulated	Sod3	Superoxide dismutase, oxidoreductase	Homo sapiens	100
	Mvl	Divalent metal cation transporter MntH	Eremococcus coleocola	100
edgeR BPS-upregulated	CG18179	Hemoglobin subunit alpha	Sus scrofa	100
	CG13078	Cytochrome b reductase 1,Oxidoreductase	Homo sapiens	99.89
	CG17580	Cytochrome C Oxidase, oxidoreductase	Paracoccus denitrificans	79.8
	CG14205	Cytochrome b reductase 1	Homo sapiens	72.57
Common BPS-upregulated	CG13077	Cytochrome b reductase 1,Oxidoreductase	Homo sapiens	99.86
	CG5157	Cytochrome b5 reductase	Homo sapiens	99.58
Deseq2 FAC-upregulated	CG8745	5-aminolevulinate synthase, mitochondrial	Homo sapiens	99.89
	CG3732	GTP-binding nuclear protein Ran	Homo sapiens	98.9
	CG14989	PCSK9, Proprotein convertase subtilisin/kexin type 9	Homo sapiens	59.58
	Lk	Ferritin	Rhodospirillum rubrum	31.2
	dgt2	CHMP3, Charged multivesicular body protein 3	Homo sapiens	29.01
edgeR FAC-upregulated	CG10505	ABC transporter, anion channel		100
	Zip99C	transporter, zinc, cadmium	Bordetella bronchiseptica	100
Common FAC-upregulated	Fer2LCH	Ferritin light chain	Trichoplusia ni	100
	Ctr1B	Ion transporters	Salmo salar	100
	Fer1HCH	Ferritin heavy chain; Oxidoreductase	Homo sapiens	99.83
	CG7720	4F2 cell-surface antigen heavy chain, transporter	Homo sapiens	97.23
	galla-1	NifU1, iron-sulfur cluster binding	Oryza sativa	72.69
	MtnB	CD-7 metallothionein	Homo sapiens	53.79

[A] Probability indicates relevant representations of significance of identified hit (Probability > 50 considered as a true positive hit).

Table 4. 17 Signal-P analysis of BRGC media analysis genes

Analysis	Symbol	Cellular Compartment[A]	Likelihood[B]
Deseq2 BPS-upregulated	CG17028	Cytoolasm	0.00
	dmGlut	Plasma membrane	0.01
	GstE6	Cytoolasm	0.01
	Ugt302K1	Intracellular membrane-bounded organelle	0.98
edgeR BPS-upregulated	Cda9	-	1.00
	Mco4	Plasma membrane	0.93
	Kaz-m1	-	1.00
	CG14273	-	1.00
	CG6933	Extracellular space	0.93
	CG43896	Extracellular space	1.00
	CG6244	Nucleus	0.00
	CG7567	-	0.92
	Dup99B	Extracellular space	1.00
	Peritrophin-15a	Extracellular space	1.00
	CG12934	-	0.98
	CG10405	-	0.99
	CG10725	Extracellular space	1.00
	CG13912	-	0.74
	Peritrophin-15b	Extracellular space	1.00
	CG10154	Extracellular space	0.99
	CG7715	-	1.00
	Muc96D	Extracellular space	1.00
	CG14300	-	1.00
	CG11470	-	0.93
	CG33986	Extracellular space	0.80
	obst-J	Extracellular space	1.00
	obst-I	Extracellular space	1.00
	CG33272	-	1.00
	CG7017	Extracellular space	0.99
	CheB93b	Extracellular space	0.84
	CG17826	Extracellular space	1.00
	CG32302	Extracellular space	1.00
	CG5084	-	0.98
	Ag5r	Extracellular space	1.00
	CG10140	Extracellular space	0.93
Deseq2 FAC-upregulated	CG6295	Extracellular space	1.00
	Rpt3	Cytoolasm/nucleus/synapse	0.00
edgeR FAC-upregulated	CG33128	-	1.00
	Hsp26	Cytoolasm	0.00
	lectin-22C	-	1.00

	Gr58b	Membrane/axon	0.00
	CG13721	-	0.99
	CG14095	-	0.90
Common FAC-upregulated	Hsp68	Cytosol/Mitochondrion	0.00
	Hsp70Ba	Cytoolasm	0.00
	Hsp70Bc	Cytoolasm	0.00
	Hsp70Aa	Cytoolasm	0.00
	Hsp70Ab	Cytoolasm	0.00
	Hsp70Bbb	Cytoolasm	0.00
	Hsp22	Mitochondrial matrix	0.01

[A] Cellular Compartment inferred for Flybase database.

[B] Likelihood indicates the probabilities of the presence of signal peptide within proteins.

Table 4. 18 Signal-P analysis of gut media analysis genes

Analysis	Symbol	Cellular Compartment[A]	Likelihood[B]
Deseq2 BPS-upregulated	Sod3	Cytoolasm/plasma membrane/nucleus/extracellular space	1.00
	yellow-k	Extracellular space	0.74
	CG43799	-	0.97
	CG13454	-	0.00
	CG14626	-	0.99
	Desi	Apical membrane	0.90
	CG33474	Integral component of peroxisomal membrane	0.00
edgeR BPS-upregulated	Ugt37a1	Intracellular membrane-bounded organelle	0.00
	CG14014	-	0.00
	IM4	Extracellular space	1.00
	pre-mod(mdg4)-Z	-	0.00
	pre-mod(mdg4)-I	-	0.00
	pre-mod(mdg4)-V	-	0.00
	CG44040	-	1.00
	ng3	-	0.99
	CG44139	-	1.00
	CG46308	-	0.02
Common BPS-upregulated	Mvl	Endosome/apical plasma membrane	0.00
	CG18179	-	1.00
	Rift	Plasma membrane/Cytoplasm	0.00
	CG13078	-	0.00
	CG13077	-	0.00
	CG33061	Membrane	0.00
	Ugt302E1	intracellular membrane-bounded organelle	0.95
	CG5157	-	0.00

Deseq2 FAC-upregulated	RpS5b	Cytoolasm	0.00
edgeR FAC-upregulated	tRNA:Leu-TAA-1-1	Cytoolasm	-
	CG10505	Membrane	0.00
	Zip89B	Apical plasma membrane	0.00
	pre-mod(mdg4)-N	-	0.00
	CG42579	-	0.00
	MtnE	-	0.00
	Hydra	-	0.00
	CG14598	-	0.99
	CG7203	-	0.99
	CG14488	-	0.00
	CG14269	-	0.16
	CG17376	-	0.01
Common FAC-upregulated	Zip99C	ER/Golgi apparatus/Plasma membrane	0.00
	Fer2LCH	Cytoplasm/Golgi apparatus/Extracellular	1.00
	Drip	Plasma membrane	0.00
	Ctr1B	Plasma membrane	0.00
	Fer1HCH	Cytoplasm/Golgi apparatus/Extracellular	0.99
	CG7763	-	1.00
	MtnA	-	0.01
	CG33270	-	1.00
	galla-1	Cytoskeleton/spindle microtubule	0.00
	MtnB	-	0.02

[A] Cellular Compartment inferred for Flybase database.

[B] Likelihood indicates the probabilities of the presence of signal peptide within proteins.

Table 4. 19 Signal-P analysis of WB media analysis genes.

Analysis	Symbol	Cellular Compartment[A]	Likelihood[B]
Deseq2 BPS-upregulated	Sod3	Cytoplasm/plasma membrane/nucleus/extracellular space	1.00
	Mvl	Endosome/apical plasma membrane	0.00
edgeR BPS-upregulated	CG18179	-	1.00
	CG13078	-	0.00
	CG17580	-	0.00
	CG14205	-	0.98
Common BPS-upregulated	CG13077	-	0.00
	CG5157	-	0.00
Deseq2 FAC-upregulated	CG8745	-	0.00
	CG3732	-	0.00
	CG14989	-	0.70
	Lk	Extracellular space	0.99
	dgt2	Cytoskeleton	0.00
edgeR FAC-upregulated	CG10505	Membrane	0.00
	Zip99C	ER/Golgi apparatus/Plasma membrane	0.00
Common FAC-upregulated	Fer2LCH	Cytoplasm/Golgi apparatus/Extracellular	1.00
	Ctr1B	Plasma membrane	0.00
	Fer1HCH	Cytoplasm/Golgi apparatus/Extracellular	0.99
	CG7720	Membrane	0.01
	galla-1	Cytoskeleton/spindle microtubule	0.00
	MtnB	-	0.02

[A] Cellular Compartment inferred for Flybase database.

[B] Likelihood indicates the probabilities of the presence of signal peptide within proteins.

Chapter 5 Examining the Role of Spen in steroid hormone production during *Drosophila* larval development

5.1 Introduction

5.1.1 *Drosophila* an excellent model to study steroids

Developmental and physiological processes in higher organisms are highly dependent on gene regulation. Spatial and temporal gene regulation is often coordinated by systemic signals such as steroid hormones. Steroids are one of the oldest growth and developmental signaling molecules, and known to regulate puberty, cellular osmosis pressure, and cellular stress responses [73–76]. In animals, steroids are bound to their cognate nuclear receptors in the target tissues to synchronize the gene expression with signaling pathways. The steroid hormone glands release steroids mainly in the form of pulses [83,84,114]. This form of release is a vital cellular process because the onset, size and duration of the hormone pulses have to be controlled [79,83].

In *Drosophila*, the molting hormone ecdysone regulates developmental transitions and differentiation of the adult tissues [328]. As mentioned before, in the larval stages, the prothoracic gland (PG) cells produce ecdysone pulses to regulate larval molts and the onset of metamorphosis [84]. In the PG cells a series of enzymatic steps converts cholesterol to a prohormone termed α-ecdysone. Upon the release of prohormone into the target tissues, the α- ecdysone is converted to its biologically active form, 20-Hydroxyecdysone (20E), and fulfills its functions. Consequently, to have an accurate timing in the production of hormone pulses, the ecdysone-producing genes have to be expressed dynamically and further controlled tightly. Besides, ecdysone-deficient animals typically show arrested or delayed developmental phenotypes with lethality in the larval or pupae stage. Therefore, the *Drosophila* prothoracic gland is a useful model to study the dynamic regulation of steroidogenic genes in the context of a developing animal.

5.1.2 Genetic regulation of ecdysone biosynthesis

The genetic action and regulation of ecdysone are similar to human steroid hormones. In the target tissues, 20E as a ligand binds to the ecdysone nuclear receptor EcR (Ecdysone receptor) and then forms a heterodimer with another nuclear receptor USP (ultraspiracle) [114,329]. The 20E/EcR/USP heterodimer binds to DNA and mediates a cascade to regulate early genes' expression [114,329,330]. These ecdysone-induced early genes encode regulatory transcription factors that advance the expression of many downstream genes (late genes) and further inhibit their own expression. Most Early and some late genes encode transcription factors that regulate ecdysone

genes' expression [114]. In the PG cells, the genes encoding ecdysone-producing enzymes are called Halloween genes (*Neverland*, *shroud*, *spookier*, *Cyp6t3*, *Phantom*, *Disembodied*, *Shadow*, and *Shade*) [79,80]. Previously, it has been shown that the early and late *E75*, *DHR3*, *DHR4 and βFtz-F1*genes govern the expression of Halloween genes during the L3 stage [114,331]. βFtz-F1 is a nuclear receptor that induces Halloween genes expression at the end of the L3 stage (*Phantom* and *Disembodied*). It is noted that the DHR3 transcription factor positively regulates the βFtz-F1 activity. However, when the 20E level rises to the max, the early ecdysone-induced protein E75 represses the βFtz-F1 by binding to the DHR3 [331]. Thus, this drops the 20E level and results in the initiation of metamorphosis [331]. On the other hand, DHR4 has been shown to repress the expression of *Cyp6t3*. The nuclear receptor DHR4 represses the 20E production during the feeding stage of the L3 stage. At the end of the L3 stage, when a pulse of 20E is required, the DHR4 is transported to the cytosol and consequently induces the *Cyp6t3 and* 20E levels.

Therefore, this early-late-induction-inhibition model, also known as the Ashburner model [114], provides a regulatory framework for the release of ecdysone pulses. The Ashburner model has further been proposed for human steroids. Androgen and Estrogen steroids regulate the gene expression in the similar fashion to ecdysone. They are bound to their nuclear receptors and form heterodimers upon ligand-receptor binding. They are then translocated to the nucleus and where they bind to hormone response elements in the DNA to regulate gene expression [332–334].

5.1.3 Ecdysone upstream regulatory signaling pathways

Different signaling pathways control the onset, amplitude, and duration of the ecdysone peaks. The exact molecular mechanism and the cross-talk between the regulatory signaling pathways in the PG still remain unknown. Here, I will focus on the MAPK/ERK, PTTH, EGFR, TGFβ/Activin, and insulin signaling pathways in the PG.

The MAPK/ERK pathway induces ecdysone release; however, its regulatory mechanism is yet unclear. It has been proposed that PG-specific disruption of the PTTH/MAP kinase pathway either directly activates Halloween genes or inactivates repressor transcription factors such as DHR4 [83,114,328,329,335]. Consistently, depletion of the core components of the MAPK/ERK signaling (Ras85D, Raf and ERK) in the PG induces developmental arrest at the L3 stage [336]. This suggests the MAPK/ERK signaling is required for the ecdysone production at the end of the L3 stage and

initiation of metamorphosis. Two upstream regulatory mechanisms are proposed for the MAPK/ERK pathway in PG cells. One of the signal molecules that play a central role in ecdysone secretion by regulating the MAPK/ERK is the Prothoracicotropic hormone (PTTH) [328,337]. The PTTH is a brain-derived peptide that is produced in two pairs of neurons that innervate the PG. PTTH is secreted rhythmically and synergistically activates the Ras/Raf/ERK pathway (MAPK/ERK) via binding to the receptor tyrosine kinase (RTK) Torso [79]. The depletion of Torso, Ras, Raf and ERK in the PG also slows down the L3 larval-pupa transition [169].

A recent study further demonstrated that Epidermal growth factor receptor (EGFR) signaling also governs ecdysone biosynthesis by activating the MAPK/ERK pathway in the PG cells [336]. Knocking down or overexpression of the EGFR receptor in the PG cells causes L3 arrest and premature pupariation phenotypes, respectively. Furthermore, the *PG- loss-of-Vien* and *Spitz* (EGFR ligands) and *pointed* (*pnt*), the principal transcription factor of the EGFR signaling, also causes the L3 arrested phenotype [336].

The TGFβ/Activin signaling is another regulatory pathway that has been demonstrated to regulate the ecdysone release in the PG cells [338]. The function of TGFβ/Activin signaling pathways is required for the proper onset of metamorphosis at the end of the L3 stage [338]. It has been shown that the PG loss of *babo* and *Smad2*, the major players of the TGFβ/Activin pathway, cause the ecdysone deficiency phenotypes and results in a prolonged L3 stage [338].

Finally, insulin also has been determined to stimulate ecdysone synthesis. Insulin signaling in PG cells coordinates nutrient availability and development by regulating ecdysone synthesis. The neurosecretory insulin-producing cells in the brain produce insulin-like peptides (ILPs) that bind to the insulin-like receptor (InR) in the PG cells' membrane [79,338]. This triggers the downstream effectors such as Pi3K (Phosphoinositide 3-kinases) and AKT kinase that regulate Halloween genes expression directly or indirectly [79,114]. Antagonizing or enhancing the function of Pi3K in PG cells further results in impaired developmental progress and suggests that insulin plays a critical role upstream of ecdysone synthesis [339].

5.1.4 The *Drosophila* Spen is a regulatory protein that functions in several signaling pathways

In 1995, Kolodziej and his colleagues reported a recessive lethal mutation with abnormal lateral chordotonal axons in the abdominal segments of *Drosophila* embryos [340]. The gene was

named *Spen* (Split-ends) and later work showed that it plays different roles during *Drosophila* development. Spen belongs to a conserved family of nuclear proteins that vary considerably in size (Figure 5.1A). It has two critical regulatory protein parts and can localize to the nucleus, cytoplasm or both cellular compartments. Spen harbors three N-terminal RNA Recognition Motifs (RRMs) and a highly conserved C-terminal domain called Spen Paralog and Ortholog C-terminal domain (SPOC). The RRMs function in the mRNA transcription, splicing, stability, localization, and translation [341]. However, the SPOC domain is an essential transcriptional motif in the repressor proteins that enable them to physically interact with other co-repressors and regulate gene expression [341].

Drosophila Spen encodes eight annotated transcripts and functions in a highly similar manner to its human and mouse orthologs, the Sharp and Mint proteins, respectively. Spen has been shown to have a role in the cell fates of neurons and glial cells, axon guidance, regulation of the cell cycle, the polarity of epithelial cells and head identity during embryo development [341–343]. To fulfill these functions mechanistically, Spen regulates gene expression translationally via acting in the Notch, EGFR, MAPK/ERK and Wingless (Wg) signaling [342,344–346].

Loss of Spen function has been indicated to affect the expression of *ERK*, *Suppressor of Hairless Su(H)*, and *Yan* in different tissues. ERK is a key protein downstream of the MAPK pathway and regulates the cell cycle and differentiation once activated via phosphorylation. The Su(H) is a key transcription inhibitor of the Notch signaling, and mutation in *Spen* was shown to reduce the expression of Su(H) and has an inhibitory effect on the Notch pathway. Yan, on the other hand, is an ETS domain-containing (E26 transformation specific) transcription factor of the EGFR signaling pathway [342,345]. Loss of Spen in the cells results abnormal *Yan* expression and an antagonizing effect on EGFR signaling. This further impairs the cell fate and proliferation during embryonic development [341,342,344].

In addition, Spen has a role in the wingless signaling during eye and wing development. Spen has been shown to positively activate the Senseless (Sens) zinc-finger transcription factor. The Sens is a critical protein for the differentiation of the wings and eyes from the larval imaginal discs [342].

All these data suggest that Spen is a critical protein in the cross-talk between different signaling pathways and lack of its function in the cells causes severe developmental defects.

5.1.5 *Drosophila* Spen and ecdysone

Spen is a unique transcription cofactor that can regulate gene expression at the chromosomal or mRNA levels. Surprisingly, the human Spen ortholog, Sharp, has been demonstrated to recruit the histone deacetylases HDAC1 and HDAC2 to chromatin via its SPOC domain to promote gene expression. Sharp also interacts with RNA coactivators to govern mRNAs translation [347]. Interestingly, an *in vivo* assay indicated that Sharp physically interacts with the Steroid Receptor RNA Activator (SRA). SRA is an RNA cofactor that enhances the transcriptional activity of the liganded steroid receptor such as the estrogen and tyrosine receptors [347,348]. Sharp binds to SRA via the RRM and attenuates the transcriptional activity of SRA-steroid receptors. This would result in the repression of steroid receptor transcriptional activity. A similar function has not been identified for the *Drosophila* Spen. However, given the function of Spen in the cell fates and differentiation, it is possible that Spen might regulate ecdysone biosynthesis by acting downstream of the EGFR and Ras/MAP kinase signaling pathways.

Here I provide preliminary evidence that Spen function is required to properly express the Halloween genes and release ecdysone titers at the L3 larval stage. The PG loss of *Spen* further causes larval molting defects that can be rescued by 20E or ecdysone precursors supplementations.

5.2 Materials and methods

5.2.1 Fly stocks

The list of flies that were ordered from the stock centers (Bloomington *Drosophila* stock center, Kyoto Stock center and Vienna *Drosophila* Resource center) is presented in Table 2.1 (Chapter 2, Section 2.1). In all experiments, w^{1118} (#3605) flies were used as controls. Further, *phm22-GAL4* and *phmN12-GAL4* (PG-specific GAL4 driver) were generous gifts from Michael O'Connor's lab.

5.2.2 medium supplementation analysis

A cornmeal standard food was used for expanding fly populations, stock maintenance, and setting up crosses to combine different genotypes. Nutri-Fly (DGRC) was used for supplemented media studies. The list of sterol compounds and their concentrations are shown in table 2.2

5.2.3 Other conducted experiments

A detail-oriented description of the survival and developmental analysis, microscopy analysis, antibody immunostaining, and qPCR experiments are presented in Chapter 2.

5.3 Results

5.3.1 Spen is required for *Drosophila* ecdysone production

Spen was one of the hits in the second round of the genome-wide screen with the aim of identifying genes involved in heme and ecdysone biosynthesis (appendix A.1 section). I became interested in studying Spen further as it was one of the proteins that have putative transcriptional activity. According to the original screen result, the PG-specific knockdown of *Spen* caused larval molting defects with the majority of the animals arrested at the L3 stage. Further, it was reported that the arrested animals had an enlarged ring gland but did not display the porphyria phenotype. These original experiments were conducted with the *Spen-RNAi^{VDRC1}* line. I then aimed at validating these results with the same line and additional RNAi lines that target different regions of the *Spen* mRNA.

Spen encodes a very large mRNA with 10 exons (Figure 5.1B). Upon alternative splicing, the Spen mRNA is converted to eight transcripts with divergent sizes. Eight exons are common among all the transcript variants, and I selected only the RNAi lines that target these exons to knockdown all transcripts in PG cells. There are nine RNAi lines available for Spen in the VDRC (six lines) and BDSC (three lines) stock centers. I tested three VDRC lines (RNAi^{VDRC1}, RNAi^{VDRC2} and RNAi^{VDRC3}) and two Trip lines (RNAi^{TRIP1} and RNAi^{TRIP2}) to validate the previous results (Figure 5.1B). All the VDRC lines and TRIP1 lines target different regions, but TRIP2 targets the same mRNA region as TRIP1. Therefore, I did not use this line in the subsequent experiment.

PG knockdown of *Spen* with all tested RNAi lines resulted in a significant L3 arrested phenotype with very few pupae and adults (Figure 5.1C and Figure 5.2A). In brief, I observed approximately 81% L3 larvae, 13% pupae and 6% adults for the RNAi^{VDRC1} line, but these numbers were ~84%, 21% and 9% for the RNAi^{VDRC2} line, respectively. The third VDRC line was also similar to the other two lines, and I observed survival of 84% L3 larvae, 19% pupae and 11% adults. The TRIP lines further exhibited a similar phenotype as the VDRC lines. The percentage

of L3 larvae, pupae and adults for the TRIP1 were 83%, 13% and 6%. Finally, I observed 78%, 8% and 4%, representing L3 larvae, pupae and adults, for the TRIP2 line. All these quantification data indicated that the function of Spen in the PG cells is critical for the L3 larval-pupal developmental transition. Furthermore, the overlap results of different RNAi lines eliminate the possibility that off-targets are responsible for the observed phenotypes.

Next, I sought to test whether loss of Spen function in PG cells affects the expression of Halloween genes in the PG cells. To test this, I dissected and collected ring glands from *Spen*-RNAi animals (*spen*-RNAi^{VDRC1}) and conducted a qPCR analysis to measure the expression of the Halloween genes (Figure 5.2B). The qPCR analysis demonstrated that the expression *nvd* (*neverland)*, *dib* (*disembodied)* and *spok* (*spookier*) were substantially downregulated in both tested spen-RNAi lines (Figure 5.2C). I observed no statistically significant change in the expression of other Halloween genes compared to the control. I further confirmed this data in the *spen*-RNAi^{TRIP1} animals (Figure 5.2B). This data illustrated the lack of Spen function in PG cells leads to a substantial down-regulation of Halloween genes and suggests that Spen is required for ecdysone production at the end of the L3 stage.

To further support the phenotypic results seen in PG>RNAi larvae and the effects on Halloween gene expression, I conducted a media survival analysis using the precursors and the end product of ecdysone pathways (Figure 5.2D). In the first step of the ecdysone pathway, Neverland converts the cholesterol (C) to 7-dehydrocholesterol (7DC). 7DC is then entered into the "black box" and is converted to 5β-ketodiol (5βk) and then to α-ecdysone (αE) via the three subsequent steps. The intermediates in the black box are yet unidentified. However, three enzymes, including Spookier, have been associated with the black box. Finally, αE is converted to 20-hydroxyecdysone (20E) after being taken up by target tissues [79,114,349]. I examined the C, 7DC, 5βk*, αE* and 20E administration on the arrested larvae. Remarkably, upon rearing *PG>Spen-RNAi^{VDRC1}* and *PG>Spen-RNAi^{TRIP1}* animals on the correspondingly supplemented foods, the arrested animals were rescued to adults on the C and 7DC diets. I observed ~ 75 % percent adults in the C supplemented, and ~79 % adults in the 7DC supplemented foods (Figure 5.2D). This indicated approximately 65 % more normal adults compared to the <10 % animals in the control food. Furthermore, in the 20E feeding, I observed ~50-60% adults, but nearly 30-40% of the

arrested larvae developed into normal adults. However, in the 5βk food, I observed no significant differences, and about 15-20% of the arrested larvae developed into adults.

These results illustrated that the lack of *Spen* in the PG cells leads to a significant down-regulation of Halloween genes and suggested that Spen is required for the ecdysone pulse at the end of the L3 stage.

5.3.2 PG loss of function of Spen induces morphological defects in the PG and reduces cell numbers

I then addressed whether *PG>Spen-RNAi* affects RG morphology. In the second stage of the original RNAi screen (where the King-Jones lab searched for red autofluorescence ring glands in ~ 800 RNAi lines), it was reported that depletion of *Spen* in PG cells results in an overgrown RG. To confirm this, I first crossed all five tested RNAi lines with a PG-specific GAL4 driver *PhmN1-GAL4* driver line and dissected the RG. The *PhmN1-GAL4* flies is are recombination line between the 3rd chromosome *Phm-GAL4* driver and *UAS- mCD::GFP* line [316] that express the eGFP protein predominantly in the plasma membrane (Phm-GAL4,*UAS- mCD::GFP*). Upon RG observation under the microscope, I confirmed that the *PG>Spen-RNAi* results in an enlarged ring gland due to the increase in PG cell size (Figure 5.3A). However, the RG morphology in the *PG>Spen-RNAi* animals was abnormal. I refer to this phenotype as "malformed" morphology where the PG cells exhibited a non-uniform shape with various sizes, from the small to remarkably enlarged cells.

To further substantiate the malformed phenotype, I quantified the number of PG cells in the RNAi and control animals. For this, I used the Spen-RNAi^{VDRC1} and Spen-RNAi^{TRIP1} lines. Consistently, the RNAi animals have significantly fewer number of cells than control (Figure 5.3B). I counted ~ 40 cells for the *Spen*-RNAi^{VDRC1} and *Spen*-RNAi^{TRIP1} lines versus ~60 cells in control. The missing 20 cells upon depletion of *Spen* may result in a lower ecdysone level in these animals.

Next, I examined whether the sterol feeding would rescue the malformed PG phenotype and/or the lessen PG cells number, as it efficiently rescued the arrested larvae. Surprisingly, in the RNAi animals (VDRC1 and TRIP1) that were reared in the C, 7DC, 20E supplemented media, the malformed phenotype was absent (Figure 5.4A), the number of PG cells were nearly similar to the

control (50-60 cells). However, the 5βk and αE feeding did not significantly improve the malformed phenotype of *PG>Spen-RNAi* animals (Figure 5.4B).

This suggests that Spen is critical for the typical morphology of the PG cells, and the adverse effects of the lack of Spen could be compensated with the administration of ecdysone or ecdysone biosynthesis intermediates.

5.3.3 Spen may act downstream of the MAPK/ERK pathway

The interplay of Spen between Notch and EGFR/Ras/MAPK signaling led me to hypothesize that Spen may be a downstream regulatory protein in these pathways. Furthermore, studies have shown that the Torso/Ras/MAPK and EGFR/Ras/MAPK pathways regulate ecdysone production through the Ras/MAPK component (Ras85D, Raf and ERK) [169,336]. However, whether PTTH/Torso signaling or EGFR signaling is the primary governing factor for PG's Ras/MAPK pathway is yet unclear. Therefore, I decided to mainly focus on the Ras/MAPK pathway. On the other hand, Notch signaling has not been reported to be involved in ecdysone biosynthesis. Using a gene knockdown approach, I provided evidence that Spen further functions in the Ras/MAPK signaling pathway and not in the Notch signaling.

The Notch signaling pathway is the master coordinator of cellular differentiation and cellular proliferation [350]. The membrane-bound Notch receptor regulates transcription upon binding to its ligands Delta (Dl) and Serrate (Ser) [350,351]. It triggers different transcription factors, such as the Suppressor of Hairless Su(H), to regulate cell fate and differentiation [345,351]. The loss of function of *Notch*, *Delta* and *Serrate* in PG neither caused the delay in the developmental progression nor the developmental arrest during the L3 stage (Figure 5.5A). Adults looked also similar to controls. This was further supported with a qPCR analysis for the *Notch* expression in *PG>Spen-RNAi*^{VDRC1} animals. The PG-specific loss of *Spen* also did not affect the expression of Notch in the PG (Figure 5.6C), at least when assessed by qPCR. This suggests that Spen does not control ecdysone biosynthesis through the Notch signaling pathway.

Next, I recapitulated the previous results for the *PG>Ras85D-RNAi*, *PG>Raf-RNAi* and *PG>ERK-RNAi* animals (Figure 5.5B). For this, I chose to use the TRIP lines from the BDSC stock center as the tested VDRC lines indicated no phenotype in the genome-wide screening. The PG-specific knockdown of the Ras/MAPK pathway was reported to cause a developmental delay

phenotype [169]. Consistently, I observed ~140, ~100 and ~195 hours delay during the L3 stage upon PG-lack of *Ras*, *Raf* and *ERK* genes, respectively. Depletion of the Ras/MAPK pathway further led to the L3 arrest larvae. The *PG>Ras85D-RNAi* animals formed ~45 % pupae and ~ 25-30% adults, but the percentages for the *PG>Raf-RNAi* animals were ~35% pupae and ~20% adult flies. Likewise, *PG>ERK-RNAi* resulted in ~50% pupae and only ~25 % of the arrested animals developed into adults. The L3 arrested data was similar to the developmentally arrested phenotype of the *Spen-RNAi* animals. However, this was inconsistent with a previous report that only demonstrated a delay phenotype for interfering with the Ras/MAPK signaling in PG [169]. This was possibly caused by the different RNAi lines that I used in my experiments. Moreover, my observations were further supported by a recently published report that showed PG-specific depletion of the Ras/MAPK pathway results in the L3 arrested phenotype [336]. However, the authors did not provide quantification data in their report.

In order to further examine whether Spen functions downstream of Ras/MAPK signaling, I measured the expression of *Torso* and *Ras* genes in the *PG>Spen-RNAi^{VDRC1}* animals. Torso is an RTK (Receptor Tyrosine Kinase) that activates Ras/MAPK signaling in the PG via binding to its ligand PTTH. Remarkably, depletion of *Spen* in the PG cells increased *Torso*'s expression ~4 fold, but it reduced Ras expression significantly (Figure 5.6C). This indicates PG depletion of *Spen* reduces the Ras/MAPK signaling in the cells.

The qPCR results led me to test whether activation of the Ras/MAPK pathway in the PG can rescue the arrested animals of *PG>Spen-RNAi*. I next expressed the constitutively activated form of Ras (Ras^{V12}) in Spen-depleted PG cells to examine this. The Ras^{V12} is a *Ras85D* transgene under control of the Gal4/UAS with a point mutation (G12V). The expression of Ras^{V12} in cells can hyperactivate the Ras/MAPK pathway since it codes an activated form of Ras [352]. Surprisingly, the *PG> Spen-RNAi^{VDRC1};Ras^{V12}* animals formed ~70% pupae, approximately 60% more pupae than using *PG> Spen-RNAi^{VDRC1}* without Ras^{V12} (Figure 5.6B). Furthermore, I observed ~45% of animals that eclosed into adult flies (30-35% increase). Consistently, the overexpression of *Ras^{V12}* in the *PG> Spen-RNAi^{VDRC1}* animals also improved the malformed phenotype of the RG (Figure 5.6A).

All these data strongly suggest that Spen is a novel component of the Ras/MAPK signaling in the PG cells acting in the ecdysone biosynthesis regulation.

5.4 Discussion and conclusion

A precise communication between various signaling pathways is required to coordinate the ecdysone synthesis and *Drosophila* development. Results from individual studies indicated that the Ras/MAPK pathway acts in the *Drosophila* prothoracic glands to regulate ecdysone biosynthesis. In this project, I showed that Spen is a novel regulator of ecdysone biosynthesis in the Ras/MAPK pathway. I have demonstrated that the loss of *Spen* reduces the expression of Halloween genes, induces the formation of an enlarged malformed RG and blocks pupariation. The malformed RG further has a lowered number of cells that could partly explain the reduced ecdysone level.

5.4.1 Spen function in PG and its dependence on Ras/MAPK signaling

Ras/MAPK is a signal-dependent pathway that promotes gene regulation upon receptor binding of the extracellular stimuli. In humans, there is evidence that the genes that encode enzymes in steroidogenesis are regulated by Ras/MAPK signaling [353–355]. Surprisingly, it has been shown that the hyperactivated Ras-MAPK pathway mediates the steroidogenic acute regulatory protein (StAR), which is the rate-limiting enzyme in the biosynthesis of all steroid hormones [353]. StAR transfers cholesterol across mitochondrial membranes to facilitate the onset of steroid production in steroidogenic cells [354]. Furthermore, active Ras can induce the expression of Cytochrome P450 enzyme genes in the human adrenocortical cells to promote cortisol production and secretion [355].

Success in rescuing the *PG>Spen-RNAi* arrested animals with the expression of hyperactivated Ras in PG supports the idea that Spen is recruited to the transcriptional cascade of the Ras/MAPK signaling pathway. Furthermore, the induction of *Torso* in PG> *Spen-RNAi*^{VDRC} supports this functional redundancy between Spen and Ras/MAPK pathways in the context of ecdysone synthesis (Figure 5.7). This is consistent with the downregulation of *Ras* in *Spen*-depleted cells as the PTTH/Torso signaling activates Ras/MAPK pathways in PG. Future experiments will have to evaluate whether the EGFR receptor is also induced in PG upon loss of function of Spen.

Additionally, the development of arrested larvae into adults with C, 7DC, and 20E supplementations, further support the idea for a role of Spen in the Ras/MAPK signaling cascade. Given the fact that Spen is a transcriptional corepressor, the Ras/MAPK-Spen mechanism in the

PG seems to be a negative regulatory process. One supporting clue for this is the role of SHARP in estrogen synthesis. It has been shown that in the MCF-7 cells, SHARP represses the transcriptional activity of the estrogen receptor through a negative feedback loop. When estrogen levels are high, *SHARP* expression is induced to suppress transcription by binding to the estrogen receptor [347]. On the other hand, loss of *Spen* function in the PG reduces ecdysone levels (inferred from reduced Halloween gene expression) and suggests that Spen positively regulates ecdysone biosynthesis. Therefore, Spen may control a transcriptional repressor of the Halloween genes. Interestingly, Ras/MAPK signaling also attenuates the transcriptional activity of the DHR4 nuclear receptor on the PG cells. DHR4 represses ecdysone synthesis by downregulating the putative Halloween gene *Cyp6t3* in the nucleus [83]. The Ras/MAPK promotes the cytosolic localization of DHR4 in PG cells to induce the expression of the *Cyp6t3* [83] via the removal of its repressor (i.e., DHR4) from the nucleus. Thus, the Ras/MAPK signaling exerts its positive regulatory effects on ecdysone production likely by recruiting Spen. This, however, requires further confirmations.

Finally, depending on the cellular contexts, Spen functions in the divergent complex processes. It may control the effector proteins of the Ras/MAPK when the ecdysone titer is required. Therefore, a lack of Spen function has an indirect adverse effect on ecdysone synthesis. Furthermore, members of the Spen protein family have been demonstrated to regulate transcription by governing alternative splicing [356]. The RBM15 protein (a member of Spen protein family) binds to the 3'UTR and intronic regions of pre-mRNAs via its RRM motif to regulate transcription [357,358]. This transcription-coupled RNA splicing regulation has been proposed to be a common function for all the Spen proteins. Correspondingly, alternative splicing of Ras, Raf and ERK has been demonstrated to affect downstream transcriptional regulation of the Ras/MAPK pathway [359,360]. This suggests that Spen may mediate the alternative splicing of Ras, Raf and ERK transcripts in PG cells. Therefore, interfering Spen function reduces the MAPK/ERK signaling and ecdysone biosynthesis. Future studies will have to address the exact mechanism by which Spen regulates ecdysone biosynthesis in the PG.

5.4.2 Conclusion

The *Spen* (also called *Split-ends*) genes encode a conserved family of nuclear proteins with considerably varying protein sizes (90-600 kD). However, they all harbor three N-terminus RNA recognition motifs (RRM) and a C-terminus SPOC domain. The conserved domain structure

suggests Spen proteins may have shared molecular functions, but their role in steroidogenesis needs to be elucidated. The potential role of *Drosophila* Ras/MAPK/Spen in the ecdysone biosynthesis will provide new insight into how Spen transcriptional effectors regulate steroid biosynthesis.

5.5 Figures

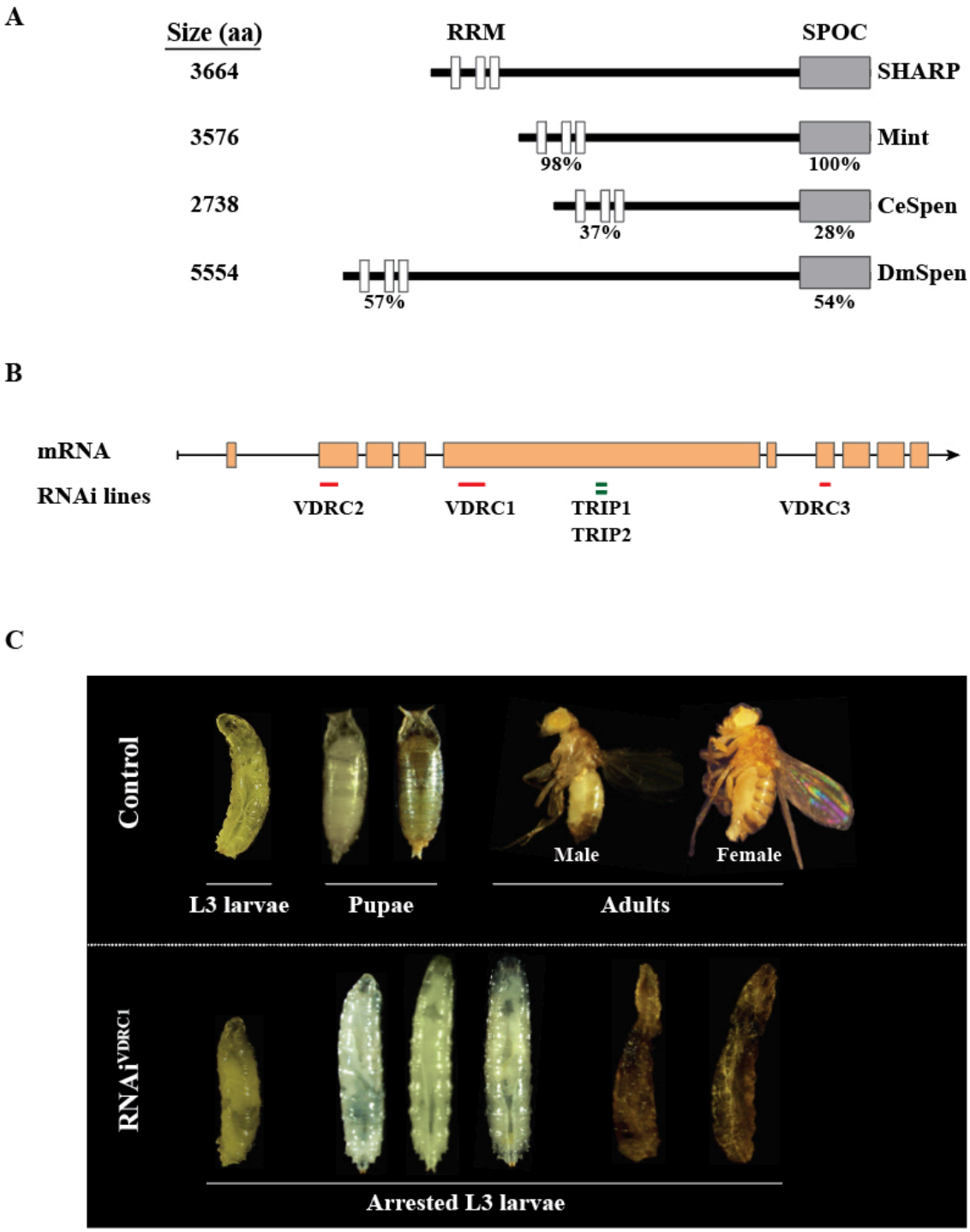
A
Size (aa)
RRM
SPOC
3664
SHARP
3576
Mint
98%
100%
2738
CeSpen
37%
28%
5554
DmSpen
57%
54%
B
mRNA
RNAi lines
VDRC2
VDRC1
TRIP1
TRIP2
VDRC3
C
Control
Male
Female
L3 larvae
Pupae
Adults
RNAi VDRC1
Arrested L3 larvae

Figure 5. 1 *Drosophila* Spen protein, mRNA and RNAi lines

A) Members of the Spen protein family in humans (SHARP), mouse (Mint), *C. elegans* (CeSpen), and *Drosophila* (DmSpen). Spen proteins have three conserved N-terminal RNA Recognition Motifs (RRMs, white boxes) and a Spen Paralog and Ortholog C-terminal domain (SPOC, gray boxes). The percentages indicate the sequence similarity between human protein domains and the corresponding domains in the other orthologs. The protein size of the orthologs (aa: amino acid) is further shown. **B)** the schematic drawing of Spen mRNA in *Drosophila*. Orange boxes represent the exonic regions of the mRNA. The tested VDRC1-3 (three red lines) and TRIP1-2 (two green lines) RNAi lines and their target regions on the mRNA are shown. **C)** The developmental phenotype of *PG>Spen-RNAi*^{VDRC1} compared to control animals. The PG loss of *Spen* results in the 3rd instar larval (L3) arrested phenotype and L3 larval lethality.

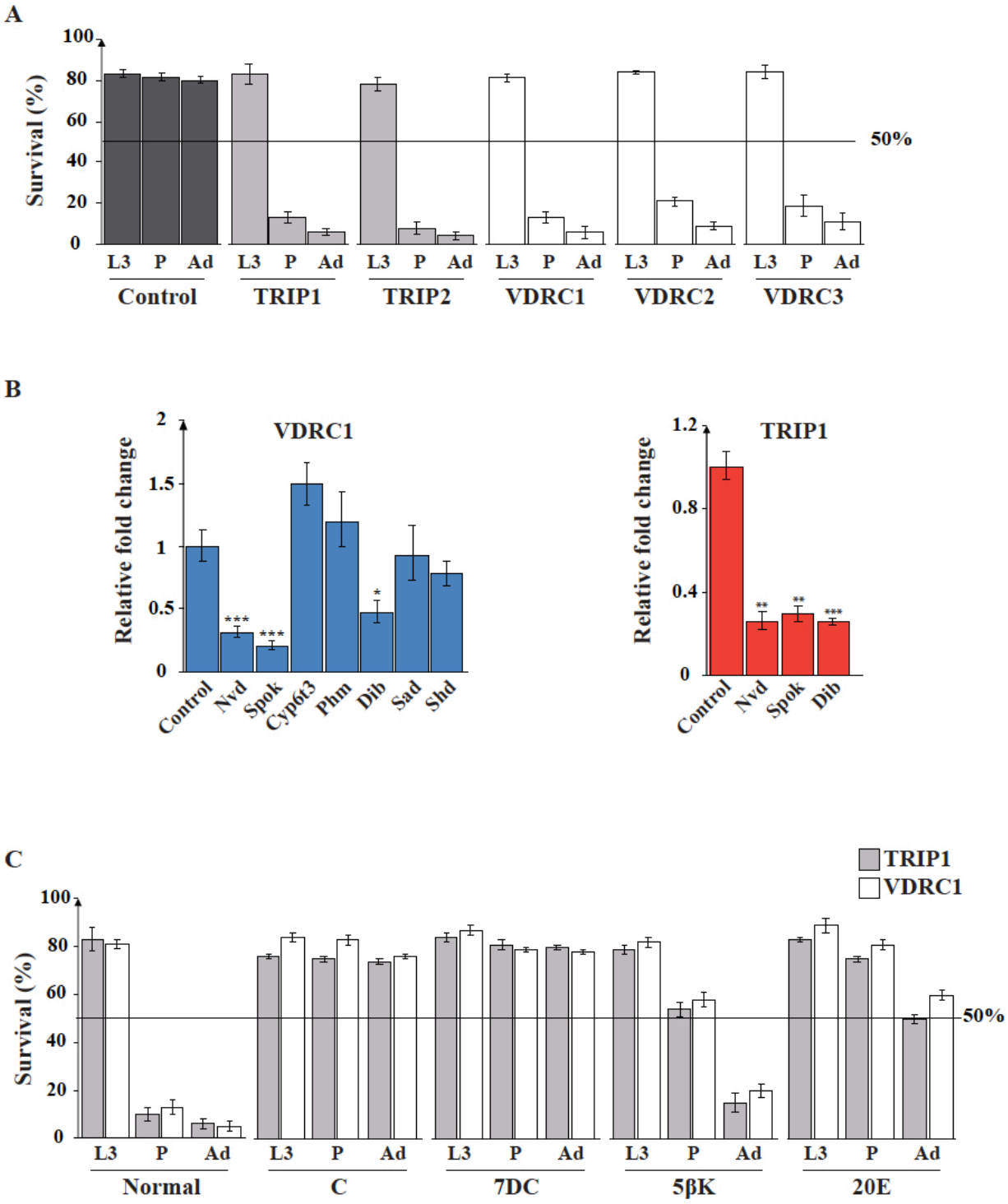
A
Survival (%)
100
80
60
40
20
0
50%
L3 P Ad
Control
TRIP1
TRIP2
VDRC1
VDRC2
VDRC3
B
VDRC1
Relative fold change
2
1.5
1
0.5
0
Control
Nvd
Spok
Cyp6t3
Phm
Dib
Sad
Shd
TRIP1
1.2
0.8
0.4
0
C
TRIP1
VDRC1
Normal
C
7DC
5βK
20E

Figure 5. 2 *PG>Spen*-RNAi developmental defect reduces expression of Halloween genes and can be rescued by sterol administration

A) Survival percent of 3rd instar larval (L3), pupae (P) and adult flies (Ad) in all five tested Spen-RNAi lines. **B)** Ring gland expression of Halloween genes in the VDRC1 and TRIP RNAi lines. **C)** Survival analysis of VDRC1 and TRIP1 RNAi animals in the normal, cholesterol (C), 7-dehydrocholesterol (7DC), 5β-ketodiol (5βk) and 20-hydroxyecdysone (20E). In **A** and **C**, error bars represent standard deviation error between three tested replicates. However, in **B**, the error bars are 95% confidence intervals between replicates, and the asterisk represents the P-value of the student's t-test analysis (*$p < 0.05$ and ***$p < 0.001$). The student's t-test was used to compare experimental samples to control samples.

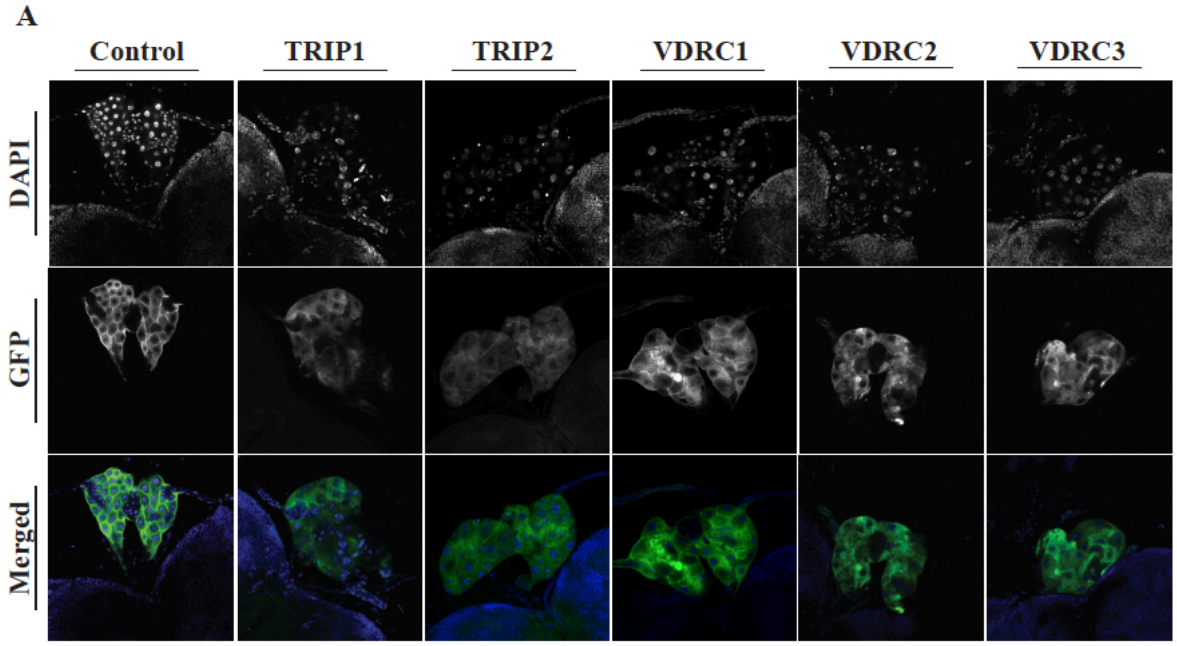
A
Control
TRIP1
TRIP2
VDRC1
VDRC2
VDRC3
DAPI
GFP
Merged

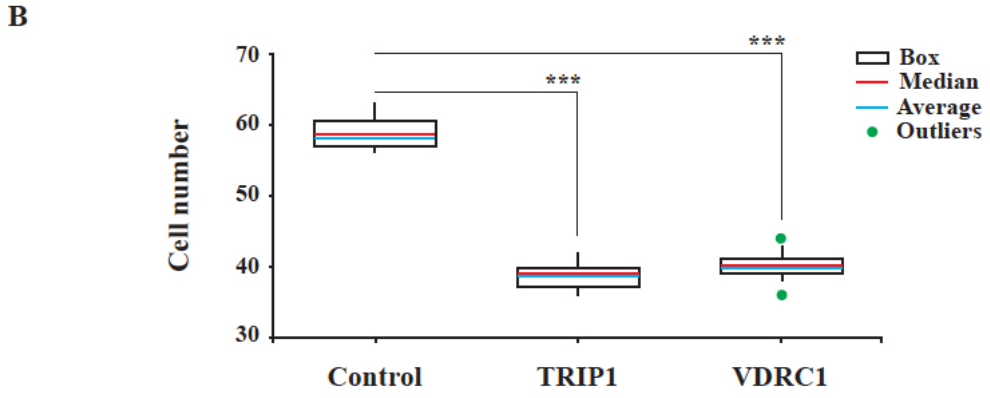
B
Cell number
70
60
50
40
30
***
***
Box
Median
Average
Outliers
Control
TRIP1
VDRC1

Figure 5. 3 PG-specific depletion of *Spen* reduces the number of RG cells and results in malformed RG morphology

A) Brain-ring gland complexes (BRGC) of all five tested *Spen-RNAi* animals compared to the control animals. DAPI is used to stain nuclei (gray color in DAPI panel and Blue color in merge panel). The gray GFP panel and green color in the merge panel show the GFP signal of the recombined *UAS-mCD::GFP* in *phm-GAL4 (PhmN1-GAL4).* In the *phmN1-GAL4* driver, GFP is expressed in the membrane of the PG cells. **B)** Box plot of the average RG cell number in control, VDRC1 and TRIP1 RNAi animals. In each genotype, cells were counted in 10 RG samples. The upper error bar represents the maximum number of cells in each group, and the lower error bar shows the minimum number of cells. The red line in boxes shows the average number of cells, and blue lines are the median lines of each box. The green dots indicate outliers of each line. Asterisks are based on *P*-values in the student's t-test analysis (*$p < 0.05$ and ***$p < 0.001$).

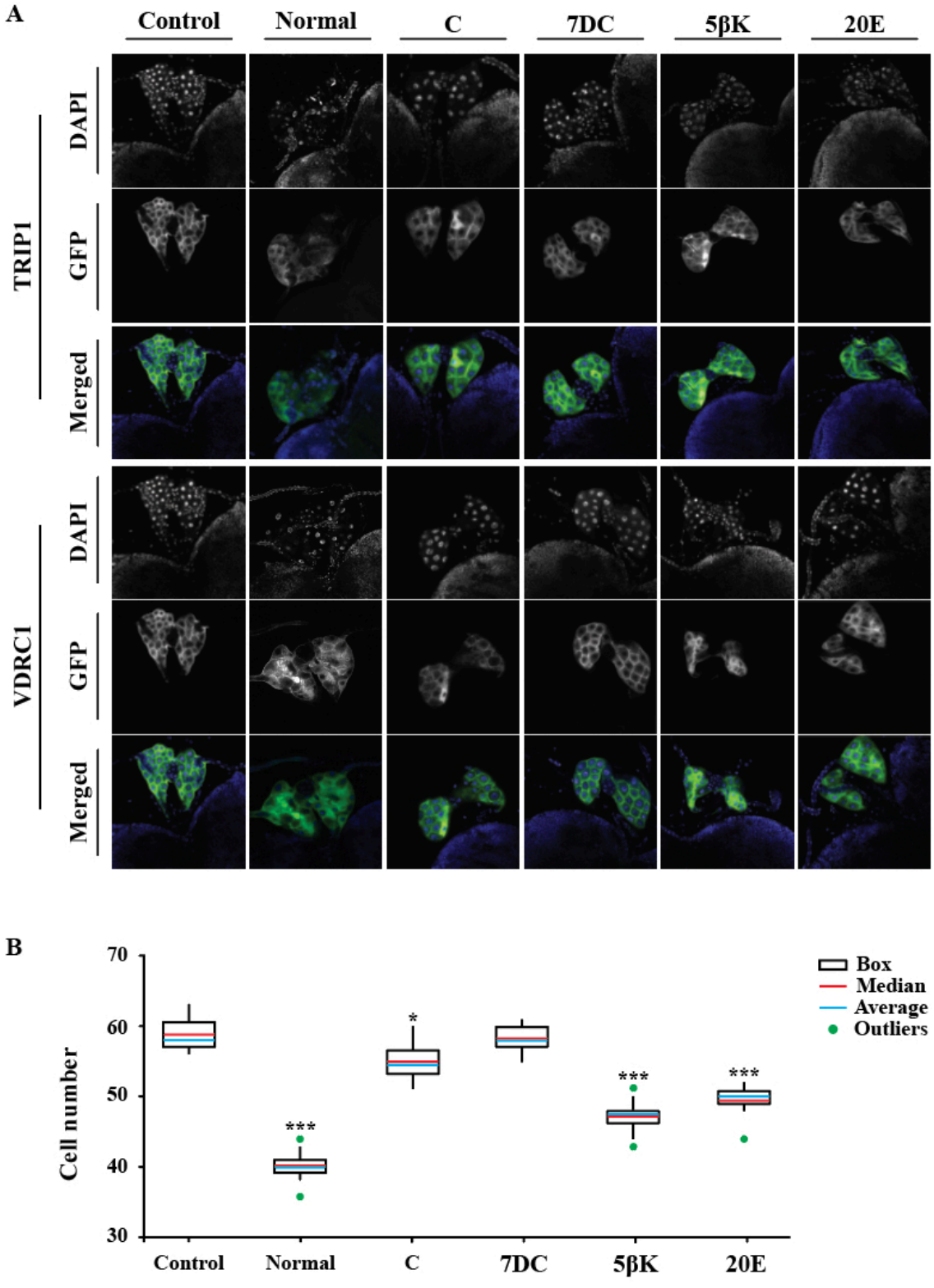
A
Control
Normal
C
7DC
5βK
20E
TRIP1
VDRC1
DAPI
GFP
Merged
B
Cell number
70
60
50
40
30
Box
Median
Average
Outliers
***
*
***
***
Control
Normal
C
7DC
5βK
20E

Figure 5. 4 Sterol feeding rescues the malformed RG phenotype and partially restores RG cell number in *PG>Spen*-RNAi animals

A) Brain-ring gland complex (BRGC) images of *Spen-RNAi* ^{TRIP1} and *Spen-RNAi* ^{VDRC1} animals reared in the normal, cholesterol (C), 7-dehydrocholesterol (7DC), 5β-ketodiol (5βk) and 20-hydroxyecdysone (20E) supplemented media. The BRGC of control flies is examined only in the normal diet. DAPI was used to stain nuclei. GFP is the signal of *phmN1-GAL4*. **B)** Box plot of *Spen-RNAi*^{VDRC1} RG cells in food supplemented with C, 7DC, 5βk and 20E sterols. Red and blue lines indicate the average and the median number of cells, but green dots are outliers. The significance asterisks are *$p < 0.05$ and ***$p < 0.01$ (based on the student's t-test analysis).

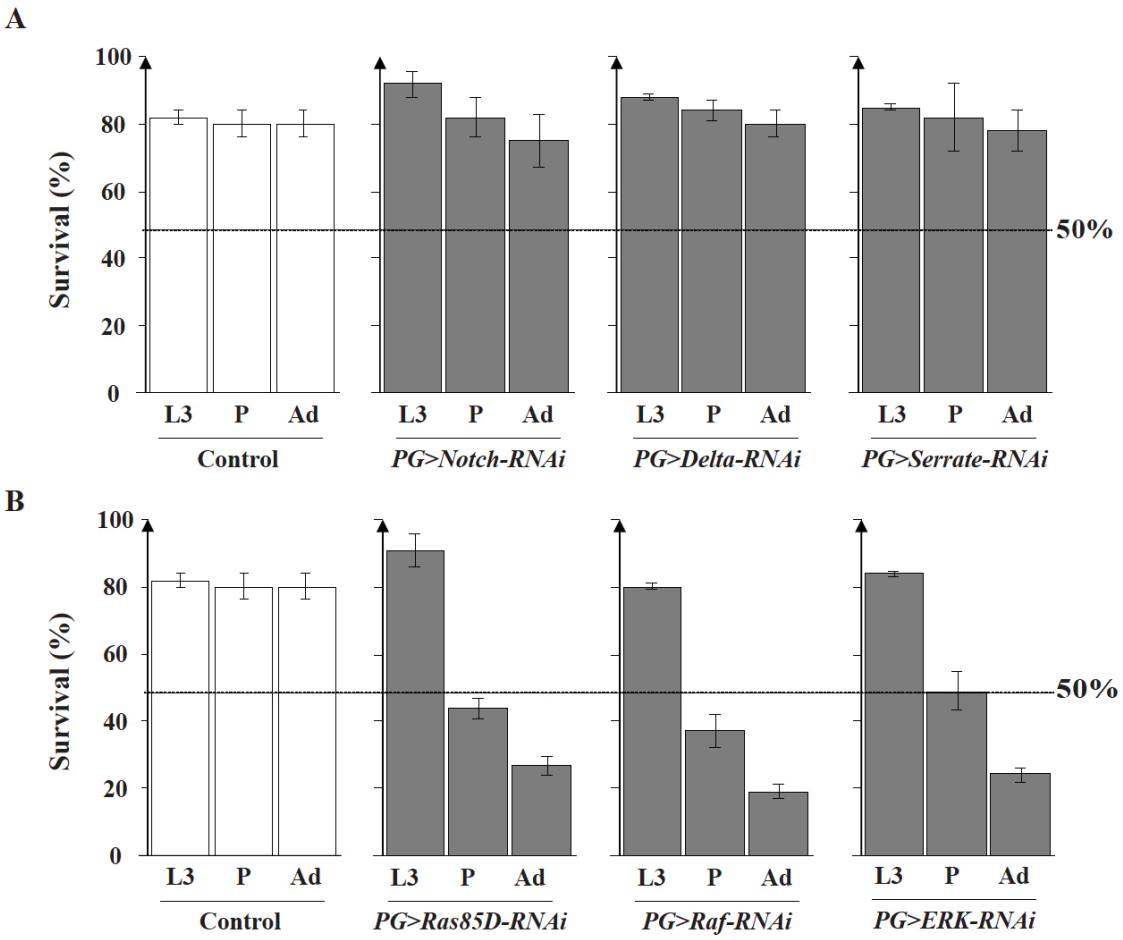

Figure 5. 5 Depletion of MAPK/ERK signaling in PG cells causes developmental defect

A) and **B)** Survival analysis of PG-specific depletion of *Notch* and MAPK/ERK signaling pathways genes. For the Notch signaling, the *PG>Notch*-RNAi, *PG>Delta*-RNAi and *PG> Serrate-RNAi* animals were tested. For the MAPK/ERK signaling, the *PG>Ras85D*-RNAi, *PG>Raf*-RNAi and *PG>ERK*-RNAi were examined. Error bars indicate the standard deviation error among three replicates. L3: 3rd instar larval, P: pupae and Ad: adults.

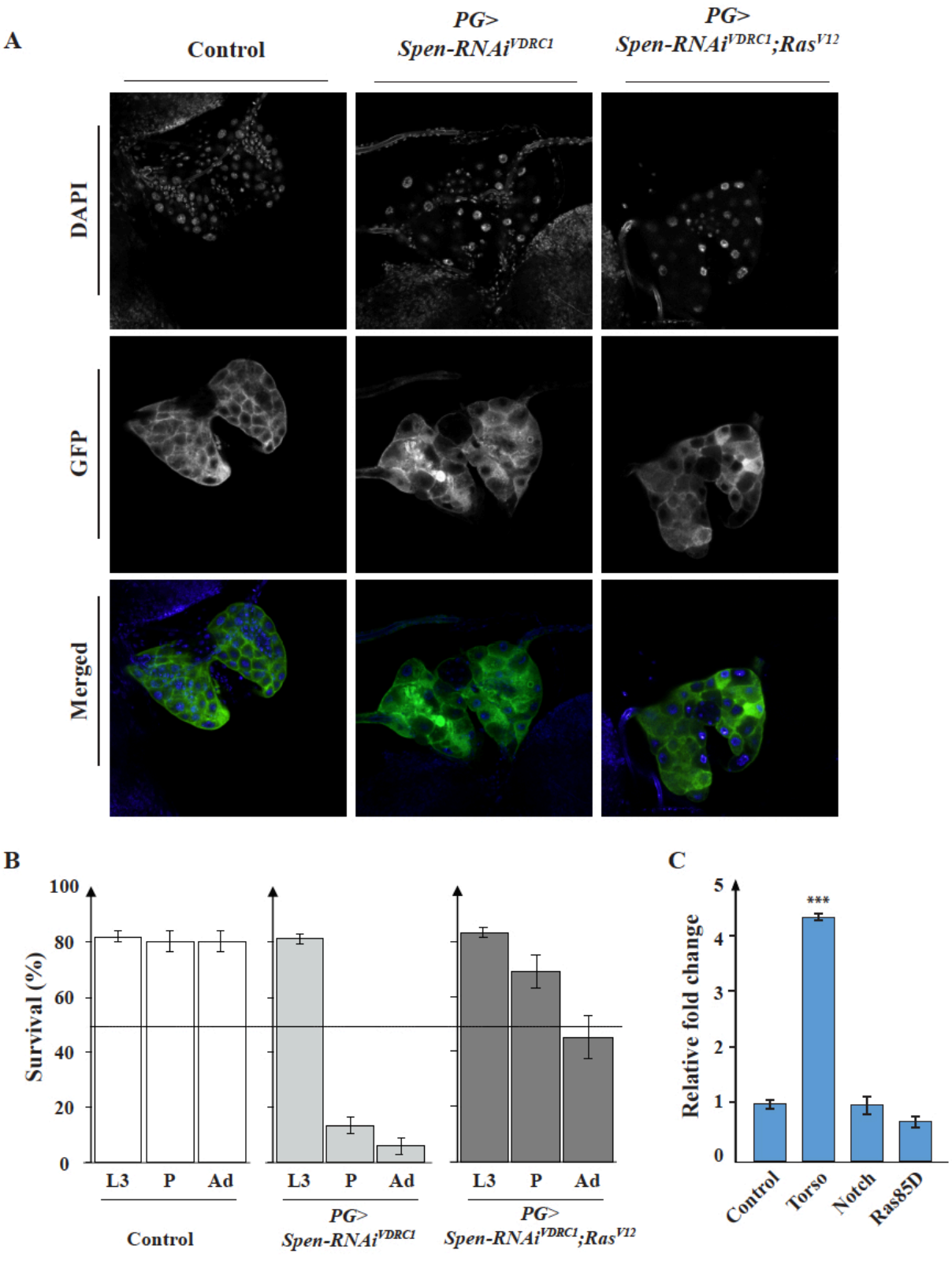
A
Control
PG>
Spen-RNAi^VDRC1
PG>
Spen-RNAi^VDRC1;Ras^V12
DAPI
GFP
Merged
B
Survival (%)
100
80
60
40
20
0
L3
P
Ad
Control
PG>
Spen-RNAi^VDRC1
PG>
Spen-RNAi^VDRC1;Ras^V12
C
Relative fold change
5
4
3
2
1
0
***
Control
Torso
Notch
Ras85D

Figure 5. 6 Spen functions downstream of MAPK/ERK signaling in PG cells

Expression of hyperactive Ras (Ras^{V12}) in PG cells of VDRC1 RNAi animals (*PG>Spen-RNAi^{VDRC1}; RasV^{12}*). **A)** The BRGC images of *PG>Spen-RNAi^{VDRC1}; RasV^{12}*, *Spen-RNAi^{VDRC1}* and control animals. DAPI: Nuclei dye, GFP: the signal of the *PhmN1-GAL4* driver. **B)** Survival analysis of *PG>Spen-RNAi^{VDRC1}; RasV^{12}* compared to *Spen-RNAi^{VDRC1}* and control animals. Error bars indicate standard deviation among three replicates of 3rd instar larval (L3), pupae (P) and adults (Ad). **C)** Relative expression analysis of *Torso*, *Notch* and *Ras85D* genes in the *Spen-RNAi ^{VDRC1}* animals via qPCR. The expression of genes was measured by collecting RG samples from RNAi animals. The error bars represent 95% confidence intervals between the replicates. The significance asterisks determine the P-value of the student's t-test analysis (*$p < 0.05$ and ***$p < 0.01$) between control and experimental samples.

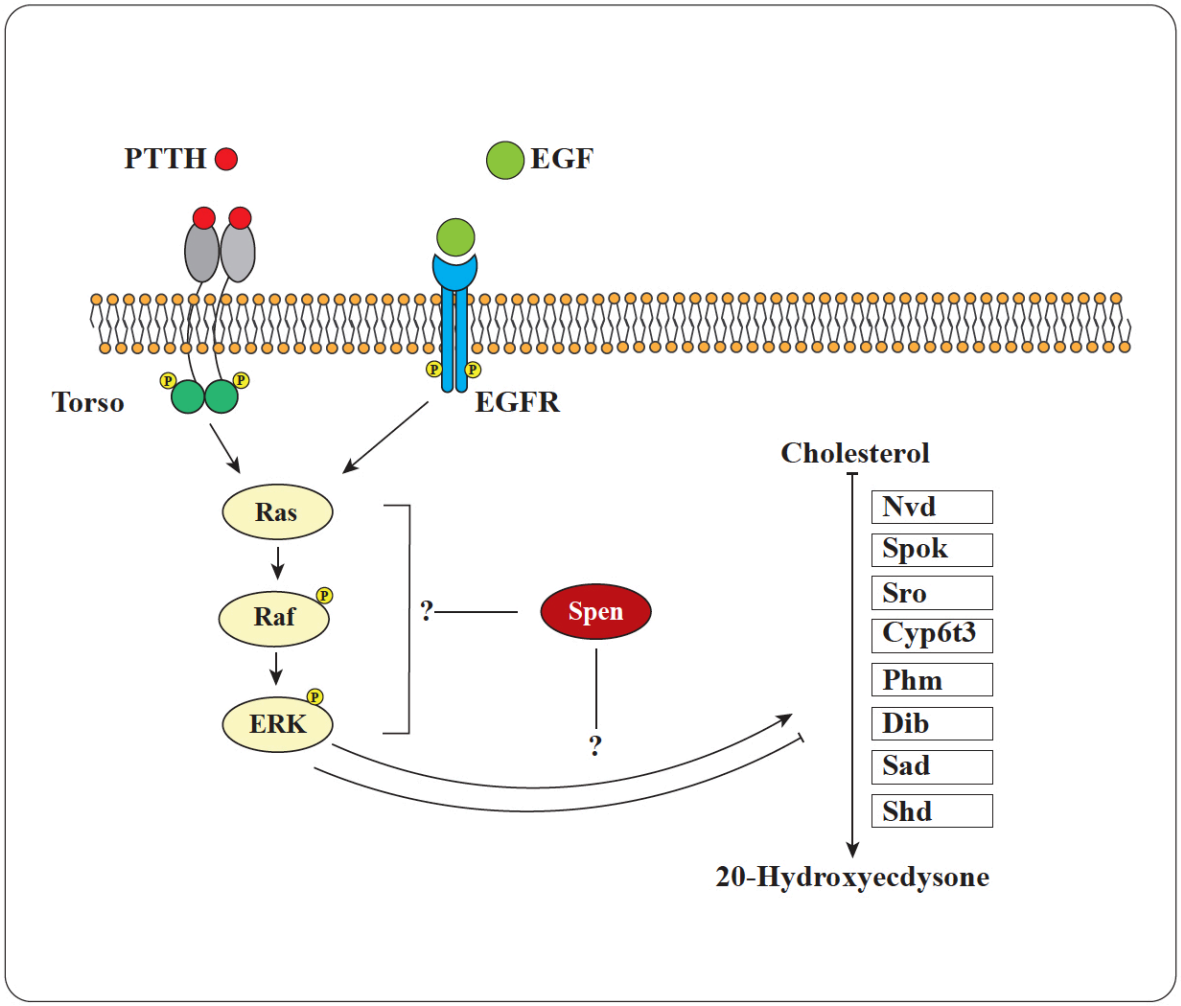

Figure 5. 7 A model for Spen function in PG cells

The downstream transcription factors of MAPK/ERK signaling cascade have been demonstrated to inhibit or induce ecdysone production in PG cells [114]. The binding of Prothoracicotropic hormone (PTTH) to Torso or EGF to EGFR activates the MAPK/ERK pathway. Once ligands are bound to receptors, it recruits Ras (Ras85D) that activates Raf oncogene (Raf) and Extracellular signal-regulated kinase (ERK), respectively. ERK is then activating target transcription factors that govern the expression of the Halloween genes. Spen may govern the MAPK/ERK proteins directly at the mRNA level or the expression of downstream transcription factors in the nucleus.

References

1. Cantu, D., Schaack, J. & Patel, M. Oxidative inactivation of mitochondrial aconitase results in iron and H2O2-mediated neurotoxicity in rat primary mesencephalic cultures. *PLoS One* **4**, e7095 (2009).
2. Koorts, A. M. & Viljoen, M. Ferritin and ferritin isoforms I: Structure–function relationships, synthesis, degradation and secretion. *Archives of physiology and biochemistry* **113**, 30-54 (2007).
3. Lill, R. Function and biogenesis of iron-sulphur proteins. *Nature* **460**, 831-838 (2009).
4. Netz, D. J. et al. Eukaryotic DNA polymerases require an iron-sulfur cluster for the formation of active complexes. *Nat Chem Biol* **8**, 125-132 (2011).
5. Philpott, C. C., Ryu, M. S., Frey, A. & Patel, S. Cytosolic iron chaperones: Proteins delivering iron cofactors in the cytosol of mammalian cells. *J Biol Chem* **292**, 12764-12771 (2017).
6. Rouault, T. A. & Tong, W.-H. Iron–sulphur cluster biogenesis and mitochondrial iron homeostasis. *Nature Reviews Molecular Cell Biology* **6**, 345-351 (2005).
7. Shouman, B. O., Mesbah, A. & Aly, H. Iron metabolism and lipid peroxidation products in infants with hypoxic ischemic encephalopathy. *J Perinatol* **28**, 487-491 (2008).
8. Yiannikourides, A. & Latunde-Dada, G. O. A Short Review of Iron Metabolism and Pathophysiology of Iron Disorders. *Medicines (Basel)* **6**, (2019).
9. Tvrda, E., Peer, R., Sikka, S. C. & Agarwal, A. Iron and copper in male reproduction: a double-edged sword. *J Assist Reprod Genet* **32**, 3-16 (2015).
10. Reddy, S. et al. Immunity, transferrin, and survival in kwashiorkor. *Br Med J* **4**, 268-270 (1970).
11. Andrews, N. C. Iron metabolism: iron deficiency and iron overload. *Annual review of genomics and human genetics* **1**, 75-98 (2000).
12. Batts, K. P. Iron overload syndromes and the liver. *Modern Pathology* **20**, S31-S39 (2007).
13. Bajoria, R. & Chatterjee, R. Hypogonadotrophic hypogonadism and diminished gonadal reserve accounts for dysfunctional gametogenesis in thalassaemia patients with iron overload presenting with infertility. *Hemoglobin* **35**, 636-642 (2011).
14. Santos, P. C. J. D. L. et al. Non-HFE hemochromatosis. *Revista brasileira de hematologia e hemoterapia* **34**, 311-316 (2012).
15. Fonseca-Nunes, A., Jakszyn, P. & Agudo, A. Iron and cancer risk—a systematic review and meta-analysis of the epidemiological evidence. *Cancer epidemiology and prevention biomarkers* **23**, 12-31 (2014).
16. Manz, D. H., Blanchette, N. L., Paul, B. T., Torti, F. M. & Torti, S. V. Iron and cancer: recent insights. *Annals of the New York Academy of Sciences* **1368**, 149 (2016).
17. Steegmann-Olmedillas, J. L. The role of iron in tumour cell proliferation. *Clin Transl Oncol* **13**, 71-76 (2011).
18. Frazer, D. M. & Anderson, G. J. The regulation of iron transport. *Biofactors* **40**, 206-214 (2014).
19. Carpenter, C. E. & Mahoney, A. W. Contributions of heme and nonheme iron to human nutrition. *Crit Rev Food Sci Nutr* **31**, 333-367 (1992).
20. Pantopoulos, K., Porwal, S. K., Tartakoff, A. & Devireddy, L. Mechanisms of mammalian iron homeostasis. *Biochemistry* **51**, 5705-5724 (2012).
21. Muckenthaler, M. U., Rivella, S., Hentze, M. W. & Galy, B. A Red Carpet for Iron Metabolism. *Cell* **168**, 344-361 (2017).

22. McKie, A. T. The role of Dcytb in iron metabolism: an update. *Biochem Soc Trans* **36**, 1239-1241 (2008).
23. Knutson, M. D. Iron transport proteins: gateways of cellular and systemic iron homeostasis. *Journal of Biological Chemistry* **292**, 12735-12743 (2017).
24. Garrick, M. D. et al. DMT1: a mammalian transporter for multiple metals. *Biometals* **16**, 41-54 (2003).
25. Yanatori, I. & Kishi, F. DMT1 and iron transport. *Free Radic Biol Med* **133**, 55-63 (2019).
26. Fuqua, B. K. et al. The multicopper ferroxidase hephaestin enhances intestinal iron absorption in mice. *PLoS One* **9**, e98792 (2014).
27. Jiang, R. et al. Hephaestin and ceruloplasmin play distinct but interrelated roles in iron homeostasis in mouse brain. *J Nutr* **145**, 1003-1009 (2015).
28. Petrak, J. & Vyoral, D. Hephaestin--a ferroxidase of cellular iron export. *Int J Biochem Cell Biol* **37**, 1173-1178 (2005).
29. Lambert, L. A., Perri, H., Halbrooks, P. J. & Mason, A. B. Evolution of the transferrin family: conservation of residues associated with iron and anion binding. *Comp Biochem Physiol B Biochem Mol Biol* **142**, 129-141 (2005).
30. Kawabata, H. Transferrin and transferrin receptors update. *Free Radic Biol Med* **133**, 46-54 (2019).
31. Aisen, P., Enns, C. & Wessling-Resnick, M. Chemistry and biology of eukaryotic iron metabolism. *The international journal of biochemistry & cell biology* **33**, 940-959 (2001).
32. Brummett, L. M., Kanost, M. R. & Gorman, M. J. The immune properties of Manduca sexta transferrin. *Insect Biochem Mol Biol* **81**, 1-9 (2017).
33. Cheng, Y., Zak, O., Aisen, P., Harrison, S. C. & Walz, T. Structure of the human transferrin receptor-transferrin complex. *Cell* **116**, 565-576 (2004).
34. Gammella, E., Buratti, P., Cairo, G. & Recalcati, S. The transferrin receptor: the cellular iron gate. *Metallomics* **9**, 1367-1375 (2017).
35. Gkouvatsos, K., Papanikolaou, G. & Pantopoulos, K. Regulation of iron transport and the role of transferrin. *Biochim Biophys Acta* **1820**, 188-202 (2012).
36. Zhao, N. & Enns, C. A. Iron transport machinery of human cells: Players and their interactions. *Current topics in membranes* **69**, 67-93 (2012).
37. Changyi J, D. J. Molecular mechanisms of non-transferrin-bound and transferring-bound iron uptake in primary hippocampal neurons. *Journal of Neurochemistry* **133**, (2015).
38. Sterling, J. et al. Iron importers Zip8 and Zip14 are expressed in retina and regulated by retinal iron levels. *Exp Eye Res* **155**, 15-23 (2017).
39. Fisher, J. et al. Ferritin: a novel mechanism for delivery of iron to the brain and other organs. *Am J Physiol Cell Physiol* **293**, C641-9 (2007).
40. Meyron-Holtz, E. G., Moshe-Belizowski, S. & Cohen, L. A. A possible role for secreted ferritin in tissue iron distribution. *J Neural Transm (Vienna)* **118**, 337-347 (2011).
41. Meyron-Holtz, E. G. et al. Ferritin polarization and iron transport across monolayer epithelial barriers in mammals. *Front Pharmacol* **5**, 194 (2014).
42. Friedman, A., Arosio, P., Finazzi, D., Koziorowski, D. & Galazka-Friedman, J. Ferritin as an important player in neurodegeneration. *Parkinsonism Relat Disord* **17**, 423-430 (2011).
43. González-Morales, N., Mendoza-Ortíz, M. Á., Blowes, L. M., Missirlis, F. & Riesgo-Escovar, J. R. Ferritin Is Required in Multiple Tissues during Drosophila melanogaster Development. *PLoS One* **10**, e0133499 (2015).
44. Levi, S. & Arosio, P. Mitochondrial ferritin. *Int J Biochem Cell Biol* **36**, 1887-1889 (2004).

45. Alkhateeb, A. A. & Connor, J. R. Nuclear ferritin: A new role for ferritin in cell biology. *Biochim Biophys Acta* **1800**, 793-797 (2010).
46. Thompson, K. J., Fried, M. G., Ye, Z., Boyer, P. & Connor, J. R. Regulation, mechanisms and proposed function of ferritin translocation to cell nuclei. *Journal of cell science* **115**, 2165-2177 (2002).
47. Asano, T. et al. Distinct mechanisms of ferritin delivery to lysosomes in iron-depleted and iron-replete cells. *Mol Cell Biol* **31**, 2040-2052 (2011).
48. Dowdle, W. E. et al. Selective VPS34 inhibitor blocks autophagy and uncovers a role for NCOA4 in ferritin degradation and iron homeostasis in vivo. *Nat Cell Biol* **16**, 1069-1079 (2014).
49. Santana-Codina, N. & Mancias, J. D. The Role of NCOA4-Mediated Ferritinophagy in Health and Disease. *Pharmaceuticals (Basel)* **11**, (2018).
50. Srivastava, A. K. et al. Thermodynamic and Kinetic Studies of the Interaction of Nuclear Receptor Coactivator-4 (NCOA4) with Human Ferritin. *Biochemistry* **59**, 2707-2717 (2020).
51. Rouault, T. A. The role of iron regulatory proteins in mammalian iron homeostasis and disease. *Nat Chem Biol* **2**, 406-414 (2006).
52. Wilkinson, N. & Pantopoulos, K. The IRP/IRE system in vivo: insights from mouse models. *Front Pharmacol* **5**, 176 (2014).
53. Dutkiewicz, R. & Nowak, M. Molecular chaperones involved in mitochondrial iron-sulfur protein biogenesis. *J Biol Inorg Chem* **23**, 569-579 (2018).
54. Jiang, H. et al. Up-regulation of divalent metal transporter 1 in 6-hydroxydopamine intoxication is IRE/IRP dependent. *Cell Res* **20**, 345-356 (2010).
55. Miyazawa, M., Bogdan, A. R., Hashimoto, K. & Tsuji, Y. Regulation of transferrin receptor-1 mRNA by the interplay between IRE-binding proteins and miR-7/miR-141 in the 3′-IRE stem–loops. *Rna* **24**, 468-479 (2018).
56. Andrews, N. C. Forging a field: the golden age of iron biology. *Blood* **112**, 219-230 (2008).
57. Nemeth, E. et al. Hepcidin regulates cellular iron efflux by binding to ferroportin and inducing its internalization. *science* **306**, 2090-2093 (2004).
58. Brasse-Lagnel, C. et al. Intestinal DMT1 cotransporter is down-regulated by hepcidin via proteasome internalization and degradation. *Gastroenterology* **140**, 1261-1271.e1 (2011).
59. Atanasiu, V., Manolescu, B. & Stoian, I. Hepcidin--central regulator of iron metabolism. *Eur J Haematol* **78**, 1-10 (2007).
60. D'Alessio, F., Hentze, M. W. & Muckenthaler, M. U. The hemochromatosis proteins HFE, TfR2, and HJV form a membrane-associated protein complex for hepcidin regulation. *Journal of hepatology* **57**, 1052-1060 (2012).
61. Mandilaras, K., Pathmanathan, T. & Missirlis, F. Iron absorption in Drosophila melanogaster. *Nutrients* **5**, 1622-1647 (2013).
62. Geiser, D. L. & Winzerling, J. J. Insect transferrins: multifunctional proteins. *Biochim Biophys Acta* **1820**, 437-451 (2012).
63. Xiao, G., Liu, Z. H., Zhao, M., Wang, H. L. & Zhou, B. Transferrin 1 Functions in Iron Trafficking and Genetically Interacts with Ferritin in Drosophila melanogaster. *Cell Rep* **26**, 748-758.e5 (2019).
64. Dunkov, B. & Georgieva, T. Insect iron binding proteins: insights from the genomes. *Insect Biochem Mol Biol* **36**, 300-309 (2006).

65. Tiklová, K., Senti, K. A., Wang, S., Gräslund, A. & Samakovlis, C. Epithelial septate junction assembly relies on melanotransferrin iron binding and endocytosis in Drosophila. *Nat Cell Biol* **12**, 1071-1077 (2010).
66. Mehta, A., Deshpande, A., Bettedi, L. & Missirlis, F. Ferritin accumulation under iron scarcity in Drosophila iron cells. *Biochimie* **91**, 1331-1334 (2009).
67. Tang, X. & Zhou, B. Ferritin is the key to dietary iron absorption and tissue iron detoxification in Drosophila melanogaster. *The FASEB Journal* **27**, 288-298 (2013).
68. Metzendorf, C. & Lind, M. I. Drosophila mitoferrin is essential for male fertility: evidence for a role of mitochondrial iron metabolism during spermatogenesis. *BMC Dev Biol* **10**, 68 (2010).
69. Missirlis, F. et al. Characterization of mitochondrial ferritin in Drosophila. *Proceedings of the National Academy of Sciences* **103**, 5893-5898 (2006).
70. Huynh, N., Ou, Q., Cox, P., Lill, R. & King-Jones, K. Glycogen branching enzyme controls cellular iron homeostasis via Iron Regulatory Protein 1 and mitoNEET. *Nat Commun* **10**, 5463 (2019).
71. Fernández-Moreno, M. A., Farr, C. L., Kaguni, L. S. & Garesse, R. Drosophila melanogaster as a model system to study mitochondrial biology. *Methods Mol Biol* **372**, 33-49 (2007).
72. Thummel, C. S. Molecular mechanisms of developmental timing in C. elegans and Drosophila. *Developmental Cell* **Vol. 1**, 453-465
73. Peper, J. S. et al. Sex steroids and brain structure in pubertal boys and girls. *Psychoneuroendocrinology* **34**, 332-342 (2009).
74. Shibata, S. & Fujita, T. The kidneys and aldosterone/mineralocorticoid receptor system in salt-sensitive hypertension. *Curr Hypertens Rep* **13**, 109-115 (2011).
75. Ropero, A. B., Alonso-Magdalena, P., Quesada, I. & Nadal, A. The role of estrogen receptors in the control of energy and glucose homeostasis. *Steroids* **73**, 874-879 (2008).
76. Furay, A. R., Bruestle, A. E. & Herman, J. P. The role of the forebrain glucocorticoid receptor in acute and chronic stress. *Endocrinology* **149**, 5482-5490 (2008).
77. Guengerich, F. P., Waterman, M. R. & Egli, M. Recent Structural Insights into Cytochrome P450 Function. *Trends Pharmacol Sci* **37**, 625-640 (2016).
78. Hall, P. F. Role of cytochromes P-450 in the biosynthesis of steroid hormones. *Vitam Horm* **42**, 315-368 (1985).
79. Pan, X., Connacher, R. P. & O'Connor, M. B. Control of the insect metamorphic transition by ecdysteroid production and secretion. *Curr Opin Insect Sci* **43**, 11-20 (2020).
80. Rewitz, K. F., O'Connor, M. B. & Gilbert, L. I. Molecular evolution of the insect Halloween family of cytochrome P450s: phylogeny, gene organization and functional conservation. *Insect Biochem Mol Biol* **37**, 741-753 (2007).
81. Gilbert, L. I. Halloween genes encode P450 enzymes that mediate steroid hormone biosynthesis in Drosophila melanogaster. *Molecular and Cellular Endocrinology* **215**, 1-10 (2004).
82. Yoshiyama, T., Namiki, T., Mita, K., Kataoka, H. & Niwa, R. Neverland is an evolutionally conserved Rieske-domain protein that is essential for ecdysone synthesis and insect growth. *Development* **133**, 2565-2574 (2006).
83. Ou, Q., Magico, A. & King-Jones, K. Nuclear receptor DHR4 controls the timing of steroid hormone pulses during Drosophila development. *PLoS Biol* **9**, e1001160 (2011).

84. Ou, Q. et al. The Insect Prothoracic Gland as a Model for Steroid Hormone Biosynthesis and Regulation. *Cell Rep* **16**, 247-262 (2016).
85. Simcox, J. A. et al. Dietary iron controls circadian hepatic glucose metabolism through heme synthesis. *Diabetes* **64**, 1108-1119 (2015).
86. Tsiftsoglou, A. S., Tsamadou, A. I. & Papadopoulou, L. C. Heme as key regulator of major mammalian cellular functions: molecular, cellular, and pharmacological aspects. *Pharmacol Ther* **111**, 327-345 (2006).
87. Ferreira, G. C. Heme biosynthesis: biochemistry, molecular biology, and relationship to disease. *Journal of bioenergetics and biomembranes* **27**, 147-150 (1995).
88. Layer, G., Reichelt, J., Jahn, D. & Heinz, D. W. Structure and function of enzymes in heme biosynthesis. *Protein Sci* **19**, 1137-1161 (2010).
89. Wu, N., Yin, L., Hanniman, E. A., Joshi, S. & Lazar, M. A. Negative feedback maintenance of heme homeostasis by its receptor, Rev-erbalpha. *Genes Dev* **23**, 2201-2209 (2009).
90. Kim, J., Lim, S.-H., Yoon, Y., Thangadurai, T. D. & Yoon, S. A fluorescent ammonia sensor based on a porphyrin cobalt(II)–dansyl complex. *Tetrahedron Letters* **52**, 2645-2648 (2011).
91. Masilamani, V., Al-Zhrani, K., Al-Salhi, M., Al-Diab, A. & Al-Ageily, M. Cancer diagnosis by autofluorescence of blood components. *Journal of Luminescence* **109**, 143-154 (2004).
92. de Oliveira Silva, F. R. et al. Intrinsic fluorescence of protoporphyrin IX from blood samples can yield information on the growth of prostate tumours. *J Fluoresc* **20**, 1159-1165 (2010).
93. Khan, A. A. & Quigley, J. G. Control of intracellular heme levels: heme transporters and heme oxygenases. *Biochim Biophys Acta* **1813**, 668-682 (2011).
94. Lesuisse, E. et al. Iron use for haeme synthesis is under control of the yeast frataxin homologue (Yfh1). *Hum Mol Genet* **12**, 879-889 (2003).
95. Correia, M. A., Sinclair, P. R. & De Matteis, F. Cytochrome P450 regulation: the interplay between its heme and apoprotein moieties in synthesis, assembly, repair, and disposal. *Drug Metab Rev* **43**, 1-26 (2011).
96. Kumar, S. & Bandyopadhyay, U. Free heme toxicity and its detoxification systems in human. *Toxicol Lett* **157**, 175-188 (2005).
97. Chiang, S. K., Chen, S. E. & Chang, L. C. A Dual Role of Heme Oxygenase-1 in Cancer Cells. *Int J Mol Sci* **20**, (2018).
98. Besur, S., Schmeltzer, P. & Bonkovsky, H. L. Acute Porphyrias. *J Emerg Med* **49**, 305-312 (2015).
99. Schulenburg-Brand, D., Katugampola, R., Anstey, A. V. & Badminton, M. N. The cutaneous porphyrias. *Dermatol Clin* **32**, 369-84, ix (2014).
100. Edel, Y. & Mamet, R. Porphyria: What Is It and Who Should Be Evaluated. *Rambam Maimonides Med J* **9**, (2018).
101. To-Figueras, J. et al. ALAS2 acts as a modifier gene in patients with congenital erythropoietic porphyria. *Blood* **118**, 1443-1451 (2011).
102. Strober, W. Trypan Blue Exclusion Test of Cell Viability. *Curr Protoc Immunol* **111**, A3.B.1-A3.B.3 (2015).

103. Daniels, R. W., Rossano, A. J., Macleod, G. T. & Ganetzky, B. Expression of multiple transgenes from a single construct using viral 2A peptides in Drosophila. *PLoS One* **9**, e100637 (2014).
104. Wang, J. W., Beck, E. S. & McCabe, B. D. A modular toolset for recombination transgenesis and neurogenetic analysis of Drosophila. *PLoS One* **7**, e42102 (2012).
105. Gratz, S. J. et al. Highly specific and efficient CRISPR/Cas9-catalyzed homology-directed repair in Drosophila. *Genetics* **196**, 961-971 (2014).
106. Linford, A. et al. Rab14 and its exchange factor FAM116 link endocytic recycling and adherens junction stability in migrating cells. *Dev Cell* **22**, 952-966 (2012).
107. Li, H. et al. The Sequence Alignment/Map format and SAMtools. *Bioinformatics* **25**, 2078-2079 (2009).
108. Anders, S., Pyl, P. T. & Huber, W. HTSeq--a Python framework to work with high-throughput sequencing data. *Bioinformatics* **31**, 166-169 (2015).
109. Jolliffe, I. T. in *Principal component analysis* 129-155 (Springer, 1986).
110. Jolliffe, I. T. & Cadima, J. Principal component analysis: a review and recent developments. *... Transactions of the Royal Society A ...* (2016).
111. Ringnér, M. What is principal component analysis. *Nature biotechnology* (2008).
112. Hiroyasu, A., DeWitt, D. C. & Goodman, A. G. Extraction of Hemocytes from Drosophila melanogaster Larvae for Microbial Infection and Analysis. *J Vis Exp* (2018).
113. Yamanaka, N., Rewitz, K. F. & O'Connor, M. B. Ecdysone control of developmental transitions: lessons from Drosophila research. *Annu Rev Entomol* **58**, 497-516 (2013).
114. Ou, Q. & King-Jones, K. What goes up must come down: transcription factors have their say in making ecdysone pulses. *Curr Top Dev Biol* **103**, 35-71 (2013).
115. Lavrynenko, O. et al. The ecdysteroidome of Drosophila: influence of diet and development. *Development* **142**, 3758-3768 (2015).
116. Conrad, M. E. & Umbreit, J. N. Iron absorption and transport—an update. *American journal of hematology* **64**, 287-298 (2000).
117. Mills, E., Dong, X. P., Wang, F. & Xu, H. Mechanisms of brain iron transport: insight into neurodegeneration and CNS disorders. *Future Med Chem* **2**, 51-64 (2010).
118. Kobayashi, H. & Fukuda, M. Arf6, Rab11 and transferrin receptor define distinct populations of recycling endosomes. *Commun Integr Biol* **6**, e25036 (2013).
119. Higa, A., Mori, Y. & Kitamura, Y. Iron deficiency induces changes in riboflavin secretion and the mitochondrial electron transport chain in hairy roots of Hyoscyamus albus. *J Plant Physiol* **167**, 870-878 (2010).
120. Mackenzie, B. & Garrick, M. D. Iron Imports. II. Iron uptake at the apical membrane in the intestine. *Am J Physiol Gastrointest Liver Physiol* **289**, G981-6 (2005).
121. Iatsenko, I., Marra, A., Boquete, J. P., Peña, J. & Lemaitre, B. Iron sequestration by transferrin 1 mediates nutritional immunity in Drosophila melanogaster. *Proc Natl Acad Sci U S A* **117**, 7317-7325 (2020).
122. Guz, N., Attardo, G. M., Wu, Y. & Aksoy, S. Molecular aspects of transferrin expression in the tsetse fly (Glossina morsitans morsitans). *J Insect Physiol* **53**, 715-723 (2007).
123. do Nascimento, A. M., Cuvillier-Hot, V., Barchuk, A. R., Simões, Z. L. & Hartfelder, K. Honey bee (Apis mellifera) transferrin-gene structure and the role of ecdysteroids in the developmental regulation of its expression. *Insect Biochem Mol Biol* **34**, 415-424 (2004).
124. Kim, B. Y. et al. Insect transferrin functions as an antioxidant protein in a beetle larva. *Comp Biochem Physiol B Biochem Mol Biol* **150**, 161-169 (2008).

125. Truman-Rosentsvit, M. et al. Ferritin is secreted via 2 distinct nonclassical vesicular pathways. *Blood* **131**, 342-352 (2018).
126. Arndt, V. et al. Chaperone-assisted selective autophagy is essential for muscle maintenance. *Curr Biol* **20**, 143-148 (2010).
127. Dice, J. F. Chaperone-mediated autophagy. *Autophagy* **3**, 295-299 (2007).
128. Cuervo, A. M. & Wong, E. Chaperone-mediated autophagy: roles in disease and aging. *Cell Res* **24**, 92-104 (2014).
129. Mancias, J. D., Wang, X., Gygi, S. P., Harper, J. W. & Kimmelman, A. C. Quantitative proteomics identifies NCOA4 as the cargo receptor mediating ferritinophagy. *Nature* **509**, 105-109 (2014).
130. Moore, R. H., Millman, E. E., Alpizar-Foster, E., Dai, W. & Knoll, B. J. Rab11 regulates the recycling and lysosome targeting of beta2-adrenergic receptors. *J Cell Sci* **117**, 3107-3117 (2004).
131. Szatmári, Z. et al. Rab11 facilitates cross-talk between autophagy and endosomal pathway through regulation of Hook localization. *Mol Biol Cell* **25**, 522-531 (2014).
132. Lim, Y. S. & Tang, B. L. The Evi5 family in cellular physiology and pathology. *FEBS Lett* **587**, 1703-1710 (2013).
133. Dabbeekeh, J. T., Faitar, S. L., Dufresne, C. P. & Cowell, J. K. The EVI5 TBC domain provides the GTPase-activating protein motif for RAB11. *Oncogene* **26**, 2804-2808 (2007).
134. Faitar, S. L., Dabbeekeh, J. T., Ranalli, T. A. & Cowell, J. K. EVI5 is a novel centrosomal protein that binds to alpha- and gamma-tubulin. *Genomics* **86**, 594-605 (2005).
135. Faitar, S. L., Sossey-Alaoui, K., Ranalli, T. A. & Cowell, J. K. EVI5 protein associates with the INCENP-aurora B kinase-survivin chromosomal passenger complex and is involved in the completion of cytokinesis. *Exp Cell Res* **312**, 2325-2335 (2006).
136. Laflamme, C. et al. Evi5 promotes collective cell migration through its Rab-GAP activity. *J Cell Biol* **198**, 57-67 (2012).
137. Stenmark, H. Rab GTPases as coordinators of vesicle traffic. *Nat Rev Mol Cell Biol* **10**, 513-525 (2009).
138. Bernards, A. GAPs galore! A survey of putative Ras superfamily GTPase activating proteins in man and Drosophila. *Biochim Biophys Acta* **1603**, 47-82 (2003).
139. Pan, X., Eathiraj, S., Munson, M. & Lambright, D. G. TBC-domain GAPs for Rab GTPases accelerate GTP hydrolysis by a dual-finger mechanism. *Nature* **442**, 303-306 (2006).
140. Alcina, A. et al. Tag-SNP analysis of the GFI1-EVI5-RPL5-FAM69 risk locus for multiple sclerosis. *Eur J Hum Genet* **18**, 827-831 (2010).
141. D'Netto, M. J. et al. Risk alleles for multiple sclerosis in multiplex families. *Neurology* **72**, 1984-1988 (2009).
142. Didonna, A. et al. A non-synonymous single-nucleotide polymorphism associated with multiple sclerosis risk affects the EVI5 interactome. *Hum Mol Genet* **24**, 7151-7158 (2015).
143. Hoppenbrouwers, I. A. et al. EVI5 is a risk gene for multiple sclerosis. *Genes Immun* **9**, 334-337 (2008).
144. Johnson, B. A. et al. Multiple sclerosis susceptibility alleles in African Americans. *Genes Immun* **11**, 343-350 (2010).
145. Liu, J. et al. Association of EVI5 rs11808092, CD58 rs2300747, and CIITA rs3087456 polymorphisms with multiple sclerosis risk: A meta-analysis. *Meta Gene* **9**, 97-103 (2016).

146. Mazdeh, M. et al. Ecotropic Viral Integration Site 5 (EVI5) variants are associated with multiple sclerosis in Iranian population. *Mult Scler Relat Disord* **18**, 15-19 (2017).
147. Mowry, E. M. et al. Multiple sclerosis susceptibility genes: associations with relapse severity and recovery. *PLoS One* **8**, e75416 (2013).
148. Hametner, S. et al. Iron and neurodegeneration in the multiple sclerosis brain. *Ann Neurol* **74**, 848-861 (2013).
149. Chung, H. et al. Characterization of Drosophila melanogaster cytochrome P450 genes. *Proceedings of the National Academy of Sciences* **106**, 5731-5736 (2009).
150. Camadro, J. M., Ibraham, N. G. & Levere, R. D. Kinetic studies of human liver ferrochelatase. Role of endogenous metals. *J Biol Chem* **259**, 5678-5682 (1984).
151. Davidson, R. E., Chesters, C. J. & Reid, J. D. Metal ion selectivity and substrate inhibition in the metal ion chelation catalyzed by human ferrochelatase. *J Biol Chem* **284**, 33795-33799 (2009).
152. Hunter, G. A., Sampson, M. P. & Ferreira, G. C. Metal ion substrate inhibition of ferrochelatase. *Journal of Biological Chemistry* (2008).
153. Jacobs, J. M. et al. Formation of zinc protoporphyrin in cultured hepatocytes: effects of ferrochelatase inhibition, iron chelation or lead. *Toxicology* **125**, 95-105 (1998).
154. Danielsen, E. T. et al. A Drosophila Genome-Wide Screen Identifies Regulators of Steroid Hormone Production and Developmental Timing. *Dev Cell* **37**, 558-570 (2016).
155. Gillingham, A. K., Sinka, R., Torres, I. L., Lilley, K. S. & Munro, S. Toward a comprehensive map of the effectors of rab GTPases. *Dev Cell* **31**, 358-373 (2014).
156. Zhang, J. et al. Thirty-one flavors of Drosophila rab proteins. *Genetics* **176**, 1307-1322 (2007).
157. Xiong, B. et al. Crag is a GEF for Rab11 required for rhodopsin trafficking and maintenance of adult photoreceptor cells. *PLoS Biol* **10**, e1001438 (2012).
158. Lock, J. G. & Stow, J. L. Rab11 in recycling endosomes regulates the sorting and basolateral transport of E-cadherin. *Molecular biology of the cell* **16**, 1744-1755 (2005).
159. Nichol, H., Law, J. H. & Winzerling, J. J. Iron metabolism in insects. *Annu Rev Entomol* **47**, 535-559 (2002).
160. Almagro Armenteros, J. J. et al. SignalP 5.0 improves signal peptide predictions using deep neural networks. *Nat Biotechnol* **37**, 420-423 (2019).
161. Nielsen, H., Engelbrecht, J. & Brunak…, S. Identification of prokaryotic and eukaryotic signal peptides and prediction of their cleavage sites. *Protein …* (1997).
162. Viotti, C. ER to Golgi-Dependent Protein Secretion: The Conventional Pathway. *Methods Mol Biol* **1459**, 3-29 (2016).
163. Nahorski, M. S. et al. Clathrin heavy chain 22 contributes to the control of neuropeptide degradation and secretion during neuronal development. *Sci Rep* **8**, 2340 (2018).
164. Rigg, R. A. et al. Heat shock protein 70 regulates platelet integrin activation, granule secretion and aggregation. *Am J Physiol Cell Physiol* **310**, C568-75 (2016).
165. Fang, X. et al. Dynamin Regulates Autophagy by Modulating Lysosomal Function. *J Genet Genomics* **43**, 77-86 (2016).
166. Uytterhoeven, V. et al. Hsc70-4 Deforms Membranes to Promote Synaptic Protein Turnover by Endosomal Microautophagy. *Neuron* **88**, 735-748 (2015).
167. Melkani, G. C. et al. TRiC/CCT chaperonins are essential for maintaining myofibril organization, cardiac physiological rhythm, and lifespan. *FEBS Lett* **591**, 3447-3458 (2017).

168. Koh, T. W. et al. Eps15 and Dap160 control synaptic vesicle membrane retrieval and synapse development. *J Cell Biol* **178**, 309-322 (2007).
169. Rewitz, K. F., Yamanaka, N., Gilbert, L. I. & O'Connor, M. B. The insect neuropeptide PTTH activates receptor tyrosine kinase torso to initiate metamorphosis. *Science* **326**, 1403-1405 (2009).
170. Melani, M., Simpson, K. J., Brugge, J. S. & Montell, D. Regulation of cell adhesion and collective cell migration by hindsight and its human homolog RREB1. *Curr Biol* **18**, 532-537 (2008).
171. Satoh, A. K., O'Tousa, J. E., Ozaki, K. & Ready, D. F. Rab11 mediates post-Golgi trafficking of rhodopsin to the photosensitive apical membrane of Drosophila photoreceptors. *Development* **132**, 1487-1497 (2005).
172. Rosas-Arellano, A. et al. Ferritin Assembly in Enterocytes of Drosophila melanogaster. *Int J Mol Sci* **17**, 27 (2016).
173. Junutula, J. R. et al. Rab14 is involved in membrane trafficking between the Golgi complex and endosomes. *Molecular biology of the cell* **15**, 2218-2229 (2004).
174. Morelli, E. et al. Multiple functions of the SNARE protein Snap29 in autophagy, endocytic, and exocytic trafficking during epithelial formation in Drosophila. *Autophagy* **10**, 2251-2268 (2014).
175. Ojelade, S. A. et al. cindr, the Drosophila Homolog of the CD2AP Alzheimer's Disease Risk Gene, Is Required for Synaptic Transmission and Proteostasis. *Cell Rep* **28**, 1799-1813.e5 (2019).
176. Salcini, A. E., Chen, H., Iannolo, G., De Camilli, P. & Di Fiore, P. P. Epidermal growth factor pathway substrate 15, Eps15. *The international journal of biochemistry & cell biology* **31**, 805-809 (1999).
177. Trombetta, E. S., Simons, J. F. & Helenius, A. Endoplasmic reticulum glucosidase II is composed of a catalytic subunit, conserved from yeast to mammals, and a tightly bound noncatalytic HDEL-containing subunit. *Journal of Biological Chemistry* **271**, 27509-27516 (1996).
178. Pennetta, G., Hiesinger, P. R., Fabian-Fine, R., Meinertzhagen, I. A. & Bellen, H. J. Drosophila VAP-33A directs bouton formation at neuromuscular junctions in a dosage-dependent manner. *Neuron* **35**, 291-306 (2002).
179. Namusamba, M. et al. Biological roles of the B cell receptor-associated protein 31: Functional Implication in Cancer. *Molecular Biology Reports* **48**, 773-786 (2021).
180. da Cruz Fernandes, M. et al. Iron localization in the guinea pig choroid plexus: A light and transmission electron microscopy study. *J Trace Elem Med Biol* **49**, 128-133 (2018).
181. Iancu, T. C. Ferritin and hemosiderin in pathological tissues. *Electron microscopy reviews* **5**, 209-229 (1992).
182. Kidane, T. Z., Sauble, E. & Linder, M. C. Release of iron from ferritin requires lysosomal activity. *Am J Physiol Cell Physiol* **291**, C445-55 (2006).
183. Bellelli, R. et al. NCOA4 Deficiency Impairs Systemic Iron Homeostasis. *Cell Rep* **14**, 411-421 (2016).
184. Lőrincz, P., Mauvezin, C. & Juhász, G. Exploring Autophagy in Drosophila. *Cells* **6**, (2017).
185. Mauvezin, C., Ayala, C., Braden, C. R., Kim, J. & Neufeld, T. P. Assays to monitor autophagy in Drosophila. *Methods* **68**, 134-139 (2014).

186. Morel, E. et al. Autophagy: A Druggable Process. *Annu Rev Pharmacol Toxicol* **57**, 375-398 (2017).
187. Nagy, P., Varga, Á., Kovács, A. L., Takáts, S. & Juhász, G. How and why to study autophagy in Drosophila: it's more than just a garbage chute. *Methods* **75**, 151-161 (2015).
188. Jacomin, A. C. et al. Impact of Autophagy and Aging on Iron Load and Ferritin in Drosophila Brain. *Front Cell Dev Biol* **7**, 142 (2019).
189. Dutkiewicz, R., Nowak, M., Craig, E. A. & Marszalek, J. Fe-S Cluster Hsp70 Chaperones: The ATPase Cycle and Protein Interactions. *Methods Enzymol* **595**, 161-184 (2017).
190. Puglisi, R. & Pastore, A. The role of chaperones in iron–sulfur cluster biogenesis. *FEBS Letters* **592**, 4011-4019 (2018).
191. Kruppa, A. J., Kendrick-Jones, J. & Buss, F. Myosins, Actin and Autophagy. *Traffic* **17**, 878-890 (2016).
192. Radisky, D. C. & Kaplan, J. Iron in cytosolic ferritin can be recycled through lysosomal degradation in human fibroblasts. *Biochemical Journal* (1998).
193. Missirlis, F. et al. Homeostatic mechanisms for iron storage revealed by genetic manipulations and live imaging of Drosophila ferritin. *Genetics* **177**, 89-100 (2007).
194. Roberts, T. M. et al. Identification and Characterisation of a pH-stable GFP. *Sci Rep* **6**, 28166 (2016).
195. LeVine, S. M. et al. Ferritin, transferrin and iron concentrations in the cerebrospinal fluid of multiple sclerosis patients. *Brain research* **821**, 511-515 (1999).
196. Craelius, W., Migdal, M. W., Luessenhop, C. P., Sugar, A. & Mihalakis, I. Iron deposits surrounding multiple sclerosis plaques. *Archives of pathology & laboratory medicine* **106**, 397-399 (1982).
197. Nezis, I. P. et al. Autophagic degradation of dBruce controls DNA fragmentation in nurse cells during late Drosophila melanogaster oogenesis. *J Cell Biol* **190**, 523-531 (2010).
198. Nichol, H., Law, J. H. & Winzerling, J. J. Iron metabolism in insects. *Annual review of entomology* **47**, 535-559 (2002).
199. Sheftel, A. D., Mason, A. B. & Ponka, P. The long history of iron in the Universe and in health and disease. *Biochim Biophys Acta* **1820**, 161-187 (2012).
200. Kalsbeck, W. A. et al. Structural and electronic properties of the heme cofactors in a multi-heme synthetic cytochrome. *Biochemistry* **35**, 3429-3438 (1996).
201. Andrews, N. C. Iron metabolism: iron deficiency and iron overload. *Annual review of genomics and human genetics* **1**, 75-98 (2000).
202. Ganz, T. & Nemeth, E. Hepcidin and iron homeostasis. *Biochim Biophys Acta* **1823**, 1434-1443 (2012).
203. Hentze, M. W., Muckenthaler, M. U., Galy, B. & Camaschella, C. Two to tango: regulation of Mammalian iron metabolism. *Cell* **142**, 24-38 (2010).
204. Singh, N. et al. Brain iron homeostasis: from molecular mechanisms to clinical significance and therapeutic opportunities. *Antioxid Redox Signal* **20**, 1324-1363 (2014).
205. Linert, W. & Kozlowski, H. *Metal ions in neurological systems* (Springer Science & Business Media, 2012).
206. White, A. R. *Metals in the Brain* (Humana Press, 2018).
207. Anderson, C. P., Shen, M., Eisenstein, R. S. & Leibold, E. A. Mammalian iron metabolism and its control by iron regulatory proteins. *Biochim Biophys Acta* **1823**, 1468-1483 (2012).
208. Eisenstein, R. S. & Blemings, K. P. Iron regulatory proteins, iron responsive elements and iron homeostasis. *The Journal of nutrition* (1998).

209. Lind, M. I. et al. Of two cytosolic aconitases expressed in Drosophila, only one functions as an iron-regulatory protein. *J Biol Chem* **281**, 18707-18714 (2006).
210. Thomson, A. M., Rogers, J. T. & Leedman, P. J. Iron-regulatory proteins, iron-responsive elements and ferritin mRNA translation. *The international journal of biochemistry & cell biology* **31**, 1139-1152 (1999).
211. Dev, S. & Babitt, J. L. Overview of iron metabolism in health and disease. *Hemodial Int* **21 Suppl 1**, S6-S20 (2017).
212. Gozzelino, R. & Arosio, P. Iron Homeostasis in Health and Disease. *Int J Mol Sci* **17**, (2016).
213. Grönke, S. et al. Dual lipolytic control of body fat storage and mobilization in Drosophila. *PLoS Biol* **5**, e137 (2007).
214. Ward, D. M. & Cloonan, S. M. Mitochondrial Iron in Human Health and Disease. *Annu Rev Physiol* **81**, 453-482 (2019).
215. Camaschella, C. Iron-deficiency anemia. *N Engl J Med* **372**, 1832-1843 (2015).
216. Muñoz, M., García-Erce, J. A. & Remacha, Á. F. Disorders of iron metabolism. Part II: iron deficiency and iron overload. *J Clin Pathol* **64**, 287-296 (2011).
217. Steinbicker, A. U. & Muckenthaler, M. U. Out of balance--systemic iron homeostasis in iron-related disorders. *Nutrients* **5**, 3034-3061 (2013).
218. Allen, K. J. et al. Iron-overload–related disease in HFE hereditary hemochromatosis. *New England Journal of Medicine* **358**, 221-230 (2008).
219. Anderson, E. R. & Shah, Y. M. Iron homeostasis in the liver. *Compr Physiol* **3**, 315-330 (2013).
220. Milic, S. et al. The Role of Iron and Iron Overload in Chronic Liver Disease. *Med Sci Monit* **22**, 2144-2151 (2016).
221. Puig, S., Askeland, E. & Thiele, D. J. Coordinated remodeling of cellular metabolism during iron deficiency through targeted mRNA degradation. *Cell* **120**, 99-110 (2005).
222. Gulec, S., Anderson, G. J. & Collins, J. F. Mechanistic and regulatory aspects of intestinal iron absorption. *Am J Physiol Gastrointest Liver Physiol* **307**, G397-409 (2014).
223. Rouault, T. A. Iron metabolism in the CNS: implications for neurodegenerative diseases. *Nat Rev Neurosci* **14**, 551-564 (2013).
224. Zhou, Z. D. & Tan, E. K. Iron regulatory protein (IRP)-iron responsive element (IRE) signaling pathway in human neurodegenerative diseases. *Mol Neurodegener* **12**, 75 (2017).
225. Ganz, T. & Nemeth, E. Iron homeostasis in host defence and inflammation. *Nature Reviews Immunology* **15**, 500-510 (2015).
226. Verbon, E. H. et al. Iron and immunity. *Annual review of phytopathology* **55**, (2017).
227. Ducey, T. F., Carson, M. B., Orvis, J., Stintzi, A. P. & Dyer, D. W. Identification of the Iron-Responsive Genes of Neisseria gonorrhoeae by Microarray Analysis in Defined Medium. *Journal of Bacteriology* **187**, 4865-4874 (2005).
228. Flanagan, J. M. et al. Microarray analysis of liver gene expression in iron overloaded patients with sickle cell anemia and beta-thalassemia. *Am J Hematol* **84**, 328-334 (2009).
229. Johnstone, D. & Milward, E. A. Genome-wide microarray analysis of brain gene expression in mice on a short-term high iron diet. *Neurochem Int* **56**, 856-863 (2010).
230. Kulshreshtha, R. et al. A microRNA signature of hypoxia. *Mol Cell Biol* **27**, 1859-1867 (2007).
231. Liu, Y., Popovich, Z. & Templeton, D. M. Global genomic approaches to the iron-regulated proteome. *Annals of Clinical & Laboratory Science* **35**, 230-239 (2005).

232. Singh, A. K., McIntyre, L. M. & Sherman, L. A. Microarray analysis of the genome-wide response to iron deficiency and iron reconstitution in the cyanobacterium Synechocystis sp. PCC 6803. *Plant Physiol* **132**, 1825-1839 (2003).
233. van de Mortel, J. E. et al. Large expression differences in genes for iron and zinc homeostasis, stress response, and lignin biosynthesis distinguish roots of Arabidopsis thaliana and the related metal hyperaccumulator Thlaspi caerulescens. *Plant Physiol* **142**, 1127-1147 (2006).
234. Yepiskoposyan, H. et al. Transcriptome response to heavy metal stress in Drosophila reveals a new zinc transporter that confers resistance to zinc. *Nucleic Acids Res* **34**, 4866-4877 (2006).
235. Zamboni, A. et al. Genome-wide microarray analysis of tomato roots showed defined responses to iron deficiency. *BMC Genomics* **13**, 101 (2012).
236. Zhou, Y. et al. Applying microarray-based technique to study and analyze silkworm (Bombyx mori) transcriptomic response to long-term high iron diet. *Genomics* **111**, 1504-1513 (2019).
237. Bolón-Canedo, V., Sánchez-Maroño, N., Alonso-Betanzos, A., Benítez, J. M. & Herrera, F. A review of microarray datasets and applied feature selection methods. *Information Sciences* **282**, 111-135 (2014).
238. Ramasamy, A., Mondry, A., Holmes, C. C. & Altman, D. G. Key issues in conducting a meta-analysis of gene expression microarray datasets. *PLoS Med* **5**, e184 (2008).
239. Fang, Z., Martin, J. & Wang, Z. Statistical methods for identifying differentially expressed genes in RNA-Seq experiments. *Cell Biosci* **2**, 26 (2012).
240. Zhang, Z. H. et al. A comparative study of techniques for differential expression analysis on RNA-Seq data. *PLoS One* **9**, e103207 (2014).
241. Conesa, A. et al. A survey of best practices for RNA-seq data analysis. *Genome Biol* **17**, 13 (2016).
242. Costa-Silva, J., Domingues, D. & Lopes, F. M. RNA-Seq differential expression analysis: An extended review and a software tool. *PloS one* **12**, (2017).
243. Oshlack, A., Robinson, M. D. & Young, M. D. From RNA-seq reads to differential expression results. *Genome Biol* **11**, 220 (2010).
244. Tang, X. & Zhou, B. Iron homeostasis in insects: Insights from Drosophila studies. *IUBMB Life* **65**, 863-872 (2013).
245. Winzerling, J. J. & Pham, D. Q. Iron metabolism in insect disease vectors: mining the Anopheles gambiae translated protein database. *Insect Biochem Mol Biol* **36**, 310-321 (2006).
246. Sewell, D., Burnet, B. & Connolly, K. Genetic analysis of larval feeding behaviour in Drosophila melanogaster. *Genetical Research* **24**, 163-173 (1974).
247. Love, M. I., Huber, W. & Anders, S. Moderated estimation of fold change and dispersion for RNA-seq data with DESeq2. *Genome Biol* **15**, 550 (2014).
248. Nookaew, I. et al. A comprehensive comparison of RNA-Seq-based transcriptome analysis from reads to differential gene expression and cross-comparison with microarrays: a case study in Saccharomyces cerevisiae. *Nucleic Acids Res* **40**, 10084-10097 (2012).
249. Robinson, M. D., McCarthy, D. J. & Smyth, G. K. edgeR: a Bioconductor package for differential expression analysis of digital gene expression data. *Bioinformatics* **26**, 139-140 (2010).

250. Bettencourt, B. R. & Feder, M. E. Hsp70 duplication in the Drosophila melanogaster species group: how and when did two become five. *Molecular biology and evolution* **18**, 1272-1282 (2001).
251. Kabani, M. & Martineau, C. N. Multiple hsp70 isoforms in the eukaryotic cytosol: mere redundancy or functional specificity. *Current genomics* **9**, 338-348 (2008).
252. van de Wetering, J. K., van Golde, L. M. & Batenburg, J. J. Collectins: players of the innate immune system. *Eur J Biochem* **271**, 1229-1249 (2004).
253. Ghazarian, H., Idoni, B. & Oppenheimer, S. B. A glycobiology review: carbohydrates, lectins and implications in cancer therapeutics. *Acta Histochem* **113**, 236-247 (2011).
254. Klang, I. M. et al. Iron promotes protein insolubility and aging in C. elegans. *Aging (Albany NY)* **6**, 975 (2014).
255. Singh, A., Severance, S., Kaur, N., Wiltsie, W. & Kosman, D. J. Assembly, activation, and trafficking of the Fet3p.Ftr1p high affinity iron permease complex in Saccharomyces cerevisiae. *J Biol Chem* **281**, 13355-13364 (2006).
256. Mittal, R. D., Pandey, A., Mittal, B. & Agarwal, K. N. Effect of latent iron deficiency on GABA and glutamate neuroreceptors in rat brain. *Indian Journal of Clinical Biochemistry* **18**, 111-116 (2003).
257. Knutson, M. D., Walter, P. B., Ames, B. N. & Viteri, F. E. Both iron deficiency and daily iron supplements increase lipid peroxidation in rats. *The Journal of nutrition* **130**, 621-628 (2000).
258. Stangl, G. I. & Kirchgessner, M. Different degrees of moderate iron deficiency modulate lipid metabolism of rats. *Lipids* **33**, 889-895 (1998).
259. Zafon, C., Lecube, A. & Simó, R. Iron in obesity. An ancient micronutrient for a modern disease. *Obes Rev* **11**, 322-328 (2010).
260. Zhang, J., Lewis, R. M., Wang, C., Hales, N. & Byrne, C. D. Maternal dietary iron restriction modulates hepatic lipid metabolism in the fetuses. *Am J Physiol Regul Integr Comp Physiol* **288**, R104-11 (2005).
261. Letelier, M. E., Sánchez-Jofré, S., Peredo-Silva, L., Cortés-Troncoso, J. & Aracena-Parks, P. Mechanisms underlying iron and copper ions toxicity in biological systems: Pro-oxidant activity and protein-binding effects. *Chem Biol Interact* **188**, 220-227 (2010).
262. Araújo, S. J., Aslam, H., Tear, G. & Casanova, J. mummy/cystic encodes an enzyme required for chitin and glycan synthesis, involved in trachea, embryonic cuticle and CNS development--analysis of its role in Drosophila tracheal morphogenesis. *Dev Biol* **288**, 179-193 (2005).
263. Merzendorfer, H. & Zimoch, L. Chitin metabolism in insects: structure, function and regulation of chitin synthases and chitinases. *J Exp Biol* **206**, 4393-4412 (2003).
264. Muthukrishnan, S., Merzendorfer, H., Arakane, Y. & Kramer, K. J. in *Insect Molecular Biology and Biochemistry* 193-235 (Elsevier, 2012).
265. Liu, H. & Kubli, E. Sex-peptide is the molecular basis of the sperm effect in Drosophila melanogaster. *Proceedings of the National Academy of Sciences* **100**, 9929-9933 (2003).
266. Tellier, A. P., Archambault, D., Tremblay, K. D. & Mager, J. The elongation factor Elof1 is required for mammalian gastrulation. *PloS one* **14**, (2019).
267. Xiao, G. & Zhou, B. ZIP13: A Study of Drosophila Offers an Alternative Explanation for the Corresponding Human Disease. *Front Genet* **8**, 234 (2017).

268. Maione, V., Cantini, F., Severi, M. & Banci, L. Investigating the role of the human CIA2A-CIAO1 complex in the maturation of aconitase. *Biochim Biophys Acta Gen Subj* **1862**, 1980-1987 (2018).
269. Stehling, O. et al. Human CIA2A-FAM96A and CIA2B-FAM96B integrate iron homeostasis and maturation of different subsets of cytosolic-nuclear iron-sulfur proteins. *Cell Metab* **18**, 187-198 (2013).
270. Gabler, M. et al. Trans-splicing of the mod(mdg4) complex locus is conserved between the distantly related species Drosophila melanogaster and D. virilis. *Genetics* **169**, 723-736 (2005).
271. Dorn, R. & Krauss, V. The modifier of mdg4 locus in Drosophila: functional complexity is resolved by trans splicing. *Genetica* **117**, 165-177 (2003).
272. Tikhonov, M., Utkina, M., Maksimenko, O. & Georgiev, P. Conserved sequences in the Drosophila mod(mdg4) intron promote poly(A)-independent transcription termination and trans-splicing. *Nucleic Acids Res* **46**, 10608-10618 (2018).
273. Bettedi, L., Aslam, M. F., Szular, J., Mandilaras, K. & Missirlis, F. Iron depletion in the intestines of Malvolio mutant flies does not occur in the absence of a multicopper oxidase. *J Exp Biol* **214**, 971-978 (2011).
274. Southon, A., Farlow, A., Norgate, M., Burke, R. & Camakaris, J. Malvolio is a copper transporter in Drosophila melanogaster. *J Exp Biol* **211**, 709-716 (2008).
275. Yeh, K.-Y., Yeh, M., Watkins, J. A., Rodriguez-Paris, J. & Glass, J. Dietary iron induces rapid changes in rat intestinal divalent metal transporter expression. *American Journal of Physiology-Gastrointestinal and Liver Physiology* **279**, G1070-G1079 (2000).
276. Ogishima, T., Kinoshita, J. Y., Mitani, F., Suematsu, M. & Ito, A. Identification of outer mitochondrial membrane cytochrome b5 as a modulator for androgen synthesis in Leydig cells. *J Biol Chem* **278**, 21204-21211 (2003).
277. Ma, A. G. et al. Retinol and riboflavin supplementation decreases the prevalence of anemia in Chinese pregnant women taking iron and folic acid supplements. *The Journal of nutrition* **138**, 1946-1950 (2008).
278. Schrader, M. & Fahimi, H. D. Peroxisomes and oxidative stress. *Biochim Biophys Acta* **1763**, 1755-1766 (2006).
279. Liu, L. et al. Biochemical characterization of three midgut chitin deacetylases of the Lepidopteran insect Bombyx mori. *J Insect Physiol* **113**, 42-48 (2019).
280. Ekiz, C., Agaoglu, L., Karakas, Z., Gurel, N. & Yalcin, I. The effect of iron deficiency anemia on the function of the immune system. *Hematol J* **5**, 579-583 (2005).
281. Hassan, T. H. et al. Impact of iron deficiency anemia on the function of the immune system in children. *Medicine (Baltimore)* **95**, e5395 (2016).
282. Verleyen, P. et al. Identification of new immune induced molecules in the haemolymph of Drosophila melanogaster by 2D-nanoLC MS/MS. *J Insect Physiol* **52**, 379-388 (2006).
283. Kawano, T. et al. Identification of a gene, Desiccate, contributing to desiccation resistance in Drosophila melanogaster. *J Biol Chem* **285**, 38889-38897 (2010).
284. Yu, L.-X., Djebrouni, M., Chamberland, H., Lafontaine, J. G. & Tabaeizadeh, Z. Chitinase: differential induction of gene expression and enzyme activity by drought stress in the wild (Lycopersicon chilense Dun.) and cultivated (L. esculentum Mill.) tomatoes. *Journal of plant physiology* **153**, 745-753 (1998).

285. D'Avino, P. P., Crispi, S. T. E. F. A. N. I. A. & Furia, M. A. R. I. A. Hormonal regulation of the Drosophila melanogaster ng-gene. *EUROPEAN JOURNAL OF ENTOMOLOGY* **92**, 259-259 (1995).
286. Karim, F. D. & Thummel, C. S. Temporal coordination of regulatory gene expression by the steroid hormone ecdysone. *The EMBO Journal* **11**, 4083-4093 (1992).
287. Danzeisen, R. et al. Superoxide dismutase 1 modulates expression of transferrin receptor. *J Biol Inorg Chem* **11**, 489-498 (2006).
288. Jung, I., Kim, T. Y. & Kim-Ha, J. Identification of Drosophila SOD3 and its protective role against phototoxic damage to cells. *FEBS Lett* **585**, 1973-1978 (2011).
289. Misra, H. P. & Fridovich, I. Purification and properties of superoxide dismutase from a red alga, Porphyridium cruentum. *Journal of Biological Chemistry* **252**, 6421-6423 (1977).
290. Molassiotis, A., Tanou, G., Diamantidis, G., Patakas, A. & Therios, I. Effects of 4-month Fe deficiency exposure on Fe reduction mechanism, photosynthetic gas exchange, chlorophyll fluorescence and antioxidant defense in two peach rootstocks differing in Fe deficiency tolerance. *J Plant Physiol* **163**, 176-185 (2006).
291. Leader, D. P., Krause, S. A., Pandit, A., Davies, S. A. & Dow, J. A. T. FlyAtlas 2: a new version of the Drosophila melanogaster expression atlas with RNA-Seq, miRNA-Seq and sex-specific data. *Nucleic Acids Res* **46**, D809-D815 (2018).
292. Goshima, G., Mayer, M., Zhang, N., Stuurman, N. & Vale, R. D. Augmin: a protein complex required for centrosome-independent microtubule generation within the spindle. *The Journal of Cell Biology* **181**, 421-429 (2008).
293. Goshima, G. et al. Genes required for mitotic spindle assembly in Drosophila S2 cells. *Science* **316**, 417-421 (2007).
294. Shevtsov, P. N., Shevtsova, E. F. & Burbaeva, G. S. Effect of Aluminum, Iron, and Zinc Ions on the Assembly of Microtubules from Brain Microtubule Proteins. *Bull Exp Biol Med* **161**, 451-455 (2016).
295. Yung, K. C. et al. Preliminary investigation about the expression of tubulin in platelets from patients with iron deficiency anemia and thrombocytosis. *Hematology* **23**, 549-557 (2018).
296. de Haro, M. et al. Detailed analysis of leucokinin-expressing neurons and their candidate functions in the Drosophila nervous system. *Cell Tissue Res* **339**, 321-336 (2010).
297. Radford, J. C., Davies, S. A. & Dow, J. A. T. Systematic G-protein-coupled Receptor Analysis inDrosophila melanogasterIdentifies a Leucokinin Receptor with Novel Roles. *Journal of Biological Chemistry* **277**, 38810-38817 (2002).
298. Laity, J. H., Lee, B. M. & Wright, P. E. Zinc finger proteins: new insights into structural and functional diversity. *Current opinion in structural biology* (2001).
299. Hoeft, K. et al. Iron Loading Exaggerates the Inflammatory Response to the Toll-like Receptor 4 Ligand Lipopolysaccharide by Altering Mitochondrial Homeostasis. *Anesthesiology* **127**, 121-135 (2017).
300. Aigner, E. et al. Iron stores, liver transaminase levels and metabolic risk in healthy teenagers. *Eur J Clin Invest* **40**, 155-163 (2010).
301. Guiran X, Z. W., Qiangwang F, Xiaona T, Bing Z. The metal transporter ZIP13 supplies iron into the secretory pathway in Drosophila melanogaster. *eLife*
302. Xu, J., Wan, Z. & Zhou, B. Drosophila ZIP13 is posttranslationally regulated by iron-mediated stabilization. *Biochimica et Biophysica Acta (BBA) - Molecular Cell Research* **1866**, 1487-1497 (2019).

303. Chen, K. et al. Loss of Frataxin induces iron toxicity, sphingolipid synthesis, and Pdk1/Mef2 activation, leading to neurodegeneration. *Elife* **5**, e16043 (2016).
304. Mi, H., Muruganujan, A., Ebert, D., Huang, X. & Thomas, P. D. PANTHER version 14: more genomes, a new PANTHER GO-slim and improvements in enrichment analysis tools. *Nucleic Acids Res* **47**, D419-D426 (2019).
305. Zimmermann, L. et al. A Completely Reimplemented MPI Bioinformatics Toolkit with a New HHpred Server at its Core. *J Mol Biol* **430**, 2237-2243 (2018).
306. Daniel, S. et al. Nuclear translocation of the phosphoprotein Hop (Hsp70/Hsp90 organizing protein) occurs under heat shock, and its proposed nuclear localization signal is involved in Hsp90 binding. *Biochim Biophys Acta* **1783**, 1003-1014 (2008).
307. Chen, Y. et al. Myeloid zinc-finger 1 (MZF-1) suppresses prostate tumor growth through enforcing ferroportin-conducted iron egress. *Oncogene* **34**, 3839-3847 (2015).
308. Zehr, J. P. & Turner, P. J. Nitrogen fixation: nitrogenase genes and gene expression. *Methods in microbiology* **30**, 271-286 (2001).
309. Courel, M., Lallet, S., Camadro, J. M. & Blaiseau, P. L. Direct activation of genes involved in intracellular iron use by the yeast iron-responsive transcription factor Aft2 without its paralog Aft1. *Mol Cell Biol* **25**, 6760-6771 (2005).
310. Fernández-Martín, K. G. et al. Genome-wide identification, in silico characterization and expression analysis of ZIP-like genes from Trichomonas vaginalis in response to Zinc and Iron. *Biometals* **30**, 663-675 (2017).
311. Qiang, W., Huang, Y., Wan, Z. & Zhou, B. Metal-metal interaction mediates the iron induction of Drosophila MtnB. *Biochem Biophys Res Commun* **487**, 646-652 (2017).
312. Andrews, M., Soto, N. & Arredondo-Olguín, M. Association between ferritin and hepcidin levels and inflammatory status in patients with type 2 diabetes mellitus and obesity. *Nutrition* **31**, 51-57 (2015).
313. Fernández-Real, J. M., López-Bermejo, A. & Ricart, W. Cross-talk between iron metabolism and diabetes. *Diabetes* **51**, 2348-2354 (2002).
314. Sikorska, K., Bernat, A. & Wroblewska, A. Molecular pathogenesis and clinical consequences of iron overload in liver cirrhosis. *Hepatobiliary Pancreat Dis Int* **15**, 461-479 (2016).
315. Silva, B. & Faustino, P. An overview of molecular basis of iron metabolism regulation and the associated pathologies. *Biochim Biophys Acta* **1852**, 1347-1359 (2015).
316. Zimmermann, M. B. & Hurrell, R. F. Nutritional iron deficiency. *The lancet* **370**, 511-520 (2007).
317. Robinson, M., McCarthy, D. J., Chen, Y. & Smyth, G. K. Package 'edger'. (2012).
318. Creagh, E. M., Sheehan, D. & Cotter, T. G. Heat shock proteins–modulators of apoptosis in tumour cells. *Leukemia* **14**, 1161-1173 (2000).
319. Kiang, J. G. & Tsokos, G. C. Heat shock protein 70 kDa: molecular biology, biochemistry, and physiology. *Pharmacology & therapeutics* **80**, 183-201 (1998).
320. Lee, G. J. & Vierling, E. A small heat shock protein cooperates with heat shock protein 70 systems to reactivate a heat-denatured protein. *Plant Physiology* **122**, 189-198 (2000).
321. Mayer, M. P. & Bukau, B. Hsp70 chaperones: cellular functions and molecular mechanism. *Cell Mol Life Sci* **62**, 670-684 (2005).
322. Aufricht, C. Heat-shock protein 70: molecular supertool. *Pediatr Nephrol* **20**, 707-713 (2005).

323. Cherayil, B. J. Iron and immunity: immunological consequences of iron deficiency and overload. *Arch Immunol Ther Exp (Warsz)* **58**, 407-415 (2010).
324. Drakesmith, H. & Prentice, A. M. Hepcidin and the iron-infection axis. *Science* **338**, 768-772 (2012).
325. Porto, G. & De Sousa, M. Iron overload and immunity. *World journal of gastroenterology: WJG* **13**, 4707 (2007).
326. Krauss, V. & Dorn, R. Evolution of the trans-splicing Drosophila locus mod(mdg4) in several species of Diptera and Lepidoptera. *Gene* **331**, 165-176 (2004).
327. Simó, A. L. R. Iron in obesity. An ancient micronutrient for a modern disease.
328. King-Jones, K., Charles, J. P., Lam, G. & Thummel, C. S. The ecdysone-induced DHR4 orphan nuclear receptor coordinates growth and maturation in Drosophila. *Cell* **121**, 773-784 (2005).
329. Sood, C., Doyle, S. E. & Siegrist, S. E. Steroid hormones, dietary nutrients, and temporal progression of neurogenesis. *Curr Opin Insect Sci* **43**, 70-77 (2020).
330. Beckstead, R. B., Lam, G. & Thummel, C. S. The genomic response to 20-hydroxyecdysone at the onset of Drosophila metamorphosis. *Genome Biol* **6**, R99 (2005).
331. King-Jones, K. & Thummel, C. S. Nuclear receptors--a perspective from Drosophila. *Nat Rev Genet* **6**, 311-323 (2005).
332. Annicotte, J. S. et al. The nuclear receptor liver receptor homolog-1 is an estrogen receptor target gene. *Oncogene* **24**, 8167-8175 (2005).
333. Kumar, R. et al. The dynamic structure of the estrogen receptor. *J Amino Acids* **2011**, 812540 (2011).
334. Liao, G. et al. Regulation of androgen receptor activity by the nuclear receptor corepressor SMRT. *J Biol Chem* **278**, 5052-5061 (2003).
335. Mirth, C., Truman, J. W. & Riddiford, L. M. The role of the prothoracic gland in determining critical weight for metamorphosis in Drosophila melanogaster. *Curr Biol* **15**, 1796-1807 (2005).
336. Cruz, J., Martín, D. & Franch-Marro, X. Egfr Signaling Is a Major Regulator of Ecdysone Biosynthesis in the Drosophila Prothoracic Gland. *Curr Biol* **30**, 1547-1554.e4 (2020).
337. McBrayer, Z. et al. Prothoracicotropic hormone regulates developmental timing and body size in Drosophila. *Dev Cell* **13**, 857-871 (2007).
338. Gibbens, Y. Y., Warren, J. T., Gilbert, L. I. & O'Connor, M. B. Neuroendocrine regulation of Drosophila metamorphosis requires TGFbeta/Activin signaling. *Development* **138**, 2693-2703 (2011).
339. Caldwell, P. E., Walkiewicz, M. & Stern, M. Ras activity in the Drosophila prothoracic gland regulates body size and developmental rate via ecdysone release. *Curr Biol* **15**, 1785-1795 (2005).
340. Kolodziej, P. A., Jan, L. Y. & Jan, Y. N. Mutations that affect the length, fasciculation, or ventral orientation of specific sensory axons in the Drosophila embryo. *Neuron* **15**, 273-286 (1995).
341. Kuang, B., Wu, S. C., Shin, Y., Luo, L. & Kolodziej, P. split ends encodes large nuclear proteins that regulate neuronal cell fate and axon extension in the Drosophila embryo. *Development* **127**, 1517-1529 (2000).
342. Chen, F. & Rebay, I. split ends, a new component of the Drosophila EGF receptor pathway, regulates development of midline glial cells. *Current biology* **10**, 943-S2 (2000).

343. Querenet, M., Goubard, V., Chatelain, G., Davoust, N. & Mollereau, B. Spen is required for pigment cell survival during pupal development in Drosophila. *Dev Biol* **402**, 208-215 (2015).
344. Chang, J. L., Lin, H. V., Blauwkamp, T. A. & Cadigan, K. M. Spenito and Split ends act redundantly to promote Wingless signaling. *Dev Biol* **314**, 100-111 (2008).
345. Doroquez, D. B., Orr-Weaver, T. L. & Rebay, I. Split ends antagonizes the Notch and potentiates the EGFR signaling pathways during Drosophila eye development. *Mech Dev* **124**, 792-806 (2007).
346. Lin, H. V. et al. Splits ends is a tissue/promoter specific regulator of Wingless signaling. *Development* **130**, 3125-3135 (2003).
347. Shi, Y. et al. Sharp, an inducible cofactor that integrates nuclear receptor repression and activation. *Genes & development* **15**, 1140-1151 (2001).
348. Foulds, C. E. et al. Research resource: expression profiling reveals unexpected targets and functions of the human steroid receptor RNA activator (SRA) gene. *Mol Endocrinol* **24**, 1090-1105 (2010).
349. Saito, J., Kimura, R., Kaieda, Y., Nishida, R. & Ono, H. Characterization of candidate intermediates in the Black Box of the ecdysone biosynthetic pathway in Drosophila melanogaster: Evaluation of molting activities on ecdysteroid-defective larvae. *J Insect Physiol* **93-94**, 94-104 (2016).
350. Go, M. J., Eastman, D. S. & Artavanis-Tsakonas, S. Cell proliferation control by Notch signaling in Drosophila development. *Development* **125**, 2031-2040 (1998).
351. Mumm, J. S. & Kopan, R. Notch signaling: from the outside in. *Dev Biol* **228**, 151-165 (2000).
352. Karim, F. D. & Rubin, G. M. Ectopic expression of activated Ras1 induces hyperplastic growth and increased cell death in Drosophila imaginal tissues. *Development* **125**, 1-9 (1998).
353. Manna, P. R. & Stocco, D. M. The role of specific mitogen-activated protein kinase signaling cascades in the regulation of steroidogenesis. *J Signal Transduct* **2011**, 821615 (2011).
354. Miller, W. L. Steroidogenic acute regulatory protein (StAR), a novel mitochondrial cholesterol transporter. *Biochim Biophys Acta* **1771**, 663-676 (2007).
355. Wu, C. H. et al. Mutant K-ras oncogene regulates steroidogenesis of normal human adrenocortical cells by the RAF-MEK-MAPK pathway. *Br J Cancer* **87**, 1000-1005 (2002).
356. Su, H., Liu, Y. & Zhao, X. Split end family RNA binding proteins: Novel tumor suppressors coupling transcriptional regulation with RNA processing. *Cancer translational medicine* **1**, 21 (2015).
357. Cross-talk between PRMT1-mediated methylation and ubiquitylation on RBM15 controls RNA splicing.
358. Xiao, N. et al. Ott1 (Rbm15) regulates thrombopoietin response in hematopoietic stem cells through alternative splicing of c-Mpl. *Blood* **125**, 941-948 (2015).
359. Camats, M., Kokolo, M., Heesom, K. J., Ladomery, M. & Bach-Elias, M. P19 H-ras induces G1/S phase delay maintaining cells in a reversible quiescence state. *PLoS One* **4**, e8513 (2009).

360. Siegfried, Z., Bonomi, S., Ghigna, C. & Karni, R. Regulation of the Ras-MAPK and PI3K-mTOR Signalling Pathways by Alternative Splicing in Cancer. *Int J Cell Biol* **2013**, 568931 (2013).

Appendices

A.1 Genome-wide RNAi screening for identifying Ecdysone and heme-related genes

In collaboration with Michael O'Connor's lab at the University of Minnesota, USA and Kim Rewitz's lab at the University of Copenhagen, Denmark, King-Jones lab carried out a two-step Gal4/UAS-RNAi screen (Figure A.1) [154]. The objective of the screen was to specifically disrupt gene expression in the Prothoracic gland (PG) via UAS-RNAi/GAL4 system to identify genes required for ecdysone biosynthesis.

In the first step, all the KK collection RNAi lines (12613 RNAi lines) of the VDRC stock center were used to knockdown genes specifically in the PG cells. The KK RNAi lines are transgenic flies that carry a small hairpin RNAi (shRNA) sequence for a target gene. The shRNA sequence is downstream of the GAL4 transcription factor UAS binding site (upstream activating sequence) and can knock down a target gene in a tissue-specific manner. The phm-GAL4 driver line was used in the RNAi screening as the PG-specific GAL4 driver for gene knockdown. In this transgenic line, the GAL4 transcription factor is under the control of the Phantom gene, which is a Halloween gene of the Ecdysone pathways. Upon first RNAi knockdown, 800 genes with deficiency phenotypes such as larval developmental arrest, larval developmental delay, pupae lethality and pupae delay were identified (Figure A.1 A) [154].

The second round of the screen was performed in the King-Jones' lab to identify genes with different ring glad morphology at the L3 larval stage. Out of 800 genes, a subset of 34 genes were found to have either overgrown ring glands (13 genes) or autofluorescence red enlarged ring glands (21 genes) under UV light exposure (or both). The subset includes genes with diverse functions such as heme genes (ALAS, UPDO, PPOX and FeCH), transcription regulatory proteins (Spen), enzymes, signaling proteins and a vesicle regulatory protein (Evi5) (Figure A.1 A and B).

From the 34 genes, I picked the Evi5 and Spen gene to study their functions in PG cells further. The PG depletion of *Evi5* resulted in a larval developmental delay with the autofluorescence overgrown ring glands (Chapter 3, Figure A.1 B). However, PG loss of *Spen* caused the Larval arrested phenotype with an overgrown ring gland (Chapter 5).

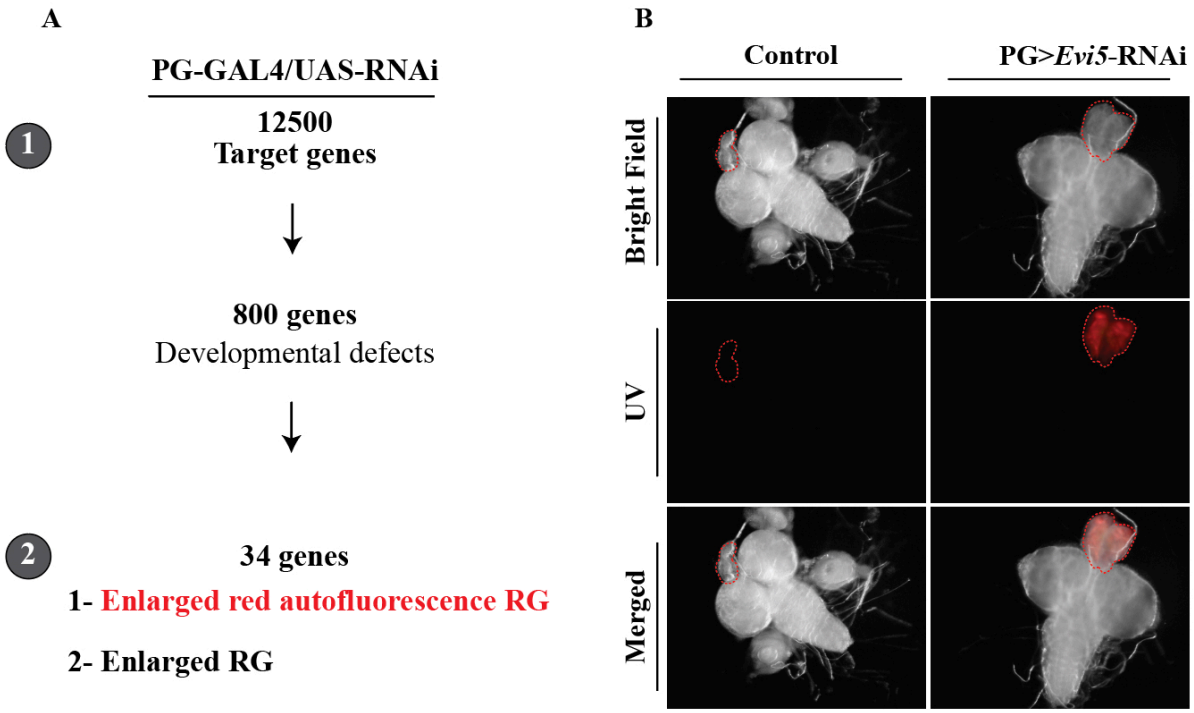

Figure A.1Genome-wide RNAi Screening.

A) An overview of the genome-wide RNAi screen steps (gray circles). In the first step, *Phm-GAL4* driver was used to knockdown 12500 genes specifically in PG-cells via GAL4/UAS-RNAi system. This step identified 800 genes that PG-specific loss of their function resulted in developmental defects associated with the ecdysone deficiency (such as larval and pupal developmental arrest or delay). In the second step out of 800 genes, a subset of 34 genes was identified that PG-specific depletion of their function caused enlarged red autofluorescence ring gland (RG) under UV light or only enlarged ring gland. **B)** An example of genes with the red autofluorescence ring gland (red dotted line). Brain and ring gland complex of PG>*Evi5*-RNAi and control animals. PG specific loss of function of Evi5 results in red autofluorescence ring gland under UV light compared to control.

A.2 Codes of RNA-sequencing analysis

In this section, the codes of the BRGC RNA-seq analysis are presented. The same codes were used for the gut and WB samples. These codes are written based on my experimental design, and for new experiments, the desired changes should be applied.

A.2.1 HISAT2 analysis code

This code is a Python software code.

Location of hisat2:

Users/sattarsoltani /software/hisat2-2.0.4/hisat2

Location of *Drosophila* BDGP6 reference genome:

data/Analysis/ https://genome-idx.s3.amazonaws.com/hisat/bdgp6.tar.gz/

Location of pair end RNA-seq files:

Users/sattarsoltani/Documents/sattar/RNA-file/

HI.4487.002.L2V12DR-BC1.FW-4-1_R2.fq

HI.4487.002.L2V12DR-BC2.FW-4-2_R1.fq

HI.4487.002.L2V12DR-BC3.BW-4-1_R2.fq

HI.4487.002.L2V12DR-BC4.BW-4-2_R1.fq

HI.4487.002.L2V12DR-BC4.BW-4-2_R2.fq

HI.4487.002.L2V12DR-BC5.FW-8-1_R2.fq

HI.4487.002.L2V12DR-BC6.FW-8-2_R1.fq

HI.4487.002.L2V12DR-BC6.FW-8-2_R2.fq

HI.4487.002.L2V12DR-BC7.BW-8-1_R1.fq

HI.4487.002.L2V12DR-BC7.BW-8-1_R2.fq

HI.4487.002.L2V12DR-BC8.BW-8-2_R2.fq

HI.4487.002.L2V12DR-BC9.Fw-12-1_R1.fq

HI.4487.002.L2V12DR-BC10.Fw-12-2_R2.fq

HI.4487.002.L2V12DR-BC11.BW-12-1_R1.fq

HI.4487.002.L2V12DR-BC12.Bw-12-2_R1.fq

HI.4487.002.L2V12DR-BC12.Bw-12-2_R2.fq

HI.4487.002.L2V12DR-BC13.FW-16-1_R2.fq

HI.4487.002.L2V12DR-BC14.FW-16-2_R1.fq

HI.4487.002.L2V12DR-BC14.FW-16-2_R2.fq

HI.4487.002.L2V12DR-BC15.BW-16-1_R1.fq

HI.4487.002.L2V12DR-BC16.BW-16-2_R2.fq

Mapping sequences to reference genome:

/home/yog/software/hisat2-2.0.4/hisat2 -p 8 -x /data/Analysis/ BDGP6 --fr -1 /data/Analysis/mapped/ HI.4487.002.L2V12DR-BC1.FW-4-1_R2.fq… HI.4487.002.L2V12DR-BC16.BW-16-2_R2.fq -2 /data/Analysis/mapped/ HI.4487.002.L2V12DR-BC1.FW-4-1_R2.sam… HI.4487.002.L2V12DR-BC16.BW-16-2_R2.sam

Outputs:

HI.4487.002.L2V12DR-BC1.FW-4-1_R2.sam

HI.4487.002.L2V12DR-BC2.FW-4-2_R1.sam

HI.4487.002.L2V12DR-BC3.BW-4-1_R2.sam

HI.4487.002.L2V12DR-BC4.BW-4-2_R1.sam

HI.4487.002.L2V12DR-BC4.BW-4-2_R2.sam

HI.4487.002.L2V12DR-BC5.FW-8-1_R2.sam

HI.4487.002.L2V12DR-BC6.FW-8-2_R1.sam

HI.4487.002.L2V12DR-BC6.FW-8-2_R2.sam

HI.4487.002.L2V12DR-BC7.BW-8-1_R1.sam

HI.4487.002.L2V12DR-BC7.BW-8-1_R2.sam

HI.4487.002.L2V12DR-BC8.BW-8-2_R2.sam

HI.4487.002.L2V12DR-BC9.Fw-12-1_R1.sam

HI.4487.002.L2V12DR-BC10.Fw-12-2_R2.sam

HI.4487.002.L2V12DR-BC11.BW-12-1_R1.sam

HI.4487.002.L2V12DR-BC12.Bw-12-2_R1.sam

HI.4487.002.L2V12DR-BC12.Bw-12-2_R2.sam

HI.4487.002.L2V12DR-BC13.FW-16-1_R2.sam

HI.4487.002.L2V12DR-BC14.FW-16-2_R1.sam

HI.4487.002.L2V12DR-BC14.FW-16-2_R2.sam

HI.4487.002.L2V12DR-BC15.BW-16-1_R1.sam

HI.4487.002.L2V12DR-BC16.BW-16-2_R2.sam

A.2.2 SAMtool analysis code

Program installation:

SAMtools (Tools for alignments in the SAM format) Version: 0.1.19-44428cd

Sorting code for :

sort -s -k HI.4487.002.L2V12DR_all _file.sam > HI.4487.002.L2V12DR _all_sorted.sam

samtools sort [options...] [in.Sam]

Options: -l INT Set compression level, from 0 (uncompressed) to 9 (best) -m INT Set maximum memory per thread; suffix K/M/G recognized [768M] -n Sort by read name -t TAG Sort by value of TAG. Uses position as secondary index (or read name if -n is set) -o FILE Write final output to FILE rather than standard output -T PREFIX Write temporary files to PREFIX.nnnn.bam--input-fmt-option OPT[=VAL] Specify a single input file format option in the form of OPTION or OPTION=VALUE -O, --output-fmt FORMAT[,OPT[=VAL]]... Specify output format (SAM)

Outputs:

HI.4487.002.L2V12DR-BC1.FW-4-1_R2.sorted.sam

HI.4487.002.L2V12DR-BC2.FW-4-2_R1.sorted.sam

HI.4487.002.L2V12DR-BC3.BW-4-1_R2.sorted.sam,

HI.4487.002.L2V12DR-BC4.BW-4-2_R1.sorted.sam,

HI.4487.002.L2V12DR-BC4.BW-4-2_R2.sorted.sam,

HI.4487.002.L2V12DR-BC5.FW-8-1_R2.sorted.sam,

HI.4487.002.L2V12DR-BC6.FW-8-2_R1.sorted.sam

HI.4487.002.L2V12DR-BC6.FW-8-2_R2.sorted.sam,

HI.4487.002.L2V12DR-BC7.BW-8-1_R1.sorted.sam,

HI.4487.002.L2V12DR-BC7.BW-8-1_R2.sorted.sam,

HI.4487.002.L2V12DR-BC8.BW-8-2_R2.sorted.sam,

HI.4487.002.L2V12DR-BC9.Fw-12-1_R1.sorted.sam

HI.4487.002.L2V12DR-BC10.Fw-12-2_R2.sorted.sam

HI.4487.002.L2V12DR-BC11.BW-12-1_R1.sorted.sam

HI.4487.002.L2V12DR-BC12.Bw-12-2_R1.sorted.sam

HI.4487.002.L2V12DR-BC12.Bw-12-2_R2.sorted.sam

HI.4487.002.L2V12DR-BC13.FW-16-1_R2.sorted.sam

HI.4487.002.L2V12DR-BC14.FW-16-2_R1.sorted.sam

HI.4487.002.L2V12DR-BC14.FW-16-2_R2.sorted.sam

HI.4487.002.L2V12DR-BC15.BW-16-1_R1.sorted.sam

HI.4487.002.L2V12DR-BC16.BW-16-2_R2.sorted.sam

A.2.3 HTSeq analysis code

Import HTSeq in the Python software:

gtf_file = HTSeq.GFF_Reader(" Drosophila_melanogaster.BDGP6.75.gtf.gz") exons = HTSeq.GenomicArrayOfSets("auto", stranded=True) for feature in gtf_file: if feature.type == "exon": exons[feature.iv] += feature.attr["gene_id"]

Counting the reads:

counts = collections.Counter( ) almnt_file = HTSeq.SAM_Reader(" HI.4487.002.L2V12DR-all.sorted.sam") for almnt in almnt_file: if not almnt.aligned: count["_unmapped"] += 1 continue gene_ids = set() for iv, val in features[almnt.iv].steps(): gene_ids |= val if len(gene_ids) == 1: gene_id = list(gene_ids)[0] counts[gene_id] += 1 elif len(gene_ids) == 0: counts["_no_feature"] += 1 else: counts["_ambiguous"] += 1 for gene_id in counts: print gene_id, counts[gene_id]

annotation.gtf >

HI.4487.002.L2V12DR-BC1.FW-4-1_R2.counted.txt

HI.4487.002.L2V12DR-BC2.FW-4-2_R1.counted.txt

HI.4487.002.L2V12DR-BC3.BW-4-1_R2.counted.txt

HI.4487.002.L2V12DR-BC4.BW-4-2_R1.counted.txt

HI.4487.002.L2V12DR-BC4.BW-4-2_R2.counted.txt

HI.4487.002.L2V12DR-BC5.FW-8-1_R2.counted.txt

HI.4487.002.L2V12DR-BC6.FW-8-2_R1.counted.txt

HI.4487.002.L2V12DR-BC6.FW-8-2_R2.counted.txt

HI.4487.002.L2V12DR-BC7.BW-8-1_R1.counted.txt

HI.4487.002.L2V12DR-BC7.BW-8-1_R2.counted.txt

HI.4487.002.L2V12DR-BC8.BW-8-2_R2.counted.txt

HI.4487.002.L2V12DR-BC9.Fw-12-1_R1.counted.txt

HI.4487.002.L2V12DR-BC10.Fw-12-2_R2.counted.txt

HI.4487.002.L2V12DR-BC11.BW-12-1_R1.counted.txt

HI.4487.002.L2V12DR-BC12.Bw-12-2_R1.counted.txt

HI.4487.002.L2V12DR-BC12.Bw-12-2_R2.counted.txt

HI.4487.002.L2V12DR-BC13.FW-16-1_R2.counted.txt

HI.4487.002.L2V12DR-BC14.FW-16-2_R1.counted.txt

HI.4487.002.L2V12DR-BC14.FW-16-2_R2.counted.txt

HI.4487.002.L2V12DR-BC15.BW-16-1_R1.counted.txt

HI.4487.002.L2V12DR-BC16.BW-16-2_R2.counted.txt

A.2.4 Deseq2 analysis code

All gene counts were placed in an excel file to create an expression matrix. In the matrix, the row names are gene names, and the columns are sample names.

First step, uploading the matrix:

File name <-read.csv("/Users/sattarsoltani/Documents/sattar/RNA-file/File.csv",row.names = 1, header = TRUE)

Second step, making data frame of analysis:

Sample.id <- c("FAC.4hr", "BPS.4hr", "FAC.8hr", "BPS.8hr", "FAC.12hr", "BPS.12hr", "FAC.16hr", "BPS.16hr") Num.tech.reps <- c("1", "1", "1", "1", "1", "1", "1", "1") strain <- c("Treatment/6j", "Control/2j", "Treatment/6j", "Control/2j", "Treatment/6j", "Control/2j", "Treatment/6j", "Control/2j") experiment.number <- c("7","6","4","6","7","6","4","6") lane.number <- c("1","3","5","7","1","3","5","7") Wh.Data=data.frame(sample.id, num.tech.reps, strain, experiment.number, lane.number)

Third step, DESeq2 analysis:

library("DESeq2") dds.2repGut <- DESeqDataSetFromMatrix(countData = Wh , colData = Wh.Data, design = ~ strain) dds.2repGut <- DESeq(dds.2repGut) plotDispEsts(dds.2repGut)

Forth step, comparing control samples with experimental samples:

contrast.deseq2 <- list("strainTreatment.6j", "strainControl.2j") contrast.deseq2 <- list("strain_Treatment.6j_vs_Control.2j") deseq2_resultsGut <- results(dds.2repGut, contrast=contrast.deseq2) write.table(deseq2_resultsGut, "gut_quick_01_parameters.txt")

Final step, identifying statistically significant DEGs:

p.threshold <- 0.05

deseq2_resultsGut$threshold <- as.logical(deseq2_resultsGut$padj < p.threshold)

genes.deseqGut <- row.names(deseq2_resultsExp)[which(deseq2_resultsExp$threshold)]

write.table(genes.deseqGut, "gut_quick_01_Desq_genes_Result.txt")

>View(genes.deseq_Result)

A.2.5 edgeR analysis code

First step, uploading matrix file:

read.csv("/Users/sattarsoltani/Documents/sattar/RNAfile/ File.csv",row.names = 1, header = TRUE)

Second step, making data frame of analysis:

sample.id <- c("FAC.4hr", "BPS.4hr", "FAC.8hr", "BPS.8hr", "FAC.12hr", "BPS.12hr", "FAC.16hr", "BPS.16hr") num.tech.reps <- c("1", "1", "1", "1", "1", "1", "1", "1") strain <- c("Treatment/6j", "Control/2j", "Treatment/6j", "Control/2j", "Treatment/6j", "Control/2j", "Treatment/6j", "Control/2j") experiment.number <- c("7","6","4","6","7","6","4","6") lane.number <- c("1","3","5","7","1","3","5","7") Wh.Data=data.frame(sample.id, num.tech.reps, strain, experiment.number, lane.number)

Third step, creating edgeR model:

dgeWh <- DGEList(counts=File, group=Exp.Data$strain) # Normalize by total count dge <- calcNormFactors(dgeWh) # Create the contrast matrix design.mat <- model.matrix(~ 0 + dge$samples$group) colnames(design.mat) <- levels(dge$samples$group)

Forth step, Estimating dispersion parameter:

dge <- estimateGLMCommonDisp(dge, design.mat) dge <- estimateGLMTrendedDisp(dge, design.mat, method="power") dge<- estimateGLMTagwiseDisp(dge,design.mat)

Plot mean-variance plotBCV(dge)

Fifth step, creating design matrix:

design.mat <- model.matrix(~ 0 + dge$samples$group) colnames(design.mat) <- c("Treatment.6j", "Control.2j") # Model fitting fit.edgeR <- glmFit(dge, design.mat)

Final step, finding differentially expressed genes

contrasts.edgeR <- makeContrasts(Treatment.6j - Control.2j, levels=design.mat)

lrt.edgeR <- glmLRT(fit.edgeR, contrast=contrasts.edgeR)

p.threshold <- 0.05 edgeR_results <- lrt.edgeR$table write.table(edgeR_results, "File_edgeR_P01_parameters.txt") sig.edgeR <- decideTestsDGE(lrt.edgeR, adjust.method="BH", p.value = p.threshold) genes.edgeR <- row.names(edgeR_results)[which(sig.edgeR != 0)] View(genes.edgeR) write.table(genes.edgeR, "BRcR0_edgeR_gene.txt")

A.2.6 Principal component analysis (PCA) code

Importing matrix file:

PCA.all3 <-read.csv("/Users/sattarsoltani/Documents/sattar/RNA file/MYFile.csv",row.names = 1,header = TRUE) data("heptathlon", package = "HSAUR") heptathlon$hurdles <- max(heptathlon$hurdles) - + heptathlon$hurdles heptathlon$run200m <- max(heptathlon$run200m) - + heptathlon$run200m heptathlon$run800m <- max(heptathlon$run800m) - + heptathlon$run800m plot(heptathlon,cex=0.9,col="Red",main="My samples", xlim=c(0,20), ylim=c(0,10)) options(digits=3) par(mfrow=c(1,1))

Calculating correlations and PCA:

round(cor(PCA.my), 2) My_pca <- prcomp(PCA.all, scale = TRUE) print(My_pca) score <- which(colnames(PCA.my) == "score")

Plotting the result:

plot(PCA.my,col="Red",main="4 hour")